AN ABSTRACT OF THESIS

Kirsten R. Wolthers for the degree of Doctor of Philosophy in Biochemistry and Biophysics presented on April 24, 2001. Title: Characterization of Neuronal Nitric-Oxide Synthase Reductase Activity.

Abstract approved: Redacted for Privacy

Michael I. Schimerlik

During catalysis the flavoprotein domain of neuronal nitric-oxide synthase (nNOS) shuttles NADPH-derived reducing equivalents from FAD to FMN and then to the P450-heme enabling heme-based oxygen activation and subsequent NO-synthesis. The binding of Ca^{2+}-activated calmodulin (Ca^{2+}-CaM) to nNOS alleviates inhibition of flavin mediated electron transfer within the diflavin domain, which is demonstrated by the increase in the rate of 2,6-dichloroindolphenol (DCIP) reduction by 2 to 3 fold and that of cytochrome c^{3+} by 10 to20 fold. To investigate the effect of the Ca^{2+}-CaM on the nNOS reductase activity, the steady-state kinetics of basal and CaM-stimulated reduction of these two substrates was studied. Parallel initial velocity patterns indicated that both substrates are reduced in a ping-pong mechanism. Product and dead-end inhibition data with DCIP as the electron acceptor were consistent with a di iso ping-pong bi-bi mechanism. In contrast, product and dead-end inhibition studies with cytochrome c^{3+} as the second substrate were consistent with an iso (two-site) ping-pong mechanism. Ca^{2+}-CaM did not alter the proposed kinetic mechanisms; however,

it did effect to varying degrees the (k_{cat}/K_m) for the various substrates. The pH-dependence of basal and CaM-stimulated reduction of DCIP revealed that ionizable groups involved in the binding of substrates and catalysis are not altered by Ca^{2+}-CaM. However, the activated cofactor does influence catalytic rate constants and/or ionizable groups involved in cytochrome c^{3+} reduction. nNOS was found to abstract the pro-*R* (A-side) hydrogen from NADPH. Primary deuterium isotope effects (NADP(D)) and solvent isotope effects (SKIE) suggests that of the two half reactions, the reductive half reaction involving NADPH oxidation limits the overall reaction rate, but that hydride transfer to FAD is not the slow step. A small value of $^{D}(V/K)_{NADPH}$ (1.2-1.6) suggests hydride transfer is not the rate-limiting step within the reductive half-reaction. Large solvent kinetic isotope effects (SKIE) were observed on $(V/K)_{cytc}$ for basal and CaM-stimulated reduction of cytochrome c^{3+} suggesting that proton uptake from the solvent limits the rate of the oxidative half-reaction. A small SKIE on V and $(V/K)_{NADPH}$ indicates that proton uptake does not limit the overall reaction rate. Proton inventory analysis revealed multiple transition-state protons contributed to the observed SKIE.

Copyright by Kirsten R. Wolthers
April 24, 2001
All Rights Reserved

Characterization of Neuronal Nitric-Oxide Synthase Reductase Activity

by

Kirsten R. Wolthers

A THESIS

Submitted to

Oregon State University

in partial fulfillment of
the requirement for the
degree of

Doctor of Philosophy

Completed April 24, 2001

Commencement June 2001

Doctor of Philosophy thesis of Kirsten R. Wolthers presented on April 24, 2001.

APPROVED

Redacted for Privacy

Major Professor Representing Biochemistry and Biophysics

Redacted for Privacy

Head of the Department of Biochemistry and Biophysics

Redacted for Privacy

Dean of Graduate School

I understand that my thesis will become part of the permanent collection of Oregon State University libraries. My signature below authorizes release of my thesis to any reader upon request.

Redacted for Privacy

Kirsten R. Wolthers, Author

ACKNOWLEDGEMENTS

I thank Dr. Michael Schimerlik for is guidance, support, and teaching me the fundamentals of enzyme kinetics on paper towels. I extend my gratitude towards Dr. Gary Peterson for assistance with nucleotide and protein purification, Dr. David Broderick for helpful discussions on molecular biology strategies, Dr. Valerie Mosser for help with tissue culture, and Dr. Mark Harder for assistance with florescence and absorbance studies. I thank the members of my committee, Drs. Sonia Anderson, Dale Mosbaugh, Stephen Giovannoni, and Isaac Wong. I am also grateful to Drs. Sonia Anderson and Dean Malencik for providing the calmodulin and calmodulin-sepharose for these kinetic studies.

I thank my parents, Tim Wolthers and Anne Marie Mol for their encouragement and enthusiasm. Finally, I am grateful to David, Drew, Krista, Carl and Clay for all fun times outside the lab.

TABLE OF CONTENTS

TABLE OF CONTENTS (CONTINUED)

TABLE OF CONTENTS (CONTINUED)

TABLE OF CONTENTS (CONTINUED)

LIST OF FIGURES

LIST OF FIGURES (CONTINUED)

LIST OF TABLES

LIST OF APPENDICES

LIST APPENDIX FIGURES

Figure Page

DEDICATION

This thesis is dedicated
to the CARY 219

Characterization of Neuronal Nitric-Oxide Synthase Reductase Activity

Chapter 1

Introduction

Nitric oxide, NO, is a wide spread mediator of a vast number of physiological and pathophysiological processes (1, 2). A family of three isozymes, the nitric-oxide synthases (NOS; EC 1.14.13.39), catalyze NO biosynthesis via the five-electron oxidation of L-arginine (Figure 1.1; 3, 4;). One reaction cycle consumes 1.5 NADPH and two O_2 to produce NO, L-citrulline and two H_2O (5, 6). In the first step, O_2 and NADPH-derived electrons convert L-arginine to the intermediate N-hydroxy-arginine (NHA) and H_2O in a mixed-function oxidation reaction (7, 8). The unique second step uses 0.5 NADPH and O_2 to oxidize NHA forming NO, L-citrulline, and H_2O (5, 9).

All three isoforms - neuronal (nNOS), inducible (iNOS) and endothelial (eNOS)- are homodimers with each subunit consisting of three conserved domains (Figure 1.2; 3, 10). An iron protoporphyrin IX heme, (6*R*)-5,6,7,8-tetrahydo-L-biopterin (H_4B), and L-arginine bind to the oxygenase domain located at the N-terminal half of the polypeptide subunit (11-14). The C-terminal reductase domain contains two flavins, FAD and FMN, and the binding site for the substrate NADPH (15). During catalysis the flavins transfer NADPH-derived electrons to the heme iron enabling it to activate oxygen and catalyze NO synthesis. Dimer formation is necessary for NO synthesis because flavin to heme electron transfer proceeds exclusively between adjacent subunits (16, 17). Binding of calmodulin (CaM) to the third conserved site connecting the oxygenase and reductase

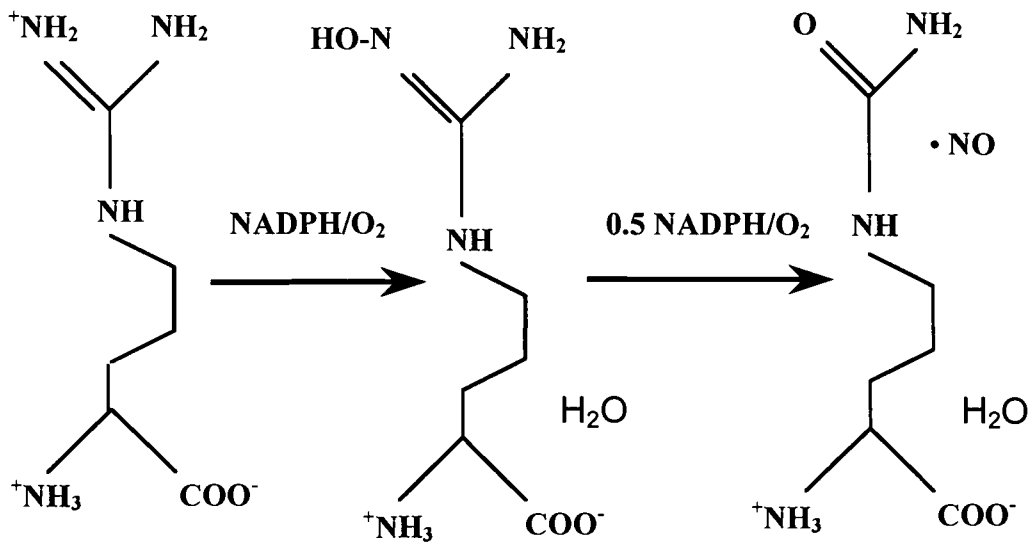

Figure 1.1 The NOS-catalyzed two-step conversion of L-arginine to L-citrulline. In the first step, O_2 and NADPH-derived electrons convert L-arginine to H_2O and the intermediate N-hydroxy-L-arginine (NHA) in a mixed-function oxidation reaction. The second step uses 0.5 NADPH and O_2 to oxidize NHA forming NO, H_2O, and L-citrulline.

Figure 1.2 Functional elements of the NOS sequence. The sequences for the PDZ domain of nNOS, the fatty acylation sites in eNOS are shown at the N-terminus (4). Site-directed mutagensis identified the cysteine axial heme ligand, the cysteine involved H_4B binding and a glutamate participating in L-arginine-NOS complex formation; these are shown in the oxygenase domain. Consensus sequences for CaM-binding and the putative contact sites for the isoalloxazine rings and phosphate portions of FMN and FAD and the ribose and adenine portions of NADPH are also depicted by the black boxes.

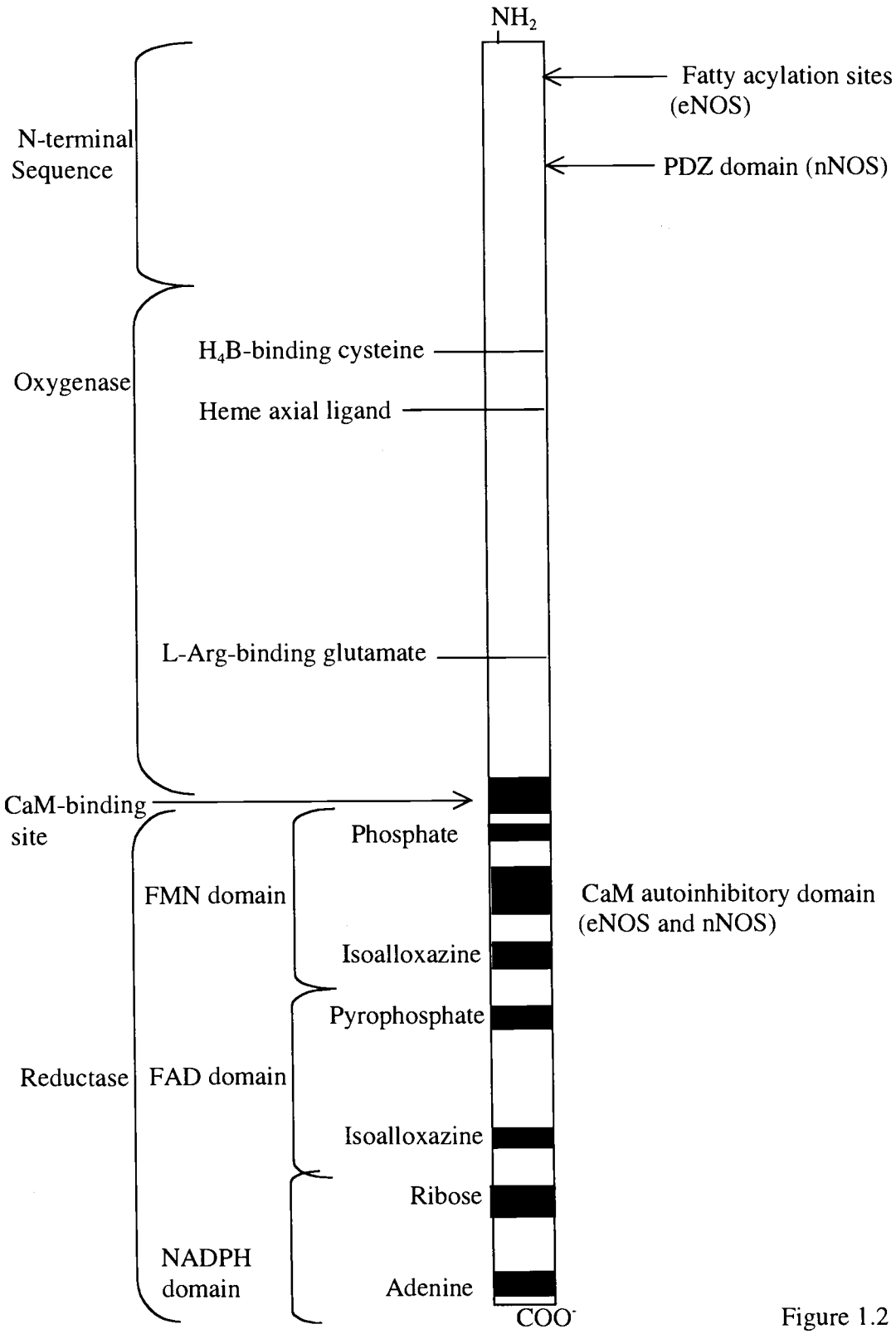
NH2
Fatty acylation sites (eNOS)
PDZ domain (nNOS)
N-terminal Sequence
H4B-binding cysteine
Oxygenase
Heme axial ligand
L-Arg-binding glutamate
CaM-binding site
Phosphate
FMN domain
CaM autoinhibitory domain (eNOS and nNOS)
Isoalloxazine
Pyrophosphate
Reductase
FAD domain
Isoalloxazine
Ribose
NADPH domain
Adenine
COO-

Figure 1.2

domains facilitates electron transfer between the flavins and heme (18). Neuronal and endothelial NOS require elevated intracellular Ca^{2+} levels to initiate the binding of Ca^{2+}-activated CaM (Ca^{2+}-CaM) required for NO synthesis (19, 20). However, CaM is a tightly bound to iNOS even at basal intracellular Ca^{2+} levels; therefore, this isoform will continually generate NO in a Ca^{2+}-independent manner (21-23).

This introductory chapter is divided into four sections. The first section will review the structure of NOS, comparing each of the isoforms with each other and with the cytochrome-P450 system. The mechanism of NO synthesis, the control of protein-mediated electron transfer, and the role of various substrate/cofactors during catalysis will be discussed in the second section. The third section will review the properties, cellular distribution and control of the expression of the NOS isoforms. The major physiological roles of NO in the nervous, immune and circulatory systems will be addressed in the last section.

1.1 Structure of NOS

1.1.1 Quaternary and tertiary structure

The three isoforms of NOS share 50-60% amino acid sequence similarity. nNOS (160 KDa; (24) is larger than eNOS (~130 KDa; 25) and iNOS (~133 KDa; 26) due to an additional ~220 N-terminal amino acid residues (27). Evidence suggests that both the monomeric and dimeric forms of NOS are elongated proteins. The elution profile for eNOS from an FPLC column with a set of globular proteins reveled that eNOS eluted immediately after apoferritin (443 KDa) and the eNOS monomer eluted very close to β-

amylase (200 KDa; 28). Furthermore, velocity sedimentation experiments with nNOS dimer revealed that the quaternary structure of the enzyme also appears to be an elongated homodimer (29).

The polypeptide subunits of NOS have a bidomain structure. Limited trypsin proteolysis of nNOS in the absence of CaM cleaved the enzyme into an N-terminal and C-terminal half, each approximately 80 KDa (30). The absorbance spectrum of the C-terminal-half showed shoulders at 450 nm and 550 nm representing the enzyme-bound FAD and FMN (30). This domain was labeled the reductase domain as it exhibited cytochrome c^{3+} reductase activity analogous to cytochrome P450 reductase (CPR; 31). The absorbance spectrum of the nNOS N-terminal half had a small shoulder at 420 nm with broad bands at lower extinction coefficients centered near 538 nm and 650 nm attributed to the heme chromophore (30). The pyridine hemochrome assay demonstrated that the enzyme contains two mols of iron protoporphyrin IX/mol of enzyme homodimer (12, 14).

Although all three isoforms function as homodimers, the protein structural components required for subunit association and the cofactor and substrates needed for inducing and stabilizing dimerization are different. Subunit association in eNOS and nNOS involves head to head interactions of the oxygenase domain, tail to tail interactions of reductase domain, and head to tail interactions between the oxygenase and reductase domain (32). In contrast, iNOS subunit association involves only oxygenase domain interactions (33). Low-temperature SDS-polyacrylamide gel electrophoresis revealed that the binding of H_4B and L-arginine synergistically convert nNOS and iNOS into stable homodimers (29). For these two isoforms, dimer

dissociation was accompanied by a concerted loss of NO synthesis activity and the release of bound H_4B from the protein (34, 35). Reif *et al.* determined that the endogenous addition of H_4B prevented monomerization (35). In contrast, dimerization in eNOS is controlled by the intracellular availability of the heme, not the binding of H_4B or L-arginine (36, 37). A set of chimeras in which the reductase and oxygenase domains where swapped between the isoforms demonstrated that the structural components in the eNOS oxygenase domain facilitate H_4B-independent dimer formation (38).

Evidence suggests the binding of H_4B and L-arginine induces large conformational changes in the iNOS and nNOS oxygenase active site. Large bulky nitrosoalkane derivatives are able to react with distal-side of the heme in the absence the cofactor and substrate. However, the binding of L-arginine and H_4B inhibits the binding of even the smallest nitrosoalkane ligand (CH_3NO; 39). Exposure of the distal side of the heme to the solvent in monomeric H_4B-free and L-arginine-free iNOS also permits DTT to form a bisthiolate complex (34). The hyperporphyrin spectra emitted by the bisthiolate complex will disappear with addition of L-arginine and H_4B indicating that structural changes are occurring in the oxygenase domain (40). Comparison of the H_4B-free and H_4B-bound crystal structures of the iNOS oxygenase domain show that the binding of the cofactor, which binds at the dimer interface, induces large conformational changes in this isoform to stabilize the dimeric form of the enzyme (41). In contrast, the crystal structure for the H_4B-free and H_4B-bound eNOS reveals that the presence of the cofactor does not induce dimerization and fails to induce any large conformational change (42).

1.1.2 Oxygenase domain

Spectral analyses of the heme ligand environment in NOS indicated that the coordination to heme was similar to that of cytochrome P450 enzymes. Similar to cytochrome P450, the binding of CO the heme results in the inhibition of substrate oxidation suggesting that the NOS-heme participates in catalysis (11). The nNOS reduced CO-difference spectrum with a λ maximum at 444 nm provided the initial evidence for a proximal thiolate linkage to the heme iron (11). Site-directed mutagenesis verified the position of the proposed thiolate donor in human eNOS, rat nNOS, and human iNOS as cysteine-184 (43), cysteine-415 (44, 45), and cysteine-200 (46), respectively. All cysteine mutants were unable to bind heme or carry out NO synthesis. The nNOS cysteine-415 mutant and iNOS cysteine-200 mutant were also unable to bind H_4B or L-arginine despite the circular dichroism (CD) spectra indicating the mutants were folded properly (44, 46).

Although both the NOS oxygenase domain and the cytochrome P450 contain cysteine thiolate-ligated heme and share several spectral properties, there is a lack of primary sequence similarity between the two enzymes, particularly within the conserved residues neighboring the distal cysteine heme ligand. The three-dimensional structures of the NOS oxygenase domains and cytochrome P450 are different in both their tertiary structure and active site geometry (42, 47). The distal heme pocket of iNOS primarily consists β structure opposed to a variety of other heme containing enzymes such as oxygenases, oxidases, peroxidases, and catalyases, which largely have α-helical distal heme pockets (47). The orientation of the cysteine proximal ligand also differs between

the two families of proteins. The cysteine-194 of iNOS lies at the carboxy-terminal end of the helix and proceeds an extended strand, whereas the cytochrome P450 cysteine lies at the N-terminal of the helix and follows an extended strand. The two cysteine thiolates also bind opposite faces of the iron protoporphyrin IX in the two proteins (47).

In the absence of substrate, the heme iron of cytochrome P450 exists as a hexacoordinate heme, four bonds to the pyrole nitrogens, one to the sulfur atom of the proximal cysteine, and the one to the sixth axial ligand, which is most often H_2O. The addition of substrate displaces the sixth axial ligand and the heme converts to the high-spin pentacoordinate state (48-50). The conversion of the heme to the high-spin form can be observed spectrally, since it coincides with a blue shift the heme Soret maximum. Unlike the majority of the cytochrome P450s, all three full-length H_4B-containing ferric NOS isoforms are predominately pentacoordinate high-spin even in the absence of substrate (51). The visible spectrum of purified nNOS displays a broad peak at 406 nm, which arises from the coalescence of a high-spin peak with an absorbance maximum at 389 nm and a low-spin peak with an absorbance maximum at 416 nm. Electron paramagnetic resonance (EPR) data on the nNOS heme confirmed that the iron exists as a population of high and low-spin heme, with the majority (>85%) in the high-spin pentacoordinate state (12). During catalysis, the sixth coordination site is occupied by O_2; however, at rest, the sixth coordination site of the heme in these enzymes is occupied by H_2O (52). The addition of L-arginine results in the conversion of the remaining fraction of hexacoordinate heme iron into the high spin-state (53). This substrate perturbation results in "type I" difference absolute spectra with a peak at 396 nm. A "type II" substrate perturbation occurs when a strong heme ligand such as

imidazole binds to the sixth axial heme ligand position and converts the heme from a high-spin pentacoordinate state back to a low-spin state hexacoordinate state. The "type II" absolute spectra has absorbance peaks ranging between 420 and 438 nm.

Imidazole inhibits NOS-catalysis formation by preventing oxygen activation (54). The binding constant for imidazole, 160 μM, was determined by following spectral changes as the ligand was titrated with the heme. The direct binding of L-arginine to NOS induces a relatively small spectral perturbation compared to imidazole; therefore, the binding constant for the substrate could not be determined by following a direct substrate-dependent shift in the heme spin equilibrium. Instead the L-arginine binding constant, 0.6 μM, was determined by following the heme absorbance change back to the high spin form accompanying imidazole displacement with the substrate (55).

If nNOS or eNOS are expressed and purified in the absence of H_4B, the heme is primarily low spin (45, 56). EPR demonstrated that the low-spin heme forms a bisthiolate complex with a cysteine thiolate located in distal heme pocket that likely becomes available to a population of the heme protein through collapse or deformation of the distal site in the absence of pterin. Prolonged incubation with H_4B (24 hrs) in the presence of dithiothreitol converts the heme of either isoform to the high spin-state. The thiol (DTT) requirement for H_4B and L-arginine binding suggests that a cysteine residue is involved in the restoration of the pterin- and substrate-binding, possibly through reductive cleavage or rearrangement of the intersubunit disulfide bond (56, 57).

In contrast, the eNOS heme is primarily high-spin in the absence of H_4B and L-arginine (28). Through a series of deletions aimed at modulating the eNOS distal heme

site, Rodriquez-Crespo *et al.* demonstrated sequence at the N-terminus stabilizes the binding of L-arginine, sequesters the heme from the bulk solvent, and retains the heme in the high-spin state even in the absence of L-arginine and H_4B. Therefore, the N-terminal portion of eNOS participates in eNOS dimerization, since these same properties are attributed to the stability of the eNOS dimer in the absence of substrate/cofactor.

Stabilization of the NOS dimers may also be attributed to the presence of a zinc tetra-thiolate in the oxygenase domain. Although the initial crystal structure of the iNOS oxygenase domain published by Crane *et al.* did not show any zinc associated with this domain, subsequent crystal structures of the oxygenase domains of all three isoforms revealed a zinc tetra-thiolate (ZnS_4) (41, 42, 58, 59). The zinc atom is tetrahedrally coordinated to two pairs of symmetry related cysteine residues located in the phylogenetically conserved CXXXXC motif present in each NOS monomer (42, 58). It is situated at the bottom of the dimer interface, 14 Å from each pterin ring and 21.7 Å from each heme iron (42, 60). In the first published crystal structure of the iNOS oxygenase domain, the cysteine ligated to the zinc, Cys-109, formed a self-symmetric disulfide bond with the Cys-109 of the adjacent subunit at the dimer interface (59). A more refined structure of the disulfide-bridge showed that an N-terminal β-hairpin hook was swapped between adjacent subunits (59). Removal of the β-hairpin hook disrupted the H-bond and packing interactions within the N-terminal and caused permanent defects in homodimer formation, H_4B binding, and enzyme activity. Thus the N-terminal hook in iNOS is thought to stabilize the dimeric structure by increasing the number of surface area contacts in the dimer interface. In the single zinc-ligated

structure, the residues on the N-terminal hook interact primarily with amino acids in the same subunit, rather than with the adjacent subunit (58). However, eight hydrogen bonds are created by the formation of the zinc tetrathiolate, which may also contribute to dimer stabilization. The formation of a disulfide between symmetry related Cys115 of eNOS in the zinc free form weakens the hydrogen-bonding to H_4B; therefore, the presence of the zinc tetrathiolate is strategic in this isoform for maintaining the integrity of the H_4B binding site (58, 59).

The presence and absence of the zinc tetrathiolate in the crystal structures of the iNOS and eNOS oxygenase domain may have arisen from the contrasting methods for expression and purification of the enzymes (60). Crane *et al.* crystallized the purified *E. coli*-expressed heme domain of iNOS, which contains only ~20 % of the theoretical zinc content based on one atom of zinc for two hemes (41). In contrast, the zinc content of the trypsin cleaved heme domain of iNOS and eNOS derived from the full length iNOS or eNOS holoenzyme contains 90% of the theoretical zinc (42, 58). Metal analysis of eNOS, nNOS and iNOS indicates that zinc is present in the eNOS at the highest ratio of 0.6 relative to the total iron. For nNOS and iNOS the ratio falls to 0.3 and 0.2, respectively. Interestingly, the ratio of zinc content roughly correlates with the stability of the homodimer, since the eNOS homodimer is the most stable and the iNOS homodimer is the least stable among the isoforms. Although the zinc binding site is conserved among all isoforms where it may contribute to stability of the homodimer, most notably for eNOS, it is not required for NO synthesis (60).

The crystal structure of eNOS and iNOS oxygenase domains also revealed that H_4B lies perpendicular to and on the proximal side to the heme (41, 42). The pterin

makes hydrogen bond contacts with the propionate of the heme, which in turn is H-bonded to the amino group of the substrate L-arginine (42). The pterin cofactor also lies at the interface of the dimer and is involved in extensive H-bonding with both subunits, which attests to its unusual high affinity (Kd ~10 nM; 42). The binding of H_4B to iNOS oxygenase induces a conformational rearrangement of the domain in which the heme becomes sequestered from the bulk solvent and a ~30 Å deep funnel-shaped channel to the active center is created (41).

Although the crystal structures show the dimer associated with two pterins, nNOS will typically purify with one molecule per dimer. This is attributed to the first molecule having a dissociation constant in the low nanomolar range (~ 10 nM), while the second molecule has a dissociation constant three orders of magnitude larger (61). Purified nNOS containing H_4B in the high affinity binding site is partially active, and the endogenous addition of micromolar concentrations of H_4B will saturate the second site and lead to an increase in NOS activity (62-64). The binding of H_4B to a pterin-deficient nNOS follows biphasic association kinetics. The Kd values obtained from radioligand binding studies are 147 ± 24.1 nM and 52 ± 9.2 nM for the binding of H_4B to eNOS in the absence and presence of 0.1 mM L-arginine, respectively (37). The positively co-operative effect of L-arginine was due to a pronounced decrease in the rate of H_4B dissociation (from 1.6 ± 0.5 to 0.3 ± 0.1 min^{-1}; 37).

1.1.3 Reductase domain

The three dimensional structure of the NOS reductase domain has not been solved; thus, any structural information on this diflavin domain is based on its close sequence

similarity with other related dual-flavin enzymes. The NOS reductase domain belongs to a subset of related reductases that contain an FMN-containing flavodoxin-like module linked to an NADPH and FAD-binding ferridoxin-like module (FNR) (15, 65). Members of the family include CPR (66), sulfite reductase (67), and methionine synthase reductase (68). The NADPH/FAD and FMN modules of these proteins appear to fold separately and function when expressed independently or after being separated by proteolysis (69, 70). The two flavins are sandwiched between aromatic residues and are positioned end to end with the two isoalloxazine rings at 150° angle with respect to each other. The closest distance separating the two flavins, about 4 Å, is through the 7- and 8- methyl groups on the isoalloxazine rings.. This close arrangement suggests that electron flow between the two flavins is not mediated by amino acid residue atoms, but occurs by direct transfer between the flavins. This structural information is consistent with kinetic data which demonstrates that electron transfer between the two flavins is rapid (69).

In the absence of NADPH, NOS maintains an air-stable one-electron reduced state (FAD-FMNH•) (71), which is unable to reduce the heme or cytochrome c^{3+} (72). The donation of two electrons through the oxidation of NADPH reduces both NOS and CPR to the three-electron reduced state. The midpoint potential for the reduction of the FAD semiquinone lies at –280 mV, suggesting that facile reduction by NADPH (reduction potential –320 mV) can occur (73). Saturation of the nNOS reductase domain with NADPH does not fully reduce the flavins (the flavins have the ability to accept 4-electrons), although full reduction of the flavins is possible with dithionite. The incomplete reduction of the flavins by NADPH could result from the binding of $NADP^+$

or NADPH stabilizing the FAD semiquinone by shifting the reduction potential to a more negative value. Similar effects have been observed for P450 BM3, adrenodoxin reductase and cytochrome b5 reductase (73). During turnover NOS, like CPR, cycles between the one and three-electron reduced states (74).

NOS and CPR are also able to reduce 2,6-dichloroindolphenol (DCIP), ferricyanide (FeCN), and cytochrome c^{3+} with electrons derived from NADPH oxidation (31, 75). However, nNOS is unique in that the binding of Ca^{2+}-CaM to the enzyme stimulates a 2 to 3 fold increase in DCIP and FeCN reduction and a 10 to 20 fold increase in cytochrome c^{3+} reduction (30, 76). The Ca^{2+}-CaM stimulation of these activities is independent of electron transfer from the flavins to the heme since the same level of stimulation of ferricyanide and cytochrome c^{3+} reduction occurs with nNOS devoid of its oxygenase domain (74, 76, 77). Stopped-flow studies indicate that the binding of Ca^{2+}-CaM increases the pre-steady state rate of electron transfer from NADPH to the flavins (76, 78). The increase in electron transfer may be facilitated by the ability of Ca^{2+}-CaM to induce a conformational change in the enzyme (30, 74, 79, 80). Bound FMN is essential for the fluorescence change associated with CaM binding to nNOS suggesting the CaM induced conformational change is restricted to the FMN module (74). Stopped-flow kinetic analysis demonstrated that FMN suppresses FAD reduction by NADPH, and the suppression is relieved by CaM binding or FMN removal (81). Potentiometric analysis of the flavin couples revealed that Ca^{2+}-CaM does not influence the thermodynamic driving force of electron transfer (73).

The FMN oxidized/semiquinone has the highest midpoint potential of –49 mV in nNOS (73), thus electron transfer from the hydroquinone state of FAD is

thermodynamically favorable. Due to the close proximity of the of the semiquinone/hydroquinone midpoint potentials for FAD (-280 mV) and FMN, (-274 mV) the two flavins can exist as a stable neutral semiquinone, and in the three-electron reduced state of the enzyme, the FMN will fluctuate between the semiquinone and hydroquinone states. Only the hydroquinone form of FMN is poised to thermodynamically deliver the first electron transfer to the ferric iron ($E'_{m,7}$ is –239mV for Fe (II)/ Fe(III)]. The midpoint potential of the semiquinone form of FMN can be accessed by the ferric-superoxy species; therefore, this intermediate may provide the second electron to heme required to generate the oxyferryl intermediate. The redox cycle of the reductase domain is completed with electron transfer from the FAD semiquinone to the oxidized FMN, generating the air-stable FMNH•.

The reductase domain of NOS also has additional amino acid sequences that are not found in CPR. nNOS and eNOS contain an additional 40-50 amino acid insert located in the FMN-binding subdomain (82). This insert is thought to be an autoinhibitory domain since it was shown to promote the dissociation of CaM from nNOS at low intracellular Ca^{2+} concentrations and to inhibit electron transfer in the absence of Ca^{2+}-CaM (82). Both iNOS and the constitutive isoforms possess an additional 21-42 amino acid-tail at the C-terminus, which is not present in CPR. This sequence is proposed to modulate electron transfer between the flavin moieties or between FMN and cytochrome c^{3+} (83).

The crystal structure of the iNOS oxygenase domain suggests that interaction with the reductase domain occurs through electrostatic interactions. The heme edge on the side opposite to the active site channel becomes exposed to the solvent upon

dimerization of the iNOS oxygenase domain (41) and may interact with the reductase domain as it contains residues which are highly conserved among the NOS isoforms. In addition, the electrostatic potential of these residues and the shape of the domain are complementary to the structure of the putative NOS reductase domain, which is based on the structure of the CPR (41). The crystal structure of the eNOS oxygenase domain revealed a lysine residue in this area, which is exposed to the solvent and lies in the region where the heme is close to the protein surface. The conversion of this lysine to a glutamic acid results in a mutant that is unable to produce NO with either L-arginine or NHA as substrates. Furthermore the low rate of electron transfer from the reductase domain to the heme iron under both aerobic and anaerobic conditions exhibited by this mutant suggests the lysine residue forms ionic interactions with the reductase domain.

1.1.4 Calmodulin-binding domain

The CaM binding domain for all three isoforms consists of a stretch of approximately 30 amino acids residues. The hydrophobic and basic composition of these amino acids along with their propensity to form an alpha helix is a diagnostic feature among CaM binding sites on target proteins. To initially demonstrate that CaM forms a complex with nNOS, a 30 amino acid synthetic peptide corresponding to the putative CaM-binding domain was used to compete for CaM and inhibit its stimulatory effect on two other CaM target proteins, cyclic nucleotide phosphodiesterase and adenylyl cyclase (84). The synthetic residue bound to CaM at an elevated Ca^{2+} concentration, with a 1:1 stoichiometry, and a binding affinity of 1 nM, typical for CaM binding targets proteins (30, 84).

A similar experiment was conducted for iNOS in which a synthetic thirty amino acid residue peptide corresponding to the putative CaM-binding domain this isoform was used to compete with full-length iNOS for CaM (21). The iNOS-peptide inhibited 90 % of iNOS activity when present in 12-fold excess. Unlike the nNOS-peptide, the presence of 5 mM EGTA only caused a 30 % maximal inhibition of activity. The addition of exogenous Ca^{2+} restored activity in a concentration-dependent fashion, demonstrating that the binding interaction between CaM is tight but reversible and requires basal concentrations of Ca^{2+} for full activity. As a result of this tight binding, CaM co-purifies with iNOS. Circular dichroism (CD) and 1H-NMR studies on the structure of the iNOS CaM binding-peptide in solution or complexed with CaM further demonstrated that the iNOS peptide retained the ability to bind CaM both in the presence and absence of Ca^{2+} (85). The 2D-NMR and CD spectra also showed that peptides corresponding to the CaM-binding domain of all three isoforms assume α-helical structures in aqueous solution and when complexed with CaM (85, 86).

To determine if the structural features that facilitate the Ca^{2+} independent CaM association lie within the thirty amino acid stretch of the iNOS CaM-binding domain or in protein sequence outside this domain, chimeric proteins were constructed in which the canonical CaM-binding domain was swapped between iNOS and nNOS. Chimeras containing the nNOS oxygenase and reductase domain tethered by the iNOS CaM-binding domain required intermediate levels of free Ca^{2+} to bind CaM and generate NO (87). Truncation analysis of iNOS suggests that residues within oxygenase domain are also required for Ca^{2+} independent binding (38). Chimeras of the two isoforms constructed by Lee *et al.* showed that Ca^{2+}-independent activity of iNOS requires

sequence in all three domains (88). The dissociation of Ca^{2+} from the CaM-nNOS complex was studied to determine the specific interactions between Ca^{2+} and CaM that lead to association and activation of NOS (89). Tryptic fragments of the C- and N-terminal lobes of CaM were bound to NOS in the presence of Ca^{2+} and the dissociation of Ca^{2+} from CaM-nNOS complex with either lobe was determined through stopped-flow fluorescent measurement using a fluorescent Ca^{2+} chelator. Fast dissociation (1000 s^{-1}) of Ca^{2+} from the N-terminal lobe corresponded to inactivation of NOS, while slower Ca^{2+} dissociation from the C-terminal lobe (1 s^{-1}) was coupled to dissociation form the CaM-nNOS complex. The bidentate glutamic acid residues, which coordinate Ca^{2+} in each of the four Ca^{2+} binding sites on CaM were changed to glutamine to examine the specific role of each Ca^{2+} in CaM-nNOS complex (90). The mutational analysis demonstrated that Ca^{2+} binding at site I is critical for all electron transfer reactions. In contrast, mutation at site III in the carboxy-terminal lobe activated NOS to similar level as wild type and mutations at sites II and IV exhibited intermediate effects on electron transfer between the flavins and heme. All single point mutations of CaM had nanomolar binding constants for nNOS, suggesting that the binding of CaM to target proteins does not necessarily lead to activation of the target protein, but rather that target activation requires specific Ca^{2+} dependent interaction between the two proteins (90).

Su *et al.* created a series of chimeras between the CaM and cardiac troponin C to determine which structural features of CaM control association and activation of nNOS (91). Although CaM and troponin C belonging to the same superfamily of Ca^{2+} signaling proteins and contain structurally related Ca^{2+} binding EF-hands, troponin C

does not bind to or activate nNOS. The study revealed that the "latch domain" of CaM (helices 2 and 6 of CaM) is essential for activation of nNOS (91).

1.2 Enzymology of NOS

1.2.1 Control of NO-synthesis and electron transfer

The three NOS isoforms differ in the rates of flavin mediated reactions (cytochrome c^{3+} and DCIP reduction) as well as in the rates of heme-mediated reactions (NO and citrulline formation). The rank order for NO-synthesis and cytochrome c^{3+}, flavin and heme reduction is iNOS > nNOS > eNOS (38). The rate of heme reduction (2.3 s^{-1} eNOS, 49 s^{-1} for nNOS, and 101 s^{-1} for iNOS $^{s-1}$) is much slower than flavin reduction (107 s^{-1} eNOS, 242 s^{-1} nNOS and 689 s^{-1} for iNOS) (92). Investigation of the activities of several chimeric NOS constructs, in which the reductase domains of eNOS and iNOS were swapped with the reductase domain of nNOS, suggests the maximal rate of NOS synthesis is determined by the maximum intrinsic ability of the reductase domain to deliver electrons to the heme domain (38).

The rate of NADPH oxidation at the reductase domain varies considerably as a function of the binding of L-arginine and H_4B, and the pattern of this variability is isoform specific. nNOS exhibits the highest degree of uncoupling in the absence of L-arginine (93). The addition of H_4B increases the rate of uncoupling 2-fold, whereas the addition of L-arginine decreases the activity 4-fold (94). In contrast, eNOS demonstrates little NADPH oxidase activity in the absence of L-arginine and the

addition of substrate or H_4B stimulates NADPH oxidation. The addition of H_4B and L-arginine to iNOS also increases the level of NADPH oxidation.

Due to the uncoupled NADPH-oxidase activity, nNOS will generate superoxide at L-arginine $\leq K_m$ and in CaM-dependent manner (7). When L-arginine is present, binding of the guanidino nitrogen in an ordered position near the heme allowing oxidation of L-arginine to proceed (47). However, in its absence, electron donation to the ferric heme leads to the subsequent activation of molecular oxygen. The transfer of the second electron from the flavins reduces the heme iron again generating superoxide (95). Under conditions of superoxide formation, the rate of NADPH oxidation increases, suggesting electron transfer from NADPH to O_2 is faster than the transfer of electrons to catalyze the formation of NO and citrulline. iNOS and eNOS can also generate superoxide in the presence of L-arginine (96-98). The inability of NaCN to significantly inhibit superoxide production in iNOS suggests that the free radical is generated through electron leakage from the flavin domain (99). NaCN was unable to block superoxide production from eNOS indicating that, like nNOS, superoxide is generated by heme-based oxygen activation (97, 100).

The constitutive (nNOS and eNOS) and inducible isoforms employ different mechanisms for controlling electron transfer to the heme. As discussed above, the binding of Ca^{2+}-CaM to nNOS and eNOS facilitates electron transfer from the flavins to heme by inducing a conformational change in the enzyme. In contrast, CaM is a tightly bound to iNOS at basal cellular levels of Ca^{2+}; therefore, an alternative mechanism for controlling electron transfer is required. Investigation of the heme midpoint potentials of the various isoforms lead to the discovery that iNOS, like P450-cam and P450-BM3,

controls heme reduction through the binding of substrates and cofactors (101). In the absence of L-arginine and H_4B, the iNOS midpoint potential is –347 mV and electron transfer from the flavins is not thermodynamically favorable. The binding of either the substrate or H_4B increases the redox potential by 100 mV making electron transfer thermodynamically feasible. In contrast the nNOS midpoint potential (-239 mV) is 100 mV higher than iNOS and this isoform is able to retain this elevated midpoint potential in the absence of L-arginine or H_4B. This feature of nNOS corresponds to the high Ca^{2+}-CaM-dependent NADPH-consumption rates exhibited in the absence of L-arginine.

NO-production by nNOS is controlled by the breakdown of a ferrous heme-NO complex. During steady-state turnover, the nNOS heme binds self-generated NO and the resulting complex is inactive (102). The ferrous heme-NO complex formation is rapid (~2 sec^{-1}; 92, 102) and results from the reduction of the ferric heme-NO-species that is an intermediate in catalysis (103). Based on the slow dissociation of the NO-heme complex (k = 0.06 sec^{-1}), an estimated 70 - 90 % of the nNOS population is inactive during steady state catalysis. Normal catalysis is resumed upon the O_2-dependent decay of the NO complex (34, 104). The apparent K_m for O_2 increases ~10-fold (38 μM to 350 μM) during steady-state NO synthesis compared to that for uncoupled NADPH oxidase activity. The ability of the nNOS heme to reversibly bind NO distinguishes it from the cytochrome P450s, which are irreversibly inactivated because the ferrous heme-NO complex rapidly break downs to form an inactive cytochrome P420 (105). NO binding is reversible albeit slow in nNOS, and multiple rounds of complex formation and decay do not slow enzyme activity (106). The binding of L-arginine and H_4B stabilizes the 6-coordinate-NO ferrous complex and prevents the

formation of the inactive P420 species (107). Aromatic stacking on the distal and proximal side of the nNOS heme by two conserved aromatic residues, Phe-584 and Trp-409 also stabilize the ferrous-NO complex (108). Although NO can recombine with the ferrous and ferric forms of eNOS (109), the ferrous heme-NO complex does not build-up to detectable levels during steady-state catalysis (110). The slow NO synthesis of eNOS is associated with slow heme reduction (92, 110).

1.2.2 Steps of NO-synthesis

NOS produces NO via two mixed-function oxidation reactions. In the first step, L-arginine is hydroxylated to form the intermediate NHA and H_2O in a reaction analogous to the two-electron substrate hydroxylation performed by cytochrome P450 enzymes. The subsequent three-electron oxidation of NHA is similar to the last step of the P450 aromatase reaction (111, 112) in which a ferric peroxide species is proposed to further oxidize NHA. The mechanism describing NO-synthesis has been largely based on P450 chemistry since the two enzymes catalyze similar substrate hydroxylations in addition to possessing a thiolate axial heme ligand, which serves as a strong internal electron donor in the process of oxygen bond scission. However, NOS is unique from the cytochrome P450s because its heme active center catalyzes two mechanistically distinct oxidations of similar substrates L-arginine and NHA, which are bound in the same conformation in the active site (113). Furthermore, NOS catalysis requires an additional cofactor, H_4B, for catalysis.

Nevertheless, the mechanism describing cytochrome P450 catalysis will be framework for the initial description of NO synthesis. Thus, catalysis begins with an

NADPH-derived electron reducing Fe(III) to Fe(II) (Figure 1.3). This facilitates the binding of O_2 to the sixth ligand position to give the intermediate [Fe(II)-O_2]. Based on the crystal structure of the iNOS oxygenase domain, L-arginine binds with the guanidinium nitrogen in the protonated form. Its close contact with a glutamic acid residue and the heme π-electrons make it a likely candidate for proton donation to the bound dioxygen (47). The thiolate axial heme ligand serves as a strong internal electron donor and this facilitates O-O bond scission, which produces an electrophilic oxo-iron intermediate (P•-Fe(IV)=O where P• is a porphyrin or protein radical). This species is thought to abstract a hydrogen atom from L-arginine and then rapidly recombine with the resulting free radical to form the hydroxylated product (113).

The second step (Figure 1.4) may occur by a mechanism where one electron from NADPH reduces the heme iron to the ferrous form. O_2 binds to Fe (II) to form a superoxo-iron (P-Fe(III)-OO^-) that removes an electron and proton, possibly from the N-hydroxy-group of NHA forming a proposed peroxo-iron intermediate [P-Fe(III)-OOH]$^{2+}$ (10, 114). The [P-Fe(III)-OOH] $^{2+}$ can participate in nucleophilic attack on the guanidino carbon of •NHA to produce a putative, tetrahedral intermediate (10, 114, 115). The collapse of the tetrahedral intermediate to the observed products, citrulline and NO can occur by proton transfer, hydride transfer or single electron chemistry.

Alternatively, once formed the [Fe(III)-OOH]$^{2+}$ intermediate can decay by subsequent heterolytic cleavage to a high valent iron-oxo complex [(Fe(IV)-O)] $^{3+}$, which can hydroxylate NHA in a P450-type catalyzed reaction. The iron-oxo intermediate has the capacity to oxidize the substrate by accepting two electrons but the

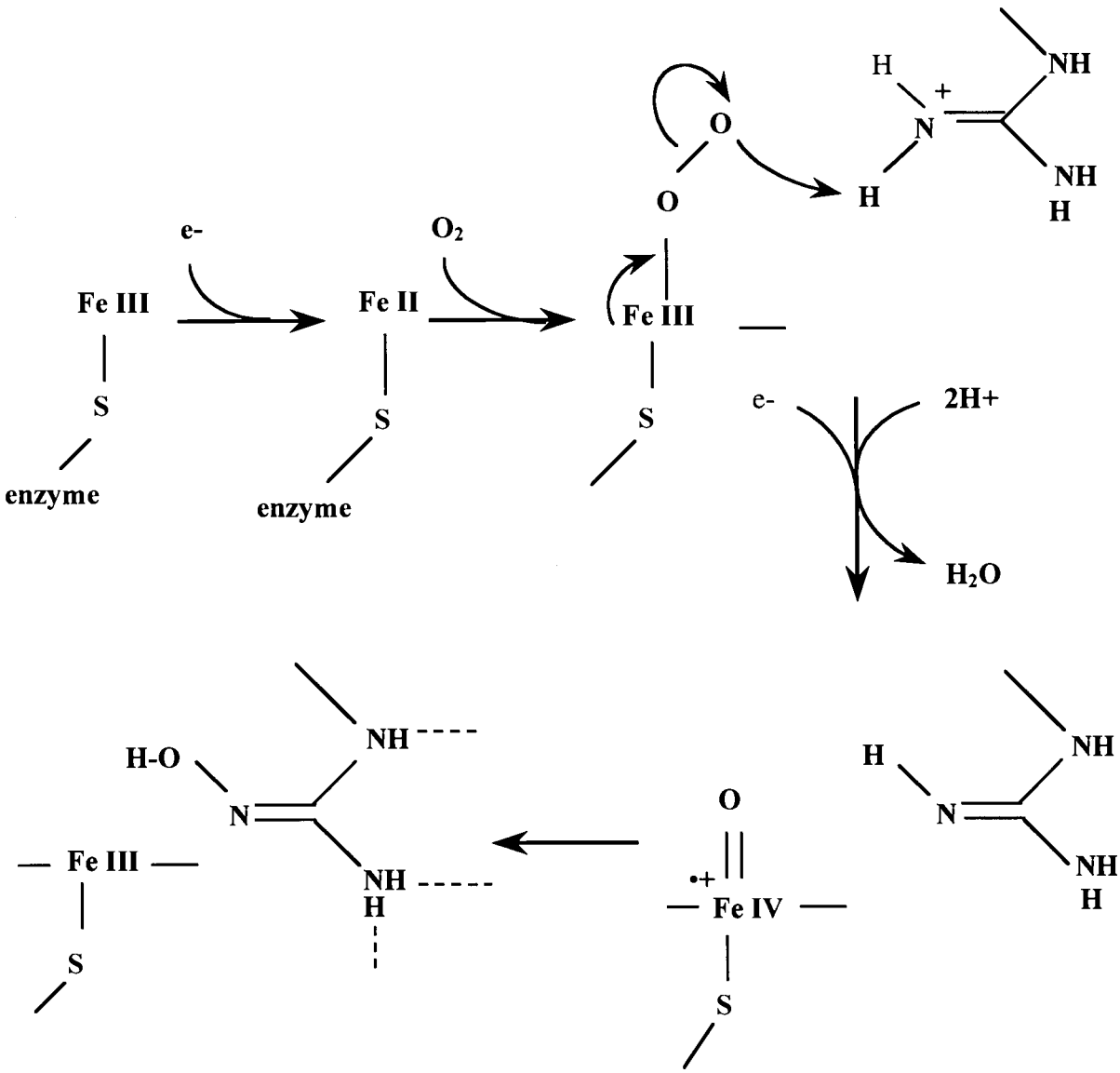

Figure 1.3 Possible mechanism for the NOS-catalyzed conversion of L-arginine to NHA. The reaction, based on P450 chemistry, begins with reduction of the heme iron from the ferric to ferrous form. This enables O_2 to bind and form a ferric super-oxo complex, which abstracts a proton from guanidinium nitrogen of L-arginine. Oxygen-oxygen bond scission accompanies this step and a high valent electrophilic oxo-iron intermediate is formed which hydroxylates the guanidinum nitrogen forming NHA.

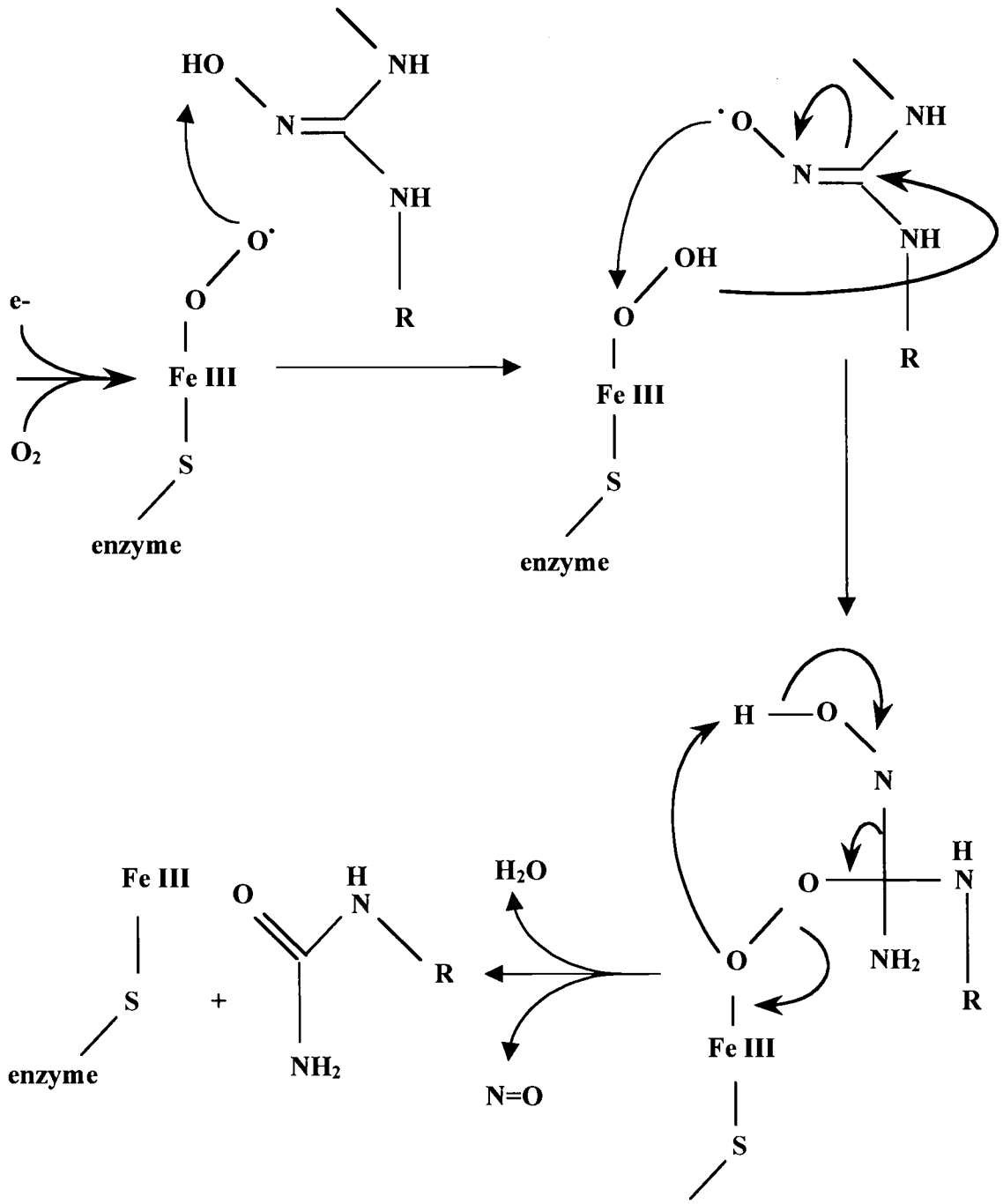

Figure 1.4 Possible mechanism for NOS-catalyzed oxidation of NHA to L-citrulline and NO. As with the first-step, the ferric heme is converted to the ferrous form and O_2 binds forming a ferric super-oxo intermediate. Hydrogen-atom abstraction from NHA generates the ferric hydroperoxo intermediate and an NHA radical. Nucleophilic addition of peroxide to the guanidino carbon produces a tetrahedral intermediate which decomposes to L-citrulline, NO and H_2O.

conversion of NHA to L-citrulline and NO is a three-electron oxidation. Therefore, there is general agreement that the second step is a peroxide-mediated reaction. Mechanistic information on NHA oxidation, derived from peroxide shunt reactions, in which H_2O_2 is substituted or NADPH and O_2 also supports the peroxide-mediated reaction (116). The hydrophobic environment of the distal pocket of the NOS heme favors a peroxide-mediated reaction, and the neutralization of the guanidinium group in NHA may discriminate between the formation of the oxo- and peroxo-iron species in the two steps of NO synthesis (47).

1.2.3 Role of tetrahydrobiopterin

Pteridines are widespread cofactors in mammalian cells that generally function as co-substrates or allosteric regulator molecules. H_4B exerts multiple allosteric effects on NOS including changing the conformation around the heme substrate binding pocket, lowering the Kd for the substrate L-arginine (117), and preventing the binding of bulky ligands such as DTT (118) or nitrosoalkanes (39) to the heme. The addition of H_4B also causes a shift in the spin equilibrium of the heme iron to the high spin state (119-121) and stabilizes the Fe-S bond in ferrous-CO or NO complexes (122). H_4B also increases the reactivity of the ferrous-O_2 complex 70-fold. For nNOS and iNOS, H_4B was shown to stabilize axial ligand geometry of the heme iron, promote dimerization and attenuate feedback inhibition of NO (123).

In the aromatic amino hydroxylases (AAH), H_4B has a redox role during catalysis, as it reacts with O_2 to form a 4α-hydroperoxy complex. Reaction of this

peroxy intermediate with a non-heme iron atom in tyrosine hydroxylase generates the Fe(IV)=O species which is responsible for the amino acid hydroxylation. The reaction generates quinoid H_2B (124). Biochemical and structural evidence indicates that H_4B does not have a similar redox role in nNOS. An accessory pterin-4a-carbinloamine dehydratase was not able to augment the reaction of H_4B to quinoid-2B and 5-methyl-H_4B was unable to support NO synthesis while it was able to stimulate phenylalanine hydroxylase. Evidence also indicates that the NOS heme is the site of O_2 activation. However, this does not exclude H_4B from participating in alternate redox chemistry since the 5-methyl derivative, although having a different redox potential than H_4B, is still able to mediate the oxidation reduction reaction (125).

Several independent studies suggest that H_4B does carry out a specific redox role. Pterin derivatives, such as dihydrobiopterin and 4-amino analog of H_4B, bind to NOS and induce the above-mentioned allosteric effects, yet they are unable to sustain NO synthesis. An oxidation-resistant deaza analog of 6-methyltetrahydrobiopterin as well as the potent dihydrobiopterin reductase inhibitor 4-amino-tetrahydrobiopterin were able to inhibit NO synthesis indicating that recycling of the cofactor may be essential for NO synthesis. These results indicate that NOS needs H_4B in a particular oxidative state that has the potential for catalysis. Heme iron reduction can take place independently of the pterin ring oxidation-state.

Studies have suggested that H_4B is a stoichiometric reactant in the first oxygenation step of NO synthesis, in a role analogous to the role of H_4B in amino acid hydroxylases. Since catalytic amounts of H_4B are required for activity, the cofactor may remain tightly bound and be regenerated throughout the catalytic cycle through a

dihydrobiopterin reductase like activity intrinsic to the enzyme (126). The neuronal isoform has this capability as it can reduce quinonoid H_2B to H_4B (127). N^G-nitro-L-arginine, NNA, an inhibitor that blocks electron transfer to the heme, increases the qH_2B reduction rate, as does the binding of Ca^{2+}-CaM. These molecules may increase the number of reducing equivalents, possibly direct flavin transfer, for qH_2B reduction.

Inspection of the x-ray crystal structure does not provide any clues as to a catalytic role for H_4B since the cofactor lies perpendicular and distant from the active site and has minimal contact with the heme edge (41). In tyrosine hydroxylase the pyrimidine portion of the pterin ring is involved in a direct oxidation/reduction reaction but there is no direct protein interaction with the N-3 of the pterin and the cofactor is weakly associated with the enzyme. In contrast, H_4B has three orders greater affinity towards NOS than tyrosine hydroxylase, primarily through its numerous hydrogen bonding contacts with the enzyme, therefore, the cofactor may go through redox recycling on the enzyme rather than be released.

H_4B may play a critical role in the first oxygenation step by supplying an electron for reducing the ferric heme superoxide species $[Fe(III)\text{-}O_2\bullet]^{2+}$ to the ferric peroxo species $[Fe(III)\text{-}OOH]^{2+}$, thereby activating the molecular oxygen for P450-type mono-oxygenation at the heme active site (128). This is suggested by experiments showing that low H_4B concentrations (100 nM) diminish the formation of superoxide but not hydrogen peroxide. During catalysis oxygen binds to the ferrous-heme group forming the ferrous-heme dioxygen complex $[Fe(II)\text{-}O_2]^{2+}$, the most stable intermediate of the reaction cycle. This complex is isoelectronic with the ferric superoxide complex $[Fe(III)\text{-}O_2\bullet]^{2+}$. In the absence of H_4B and L-arginine, the ferric superoxide complex

may readily dissociate to generate superoxide and the ferric heme $[Fe(III)]^{3+}$. H_4B may enhance the rate of reduction of the $[Fe(III)\text{-}O_2\bullet]^{2+}$ complex to generate the peroxyl iron complex $[Fe(III)\text{-}OOH]^{2+}$. The breakdown of this product would lead to the formation of hydrogen peroxide, which has been detected as the product of uncoupled oxygen reduction under limited H_4B. H_4B may mediate this activity by either favoring flavin-dependent reduction of the $[Fe(III)\text{-}O_2\bullet]^{2+}$ species or by direct hydrogen atom donation or electron transfer to the heme. Therefore, it is likely that H_4B does not inhibit the generation of superoxide by controlling electron transfer through the enzyme. Since only one electron is required for this transition to the peroxo species if H_4B is the electron donor, the trihydrobiopterin radical (H_3B) would be the oxidized pterin product formed during catalysis. Freeze quench EPR demonstrated that some H_4B can convert to an H_3B radical during the reaction of ferrous nNOS oxygenase domain with O_2 (129). H_4B may be regenerated by reduction of H_3B radical through electron donation from a downstream intermediate, possibly the heme-complexed tetrahedral intermediate.

H_4B may also participate in the second step of catalysis by donating an electron to the ferrous dioxy-species. It was originally suggested that NHA was the electron-donor candidate to the ferrous-dioxy complex; however, experiments have not demonstrated this (129-132). Electron transfer could be facilitated through the heme propionate (42, 113).

1.3 Properties, Cellular Distribution and Expressional Control of NOS Isoforms

1.3.1 Neuronal NOS

NOS activity is found in a wide variety of cells and tissues such as liver, brain, heart, artery, vein, adrenal, lung and spleen. Cells such as macrophages, endothelial cells, platelet, astrocytes, hepatocytes, mast cells, adreno-carcinoma cells, neuroblastma, mesangial, microglial and epithelial cells also contain NOS activity. The neuronal isoform is concentrated in a variety of neuronal structures in the brain, most notably the pyramidal cells of the hippocampus (13, 133, 134). The isoform is also in the epithelium of the respiratory track and skeletal muscle, where it is concentrated in fast fibers (135-139).

The human gene for nNOS is the largest of the three isoforms, spanning 150kb (140). The mRNA is encoded over 29 exons and the gene is located on human chromosome 12. There is a high conservation of protein sequence (93%) between the nNOS isolated from the rat and human brain. A human variant form of nNOS, nNOSμ arises from the splicing of an additional exon between exons 16 and 17 of the human nNOS gene, which causes an in-frame insertion of 34 amino acids (141, 142). The alternatively spliced form is expressed in various tissues, including striated muscle.

The neuronal isoform contains an additional 220 amino acids. The PDZ motif, which is a repeat of GLGF residues that spans 100 amino acids, is located in this sequence (143). This motif is found in diverse group of cytoskeletal proteins and enzymes. The PDZ motif facilitates interaction between nNOS and α1-syntrophin, a binding partner of dystrophin (144). This interaction localizes nNOS to the membrane

in this tissue, since the scarcolemma of skeletal muscle contains a family of intracellular and transmembrane glycoproteins associated with dystrophin (144). The nNOS PDZ motif also interacts with similar motif in post-synaptic density-95 protein (PSD-95) and PSD 93. This interaction concentrates nNOS at synaptic junctions in brain and motor endplates in skeletal muscle (145). Peptides binding with high affinity to the nNOS PDZ domain selectively uncouple NOS activity from the N-methly-D-aspartate (NMDA) receptor stimulation, suggesting that the interaction with post-synaptic proteins targets nNOS to the NMDA receptors, creating a link between post-synaptic glutamate binding and NO synthesis.

The two-hybrid screen led to the identification of a 10 KDa protein, which interacts with nNOS and inhibits activity by destabilizing the NOS dimer (146). The protein, named PIN for protein inhibitor of nNOS, binds in a 1:2 stoichiometry to a 17 amino acid insert in nNOS, which is absent in eNOS and iNOS (147). The expression levels of PIN and nNOS are nearly parallel in different brain regions, suggesting that PIN may function *in vivo* by regulating nNOS activity. However, results of Hemmens *et al.* showed that a 290-fold molar excess of PIN over nNOS was required for nNOS inhibition, and at this concentration PIN formed higher order aggregates (148).

1.3.2 Inducible NOS

Although iNOS was first isolated from murine macrophages (22, 149), it is also localized in heart muscle, astroglia, liver and smooth muscle cells (150). Unlike nNOS or eNOS, iNOS is regulated mainly at the transcriptional level. The transcription of the iNOS gene is induced by the presence of cytokines such as interferon gamma, tumor

necrosis factor alpha, interleukin and interleukin 2 or lippopolysaccahrides. The signaling cascades leading to iNOS production is cell-type specific, but appears to involve the activation of tyrosine kinases and NF-Kβ (151, 152).

The overproduction of NO in response to infection can cause symptoms of septic shock, such as extreme hypotension or cardiovascular disease. To prevent such occurrences, macrophage cells may institute a negative feedback loop involving p53. Accumulation of NO increases the cellular concentration of p53, which in turn down regulates iNOS expression through inhibition of the iNOS promoter (153). iNOS activity can also be affected by NAP110 (NOS-associated protein), which is expressed in murine macrophages. NAP110 inhibits the catalytic activity of the enzyme by directly interacting with the amino terminus of iNOS and preventing the formation of homodimers. Inhibition of iNOS is a possible means by which macrophage protect themselves from cytotoxic levels of NO (154).

1.3.2 Endothelial NOS

The endothelial isoform was first identified in endothelial cells (155), but immunohistochemical studies have located the enzyme in cytotrophoblasts of human placenta, kidney tubular epithelial cells, interstitial cells of the colon, and neural cells (156-159). The NO which regulates blood pressure and platelet function, originates mainly but not exclusively, from endothelial cells. The disruption of eNOS in mice or the administration inhibitors specific for eNOS significantly increases the blood pressure (160).

This isoform is myristolated and palmitolated at the N-terminus. Acylation targets eNOS to the plasmalemmal caveolae in endothelial cells and cardiac myocytes (161). The plasmalemmal caveolae are small invaginations in the plasma membrane composed of the structural transmembrane protein caveolin (162). They serve as signal transducing microdomains as they sequester signaling molecules such as receptors, G-proteins, and protein kinases (163). eNOS interacts with caveolin-1 in endothelial cells, and in cardiac myocytes eNOS associates with the muscle specific caveolin-3 (164, 165). The association with caveolin-1 or caveolin-3 suppresses eNOS enzyme activity in a manner that is reversed by Ca^{2+}-CaM (166-169).

1.4 Physiology of NO

1.4.1 Chemistry of NO

The biological effects of NO are determined by its ability to freely diffuse through plasma membranes and its chemical reactivity. NO is among the more stable of the biologically relevant free radicals, having a lifetime of several seconds in oxygenated water and much longer life span in anaerobic conditions (170). NO has to capability to diffuse unimpeded across cell membranes, because it is a small amphipathic molecule with relatively long half life (171).

The various fates of NO include the following: (1) NO may be oxidized to nitrite and nitrate, which are ultimately eliminated from the body as waste products (172) or (2) NO may diffuse into red blood cells and be consumed by reaction with hemoglobin. NO, unlike O_2 or CO can bind to Fe(III)–porphyrins; the Fe(III)-NO can undergo a

charge transfer complex reaction to form Fe(II)-NO^+ (173). (3) Non-heme metal complexes, such as iron sulfur centers are also targets for NO. (4) NO also forms reversible S-nitrosyl complexes with thiols of cysteine residues of a number of proteins (e.g. hemoglobin and glutathione) which extends its lifetime, as the free radical cycles between the free and nitrosothiol states (172, 174).

The reactivity and toxicity of NO is enormously increased by its near diffusion-limited reaction with superoxide to form the peroxynitrite anion ($ONOO^-$). Both NO and superoxide are paramagnetic species that react by a diffusion-limited reaction (6.7 X 10^9 M^{-1} s^{-1}; 175); therefore, NO successfully competes with superoxide dismutase for superoxide. Peroxynitrite can take part in a number of chemical reactions that involve the modification of lipids, carbohydrates, nucleic acids, and proteins. For example, peroxynitrite may directly initiate lipid peroxidation by abstraction of an allylic hydrogen from polyunsaturated fatty acids (176). The oxidation of liposomes by $ONOO^-$ results in the formation of dienes, aldehydes and increased consumption of oxygen, which contributes to the atherogenic processes. The pK_a of the peroxynitrite oxoanion is 6.87, so that protonation at physiological pH yields peroxynitrous acid, ($ONOOH^-$). This species decomposes to form a hydroxyl radical (•OH) and nitrogen dioxide (NO_2•), both of which are potent oxidants. The hydroxyl radical is capable of initiating lipid oxidation, oxidizing cysteine and methionine residues, deaminating nucleic acids and nitrating aromatic compounds (177, 178).

Several studies indicate that the formation of $ONOO^-$ has the potential to disrupt signal transduction events in the cell through modification of cysteine or tyrosine residues on proteins involved in a signal cascades. The $ONOO^-$ anion reacts with

reduced glutathione (GSH) and CO_2 leading to GSH oxidation and the formation of nitrosoperoxycarbonate ($ONO_2CO_2^-$), which is a potent nitrating agent of tyrosine (179). The reaction between peroxynitrite and SOD forms a powerful nitrating agent, NO^{2+}, which also modifies tyrosine residues to form nitrotyrosine.

The autooxidation of NO forms the nitrosating agent nitrous anhydride (N_2O_3) which directly damages DNA by deaminating cytosine and guanine in deoxynucleosides, forming uracil and xanthine, respectively (180). DNA damage may be central to neurotoxicity elicited by NO and other free radicals, because such types of DNA damage activates poly (ADP-ribose) synthase (PARS), a nuclear enzyme which ADP-ribosylates nuclear proteins such as histones and PARS itself (181). This activity depletes energy storage through the reduction of NAD and ATP pools, eventually leading to cell death.

1.4.2 Pathological effects of NO

Pathologies linked to excessive NO production include immune type diabetes, inflammatory bowel disease, rheumatoid arthritis, carcinogenesis, septic shock, multiple sclerosis, transplant rejection, and stroke (182). Whereas pathologies linked to insufficient NO production include hypertension, impotence, arteriosclerosis and susceptibility to infection (170, 183, 184). A consensus is emerging that the toxic or trophic properties of NO depend on the steady state concentration and the site of generation. Typically, NO is present at high concentrations in macrophages where it participates in host defense against tumor cells and pathogens. In contrast, in neuronal and endothelial cells NO is present at lower concentrations where it acts as a signaling

molecule in processes such as vasodilatation and neurotransmission. The uncontrolled generation of NO in a particular cell type will can lead to a variety of pathological disorders. For example, the over-production of NO by nNOS and iNOS is directly linked to the pathogenesis of stroke and shock (185, 186), respectively. The global inhibition of the NOS would result in complications since the NO generated by eNOS has been shown to be antiatherogenic and critical for angiogenesis. Therefore isoform-specific drugs are required to inhibit NO production by nNOS and iNOS under pathological conditions, without hindering NO generation by eNOS.

Fortunately several NOS inhibitors have proven to have differential effects on NOS activity. Roman *et al.* investigated the inhibitory effects on N-amino-, N-methyl, and N-nitro-L-arginine analogs on the various isoforms of NOS. The rank order potency for inhibition of iNOS NO biosynthesis was found to be N-amino ≥ N-methyl >> N-nitro. In contrast the rank order potency was N-nitro>> N-amino ≥ N-methyl for eNOS and nNOS (187, 188). S-methyl-L-thiocitrulline (Me-TC) and S-ethyl-L-thiocitrulline (Et-TC) were found to be more potent inhibitors of nNOS compared to eNOS. (189).

1.4.3 NO as an endothelial relaxation factor

The discovery of NO as important signaling molecule in mammals was achieved through the quest to identify an endothelium-derived relaxation factor (EDRF). EDRF was found to be unstable, transient species, which caused smooth muscle relaxation by raising intracellular cGMP concentrations via activation of guanylyl cyclase. Hemoglobin, methylene blue, and superoxide were found to inactivate EDRF activity.

Furchgott and Ignarro provided evidence, through NO-donating compounds, such as sodium nitroprusside and nitroglycerin, that NO was the primary endogenous vasodilator (190, 191). Later it was found that the enzymatic production of NO required L-arginine as a substrate, and that L-arginine analogs served as potent vasoconstrictors.

The NO, which functions as an EDRF, originates mainly, but not exclusively from endothelial cells and eNOS. The tonic production of endothelial-derived NO is crucial for maintenance of normal blood pressure and platelet function; therefore, regulation of eNOS is relevant to hypertension, atherosclerosis, and heart disease. The agonists, acetlycholine and bradykinin activate eNOS activity by increasing intracellular levels of Ca^{2+}, which leads to the binding of Ca^{2+}-CaM (192). eNOS activity is also upregulated by hemodynamic shear stress which causes local Ca^{2+} increase near the plasma membrane (193)

Vasorelaxation and platelet inhibition occurs by NO binding to the heme of soluble guanylyl cyclase, which activates the enzymes production of cGMP several hundred-fold (194, 195). The raise in intracellular level of cGMP leads to vasodilatation through the cGMP-dependent modification of several intracellular processes including activation of potassium channels through cGMP-dependent kinases. Nitric oxide also acts as an EDRF by inhibiting receptor agonist (e.g. ADP)-evoked Ca^{2+} mobilization from intracellular stores. These effects are mediated by cGMP-dependent protein kinase and involve inhibition of phospholipase C, inositol triphosphate receptor and perhaps intracellular Ca^{2+} release channels. Evidence also suggests that NO directly activates Ca^{2+}-dependent K^+ channels in rabbit aortic smooth muscle cells, possibly through

nitrosylation of sulfhydryl groups. Inhibition of platelet aggregation occurs by the cGMP-dependent extrusion of intracellular Ca^{2+} from the platelet.

The NO generated in skeletal muscle is involved contraction and relaxation of muscle cells possibly through the cGMP pathway or through interactions with reactive oxygen species (ROS) (139). The latter mechanism involves reactive oxidants modulating Ca^{2+} flux at the sarcoplasmic reticulum by redox-sensitive thiol targets on Ca^{2+} release channels and the Ca^{2+} dependent ATPase. In the actively contracting state, increased production of ROS will probably divert NO away from metal centers towards sulfydryl targets through formation of nitrosothiols. The resultant S-nitrosylation and thiol oxidation reaction would promote Ca^{2+} release and force production.

1.4.4 Role of NO in the immune system

NO constitutes a primary mechanism of defense against tumor cells and intracellular and extracellular microorganisms. At high concentrations, NO functions as a bacteriocidal or antitumorgenic agent by inhibiting mitochondrial respiration. The pioneering work of Hibbs demonstrated that tumor cells exposed to activated macrophages had impaired mitochondrial respiration due to inhibition of complexes I and II of the mitochondrial electron transport chain (196). NO was also discovered to complex with iron-sulfur groups within key enzymes necessary for DNA replication such as ribonucleotide reductase and mitochondrial energy production, *cis*-aconitase (197-199). Along with NO, activated macrophages also produce significant amounts of superoxide. The macrophage-generated NO and O_2^- can react to form peroxynitrite (ONOO-), which participates in a number of reactions leading to cell apoptosis.

1.4.5. NO in the nervous system.

NO was implicated as a key signaling molecule in the CNS when rat cerebral cells stimulated with N-methyl-D-aspartate (NMDA), a agonist for the glutamate receptor were found to release the EDRF (200, 201). Histochemical staining lead to the identification of nNOS in the rat forebrain tissue and established the existence of an L-arginine-NO pathway in the CNS. In post-synaptic terminals, binding of glutamate to NMDA-type receptors lead to Ca^{2+} influx and the activation of nNOS. The increase in NO stimulates guanylyl cyclase to produce cGMP (202, 203).

Because NO has the ability to diffuse freely from the point of synthesis to intracellular target sites in neighboring cells, it differs from the more conventional neurotransmitters in being independent of vesicular release, membrane receptors or lipid cell boundaries (1). Therefore, it was postulated to function as a retrograde messenger contributing to the formation of memory and development, e.g. long term potentiation (LTP; 204, 205). The formation of LTP is proposed to occur by the following sequence of events: (1) Glutamate, released from the presynaptic cell, activates the NMDA receptor in the postsynaptic cell. (2) Activation of the receptor causes a Ca^{2+} influx via the Ca^{2+} channel associated with the NMDA receptor or via voltage-gated Ca^{2+} channels. (3) The increase in Ca^{2+} activates NO synthase. (4) NO then diffuses randomly through the cytosol and membranes and is absorbed by the heme group of guanyly cyclase in the presynaptic cells. (5) The production of cGMP then evokes an increase in the release of transmitter and synaptic transmission.

Several biochemical and mutagenic studies support the involvement of NO in LTP. Through the use of NO donors and NOS inhibitors, Shibuki and Okado initially

demonstrated that endogenous NO was important for the development of long term depression in the cerebellum (206). Histochemical staining showed NOS post-synaptically vesicles of dendrites and NO-sensitive guanylyl cyclase has been found pre-synaptically in the hippocampus. NO was also shown to increase the release of neurotransmitter in the hippocampus and the basal ganglion (207). Postsynaptic but not presynaptic injection of NOS inhibitors block LTP indicating NO is produced in the presynaptic neuron (208). Knock-out mice that are doubly mutant in eNOS and nNOS also have reduced LTP in stratum radiatum of CA1 of the hippocampus (209).

The excessive release of excitatory amino acids, such as glutamate is associated with convulsions and neurotoxicity in addition to contributing to pathogenic mechanisms in Alzheimer's disease and amyotrophic lateral sclerosis (210). The link between excitation of the NMDA receptor and the activation of nNOS implicates the involvement of NO in these disease states. Furthermore, NMDA toxicity acting via NO may account for neural damage associated with AIDS dementia as well as neural damage in cerebral infarction. Interestingly, Ca^{2+}-dependent neurotoxicity is triggered most efficiently when Ca^{2+} influx occurs through NMDA receptors and can not be reproduced by loading neurons with equivalent quantities of Ca^{2+} through non-NMDA receptors or voltage sensitive channels (211)

NO has been shown to have neuroprotective role in CNS if the molecule changes redox state. Sodium nitroprusside (SNP), which has NO^{+} character, significantly protected rat cortical neurons against NMDA-induced neurotoxicity. The nitrosium ion was able to modify the thiolate anions on the NMDA redox sites (212). This lead to

down regulation of the receptor such that it would no longer be over stimulated by the excessive release of excitatory amino acids (174).

In the peripheral nervous system, NO functions as a nonadrenergic-noncholinergic (NANC) neurotransmitter mediating actions of autonomic motor neurons on vascular and nonvascular smooth muscle (213). Neurons that are NANC innervate a variety of smooth muscle tissues such as the gastrointestinal track, corpus caveronsum and the esophagus. NO is responsible for NANC mediated events such relaxation and dilation of the stomach (214), development of penile erections in humans (215), and regulation of bronchial smooth muscle tone (216). These NANC-mediated events appear to utilize the NO-cGMP pathway.

Due to the large number of protective and destructive effects of NO in a diverse array of physiological events, a major challenge for the medical and pharmaceutical communities will be to specifically target one site of NO-production, presumably with drugs that aim to modifying one of the isoforms. Fortunately, the NOS isoforms exhibit varying affinities for various L-arginine analogs that have proven useful for inhibiting a specific isoform. Another target for controlling NO-synthesis is the NOS reductase domain. The three isoforms display different means for controlling the rate of electron transfer, (i.e. Ca^{2+} concentration, heme-redox potentials) and have varying rates of NO synthesis which is controlled by the intrinsic rate of the flavin-mediated electron transfer. By understanding the involvement of structural features present in the NOS reductase domain, (i.e. autoinhibitory domains, residues close to the flavins and NADPH, CaM-binding residues) which control electron-transfer it may ultimately be

possible to not only decrease, but also stimulate the rate of NO-synthesis at a specific locus.

This thesis aims at gaining an understanding of the stimulatory effects Ca^{2+}-CaM on the mechanism of electron transfer in the reductase domain of nNOS by measuring the reduction of DCIP and cytochrome c^{3+} in the presence and absence of the activated cofactor. These two electron acceptors were chosen since DCIP is reduced by a two-electron transfer from reduced FAD and is stimulated only 2- to 3-fold by Ca^{2+}-CaM. In contrast, cytochrome c^{3+} is reduced by donation of one electron from FMN and the binding of Ca^{2+}-CaM causes a 10- to 20-fold increase in activity. Kinetic mechanisms were proposed for the reduction of these two-substrates based on initial velocity and product and dead-end inhibition studies in Chapter 2. The pH-dependence of the rate of electron transfer and binding of substrates was investigated to determine if Ca^{2+}-CaM influences any ionizable groups involved in these steps (Chapter 3). Finally, data from primary substrate (NADP(D)) and solvent isotope effects of the various kinetic parameters were used in conjunction with the proposed kinetic mechanism to determine the location of rate-determining step(s) (Chapter 4).

Chapter 2

The Reaction of Neuronal Nitric-oxide Synthase with 2,6-Dichloroindolphenol and Cytochrome c^{3+}: Influence of Electron Acceptor and Binding of Ca^{2+}-Activated Calmodulin on the Kinetic Mechanism

Kirsten R. Wolthers and Michael I. Schimerlik

Published in *Biochemistry*

American Chemical Society,

2001, 40, 4722-4737

2.1 Summary

Binding of Ca^{2+}-activated calmodulin (Ca^{2+}-CaM) to neuronal nitric-oxide synthase (nNOS) increases the rate of 2,6-dichloroindolphenol (DCIP) reduction 2- to 3-fold and that of cytochrome c^{3+} 10- to 20-fold. Parallel initial velocity patterns indicated that both substrates were reduced *via* two-half reactions in a ping-pong mechanism. Product and dead-end inhibition data with DCIP were consistent with an iso ping-pong bi-bi mechanism; however, product and dead-end inhibition studies with cytochrome c^{3+} were consistent with the (two-site) ping-pong mechanism previously described for the NADPH-cytochrome P450 reductase-catalyzed reduction of cytochrome c^{3+} [Sem and Kasper (1994) *Biochemistry* 33, 12012-12021]. Dead-end inhibition by 2'-adenosine monophosphate (2'-AMP) was competitive *versus* NADPH for both electron acceptors, although the value of the slope inhibition constant, K_{is}, was to 25 to 30 fold greater for DCIP as the substrate than for cytochrome c^{3+}. The difference in the apparent affinity of 2'-AMP is proposed to result from a rapidly equilibrating isomerization step that occurs in both mechanisms prior to the binding of NADPH. Thus, initial velocity, product, and dead-end inhibition data were consistent with a di-iso ping-pong bi-bi and an iso (two-site) ping-pong mechanism for the reduction of DCIP and cytochrome c^{3+}, respectively. The presence Ca^{2+}-CaM did not alter the proposed kinetic mechanisms. The activated cofactor had a negligible effect on $(k_{cat}/K_m)_{NADPH}$, while it increased $(k_{cat}/K_m)_{DCIP}$ and $(k_{cat}/K_m)_{cytc}$ 4.5- and 23-fold, respectively.

2.2 Introduction

Nitric oxide (NO) is a ubiquitous molecule involved in a diverse array of physiological and pathological roles (2, 201, 217-219). NO is synthesized in mammals by the NO-synthases, a family of three homodimeric enzymes. Each of the isoforms consumes 1.5 equivalents of NADPH and two equivalents of O_2 in the five-electron oxidation of L-arginine to produce NO and L-citrulline (3, 4). The enzymes can be classified into two distinct groups according to regulation of transcriptional expression and dependence on intracellular Ca^{2+} concentrations. The constitutively expressed neuronal (nNOS)[1] and endothelial (eNOS) isoforms require an increase in Ca^{2+} levels to promote the subsequent binding of Ca^{2+}-activated calmodulin (Ca^{2+}-CaM) for NO synthesis (133). The inducible isoform (iNOS) is transcriptionally regulated by the action of cytokines and its NO synthesis activity is independent of Ca^{2+} concentration since CaM is tightly bound to this isoform even at basal cellular levels of the divalent cation (220).

The CaM-binding domain, located at the center of the NOS polypeptide subunit, tethers the N-terminal oxygenase domain to the C-terminal reductase domain (19, 30, 220). The reductase domain is structurally similar to NADPH-cytochrome P450 oxidoreductase (CPR) since each polypeptide contains one equivalent each of FAD and FMN and the binding site for NADPH (15, 149). The oxygenase domain is structurally unique and contains a P450-type heme, the binding site for the cofactor (*6R*)–5,6,7,8-tetrahydro-L-biopterin (H_4B), and the substrate L-arginine (11, 14, 47, 221). For the constitutive isoforms, the binding of Ca^{2+}-CaM is essential for NO synthesis, because it

triggers the electron transfer between the flavins in the reductase domain and the heme in the oxygenase domain (18, 76).

Evidence from several laboratories indicates that the NOS reductase domain and CPR share the same mechanism of electron transfer to the heme. The FAD and FMN redox centers of both enzymes shuttle two electrons from the oxidation of NADPH to a one-electron heme acceptor (15). In the absence of NADPH, both CPR and NOS maintain an air-stable one-electron reduced state (FAD-FMNH•; 71, 222), which is unable to reduce the heme (72, 223). The donation of two electrons through the oxidation of NADPH reduces either enzyme to the three-electron reduced state. The flavins then subsequently reduce the P-450 heme in two one-electron transfers returning the enzyme to the one-electron reduced state (224, 225). Therefore, during turnover it is proposed that NOS, like CPR, cycles between the one-electron and three-electron reduced states (74). Furthermore, analysis of the flavin midpoint potentials and the removal of the FMN cofactor suggests that the path of electron transfer in both enzymes is from NADPH to FAD to FMN to the heme (73, 79, 81, 222, 226).

NOS and CPR are also able to reduce 2,6-dichloroindolphenol (DCIP), ferricyanide (FeCN), and cytochrome c^{3+} with electrons derived from NADPH oxidation (31, 75). However, nNOS is unique in that the binding of Ca^{2+}-CaM to the enzyme stimulates a 2- to 3-fold increase in DCIP and FeCN reduction and a 10 to 20-fold increase in cytochrome c^{3+} reduction (30, 76). The Ca^{2+}-CaM induced stimulation of these activities is independent of electron transfer from the flavins to the heme since the same level of stimulation of ferricyanide and cytochrome c^{3+} reduction occurs with nNOS devoid of its oxygenase domain (74, 76, 77). Stopped-flow studies have indicated

that the binding of Ca^{2+}-CaM increases the pre-steady state rate of electron transfer from NADPH to the flavins (76, 78). The binding of Ca^{2+}-CaM has a negligible affect on the flavin redox potentials indicating that the thermodynamic driving force of electron transfer remains unchanged (73). However, the increase in electron transfer may be facilitated by the ability of Ca^{2+}-CaM to induce a conformational change in the enzyme (30, 74).

The reductase domain of NOS also has additional amino acid sequences that are not found in CPR. nNOS and eNOS, which have slower rates of electron transfer to the heme, DCIP, and cytochrome c^{3+}, contain an additional 40-50 amino acid insert located in the FMN-binding subdomain. This insert is thought to be an autoinhibitory domain since it was shown to promote the dissociation of CaM from nNOS at low intracellular Ca^{2+} concentrations and to inhibit electron transfer in the absence of Ca^{2+}-CaM (79, 80, 82). Both iNOS and the constitutive isoforms possess an additional 21-42 amino acid-tail at the C-terminus, which is not present in CPR. This sequence is proposed to modulate electron transfer between the flavin moieties or between FMN and cytochrome c^{3+} (83).

Considering the additional structural and dynamic features in NOS that are absent in CPR, there is interest in how Ca^{2+}-CaM imparts control of electron transfer. Although several pre-steady state kinetic and mutational analyses have been performed to investigate the effects of Ca^{2+}-CaM on interflavin electron transfer, the influence of the cofactor on the kinetic mechanism of electron transfer within the reductase domain of the enzyme remains to be elucidated. Establishing a mechanism is important for studying the overall rate of NO production since the control point of electron transfer

resides within the reductase domain of the enzyme. This is suggested by the different rates of NO-synthesis exhibited by the three isoforms as determined by the rate of electron transfer between FAD and FMN or between FMN and the heme (38). The data presented below describes the steady-state kinetic mechanism of the NOS-catalyzed electron transfer to cytochrome c^{3+} and DCIP in the presence and absence of Ca^{2+}-CaM. We chose to investigate these two electron acceptors since DCIP is reduced by a two-electron transfer from reduced FAD and is stimulated only 2- to 3-fold by Ca^{2+}-CaM (81). In contrast, cytochrome c^{3+} is reduced by donation of one electron from FMN and the binding of Ca^{2+}-CaM causes a 10- to 20-fold increase in activity. Initial velocity and product inhibition data for the nNOS-catalyzed reduction of DCIP was consistent with an iso ping-pong bi-bi mechanism, with a steady-state isomerization step between the release of $NADP^+$ and the binding of DCIP. In contrast, initial velocity and product inhibition data for the reduction of cytochrome c^{3+} were best accommodated by a nonclassical (two-site) ping-pong mechanism. However, dead-end inhibition studies revealed a large difference in the K_{is} values of 2'-AMP in competitive inhibition patterns *versus* NADPH for DCIP compared to cytochrome c^{3+}. To rationalize the difference in the K_{is} value an additional rapidly equilibrating isomerization step between the enzyme form found immediately after the release of the last product (E_1') and the enzyme form competent to bind NADPH (E_1) was required in both mechanisms (E_1' binds to 2'-AMP, but not NADPH, while E_1 does not bind 2'-AMP). The rate equations describing DCIP and cytochrome c^{3+} reduction were derived for a di-iso ping-pong bi-bi and an iso (two-site) ping-pong mechanism, respectively. The presence of Ca^{2+}-CaM did not alter the observed steady-state kinetic mechanisms proposed for the reduction of DCIP and

cytochrome c^{3+}. Ca^{2+}-CaM did affect to varying degrees the kinetic parameters for the substrates NADPH, cytochrome c^{3+}, and DCIP.

2.3 Experimental Procedures

2.3.1 Materials

The cDNA for rat neuronal NOS was kindly provided by T.M. Dawson (Johns Hopkins University; 227), and the pCWori expression vector was a gift of F.W. Dalhquist (University of Oregon; 228). Tetrahydrobiopterin (H4B) was purchased from Cayman Chemical (Ann Arbor, MI), the 2', 5' ADP-Sepharose was purchased from Amersham Pharmacia Biotech (Piscataway, NJ), and the CaM-Sepharose and CaM were generous gifts of S. Anderson and D. Malencik (Oregon State University). All other reagents were from Sigma Chemical Co. (St Louis, MO).

2.3.2 Enzyme expression and purification

The enzyme was purified according to the protocol published by Gerber and Ortiz de Montellano with slight modification (229). nNOS was more than 85% pure as judged by SDS-polyacrylamide gel electrophoresis with a specific activity of 150 nmol NO min^{-1} mg^{-1} at 25 °C. The rate of NO production was measured by the hemoglobin-NO capture assay following the procedures of Stuehr *et al* (26). Protein concentration was determined with the Lowry Assay using BSA as a standard (230).

2.3.3 Measurement of reductase activities

Reactions were performed in 5 mL volume at 25 °C using either a 10 cm or 5 cm path length cuvette. The reaction rate was measured by reduction of cytochrome c^{3+} ($\Delta\varepsilon$ = 21.1 mM^{-1} cm^{-1}) at 550 nm or DCIP ($\Delta\varepsilon$ = 21 mM^{-1} cm^{-1}) at 600 nm (231). Reaction mixtures contained 50 mM Hepes-NaOH (pH 7.5), variable concentrations of substrates (NADPH, cytochrome c^{3+} or DCIP), and where appropriate, 10 μM $CaCl_2$, 100 nM CaM, and variable concentrations of inhibitor ($NADP^+$, 2'AMP, or cytochrome c^{2+}). Reactions were initiated in a total volume of 5 mL by the addition of 0.08-0.8 μg of nNOS.

2.3.4 Preparation of cytochrome c^{2+}

Cytochrome c^{2+} was prepared by reducing cytochrome c^{3+} with sodium dithionite. After 10 mins of incubation at room temperature, the sodium dithionite was removed by passing 1 mL of the solution over two, 2 mL columns of G-25 resin equilbrated in H_2O. The concentration of cytochrome c^{2+} was determined by measuring the absorbance at 550 nm before and after reduction with sodium dithionite using the extinction coefficients for reduced (ε = 29.5 mM^{-1} cm^{-1}) and oxidized (ε = 8.4 mM^{-1} cm^{-1}) cytochrome c (231).

2.3.5 Data analysis

Data were first analyzed graphically using primary plots of reciprocal velocities and reciprocal substrate concentrations. Slopes and intercepts obtained from the primary plots were then graphed as secondary plots against inhibitor concentrations. The form of

the over all rate equation was determined by examination of the results of the graphical analysis. Although the kinetic results are presented in double reciprocal plots, the computer analysis was performed by the nonlinear least-squares fit to the specific rate equation using the computer program Origin v. 4.0 (MicroCal Software Inc., North Hampton, MA). The data from initial velocity studies were fit to equation 2.1 for a ping-pong mechanism and to equation 2.2 for a sequential mechanism.

$$v_i = \frac{VAB}{K_B A + K_A B + AB} \tag{2.1}$$

$$v_i = \frac{VAB}{K_{iA} K_B + K_B A + K_A B + AB} \tag{2.2}$$

where v_i is the initial velocity, A and B are concentrations of NADPH and the electron acceptor (cytochrome c^{3+} or DCIP), respectively. V is the maximal velocity, K_A and K_B are corresponding Michaelis constants for A and B, respectively, and K_{iA} is the dissociation constant for NADPH. Data from inhibition studies were fit to equations for competitive (eq 2.3), uncompetitive (eq 2.4), and noncompetitive (eq 2.5) inhibition:

$$v_i = \frac{VA}{K_m(1 + I/K_{is}) + A} \tag{2.3}$$

$$v_i = \frac{VA}{K_m + A(1 + I/K_{ii})} \tag{2.4}$$

$$v_i = \frac{VA}{K_m(1 + I/K_{is}) + A(1 + I/K_{ii})} \tag{2.5}$$

where v_i is the initial velocity, V is the maximal velocity, A is the varied substrate, K_m is the apparent Michaelis constant, I the inhibitor concentration, K_{ii} the intercept inhibition constant, and K_{is} the slope inhibition constant. For all reactions, the non-varied substrate was present at a level close to its K_m.

2.4 Results

2.4.1 Initial velocity studies with DCIP as an electron acceptor

Initial velocity experiements demonstrated that substrate inhibition by NADPH for DCIP reduction occurred at concentrations of NADPH 2-fold above its K_m. Substrate inhibition by NADPH is also observed for the FAD-containing enzyme, nitrate reductase (232). Therefore, the concentration of NADPH with DCIP as an electron acceptor was varied between $K_m/5$ to K_m for the initial velocity experiments. A plot of $1/v_i$ *versus* 1/[DCIP] at varying fixed concentrations of NADPH showed a family of parallel lines in the absence of Ca^{2+}-CaM (Figure 2.1A) and in the presence Ca^{2+}-CaM (Figure 2.1B). Similarly, a plot of $1/v_i$ *versus* 1/[NADPH] at varying fixed concentrations of DCIP showed a family of parallel lines in the absence and presence of Ca^{2+}-CaM (Figures 2.1C and 2.1D, respectively). A parallel pattern is typical of ping-pong mechanisms in which an irreversible step such as release of a product or the addition of substrate at saturating levels separates the addition of either of the two substrates in the reaction sequence (233). A nonlinear least-squares fit of the initial velocity data yeilded a lower χ^2 value with the equation describing a ping-pong mechanism (eq 2.1) compared to that for a

Figure 2.1 Initial velocity patterns for the nNOS-catalyzed reaction involving the reduction of DCIP by NADPH. The symbols represent the experimentally determined mean of three values, while the lines are best nonlinear global fit to the data. (A) Varying concentrations of DCIP at NADPH concentrations of ■ 0.05, ● 0.08, ▲ 0.12, and ▼ 0.25 μM. (B) $CaCl_2$ at 10μM and CaM at 100 nM present with varying concentrations of DCIP at NADPH concentrations of ■ 0.059, ● 0.094 ▲ 0.142 and ▼ 0.213 μM. (C) Varying concentrations of NADPH at DCIP concentrations of ■ 3, ● 6, ▲ 12, and ▼ 25 μM. (D) $CaCl_2$ at 10 μM and CaM at 100 nM present with varying concentrations of NADPH at DCIP concentrations of ■ 6, ● 10, ▲ 20, and ▼ 35 μM.

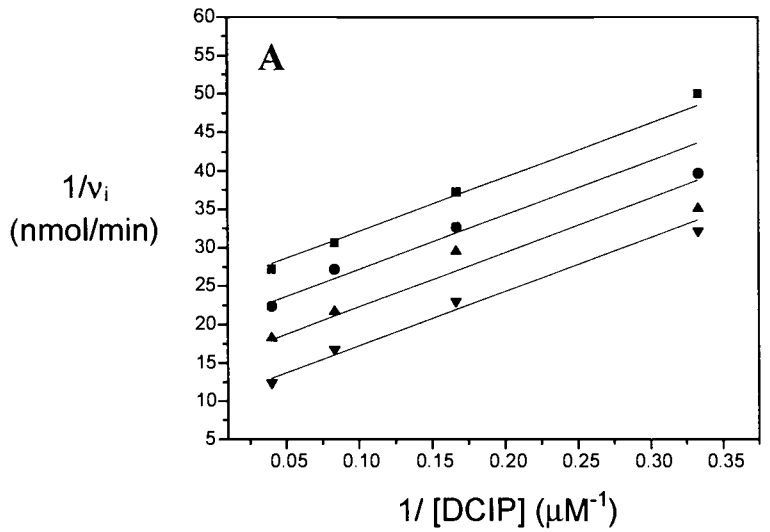
A
1/vi
(nmol/min)
60
55
50
45
40
35
30
25
20
15
10
5
0.05
0.10
0.15
0.20
0.25
0.30
0.35
1/ [DCIP] (μM-1)

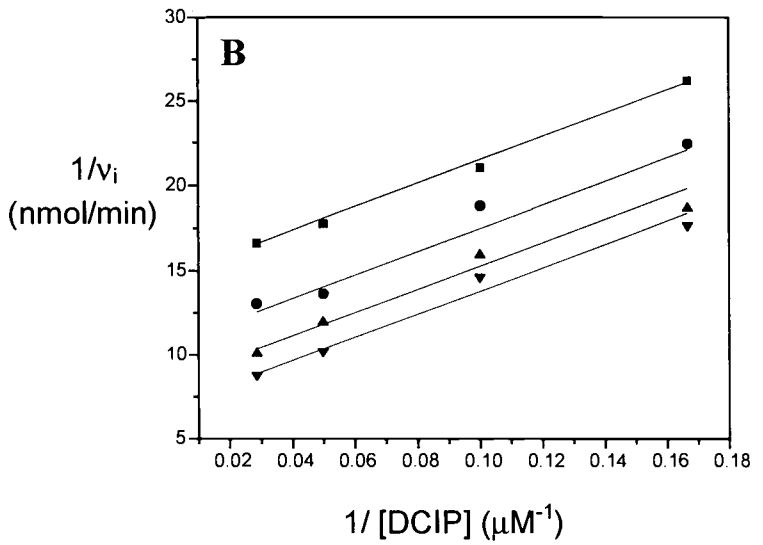
B
1/vi
(nmol/min)
30
25
20
15
10
5
0.02
0.04
0.06
0.08
0.10
0.12
0.14
0.16
0.18
1/ [DCIP] (μM-1)

Figure 2.1

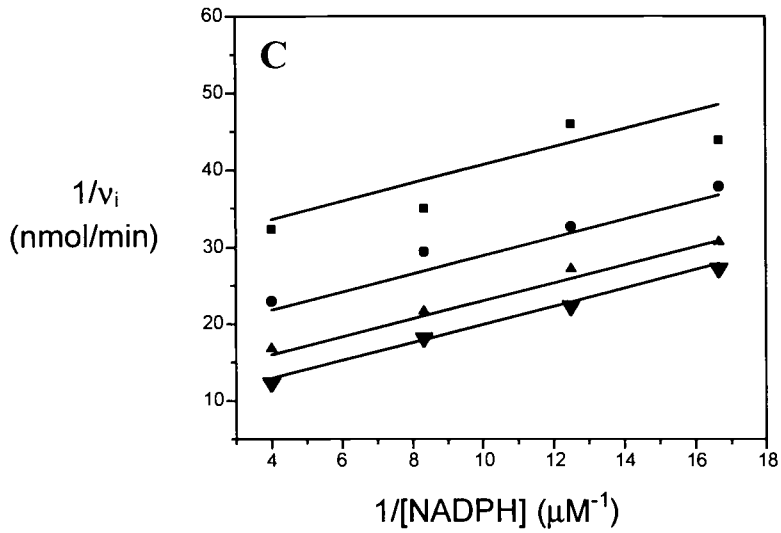

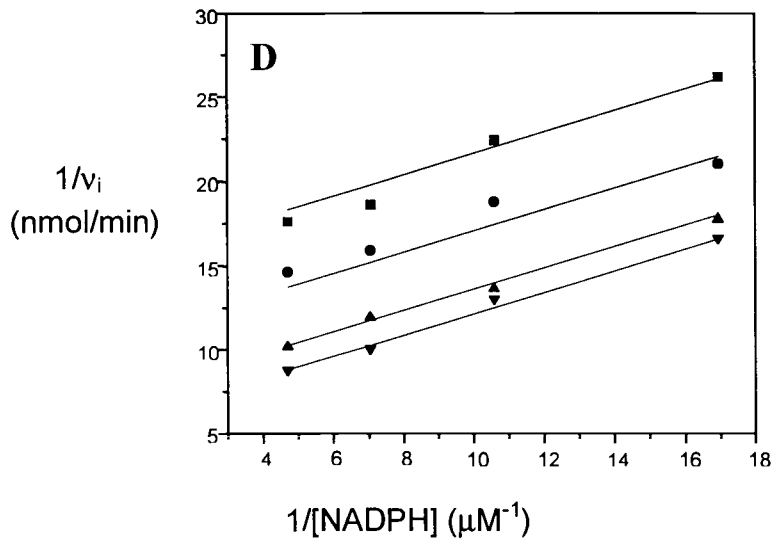

Figure 2.1 (Continued)

sequential mechanism (eq 2.2). The latter equation did not reduce the chi-squared value and gave an undefined value for K_{iA}.

Ping-pong mechanisms are characterized by the enzyme oscillating between two or more stable forms (234). As illustrated in Scheme 2.1, the air-stable one-electron reduced state of nNOS, E_1, is designated as one of these stable enzyme forms. The oxidation of one NADPH molecule generates the second stable enzyme form, the three-electron reduced state of nNOS, E_3. Since DCIP reduction is a two-electron process only one molecule is required to react with E_3 in the subsequent half-reaction to return the enzyme to E_1.

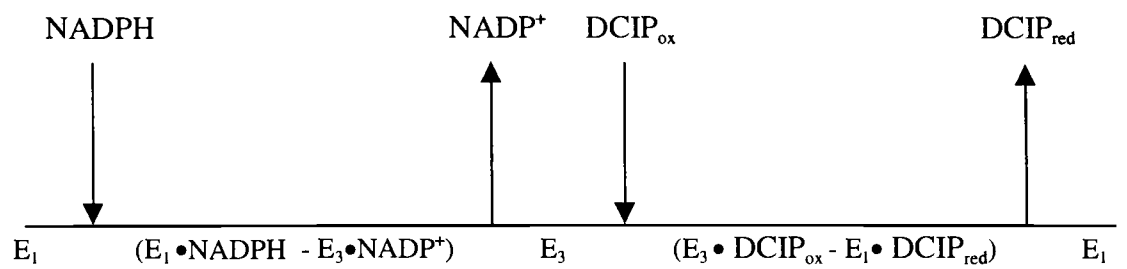

(Scheme 2.1)

If DCIP reduction were to follow this classical ping-pong mechanism, the substrates and products would bind to the enzyme in a tetra-uni fashion.

The presence of Ca^{2+}-CaM resulted in a 3-fold increase in k_{cat}, a 4.5-fold increase in $(k_{cat}/K_m)_{DCIP}$, and a 1.5-fold increase in $(k_{cat}/K_m)_{NADPH}$ (Table 2.1). The experimentally determined Michaelis constants for NADPH (22, 235) and DCIP and the turnover number (k_{cat}) for DCIP reduction with and without Ca^{2+}-CaM agree with previously reported values, which have been reported to be 300 min^{-1} - 460 min^{-1} (31).

Table 2.1 Values for the steady-state kinetic parameters of nNOS-catalyzed reduction of DCIP and cytochrome c^{3+} in the absence and presence of Ca^{2+}-CaM

Electron Acceptor	Ca^{2+} -CaM	K_{NADPH}[a,e] (μM)	K_{acc}[b,e] (μM)	k_{cat}[c,e] (s^{-1})	$\frac{k_{cat}}{K_{NADPH}}$[d] ($M^{-1}s^{-1} \times 10^5$)	$\frac{k_{cat}}{K_{acc}}$[d] ($M^{-1}s^{-1} \times 10^5$)
DCIP	-	0.18 ± 0.05 (5)	15.9 ± 1.9 (3)	5.41 ± 0.35 (5)	300.7 ± 85.7	3.43 ± 0.47
	+	0.35 ± 0.05 (5)	10.3 ± 1.7 (3)	16.10 ± 0.52 (5)	460.0 ± 67.3	15.63 ± 1.18
cytc[f]	-	0.02 ± 0.01 (6)	0.4 ± 0.1 (11)	1.64 ± 0.05 (5)	725.7 ± 261.7	43.17 ± 11.3
	+	0.25 ± 0.09 (5)	0.4 ± 0.1 (4)	37.16 ± 0.91 (5)	1486 ± 536	1004 ± 272

[a] K_{NADPH} is the Michaelis constant for NADPH
[b] K_{acc} is the Michaelis constant for the designated electron acceptor.
[c] k_{cat} is the maximal velocity, V, divided by the nNOS concentration.
[d] k_{cat}/K_{NADPH} and k_{cat}/K_{acc} are the V/K_{NADPH} and V/K_{acc} divided by the nNOS concentration, respectively.
[e] the values are the mean and standard deviation determined from n determinations where n is enclosed in parenthesis.
[f] cytc is cytochrome c^{3+}

2.4.2 Product inhibition studies with DCIP as an electron acceptor

As indicated in Table 2.2, $NADP^+$ was noncompetitive with either NADPH or DCIP as the variable substrate, and the dead-end inhibitor, 2'AMP, was competitive *versus* NADPH and uncompetitive *versus* DCIP. The inhibition patterns are consistent with the classical ping-pong mechanism illustrated in Scheme 2.1 with one exception. Product inhibition by $NADP^+$ is expected to be competitive *versus* DCIP, because they both bind to the same enzyme form, E_3 (234). However, $NADP^+$ was noncompetitive *versus* DCIP indicating that they bind to different forms of E_3. The kinetic mechanism was therefore revised to incorporate a step which allows E_3 to isomerize to a distinct three-electron reduced state, E_3', which exclusively binds DCIP (Scheme 2.2). When an isomerization of a stable form of the enzyme occurs in the reaction sequence it is referred to as an iso-mechanism (234). To follow previously established nomenclature, the mechanism is drawn in Scheme 2.2 is referred to as an iso ping-pong bi-bi (234).

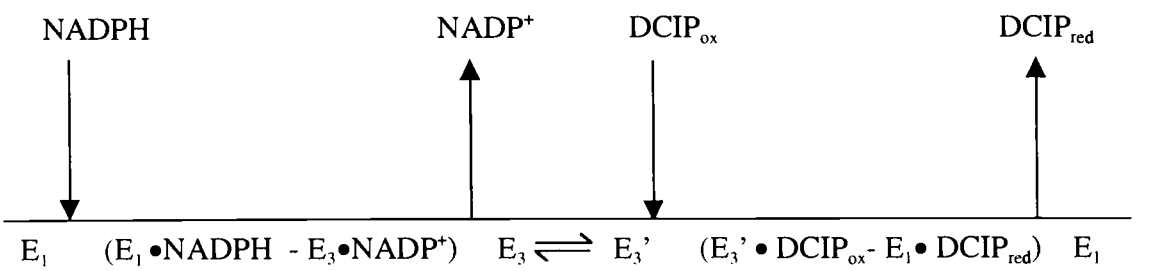

(Scheme 2.2)

Saturating levels of Ca^{2+}-CaM in the reaction mixtures did not affect the product and dead-end inhibition patterns. It did increase the K_{is} for 2'-AMP *versus* NADPH~2-fold, but did not affect the K_{ii} for 2'-AMP with DCIP as the variable substrate (Table 2.2).

2.4.3 Initial velocity studies with cytochrome c^{3+} as an electron acceptor

Cytochrome c^{3+} shows substrate inhibition at concentrations above 2 μM (5–10 times its K_m); therefore, this electron acceptor was maintained at sufficiently low concentrations to minimize this effect. Substrate inhibition by cytochrome c^{3+} also occurs with CPR at 5-10 times its K_m (236). A plot of $1/v$ *versus* 1/[cytochrome c^{3+}] at varying fixed concentrations of NADPH gave a family of parallel lines both without Ca^{2+}-CaM (Figure 2.2A) and with Ca^{2+}-CaM (Figure 2.2B). Likewise, a plot of $1/v$ *versus* 1/[NADPH] at varying fixed concentrations of cytochrome c^{3+} in the absence and presence of Ca^{2+}-CaM produced a family of parallel lines (Figures 2.2C and 2.2D, respectively). The lack of a slope effect suggests that both basal and CaM-stimulated cytochrome c^{3+} reductase activities are consistent with ping-pong mechanisms. This graphical analysis is consistent with the computer analysis as the rate equation for a ping-pong mechanism (eq 2.1) gave a better fit to the initial velocity data compared to the rate equation for a sequential mechanism (eq. 2.2). The latter equation did not reduce the chi-squared value and gave an undefined value for K_{iA}.

If the nNOS reduction of cytochrome c^{3+} were to follow the classical ping-pong mechanism the binding of substrates and release of products would proceed in a hexa-uni fashion (Scheme 2.3; 236). After the initial conversion of E_1 to E_3 by NADPH oxidation, two molecules of cytochrome c^{3+}, each of which are reduced by one electron, are required to react with the enzyme to return it to its initial state, E_1 (Scheme 2.3). Thus, the two-electron reduced state, E_2, now appears after the reduction of the first molecule of cytochrome c^{3+}. Equation 2.1 is also consistent with a nonclassical (two-

Table 2.2 Dead-end and product inhibition of nNOS-catalyzed reduction of DCIP in the absence and presence of Ca^{2+}-CaM

Varied Substrate	Ca^{2+}-CaM	Inhibitor	Type of Inhibition	Inhibition Constants (μM)
DCIP	-	$NADP^+$	noncompetitive	$K_{is} = 8.1 \pm 1.8$
				$K_{ii} = 13.0 \pm 2.0$
	+	$NADP^+$	noncompetitive	$K_{is} = 18.6 \pm 5.2$
				$K_{ii} = 12.2 \pm 5.2$
	-	2'-AMP	uncompetitive	$K_{ii} = 435.4 \pm 23.1$
	+	2'-AMP	uncompetitive	$K_{ii} = 435.6 \pm 34.0$
NADPH	-	$NADP^+$	noncompetitive	$K_{is} = 14.5 \pm 1.5$
				$K_{is} = 27.7 \pm 1.8$
	+	$NADP^+$	noncompetitive	$K_{is} = 8.1 \pm 1.4$
				$K_{ii} = 58.9 \pm 12.0$
	-	2'-AMP	competitive	$K_{is} = 840.9 \pm 92.9$
	+	2'-AMP	competitive	$K_{is} = 1437.0 \pm 280.8$

Figure 2.2 Initial velocity patterns for the nNOS-catalyzed reaction for the reduction of cytochrome c^{3+} by NADPH. The symbols represent the experimentally determined mean of three values, while the lines are best nonlinear fits to the data. (A) Varying concentrations of cytochrome c^{3+} (cytc) at NADPH concentrations of ■ 0.029, ● 0.047, ▲ 0.089, and ▼ 0.534 μM. (B) $CaCl_2$ at 10 μM and CaM at 100 nM present with varying concentrations of cytochrome c^{3+} at NADPH concentrations of ■ 0.098, ● 0.196, ▲ 0.588, and ▼ 1.96 μM. (C) Varying concentrations of NADPH at cytochrome c^{3+} concentrations of ■ 0.154, ● 0.246, ▲ 0.619, and ▼ 1.848 μM. (D) $CaCl_2$ at 10μM and CaM at 100 nM present with varying concentrations of NADPH at cytochrome c^{3+} concentrations of ■ 0.28, ● 0.51, ▲0.85, and ▼ 1.99 μM.

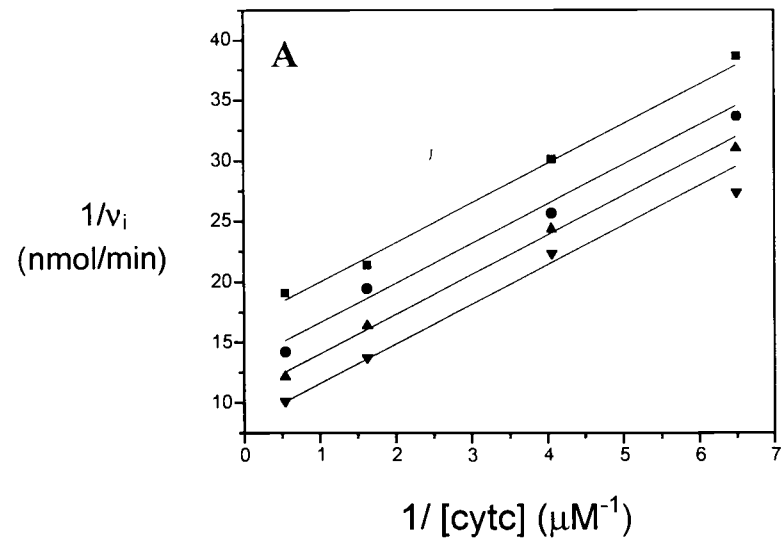

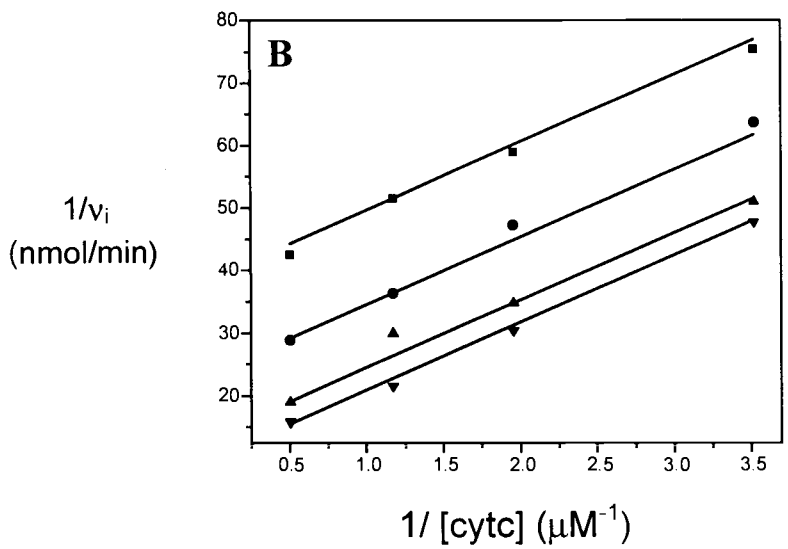

Figure 2.2

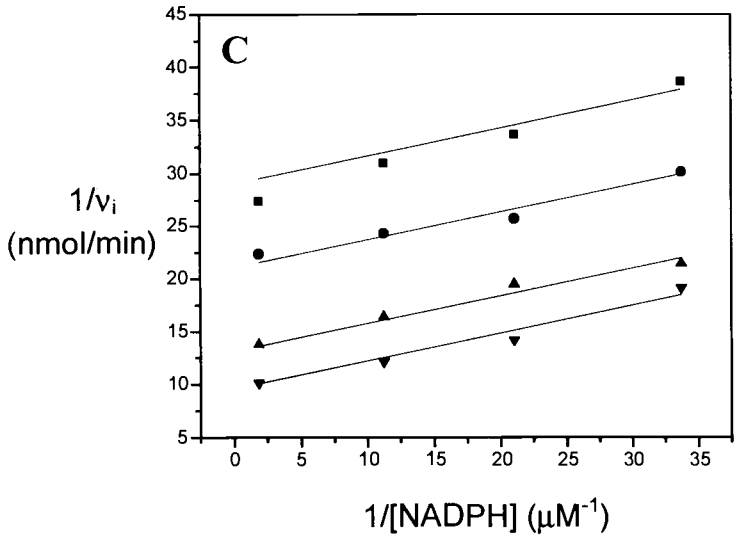

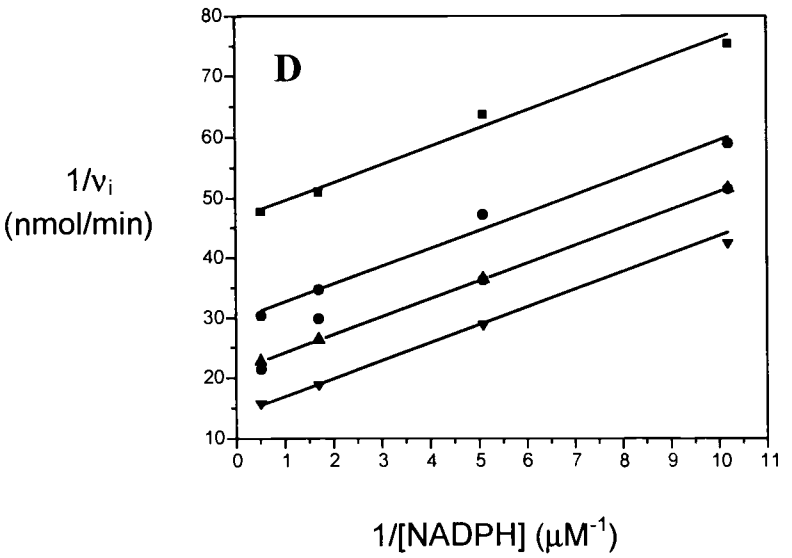

Figure 2.2 (Continued)

Table 2.3: Dead-end and product inhibition of nNOS-catalyzed reduction of cytochrome c^{3+} in the absence and presence of Ca^{2+}-CaM

Varied Substrate	Ca^{2+}-CaM	Inhibitor	Type of Inhibition	Inhibition Constants (μM)
$cytc^{3+}$	-	$cytc^{2+}$	competitive	$K_{is} = 2.3 \pm 0.3$
	+	$cytc^{2+}$	competitive	$K_{is} = 4.1 \pm 0.4$
	-	$NADP^+$	uncompetitive	$K_{ii} = 6.2 \pm 0.5$
	+	$NADP^+$	uncompetitive	$K_{ii} = 1.6 \pm 0.1$
	-	2'AMP	uncompetitive	$K_{ii} = 95.3 \pm 2.7$
	+	2'AMP	uncompetitive	$K_{ii} = 82.4 \pm 2.3$
NADPH	-	$cytc^{2+}$	noncompetitive	$K_{is} = 6.1 \pm 1.1$
				$K_{ii} = 2.3 \pm 1.0$
	+	$cytc^{2+}$	noncompetitive	$K_{is} = 7.1 \pm 1.0$
				$K_{ii} = 9.6 \pm 0.7$
	-	$NADP^+$	competitive	$K_{is} = 1.2 \pm 0.1$
	+	$NADP^+$	competitive	$K_{is} = 2.1 \pm 0.1$
	-	2'AMP	competitive	$K_{is} = 31.5 \pm 2.9$
	+	2'AMP	competitive	$K_{is} = 71.5 \pm 3.8$

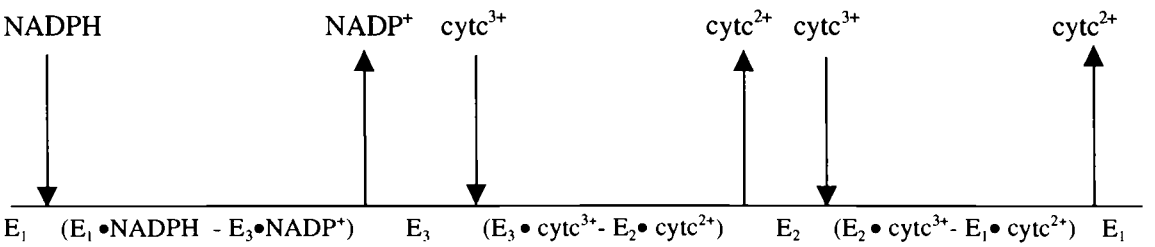

(Scheme 2.3)

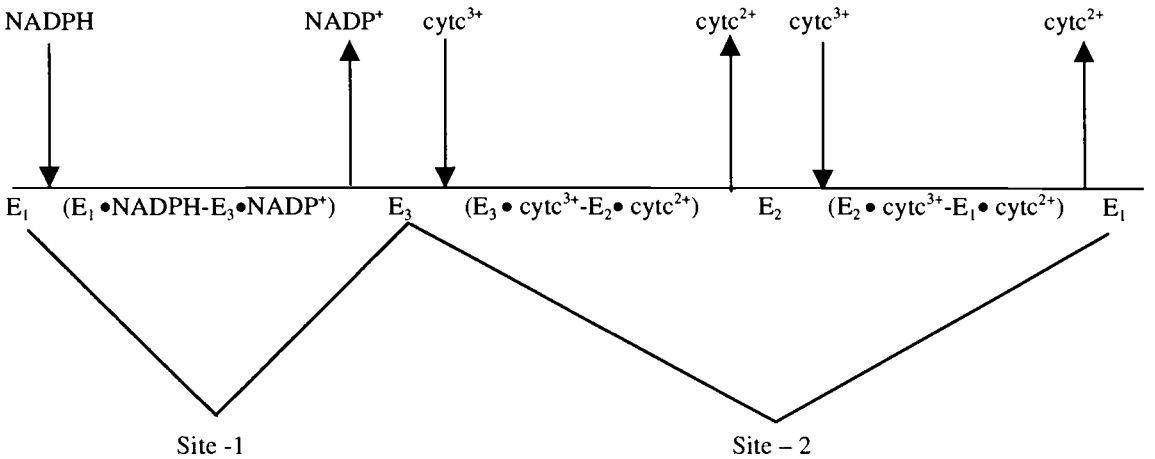

(Scheme 2.4)

site) ping-pong mechanism (236). In this kinetic mechanism, NADPH and cytochrome c^{3+} react at two catalytically independent sites on the enzyme. Scheme 2.4 illustrates the (two-site) ping-pong mechanism with the active sites for NADPH and cytochrome c^{3+} labeled as site-1 and site-2, respectively. This mechanism has been previously proposed for the CPR-catalyzed reduction of cytochrome c^{3+}. Considering the structural/functional similarities of nNOS with CPR it seems reasonable that this mechanism also applies for the nNOS cytochrome c^{3+} reductase activity. The classical (one site) and the non-classical (two-site) mechanisms drawn in Schemes 2.3 and 2.4, respectively, generate different product and dead-end inhibition patterns (236, 237);

therefore, there is a means for discerning which mechanism applies for the nNOS reduction of cytochrome c^{3+}.

The presence of Ca^{2+}-CaM did not alter the parallel pattern of the double reciprocal plots (Figures 3.2B and 3.2D); however, the presence of the activated cofactor resulted in a 23-fold increase in k_{cat} and $(k_{cat}/K_m)_{cytc}$ (Table 3.1). The average value of $(k_{cat}/K_m)_{NADPH}$ increased 2-fold with the addition of Ca^{2+}-CaM; however, due to the large errors associated with the values, the change was not considered significant (Table 3.1).

2.4.4 Product inhibition studies with cytochrome c^{3+} as an electron acceptor

Although the parallel initial velocity patterns with cytochrome c^{3+} as the terminal electron acceptor are consistent with either a classical (one-site) ping-pong mechanism, (Scheme 2.3) or a non-classical (two-site) ping-pong mechanism (Scheme 2.4), product and dead-end inhibition patterns are consistent only with the latter of these two kinetic mechanisms. The results of the inhibition studies, summarized in Table 2.3, show that product inhibition by $NADP^+$ was competitive *versus* NADPH and cytochrome c^{2+} was competitive *versus* cytochrome c^{3+}. These patterns are consistent with the (two-site) ping-pong mechanism (Appendix 2; 236). In the classical (one-site) hexa-uni ping-pong mechanism drawn in Scheme 2.3, both of these inhibition patterns are expected to be noncompetitive; therefore, this mechanism is not consistent for the nNOS-reduction of cytochrome c^{3+} (Appendix 2). The remaining inhibition patterns listed in Table 2.3 are consistent with the (two-site) ping-pong mechanism since product inhibition by $NADP^+$ was found to be uncompetitive *versus* cytochrome c^{3+} and cytochrome c^{2+} was found to be a noncompetitive product inhibitor *versus* NADPH. Finally, the dead-end inhibition

by the NADPH analog, 2'-AMP, was competitive with NADPH as the variable substrate and uncompetitive with cytochrome c^{3+} as the variable substrate.

The presence of Ca^{2+}-CaM did not effect the product and the dead-end inhibition patterns. However, a saturating amount of Ca^{2+}-CaM in the reaction mixture increased the value of K_{is} by 1.5- to 2.5- fold for both $NADP^+$ and 2'-AMP with NADPH as the variable substrate. The K_{ii} for 2'-AMP inhibition*versus* cytochrome c^{3+} or DCIP did not change significantly in the presence of Ca^{2+}-CaM. However, the K_{ii} for $NADP^+$ decreased approximately 4-fold in inhibition studies with varying concentrations of cytochrome c^{3+}.

2.4.5 Dead-end inhibition by 2'-AMP

The K_{is} for 2'-AMP in inhibition studies with NADPH as the variable substrate decreased 25- to 30-fold when the electron acceptor was changed from DCIP to cytochrome c^{3+} (Tables 2.2 and 2.3). Furthermore, the K_{ii} for 2'-AMP was 4- to 5-fold higher when DCIP rather then cytochrome c^{3+} was the variable substrate. Both K_{ii} and K_{is} values for the NADPH analog changed by similar amounts under the same conditions with Ca^{2+}-CaM. In the kinetic mechanisms proposed for DCIP (Scheme 2.2) and cytochrome c^{3+} (Scheme 2.4), 2'-AMP is expected to bind to the same enzyme form as NADPH, E_1. This would accommodate both competitive and uncompetitive patterns for 2'-AMP *versus* NADPH and *versus* the electron acceptor, respectively. If this were the case both of the apparent affinity constants for 2'-AMP should be the same regardless of the electron acceptor, because the dead-end inhibitor is binding to a substrate-free form of the enzyme, E_1, in both mechanisms. To explain the observed differences in apparent

affinity for 2'-AMP, a second form of E_1, labeled as E_1'in Figures 2.3 and 2.4, which is able bind 2'-AMP but not NADPH, is proposed to exist in both kinetic mechanisms. To satisfy the competitive dead-end inhibition patterns *versus* NADPH, the isomerization of E_1' to E_1 must be in rapid equilibrium. If this step was at steady-state, 2'-AMP would be noncompetitive *versus* NADPH. The kinetic mechanism for the reduction of DCIP was modified and renamed to include this second, faster isomerization step and is now referred to as a di-iso ping-pong bi-bi mechanism. Likewise, the reduction of cytochrome c^{3+} is now proposed to follow an iso (two-site) ping-pong mechanism.

2.5 Discussion

The classical method for distinguishing between sequential and ping-pong reaction mechanisms is by analysis of the initial velocity patterns obtained by varying the concentration of one substrate at several fixed concentrations of a second substrate. When the data are plotted in double-reciprocal form, ping-pong mechanisms give patterns of parallel lines while sequential mechanisms will yield a family of lines which intersect to the left of the vertical axis (238). The initial velocity experiments with DCIP and cytochrome c^{3+} in the presence and absence of Ca^{2+}-CaM fit best to equation 2.1 for a ping-pong mechanism. Abu-Soud *et al.* have shown that the flavin cofactors of nNOS can be reduced with the addition of excess NADPH in the absence of any electron-acceptor (92, 239). This data supports the ping-pong mechanism, because it demonstrates that a binary complex between nNOS and either electron acceptor is not a prerequisite for the binding and subsequent oxidation of NADPH.

Although nNOS maintains one electron on its flavins in the form of a flavin-semiquinone (FAD-FMNH•), it is unable to transfer this electron to either DCIP or to cytochrome c^{3+} (72). This one-electron reduced state of nNOS, E_1, is then postulated as one of the stable enzyme forms in the ping-pong mechanisms for DCIP and cytochrome c^{3+}. Since hydride transfer from NADPH results in the transfer of two electrons to the flavins, the three-electron reduced state, E_3, is thought to be the second stable enzyme form in the reaction sequences for both electron acceptors. However, the kinetic mechanisms for DCIP and cytochrome c^{3+} differ once the number of electrons required to reduce the electron acceptor is considered. The reduction of DCIP is a two-electron process; therefore, one molecule combining with E_3 is enough to return the enzyme to E_1. Scheme 2.1 illustrates the tetra-uni ping-pong mechanism for the reduction of this substrate. In contrast, cytochrome c^{3+} is reduced by one electron; therefore, it would follow hexa-uni ping-pong mechanism, which would include the formation of E_2 after the reduction of the first molecule of cytochrome c^{3+} (Scheme 2.3).

The kinetic mechanisms for the reduction of DCIP and cytochrome c^{3+} illustrated in Schemes 2.1 and 2.3, respectively, are modified to be consistent with the product and dead-end inhibition studies in Tables 2.2 and 2.3. The kinetic mechanism for DCIP reduction was revised to incorporate an iso-step, or an isomerization of E_3 to E_3' (Scheme 2.2), based on the noncompetitive inhibition by $NADP^+$ at varying concentrations of DCIP. According to the classical ping-pong mechanism depicted in Scheme 2.1, $NADP^+$ and DCIP combine with the same enzyme form, E_3; therefore, $NADP^+$ is expected to be competitive *versus* DCIP. However, if the two molecules bind

exclusively to different conformations of E_3 or to alternate forms of E_3 that arise from differences in the distribution of the three electrons on the flavins (i.e. (FADH•-$FMNH_2$) *versus* ($FADH_2$-FMNH•)), and the rate of isomerization between the two forms is at steady-state, noncompetitive inhibition is expected. Thus, this iso-step is not included in either rapid equilibrium segment *Y* or *Z* of Figure 2.3. If the iso-step were to occur in rapid equilibrium, $NADP^+$ would be a competitive inhibitor when DCIP is the variable substrate. The noncompetitive inhibition of $NADP^+$ when NADPH is the variable substrate (Table 2.2) is consistent with the proposed mechanism in Scheme 2.2 since the reduced and oxidized forms of the nucleotide bind to E_1 and E_3, respectively. Dead-end inhibition patterns with the NADPH analog, 2'-AMP, are also consistent with the proposed kinetic mechanism. The dead-end inhibitor was found to be competitive *versus* NADPH, which is consistent with them both binding to the same enzyme form. The NADPH-analog was also found to be uncompetitive *versus* DCIP (Table 2.2), which is consistent with binding to different enzyme forms connected by an irreversible step, the release of $NADP^+$.

The parallel initial velocity patterns observed with cytochrome c^{3+} as an electron acceptor agree with both the classical (one-site) ping-pong mechanism (Scheme 2.2), and the (two-site) ping-pong mechanism (Scheme 2.4; 233). However, product and dead-end inhibition studies are consistent only with the latter of these two kinetic mechanisms. The defining characteristic of the (two-site) ping-pong mechanism is presence of two separate and functionally distinct catalytic sites on the enzyme that are linked by a mobile component or by an internal electron carrier. This type of system was first used to describe enzymes that contain a mobile component, such as a biotinyl

prosthetic group (237, 240) or lipoic acid cofactor (241), which links the non-overlapping catalytic sites on the enzyme. It has also been shown to be applicable for enzymes with redox cofactors that serve as internal electron carriers, such as xanthine dehydrogenase (242), glutamate synthetase (243), nitrate reductase (232), two hydrogenases (244, 245) and dihydroorate dehydrogenase (246). The two-site ping-pong mechanism is also proposed for the CPR-catalyzed reduction of cytochrome c^{3+} in which the FAD/FMN prosthetic groups act as internal electron carriers between the NADPH and the cytochrome c^{3+} active sites. Considering the functional and structural similarity between CPR and nNOS reductase domain, it seems reasonable that the product and dead-end inhibition studies for the nNOS-catalyzed reduction of cytochrome c^{3+} are also consistent with a (two-site) ping-pong mechanism. In this mechanism, the product ($NADP^+$ or cytochrome c^{2+}) can be released before or after the addition of the substrate (NADPH or cytochrome c^{3+}) and the reaction is not restricted to either exclusive formation of binary complexes or to compulsory formation of a central ternary complex.

This is in contrast to the classical (one-site) hexa-uni ping-pong mechanism shown in Scheme 2.3 where the formation of the ternary complex is precluded. With this mechanism, product inhibition by $NADP^+$ is expected to be noncompetitive *versus* NADPH and competitive *versus* cytochrome c^{3+} (Appendix 2). Furthermore, product inhibition by cytochrome c^{2+} is expected to be noncompetitive *versus* NADPH and noncompetitive *versus* cytochrome c^{3+} (Appendix 2). Instead, $NADP^+$ was found to be a competitive inhibitor when NADPH was the variable substrate and an uncompetitive inhibitor *versus* cytochrome c^{3+}. Cytochrome c^{2+} was noncompetitive *versus* NADPH

and competitive when cytochrome c^{3+} was the variable substrate (Table 2.3). These patterns are identical with those reported for the CPR-catalyzed reduction of cytochrome c^{3+} (236) and are consistent with the unique product inhibition patterns that are commonly observed with the enzymes listed above which follow a (two-site) ping-pong mechanism. The first product (*P*) is always competitive with the first substrate (*A*). Similarly, inhibition by the second product (*Q*) is competitive with the second substrate (*B*; 232). Therefore, we propose that the nNOS-catalyzed reduction of cytochrome c^{3+} also follows a (two-site) ping-pong mechanism in which the enzyme binds NADPH at site-1 in a uni-uni fashion and follows a tetra-uni ping-pong reaction for two molecules of cytochrome c^{3+} at site-2 (Scheme 2.4). This kinetic mechanism is only applicable for CPR at high-ionic strength of 850 mM (236). At lower ionic strength (300 mM) the CPR cytochrome c^{3+} reductase activity is still consistent with a (two-site) ping-pong mechanism, but the binding of cytochrome c^{3+} follows a bi-bi random sequential mechanism at site-2 (247). This was deduced from the nonlinear initial velocity patterns observed when cytochrome c^{3+} was the variable substrate for CPR at low ionic strength. However, nNOS does not show any curvature in the initial velocity patterns for reduction of cytochrome c^{3+} at low ionic strength (Figures 2.2A and 2.2B).

Inhibition by $NADP^+$ *versus* cytochrome c^{3+} at non-saturating concentrations of NADPH should be noncompetitive for a two-site ping-pong mechanism, but CPR and nNOS both exhibited uncompetitive inhibition patterns (Table 2.3). To explain this observation it was assumed that the reverse rate of hydride transfer, k_4, catalyzed by CPR was much slower than the rate of cytochrome c^{3+} reduction, k_9 (Figure 2.4; 236). The lack of any pronounced curvature in inhibition patterns with cytochrome c^{2+} further

indicated that hydride transfer, k_3, was much slower than electron transfer from the flavins to cytochrome c^{3+}, k_9 (236). Since nNOS exhibits the same inhibition patterns as CPR and it does not display any curvature in the inhibition patterns with cytochrome c^{2+}(data not shown) this assumption ($k_9 >> k_4$) was also used in the derivation of the (two-site) ping-pong mechanism for nNOS-catalyzed reduction of cytochrome c^{3+} (Appendix 2).

In the one-site ping-pong mechanism for DCIP, only binary enzyme-substrate complexes form and the release of the first product, $NADP^+$, occurs before the addition of DCIP. However, since NADPH and cytochrome c^{3+} are proposed to act at catalytically independent sites on the enzyme the formation of a ternary complex between the two substrates and nNOS is possible. The difference may be do to the flavin cofactor that reduces the electron acceptor. Since nNOS depleted of its FMN cofactor is still able to reduce DCIP the reduction of this substrate may occur through the direct two-electron transfer from the fully reduced FAD, presumably through the conversion of ($FADH_2$-FMNH•) to (FAD-FMNH•; 81). Once NADPH reduces E_1 (FAD-FMNH•) to E_3, disproportionation of electrons on the flavins establishes an equilibrium of ($FADH_2$-FMNH•) and (FADH•-$FMNH_2$). It has been proposed that $NADP^+$ shifts the reduction potential of the FAD semiquinone to a more negative value and stabilizes the FADH•-$FMNH_2$ form of the enzyme (73). Similar effects have been observed in P450-BM3 (248), and adrenodoxin reductase (249). As such, it is possible that the oxidized nucleotide is required to dissociate from the nNOS to allow the disporportionation of electrons on the flavins to favor the reduction of DCIP, thereby

restricting the kinetic mechanism to the exclusive formation of binary enzyme-substrate complexes.

According to the two-site ping-ping mechanism NADPH oxidation and cytochrome c^{3+} reduction operate independently during nNOS catalytic turnover. This catalytic independence may be facilitated by topographically separate substrate binding sites on nNOS and/or by FMN acting as the terminal electron donator. Based on sequence comparisons, the nNOS reductase domain and CPR belong to a class of dual flavin containing proteins that have independent NADPH/FAD and FMN binding domains (70). Mutational analysis and sequence comparison with CPR suggests that cytochrome c^{3+} interacts with a cluster of acidic residues in the FMN domain, while NADPH binds in close proximity to FAD (81). Therefore, if the substrates bind to different domains, which are separated by an internal electron carrier, that stores reducing equivalents, independent reactions with either substrate could occur.

Comparison of the inhibition constants for 2'AMP determined with DCIP or cytochrome c^{3+} as electron acceptors lead to the second modification of the mechanisms proposed for DCIP and cytochrome c^{3+} reduction. In both the iso ping-pong and the (two-site) ping-pong, the NADPH analog binds to the same enzyme form as NADPH, E_1. This is consistent with 2'AMP dead-end inhibition patterns listed in Tables 2.2 and 2.3; however, if 2'AMP bound to E_1 in both mechanisms then the values of the inhibition constants for 2'AMP should be the same regardless of the electron acceptor. Nevertheless, a large increase in the apparent affinity for 2'AMP in the presence of DCIP compared to cytochrome c^{3+} was observed. To interpret these results, an additional free enzyme form, E_1', was proposed to occur in both mechanisms. The

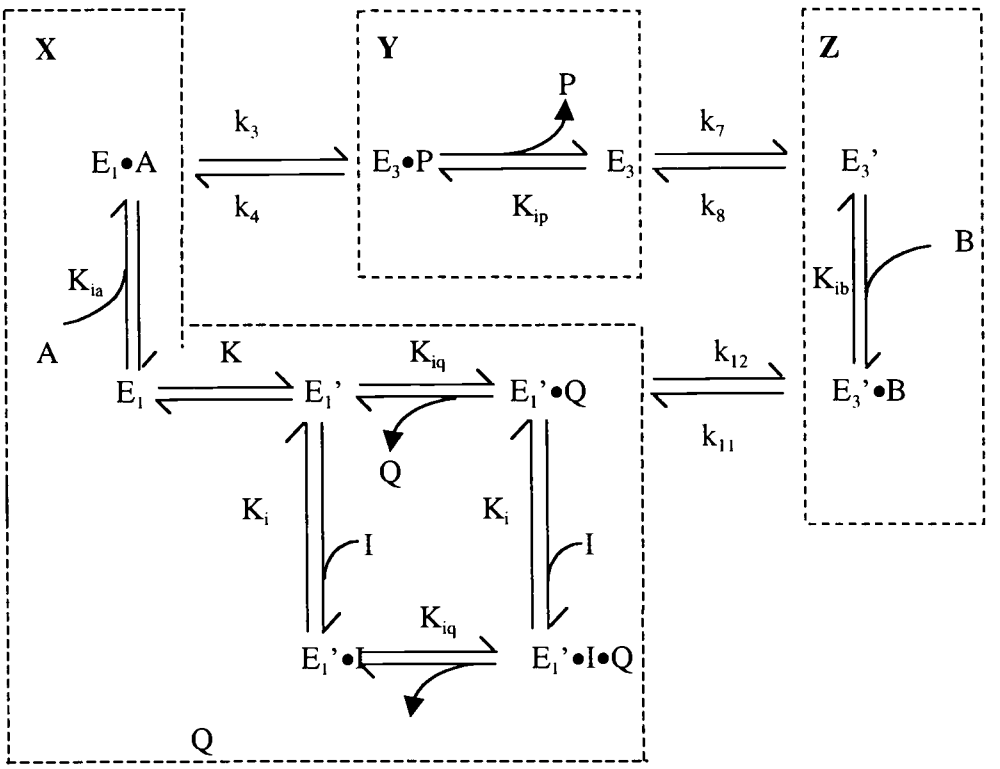

Figure 2.3 Kinetic scheme for a di-iso ping-pong bi-bi mechanism for the nNOS-catalyzed reduction of DCIP. *A, B, P, Q,* and *I* represent NADPH, $DCIP_{ox}$, $NADP^+$, $DCIP_{red}$, and 2'-AMP respectively, and the K_i values refer to their respective dissociation constants. E_1 and E_1' are the one-electron (FAD/FMNH•) forms of nNOS that exclusively bind NADPH and 2'-AMP, respectively. E_3 and E_3' are the three-electron (FADH•/$FMNH_2$) or ($FADH_2$/FMNH•) forms of nNOS that exclusively bind $NADP^+$ and $DCIP_{ox}$, respectively. *K* is the equilibrium constant for the conversion of the two enzyme forms, E_1 and E_1'. The dotted boxes labeled *X, Y,* and *Z* indicate the proposed rapid equilibrium segments for the reaction mechanism, where $X = E_1 + E_1' + E_1'I + E_1'IQ + E_1'Q + E_1A$; $Y = E_3P + E_3$; $Z = E_3' + E_3'B$.

Site-1:

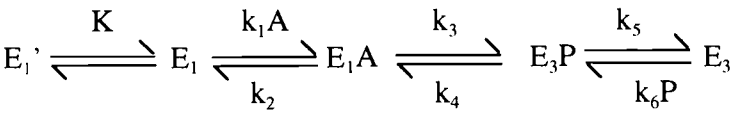

Site-2:

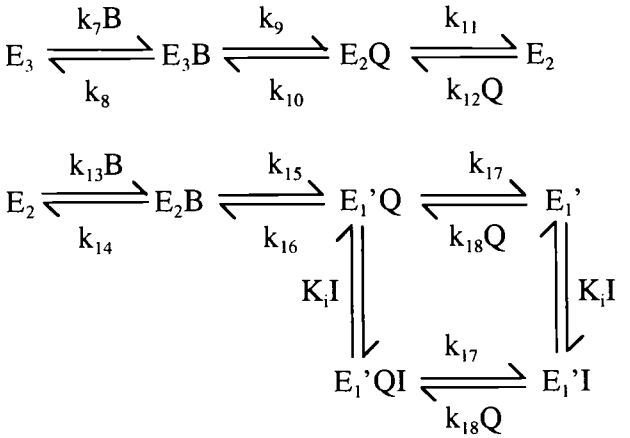

Figure 2.4 The kinetic scheme illustrating the iso (two-site) ping-pong mechanism for the nNOS-catalyzed reduction of cytochrome c^{3+}. *A*, *B*, *P*, *Q*, and *I* represent NADPH, cytochrome c^{3+}, $NADP^+$, cytochrome c^{2+}, and 2'-AMP, respectively. E_1, E_1,' and E_3 are the same as in Figure 2.3, and E_2 represents the two ($FAD/FMNH_2$) electron reduced form
of nNOS.

differences in the inhibition constants for 2'AMP would arise if the following conditions were met: (1) the NADPH analog could only form dead-end complexes with E_1' and not E_1, E_3, or in the case of cytochrome c^{3+}, E_2; (2) NADPH and $NADP^+$ could not bind to E_1'; and (3) E_1 is in rapid equilibrium with E_1'. The last assumption still results in a competitive inhibition pattern for 2'AMP *versus* NADPH. The kinetic mechanisms proposed for DCIP and cytochrome c^{3+} were revised to include the isomerization step for the free enzyme governed by the equilibrium constant, K (Figures 2.3 and 2.4). The two mechanisms also include different dead-end complexes between E_1' and 2'-AMP which could account for the differences in the apparent affinity of 2'-AMP observed in dead-end inhibition studies.

Based on sequence similarity, the putative $NADP^+$ and FAD binding motifs of nNOS belong to the family flavoenzymes of which ferridoxin-$NADP^+$ reductase (FNR) is the prototype. The early crystal structure of FNR failed to reveal the geometry between FAD and the nicotinamide ring. The only relevant structural information was obtained with the 2'AMP portion of the $NADP^+$ molecule complexed with the enzyme (250). This occurred because positioning of the nicotinamide ring in close proximity to the *re*-face of the FAD cofactor required the energetically unfavorable displacement of a tyrosine residue (251). The two alternate forms of nNOS, E_1 and E_1', may likewise result from the positioning of a similar residue in nNOS.

Rate equations were derived for the proposed di-iso ping-pong bi-bi mechanism for DCIP and the iso (two-site) ping-pong mechanism for cytochrome c^{3+} under initial velocity conditions and for product and dead-end inhibition studies (Appendix 2). The derivation of nNOS-catalyzed reduction of cytochrome c^{3+} is similar to the derivation for

the CPR-catalyzed reduction which assumes that the binding and release of ligands occurs in rapid equilibrium and the conversion of enzyme forms (i.e. E_1 to E_3) occurs at steady-state. This assumption was also used for the derivation of the nNOS-catalyzed reduction of DCIP. All of the experimental initial velocity and inhibition patterns were consistent with the patterns predicted for the rate equations derived under the appropriate conditions. The turnover rate (k_{cat}), Michaelis constant (K_m), and the values for k_{cat}/K_m for each substrate are also defined in terms of rate and equilibrium constants in the Appendix, (i.e. $(k_{cat}/K_m)_{NADPH} = k_3/K_{iA}$ (1+1/K) (Figures 2.3 and 2.4) and $(k_{cat}/K_m)_{DCIP} = k_7k_{11}/K_{iB}$ (k_7+k_8) (Figure 2.3), $(k_{cat}/K_m)_{cytc} = k_9k_{15}/K_{iB}$ (k_9+k_{15}) (Figure 2.4). The ratio of rate and equilibrium constants to define $(k_{cat}/K_m)_{NADPH}$ was the same for both mechanisms.

Although Ca^{2+}-CaM increased the rate of DCIP and cytochrome c^{3+} reduction, it did not change the proposed kinetic mechanism for the reduction of either electron acceptor. Identical types of initial velocity, product and dead-end inhibition patterns were observed in the presence or absence of Ca^{2+}-CaM. The presence of the activated cofactor did have variable effects on the kinetic parameters for the various substrates listed in Table 2.1 and on the inhibition constants listed in Table 2.2 and 2.3. The influence of Ca^{2+}-CaM on these various parameters will be discussed in the context of the mechanisms presented in Figures 2.3 and 2.4 in an effort to describe how individual rate constants are affected.

$NADP^+$ is a competitive inhibitor of NADPH in the presence of non-saturating concentrations of cytochrome c^{3+}; therefore, the reported K_{is} is a direct measure of the dissociation constant for $NADP^+$. The presence of Ca^{2+}-CaM in the inhibition study

caused a 2-fold increase in the inhibition constant for $NADP^+$ suggesting that it may slightly reduce the affinity of the enzyme for $NADP^+$. The activated cofactor also caused an increase in the K_{is} of 2'-AMP *versus* NADPH with either DCIP or cytochrome c^{3+} as the electron acceptor. Although the dead-end inhibitor is also competitive *versus* NADPH, the K_{is} value is not a direct measure of the dissociation constant because it is also a function of the equilibrium constant K, equal to E_1 /E_1', (eqs A2.19, A2.20, and A2.39 in Appendix 2). Assuming that Ca^{2+}-CaM has a negligible effect on the equilibrium between E_1 and E_1', the increase in the K_{is} value for 2'-AMP may be interpreted as the ability of the cofactor to slightly reduce the affinity of nNOS for 2'-AMP. The activated cofactor also caused a 1.5-fold increase in $(k_{cat}/K_m)_{NADPH}$ with DCIP as an electron acceptor (Table 2.1). While the average value of $(k_{cat}/K_m)_{NADPH}$ with cytochrome c^{3+} increased about 2-fold in the presence of Ca^{2+}-CaM, the large error associated with the value, which originates with the difficulty in determining the low K_m for NADPH under these conditions, did not make the change significant (Table 2.1). Assuming that the 1.5 to 2-fold increase $(k_{cat}/K_m)_{NADPH}$ is valid for both acceptors, it would be do an increase in the value of the expression: $k_3/K_{iA}(1+1/K)$ (Appendix 2). Thus, the presence of Ca^{2+}-CaM could either affect the rate of hydride transfer, k_3, the dissociation constant for NADPH, K_{iA}, or both.

Ca^{2+}-CaM caused a 4.5-fold increase $(k_{cat}/K_m)_{DCIP}$ and a 23-fold increase in $(k_{cat}/K_m)_{cytc}$ (Table 2.1). Both of these kinetic parameters are defined by ratio of forward rate constants for the reduction of the electron acceptor in the second half reaction (k_7 and k_{11} for DCIP and k_9 and k_{15} for cytochrome c^{3+}) as well as their associated binding constants shown in equations 2.6 and 2.7.

$$(k_{cat}/K_m)_{\text{DCIP}} = \frac{k_7 k_{11}}{K_{iB}(k_7 + k_8)} \tag{2.6}$$

$$(k_{cat}/K_m)_{\text{cytc}} = \frac{k_9 k_{15}}{K_{iB}(k_9 + k_{15})} \tag{2.7}$$

K_{iB} is the dissociation constant for DCIP or cytochrome c^{3+} in equations 2.6 and 2.7, respectively. The rate constants, k_7, k_8, and k_{11} in equation 2.6 are the same as those in Figure 2.3, and the rate constants, k_9 and k_{15} in equation 2.7 are the same as those in Figure 2.4. The data suggests that the binding of Ca^{2+}-CaM may stimulate the rate of electron transfer to the electron acceptors by increasing the forward rate constants for these steps and/or decreasing the dissociation constant for the electron acceptor.

The presence of Ca^{2+}-CaM also caused an approximate 2-fold increase in Michaelis constant for NADPH, K_{NADPH}, with DCIP as an electron acceptor and a 10-fold increase with cytochrome c^{3+} as an electron acceptor. Equations 2.8 and 2.9 define K_{NADPH} in terms of rate and equilibrium constants according to the derivation of the mechanisms proposed for the reduction of DCIP and cytochrome c^{3+}, respectively.

$$K_{\text{NADPH}} = \frac{K_{iA}(1+1/K)}{(1+k_3/k_7+k_3/k_{11})} \tag{2.8}$$

$$K_{\text{NADPH}} = \frac{K_{iA}(1+1/K)}{(1+k_3/k_9+k_3/k_{15})} \tag{2.9}$$

The rate constants, k_3, k_7, and k_{11} in equation 2.8 are the same as those in Figure 2.3, and the rate constants, k_3, k_9 and k_{15} in equation 2.7 are the same as those in Figure 2.4. The reason why Ca^{2+}-CaM exerts more of a change in K_{NADPH} with cytochrome c^{3+} may be the difference in the ratios of rate and equilibrium constants defined for K_{NADPH}. Assuming that Ca^{2+}-CaM had no effect on K, then the increase in K_{NADPH} may be do to the decrease in k_3/k_9 and/or k_3/k_{15} ratios. In other words, Ca^{2+}-CaM accelerates electron transfer to cytochrome c^{3+} by increasing k_9 and/or k_{15} to a greater extent then its stimulation of hydride transfer given by k_3. The Ca^{2+}-CaM-induced increase in k_9 and/or k_{15} also agrees well with the large increase (23-fold) in $(k_{cat}/K_m)_{cytc}$ (eq. 2.7). Similarly, the 2-fold change in K_{NADPH} with DCIP may be caused by changes in k_3/k_7 and/or k_3/k_{11} ratios.

The presence of Ca^{2+}-CaM does not significantly change the K_{ii} for 2'-AMP with either DCIP or cytochrome c^{3+} as the variable substrate. For DCIP, this observation is consistent with the reaction occurring in two-half reactions and for cytochrome c^{3+}, the observation is also consistent with the two-half reactions occurring at two separate catalytic sites on the enzyme.

In summary, we have shown that the nNOS-catalyzed reduction of DCIP and the nNOS-catalyzed reduction of cytochrome c^{3+} are accommodated by the di-iso ping-pong bi-bi mechanism and by the iso (two-site) ping-pong mechanism, respectively. Although the presence of Ca^{2+}-CaM accelerates the rate of electron transfer, its presence does not alter either of these mechanisms.

2.6 Acknowledgements

We are grateful to Drs. Sonia Anderson and Dean Malencik for supplying CaM and the CaM-Sepharose column and to Dr. Ted Dawson for giving us the cDNA plasmid construct for rat neuronal NOS. We would also like to acknowledge the Nucleic Acids and Proteins Core Facilities of Oregon State University Environmental Health Sciences Center in conducting these studies.

Chapter 3

The Effects of Ca^{2+}-Activated Calmodulin on Neuronal Nitric-Oxide Synthase Reductase Activity and Binding of Substrates Characterized by pH

Kirsten R. Wolthers and Michael I. Schimerlik

3.1 Summary

The pH-dependence of the basal and calmodulin (CaM)-stimulated neuronal nitric-oxide synthase reduction of 2,6-dichlorophenolindolphenol (DCIP) and cytochrome c^{3+} was investigated. The wave-shaped log V profile revealed optimal DCIP reduction occurred when a group with a pK_a of 7.1-7.3 was ionized. The $(V/K)_{NADPH}$ and $(V/K)_{DCIP}$ pH profiles increased with the protonation of a group with a pK_a of 6.5 or 5.9 and the ionization of 2 groups with the same pK_a of either 7.5 or 7.0, respectively. $(V/K)_{DCIP}$ also decreased with the ionization of a group with a pK_a of 9.0. Similar log V, $(V/K)_{NADPH}$, and $(V/K)_{DCIP}$ pH profiles for the reduction of DCIP were obtained with and without CaM, indicating it does not influence ionizable groups involved in catalysis or substrate binding. In contrast, CaM affected the pH-dependence of cytochrome c^{3+} reduction. The wave-shaped log V profile for basal cytochrome c^{3+} reduction revealed that ionization of a group, pK_a of 8.6, increased catalysis. V for CaM-stimulated cytochrome c^{3+} reduction displayed a bell-shaped pH-dependence with the protonation of a group with a pK_a of 6.4, and the ionization of a group with a pK_a of 9.25, resulting in a loss of activity. The pH profiles for $(V/K)_{cytc}$ with and without Ca^{2+}-CaM were bell-shaped with the ionization of group at pK_a of 7.1 and 7.6 (Ca^{2+}-CaM) and pK_a of 9.38 and 9.62 (Ca^{2+}-CaM), increasing and decreasing $(V/K)_{cytc}$, respectively. These results suggest that Ca^{2+}-CaM may change the nature of the rate-limiting catalytic steps or the ionizable groups involved in cytochrome c^{3+} reduction.

3.2 Introduction

The nitric-oxide synthases (NOS) are a family of three mammalian isozymes which produce the physiologically important free radical nitric oxide, NO, (for reviews see 2, 201, 217, 219, 252). Each of the isozymes functions as a homodimer to produce NO and L-citrulline via the 5-electron oxidation of L-arginine (3, 4). The polypeptide subunit for each of the three isoforms is divided into two distinct domains. The oxygenase domain contains a P450-type heme, and the binding sites for the cofactor (*6R*)–5,6,7,8-tetrahydro-L-biopterin (H_4B) and the substrate L-arginine (11, 14, 47, 221). The reductase domain contains one mol each of FAD and FMN and the binding site for NADPH (15, 149). The calmodulin (CaM)-binding motif, located at the center of the NOS polypeptide subunit, tethers the oxygenase domain to the reductase domain (19, 30, 220). A rise in intracellular Ca^{2+} concentrations promotes the binding of CaM to neuronal (nNOS) and endothelial (eNOS) which triggers interdomain electron transfer, an essential step for NO-synthesis (18, 76, 133). In contrast, CaM is tightly bound to the inducible (iNOS) isoform at basal intracellular levels of Ca^{2+}; its activity is modulated at the transcriptional level through the action of cytokines (220).

The dual flavin-containing domain of NOS is structurally and functionally similar to NADPH-cytochrome P450-reductase (CPR) (15, 149). During catalysis, the enzyme-bound flavins on nNOS and CPR cycle between the one- and three-electron reduced states as they shuttle reducing equivalents from NADPH to FAD then FMN and finally to the P450-heme (15, 73, 81, 222, 226). CPR and nNOS are both able to reduce the non-physiological flavin electron acceptors, ferricyanide (FeCN), 2,6-

dichlorophenolindophenol (DCIP), and cytochrome c^{3+} (31, 75). The binding of Ca^{2+}-CaM to nNOS alleviates the inhibition of flavin-mediated electron transfer. This allows nNOS to achieve of the same level of FeCN and DCIP reduction (2- to 3-fold increase) and cytochrome c^{3+} reduction (10- to 20-fold increase), exhibited by CPR (30, 76). The same level of Ca^{2+}-CaM induced stimulation of these activities is achieved with the nNOS reductase domain; thus, this behavior is not attributed to the cofactor triggering electron transfer to the heme (76, 77, 253). Ca^{2+}-CaM also has a negligible effect on the flavin midpoint potentials; thus, the cofactor does not change the thermodynamic driving force behind electron transfer in the reductase domain (73). However, Ca^{2+}-CaM has been shown to increase the pre-steady state rate of electron rate transfer from NADPH to the flavins (76) and induce conformational changes in the diflavin domain (30, 74, 81).

The binding of Ca^{2+}-CaM may remove the suppression of electron transfer by acting on structural components which are absent in CPR. All three NOS isoforms possess 21-40 additional amino acids at the C-terminal tail, and the constitutive isoforms (nNOS and eNOS) contain a 45-50 amino acid insert located in the FMN-binding domain. In the absence of Ca^{2+}-CaM, eNOS and nNOS lacking their C-terminal tail exhibit faster rates of flavin and cytochrome c^{3+} reduction compared to wild-type (78). The CaM-stimulated cytochrome c^{3+} reductase activity was similar for the wild-type and the truncated forms, suggesting that the C-terminal tail acts to suppress electron transfer, which can then be alleviated with the binding of Ca^{2+}-CaM (78). Removal of the 45-50 amino acid sequence in the FMN-domain demonstrated that this is a putative

autoinhibitory element as it promotes the dissociation of CaM at low intracellular Ca^{2+} concentrations and inhibits electron transfer in the absence of Ca^{2+}-CaM (79, 80, 82).

The NOS isoforms exhibit varying rates of NO-synthesis, which is correlated to the rate of interflavin electron transfer and/or transfer between the FMN and the heme (38). Because the efficiency or behavior of the reductase domain controls the rate of NO production, there is great interest in the role of Ca^{2+}-CaM in mediating electron transfer. The steady-state kinetic mechanisms for DCIP and cytochrome c^{3+} reduction were the same in the presence and absence of the activated cofactor. Both the reduction of DCIP and cytochrome c^{3+} occur in two-half reactions by a di-iso one-site ping-pong and a non-classical iso (two-site) ping-pong mechanism, respectively. (254). The role Ca^{2+}-CaM is further investigated in this manuscript by determining its influence on ionizable groups associated with catalysis or binding of substrates. The pH profile for V yields pK_a values for groups involved in rate limiting step(s) of the mechanism. In contrast, the pK_a values in the V/K pH profiles represent groups in the steady-state mechanism that participate in events from binding of the substrate up to the first irreversible step, which could be a catalytic step or product release. If the pK_a to appears in both the V and V/K profiles, it represents the particular ionization state of a group on the enzyme or substrate that is limiting for catalysis rather than one involved solely in substrate binding (255). The proposed steady-state kinetic mechanisms for the reduction of these two substrates also provided a framework for the interpretation of the dependence of V and V/K for substrates on pH.

3.3 Experimental Procedures

3.3.1 Materials

NADPH, $NADP^+$, DCIP, and horse heart cytochrome c^{3+} were purchased form Sigma Chemical Co. (St Louis, MO). Hepes was purchased from Research Organics (Cleveland, OH). Tetrahydrobiopterin was purchased from Cayman Chemical (Ann Arbor, MI), the 2', 5'-ADP-Sepharose was purchased from Amersham Pharmacia Biotech (Piscataway, NJ), and the calmodulin-Sepharose and calmodulin were generous gifts of Dr. S. Anderson (Oregon State University). All other reagents were from Sigma Chemical Co. (St Louis, MO).

3.3.2 Protein expression and purification

Recombinant rat nNOS was purified from *E. coli* strain BL21(DE3) after over expression of the cDNA with the pCWori vector. The enzyme was purified according to the protocol published by Gerber and Ortiz de Montellano with slight modification (229). The rate of NO production was measured by the hemoglobin-NO capture assay at 25 °C following the procedures of Stuehr *et al* (22). nNOS was more than 85% pure as judged by densometric scan of an SDS-polyacrylamide gel with a specific activity of 150 nmol NO min^{-1} mg^{-1} at 25° C. Protein concentration was determined with the Lowry Assay using bovine berum albumin as a standard (230).

3.3.3 Substrate titrations

^{31}P-NMR spectra for NADPH titration curves were obtained with a Bruker DRX 600 spectrometer operating at 242.9 MHz using a 90° observation pulse. Chemical shifts were referenced to H_2O. Experiments were performed at 25°C using a 5 mm Nuclear Magentic Resonance (NMR) tube. The spectra were collected unlocked with constant compensation for field drift. Titration samples contained 1 mM NADPH in the buffer used for the pH kinetic studies. The spectrophotometric titration of DCIP at 600 nm was performed at 25 °C. The samples contained 20 μM DCIP in the buffer used for the pH kinetic studies.

3.3.4 Measurement of reductase activities

A three-component buffer system consisting of 15 mM MES (p K_a 6.15), 15 mM Hepes (pK_a 7.55) and 15 mM CHES (pK_a 9.5) was used for the pH-dependence studies. The buffer was titrated to the desired pH with NaOH. Reactions were performed in a 5.0 mL volume at 25 °C using either a 1 cm or 5 cm path length cuvette. The rate of cytochrome c^{3+} was measured by following absorbance changes at 550 nm ($\Delta\ \varepsilon = 21.1\ mM^{-1}\ cm^{-1}$) (231). The rate of DCIP reduction was measured by following absorbance changes at 600 nm using an extinction coefficient for DCIP that was calculated at each pH (described below). Reaction mixtures contained variable concentrations of substrates (NADPH, cytochrome c^{3+} or DCIP), and where appropriate 10 μM $CaCl_2$ and 100 nM CaM. Reactions were initiated by the addition of 0.5 – 4 μg of nNOS to a 5 mL reaction volume. The pH profiles were extended as far as possible into the pH extremes until

enzyme or substrate instability prevented the measurement of initial rates. At pH values below 7 the level of uncatalyzed NADPH oxidation in the absence of nNOS were subtracted from initial rates obtained in the presence of the enzyme.

3.3.5 Data analysis

Values for the various parameters were derived by non-linear least-squares fitting (Levenberg-Marquardt algorithm) of a given equation to the data using the computer programs Origin v. 4.0 (MicroCal Software Inc., North Hampton, MA) or MicroMath Scientist (MicroMath Scientific Software, Salt Lake City, UT.). V and $(V/K)_{cytc}$ values for the basal and CaM-stimulated reduction of cytochrome c^{3+} were obtained by measuring the rate of cytochrome c^{3+} reduction at fixed saturating concentration of NADPH (10 μM). The initial rates were fit to the Michaelis-Menton equation (eq 3.1).

$$v_i = \frac{VA}{K_m + A} \tag{3.1}$$

where v_i represents the initial rate, V is the maximal velocity, A is variable substrate concentration, and K_m the Michaelis constant for the variable substrate. Similarly, $(V/K)_{NADPH}$ values for the basal and CaM-stimulated reduction of DCIP were obtained from a fit to eq 3.1 with DCIP present at a constant sub-saturating concentration of 20 μM. Concentrations of NADPH > $2K_{NADPH}$ inhibits DCIP reduction at DCIP concentrations < K_{DCIP}; thus, $(V/K)_{DCIP}$ in the presence and absence of Ca^{2+}-CaM was determined by fitting the initial rate at various DCIP concentrations with fixed non-

saturating levels NADPH (0.3 μM) and fitting the data to eq 3.1. This method is valid since the basal and CaM-stimulated reduction of DCIP follows a ping-pong mechanism (254); therefore, the concentration of the nonvariable substrate can be maintained at nonsaturating levels without effecting the value of (*V/K*) for the variable substrate. The log *V* profile for basal and CaM-stimulated reduction of DCIP was determined by measuring the initial rate at saturating amounts of NADPH (20 μM) and DCIP (100 μM) in the reaction mixture.

Titration curves for NADPH and DCIP (Figure 3.1A and 3.1B, respectively) were fit to the following equation:

$$Y = \frac{\left[Y_H + Y_L(H/K)\right]}{(H/K + 1)} \tag{3.2}$$

where Y is the ^{31}P-NMR chemical shift (NADPH profile) or the extinction coefficient (DCIP profile), H is the proton concentration, K is the acid dissociation constant, and Y_L and Y_H are the low- and high-pH plateau values, respectively, for Y. All plots of the kinetic data contain error bars for each the average of four data points corresponding to one standard deviation. The following equation was used to fit a wave with ionization of one group leading to an increase in the rate of catalysis.

$$\log Y = \log\left[\frac{Y_H + Y_L(H/K_2)}{(1 + H/K_2)}\right] \tag{3.3}$$

where Y denotes the maximal velocity, H is the proton concentration, K_2 is the acid dissociation constant, and Y_H and Y_L are the values for Y at the high- and low- pH

plateaus, respectively. The log V pH profile for the reduction of DCIP in the absence and presence of Ca^{2+}-CaM (Figure 3.2) and nNOS-catalyzed basal reduction of cytochrome c^{3+} (Figure 3.5A) were fit to eq 3.3. The $(V/K)_{NADPH}$ pH profiles (Figure 3.3) with DCIP as the second substrate in the presence and absence of Ca^{2+}-CaM in which the ionization of a group with a low pK_a decreases $(V/K)_{NADPH}$ and the ionization of two groups with the same pK_a leads to an increase in $(V/K)_{NADPH}$ were fit to the equation 3.4.

$$\log Y = \log\left[\frac{Y_H + Y_L(H/K_1)(H/K_2)^2}{(1+H/K_1)(1+H/K_2)^2}\right] \tag{3.4}$$

where Y is $(V/K)_{NADPH}$, H is the proton concentration, K_1 is the acid dissociation of the group which ionizes at a lower pH, K_2 is the acid dissociation constants for the two groups that ionize at a high pH, and Y_H and Y_L are the values of $(V/K)_{NADPH}$ at the high- and low-pH plateaus, respectively. The $(V/K)_{DCIP}$ pH profiles (Figure 3.4), in which the ionization of group with a low pK_a, the protonation of two groups with the same mid-range pK_a, and the ionization of a group with a high pK_a all lead to a decrease in $(V/K)_{DCIP}$ were fit to the following equation.

$$\log Y = \log\left[\frac{Y_H + Y_L(H/K_1)(H/K_2)^2}{(1+H/K_1)(1+H/K_2)^2(1+H/K_3)}\right] \tag{3.5}$$

where Y is $(V/K)_{DCIP}$, K_1, K_2, K_3 are the dissociation constants for the groups that ionize at low, neutral and high pH, respectively. Y_H and Y_L are the high- and low-pH plateau values for Y, respectively. The pH profiles that were bell-shaped, where catalysis

requires the ionization of a group at a low pH and the protonation of a group at a higher pH, were fit to the following equation

$$\log Y = \log\left[\frac{Y_H}{\left(1 + H/K_2 + K_1/H\right)}\right] \tag{3.6}$$

where Y is V or $(V/K)_{cytc}$, K_1 and K_2 are the dissociation constants for the groups that ionize at low and high pH, respectively, and Y_H is the value for V or (V/K) when both groups are in their preferred ionization states. The log V versus pH profile for CaM-stimulated cytochrome c^{3+}, reduction (Figure 3.5B) and the $(V/K)_{cytc}$ versus pH profiles with and without Ca^{2+}-CaM (Figure 3.6) where fit to eq 3.6.

3.4 Results

3.4.1 pH-characterization of substrates

The pK_a for ionizable groups on NADPH and DCIP were determined to aid in the interpretation kinetic pH profiles. The pH variation in the chemical shift of the ^{31}P by NMR has been the method previously employed to determine the pK_a of the NADPH 2'phosphate. The pK_a values were reported to be 6.1 for NADPH in 100% D_2O containing 500 mM KCl at 11°C (256) and 6.52 in 10 % D_2O and 10% (w/v) glycerol at 25°C (257). At an ionic strength of 800 mM and in the absence of D_2O, Sem and Kasper reported a pK_a of 5.91 for the 2'-phosphate of NADPH (258). From the variation in the above reported values, it is apparent that both ionic strength and the presence of D_2O will affect the pK_a of the NADPH 2'-phosphate. Therefore, it was necessary to determine the pK_a under the conditions of our pH studies. To avoid the use of D_2O in

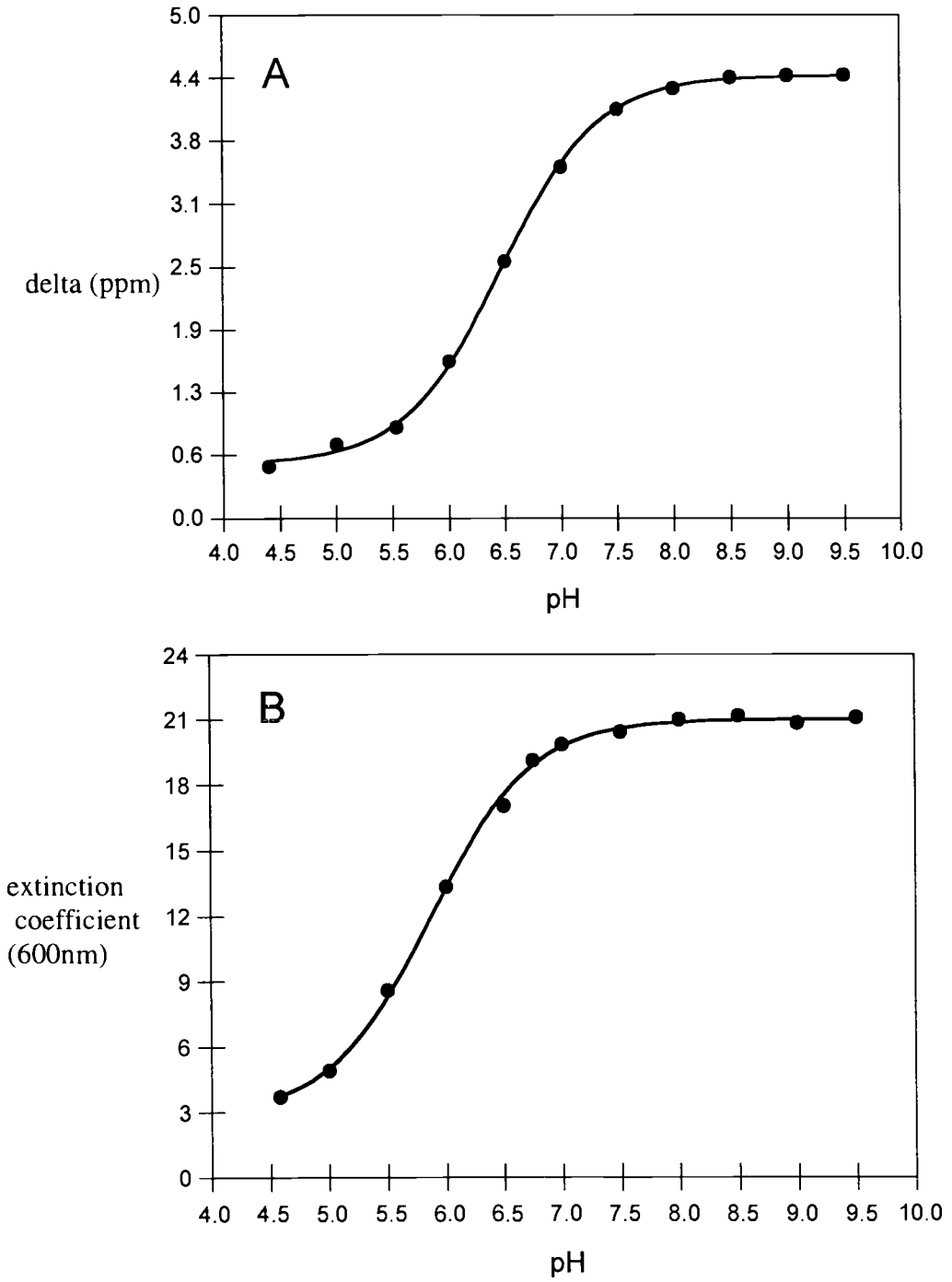

Figure 3.1 (A) pH variation of the ^{31}P-NMR chemical shift of the 2'-phosphate of NADPH in the buffer used for pH studies. (B) pH variation of the extinction coefficient for DCIP at 600 nm in the buffer used for the pH studies A fit of the data to eq 3.2 gave a pK_a of 6.46 for panal A and a pK_a of 5.87 for panal B.

Table 3.1 pH-dependence of kinetic parameters for DCIP reduction

Kinetic Parameter	Ca^{2+}-CaM	pK_1	pK_2	pK_3
V	-		7.65 ± 0.06	
V	+		7.77 ± 0.04	
$(V/K)_{NADPH}$	-	6.47 ± 0.37	7.51 ± 0.07	
$(V/K)_{NADPH}$	+	6.47 ± 0.02	7.56 ± 0.05	
$(V/K)_{DCIP}$	-	5.86[a]	6.97 ± 0.07	9.00 ± 0.22
$(V/K)_{DCIP}$	+	5.86[a]	7.08 ± 0.07	9.01 ± 0.21

[a] value was fixed

± 0.02. (B) pH variation of the extinction coefficient for DCIP at 600 nm in the buffer

the buffer the spectra were collected unlocked with constant compensation for the field drift. At 25°C the pK_a of the NADPH 2'-phosphate is 6.47 ± 0.02 (Figure 3.1A).

A hydroxyl group on DCIP is known to ionize in the pH range studied and change the extinction coefficient for the substrate. The pK_a of this group under the buffering conditions used for the nNOS pH studies was determined by measuring the absorbance of used for the pH studies. A nonlinear least squares fit of eq 3.2 yielded a pK_a for the hydroxyl group of 5.87 ± 0.02 (Figure 3.1B) which is identical within error to the value obtained by Sem and Kasper (258). The extinction coefficients used for calculating initial rates of DCIP reduction in the pH-dependence studies were calculated at each pH with eq 3.2, which assumes an extinction coefficient of 21.0 mM^{-1} cm^{-1} at pH 7.0 (259).

3.4.2 pH-dependence of kinetic parameters for DCIP reduction

The kinetic parameters for the nNOS-catalyzed reduction of DCIP were measured over the pH range of 5.5 – 9.0. The pK_a values for V, $(V/K)_{NADPH,}$, and $(V/K)_{DCIP}$ are listed in Table 3.1. The pH-dependence of V for the basal and CaM-stimulated reduction of DCIP were wave-shaped with the ionization of a group, pK_a of 7.65 ± 0.06 and 7.77 ± 0.04 (Ca^{2+}-CaM) leading to an increase the rate of DCIP reduction (Figure 3.2).

The $(V/K)_{NADPH}$ versus pH profiles for basal and CaM-stimulated DCIP reductase activity are shown Figure 3.3. $(V/K)_{NADPH}$ increased in the low-pH extreme as a group a

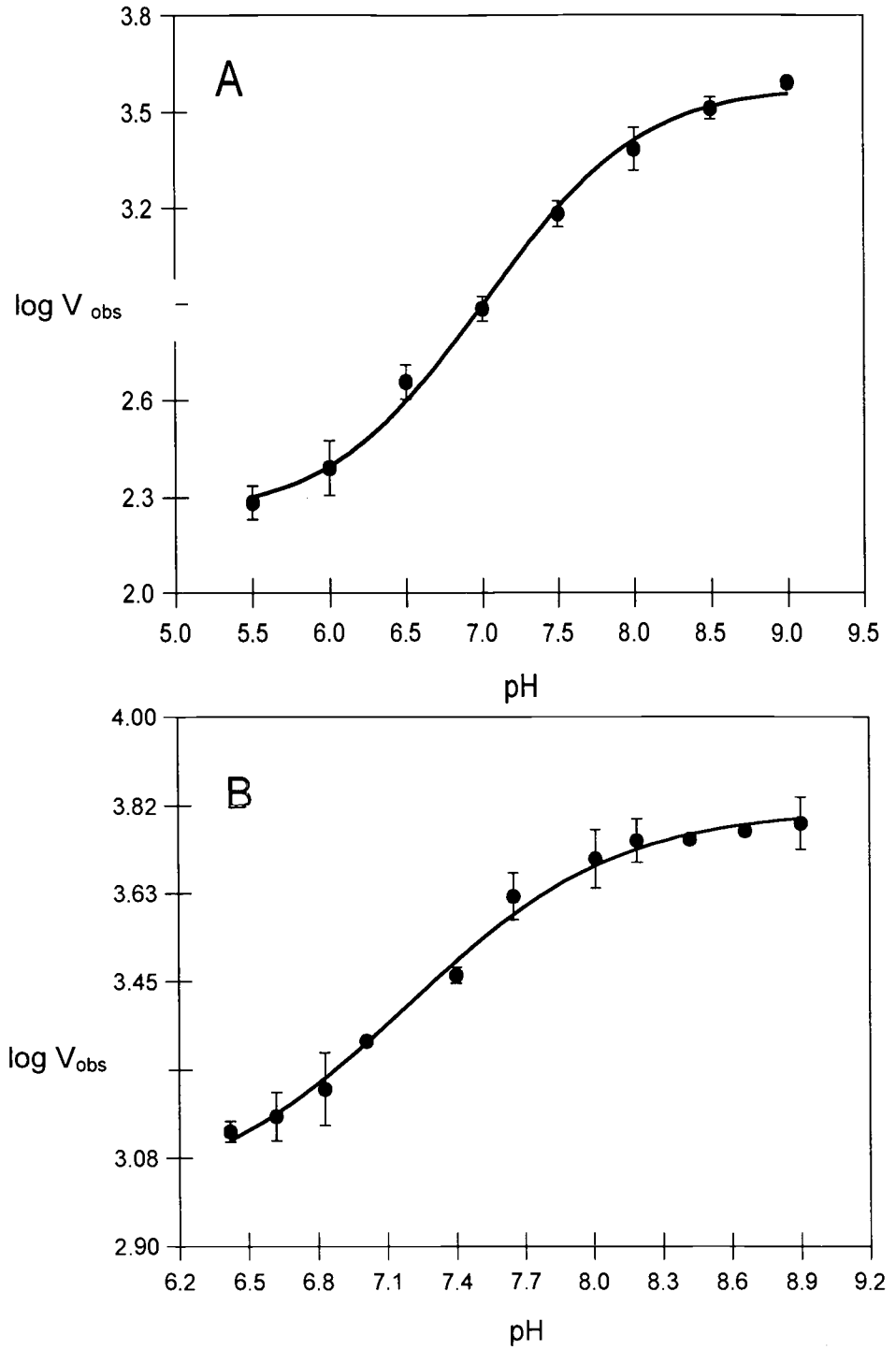

Figure 3.2 pH-dependence of V for the nNOS-catalyzed reduction of DCIP in the (A) absence and (B) presence of 10 μM $CaCl_2$ and 100 nM CaM. The reaction mixtures also contained 100 μM DCIP and 20 μM NADPH and 1.5 μg of nNOS. The data points in A and B were fit to equation 3.3 and the pK_a values are listed in Table 3.1.

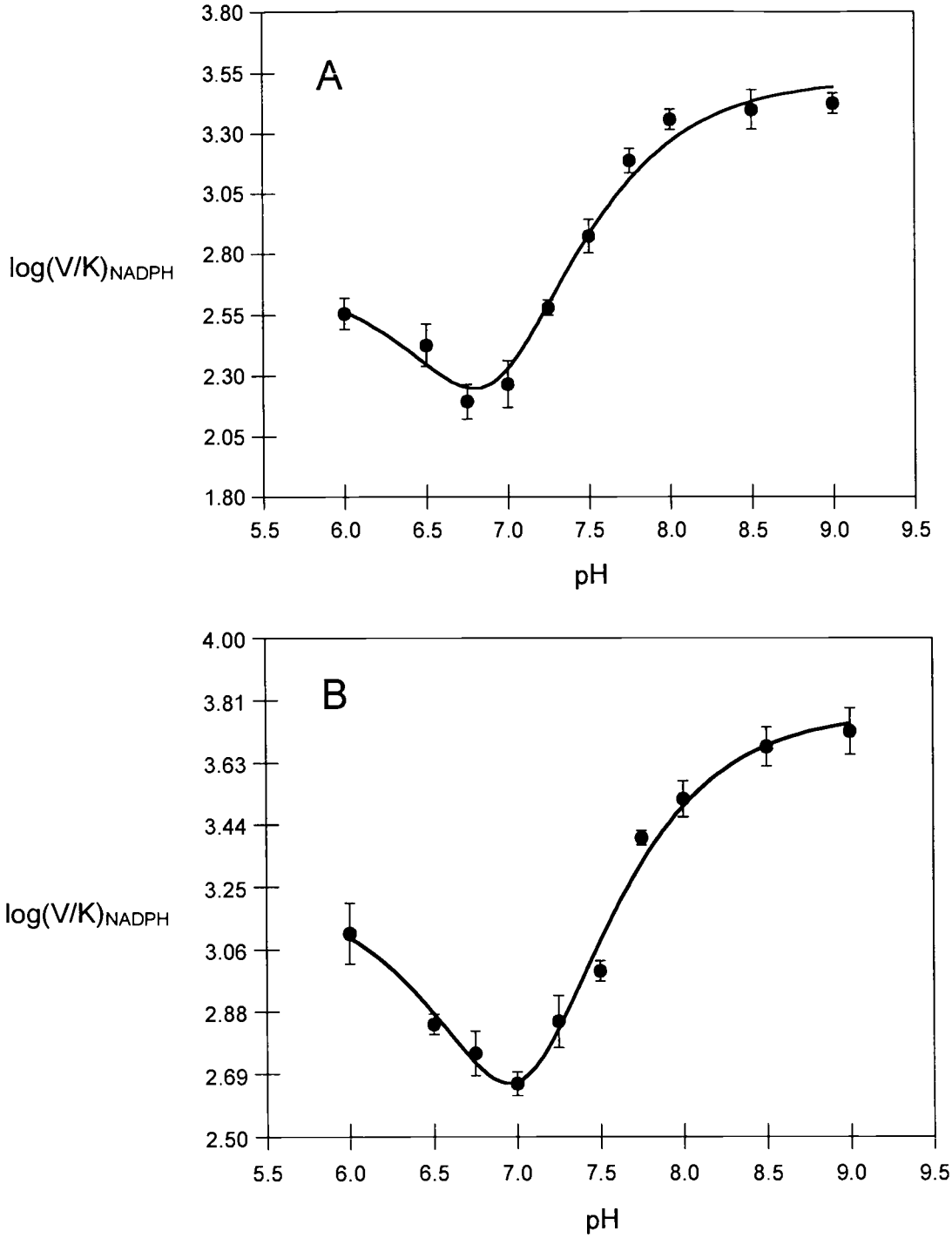

Figure 3.3 pH dependence of $(V/K)_{NADPH}$ for the nNOS-catalyzed reduction for DCIP in the (A) absence and in the (B) presence of 10 μM $CaCl_2$ and 100 nM CaM. The reaction mixtures also contained varying concentrations of NADPH, 20 μM DCIP and 0.5 μg of nNOS. The data points in A and B were fit to equation 3.4 and the pK_a values are listed in Table 3.1.

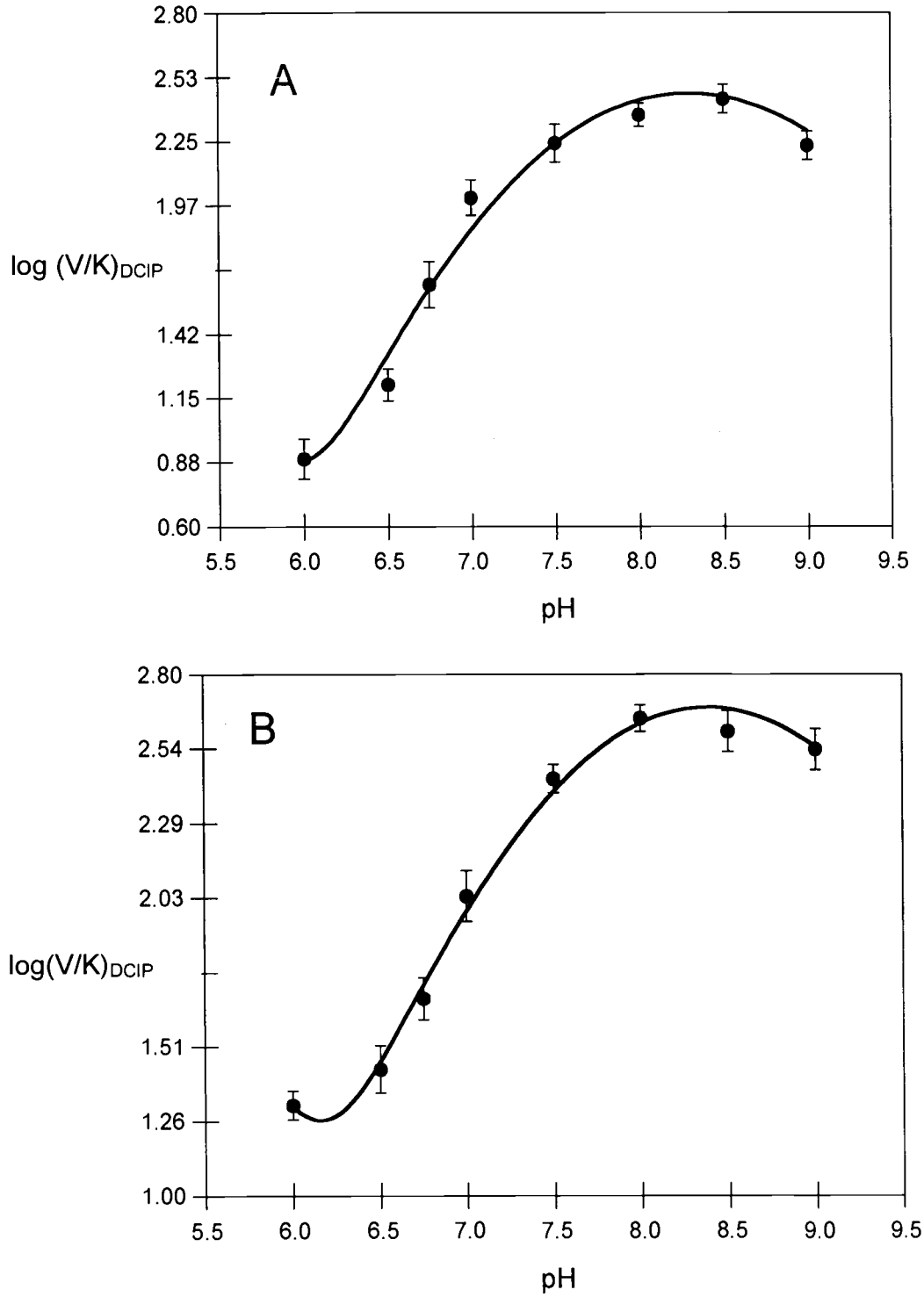

Figure 3.4 pH dependence of $(V/K)_{DCIP}$ for the nNOS-catalyzed reduction for DCIP in the (A) absence and in the (B) presence of 10 μM $CaCl_2$ and 100 nM CaM. The reaction mixtures also contained varying concentrations of DCIP, 0.25 μM NADPH and 0.5 μg of nNOS. The data points in A and B were fit to equation 3.5 and the pK_a values are listed in Table 3.1.

with a pK_{a1} of 6.47 ± 0.37 (basal) and 6.47 ± 0.20 (+Ca^{2+}-CaM) was protonated. The pK_{a1} may reflect the ionization of the 2'phosphate of NADPH, since it equals the pK_a determined in the titration of ^{31}P for NADPH (Figure 3.1A), and it does not appear in the log *V* profile (Figure 3.2). The increase in $(V/K)_{NADPH}$ at a low pH suggests that the protonated or monoanionic form of the 2'-phosphate is the preferred state for binding of the nucleotide to nNOS. $(V/K)_{NADPH}$ increases with the ionization of two groups each with pK_{a2} of 7.51 ± 0.07 (basal) and 7.56 ± 0.05 (Ca^{2+}-CaM). One of the groups in each profile reflects a group involved in catalysis since a similar pK_a is observed in the log *V* pH profile (Figure 3.2).

A plot of log $(V/K)_{DCIP}$ versus pH also increases at low pH (Figure 3.4). The pK_a for this group is shifted to the left compared to the pH profile for $(V/K)_{NADPH}$ (Figure 3.3). As such, the number of data points was insufficient to obtain an accurate determination of pK_{a1} when eq 3.4 or eq 3.5 was to fit the data. The pH profile could not be extended to lower pH values due to the increase in uncatalyzed NADPH oxidation. However, if we assume that this group originates from the ionization of the hydroxyl group on DCIP and fix pK_{a1} at 5.87 during the fitting routine, a reasonable fit of the data is obtained with eq 3.5. The ionization of two groups which lead to an increase in $(V/K)_{DCIP}$ had equal pK_a values of 6.97 ± 0.07 (basal) and 7.08 ± 0.07 (Ca^{2+}-CaM). On the basic pH limb, $(V/K)_{DCIP}$ decreased with a ionization of a group, pK_{a3} of 9.00 ± 0.22 (basal) and 9.01 ± 0.21 (Ca^{2+}-CaM). A more accurate determination of pK_{a3} could not be obtained because nNOS quickly lost stability at pH > 9.0. The value of pK_{a2} is

Table 3.2 pH-dependence of kinetic parameters for cytochrome c^{3+} reduction

Kinetic Parameter	Ca^{2+}-CaM	pK_1	pK_2
V	-	8.60 ± 0.04	
V	+	6.40 ± 0.06	9.25 ± 0.09
$(V/K)_{cytc}$	-	7.10 ± 0.12	9.38 ± 0.23
$(V/K)_{cytc}$	+	6.47 ± 0.02	9.62 ± 0.37

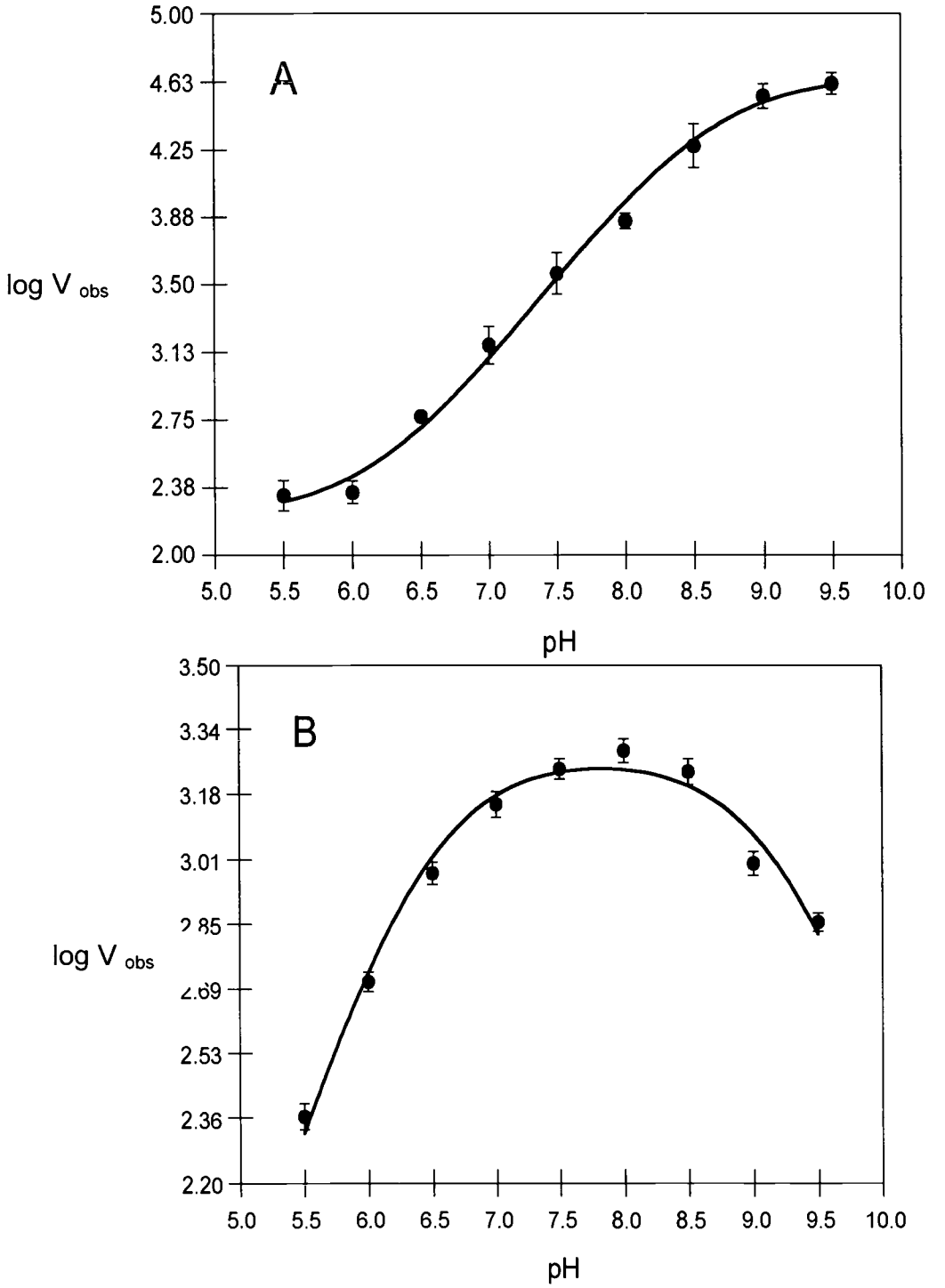

Figure 3.5 pH-dependence of V for the nNOS-catalyzed reduction of cytochrome c^{3+} in the (A) absence and (B) presence of 10 μM $CaCl_2$ and 100 nM CaM. The reaction mixtures contained varying concentration of cytochrome c^{3+} and 20 μM NADPH, 0.5 μg of nNOS. The data points in A were fit to eq 3.3 and the data points in B were fit to eq 3.6. The pK_a values are listed in Table 3.2.

comparable to the pK_{a2} in the log V pH profile for basal and CaM-stimulated reduction of DCIP (Figure 3.2); therefore it likely reflects an ionizable group involved in catalysis and not the binding of group, pK_a of 6.40 ± 0.06, which is must be unprotonated for activity and a slope of −1 for DCIP. However, the second pK_{a2} and pK_{a3}, represent ionizable groups on nNOS that affect the binding of DCIP as they only appear in the log $(V/K)_{DCIP}$ versus pH profile.

3.4.3 pH-dependence of the kinetic parameters for cytochrome c^{3+} reduction

The pK_a values associated with pH-dependence of the steady-state kinetic parameters for cytochrome c^{3+} reduction are summarized in Table 3.2. The pH profile for V for the basal reduction of cytochrome c^{3+} forms a wave, where the ionization of a group with a pK_a of 8.60 ± 0.04 leads to optimal cytochrome c^{3+} reductase activity (Figure 3.5A). In contrast, the log V pH profile for the CaM-stimulated reduction of cytochrome c^{3+} forms a bell-shaped curve (Figure 3.5B). The log V pH profile has a slope of 1 from a group, pK_a of 9.25 ± 0.09 that must be protonated for activity. Comparison of the pH-dependence on V for basal and CaM-stimulated cytochrome c^{3+} reduction indicates that Ca^{2+}-CaM incorporates either 2 different ionizable groups or shifts the lower pK_a over 2 pH units and incorporates an additional group that ionizes at a higher pH.

The pH variation for $(V/K)_{cytc}$ for the basal and CaM-stimulated reduction of cytochrome c^{3+} are shown in Figure 3.6. Both profiles show a bell-shaped curve, with the ionization of a group with a pK_{a1} of 7.10 ± 0.12 and 7.58 ± 0.12 (Ca^{2+}-CaM)

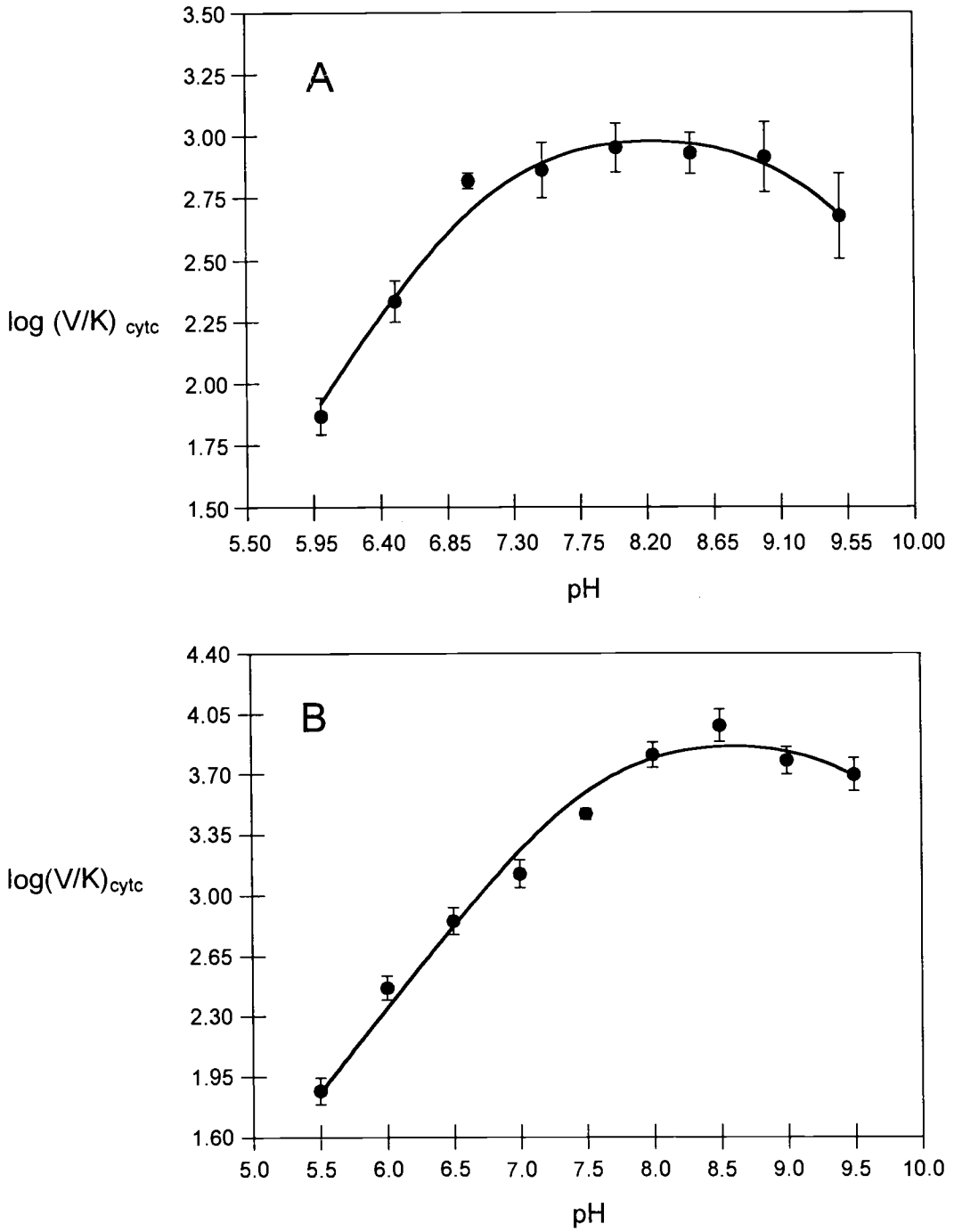

Figure 3.6 pH-dependence of $(V/K)_{cytc}$ for the nNOS-catalyzed reduction of cytochrome c^{3+} in the (A) absence and (B) presence of 10μM $CaCl_2$ and 100 nM CaM. The reaction mixtures contained varying concentration of cytochrome c^{3+} and 20 μM NADPH, 0.5 μg of nNOS. The data points in A and B were fit to equation 3.2. The pK_a values are listed in Table 3.2.

increasing $(V/K)_{cytc}$ and the ionization of a group with a pK_{a2} of 9.38 ± 0.23 and 9.62 ± 0.37 (Ca^{2+}-CaM) resulting in a decrease in $(V/K)_{cytc}$ (Table 3.2). For the basal cytochrome c^{3+} reductase activity, the pK_{a1} shifts from 8.6 in the log V pH profile to 7.1 in the log (V/K) pH profile. Since pK_{a1} appears in both profiles, it reflects an ionizable group involved in a catalytic step during the basal and CaM-stimulated reduction of cytochrome c^{3+}. The ~.1.5 pH unit perturbation for pK_{a1} for the basal cytochrome c^{3+} reductase activity to the left in the log $(V/K)_{cytc}$ profile could reflect differences in the microenvironment of the cytochrome-free enzyme compared to the nNOS complexed with the electron acceptor. The log $(V/K)_{cytc}$ pH profile also shows an additional pK_{a2} for a basic group, which is not in the corresponding log V pH profile. Thus, the ionization of this group is responsible for the decrease in binding of cytochrome c^{3+}. The calculated pK_a values appear in both bell-shaped log V and log $(V/K)_{cytc}$ versus pH profiles for CaM-stimulated cytochrome c^{3+} reduction; thus, they represent groups involved in catalysis. The pK_{a1} value shifts outward from the log V pH profile by 1.2 pH units, possibly reflecting a slow substrate release step or solvent exclusion from the active site.

3.5 Discussion

3.5.1 Interpretation of pH profiles for the reduction of DCIP

The interpretation of the pH profiles for the catalysis and binding of substrates for basal and CaM-stimulated nNOS catalyzed reduction of DCIP and cytochrome c^{3+} will be

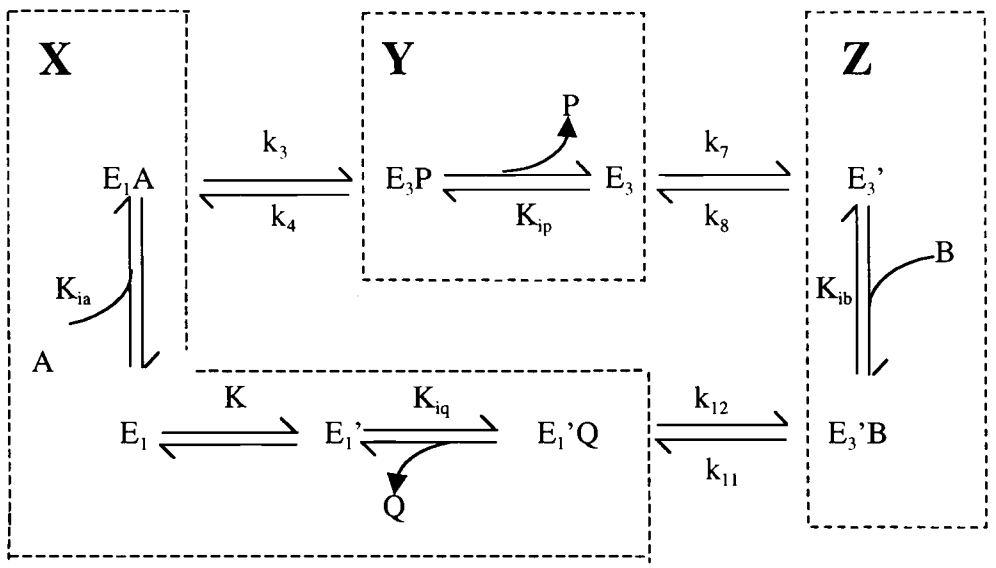

Figure 3.7 Kinetic scheme for a di-iso ping-pong bi-bi mechanism for the nNOS-catalyzed reduction of DCIP. *A*, *B*, *P*, and *Q* represent NADPH, $DCIP_{ox}$, $NADP^+$, and $DCIP_{red}$, and the K_i values refer to their respective dissociation constants. E_1 and E_1' are the one-electron (FAD/FMNH•) forms of nNOS that exclusively bind NADPH and 2'AMP, respectively. E_3 and E_3' are the three-electron ($FADH•/FMNH_2$) or ($FADH_2/FMNH•$) forms of nNOS that exclusively bind $NADP^+$ and $DCIP_{ox}$, respectively. *K* is the equilibrium constant for the conversion of the two enzyme forms, E_1 and E_1'

done in the context of their proposed steady-state kinetic mechanism (254). Initial velocity, product, and dead-end inhibition studies were consistent with DCIP reduction following a di-iso ping-pong bi-bi mechanism drawn in Figure 3.7 in the presence and absence of CaM. The features of the proposed mechanism include the following: (1) NADPH, binds to the one-electron reduced state, E_1. (2) The oxidation of NADPH reduces nNOS to the three-electron reduced state, E_3. (3) A steady-state isomerization of E_3 occurs after the release of $NADP^+$, and prior to the binding of DCIP, (i.e. E_3 to E_3'). (4) After the reduction and release of reduced DCIP, there is a rapidly equilibrating isomerization of the free enzyme form prior to the binding of NADPH, (i.e E_1' to E_1). E_1', is able to bind the NADPH analog, 2'-AMP, but not the substrate NADPH. To simplify the derivation of the di-iso ping pong mechanism the binding of substrates/inhibitors and the release of products is assumed to occur in rapid equilibrium. The derivation of the rate equation for the mechanism drawn in Figure 3.7 allowed V and the Michaelis constants for NADPH and DCIP to be defined in terms of the following rate constants.

$$\frac{V}{E_t} = \frac{k_3 k_7 k_{11}}{\left(k_3 k_7 + k_3 k_{11} + k_7 k_{11}\right)} \tag{3.7}$$

$$K_A = \frac{K_{iA}(k_7 k_{11})\left(1 + 1/K\right)}{\left(k_3 k_7 + k_3 k_{11} + k_7 k_{11}\right)} \tag{3.8}$$

$$K_B = \frac{K_{iB}\left(k_3 k_7 + k_3 k_8\right)}{\left(k_3 k_7 + k_3 k_{11} + k_7 k_{11}\right)} \tag{3.9}$$

where V is the maximal velocity, E_t is the nNOS concentration, K_A and K_B are the Michaelis constants for NADPH and DCIP, respectively and K_{iA} and K_{iB} are their

corresponding dissociation constants. The rate constants are the same as those in Figure 3.7, and K (equal to E_1/E_1') is the equilibrium constant for the conversion of the two free enzyme forms.

The log V pH profile for the basal and CaM-stimulated reduction of DCIP forms a wave where the ionization of a group with a pK_a of 7.5 to 7.6 leads to an increase in catalysis (Figure 3.2). The rate of catalysis reaches a plateau at high and low pH; therefore, it follows the simplified mechanism shown in Scheme 3.1; where the proton can associate with either the substrate free or substrate-enzyme binary complex, and both the ionized and protonated forms of nNOS are catalytically active.

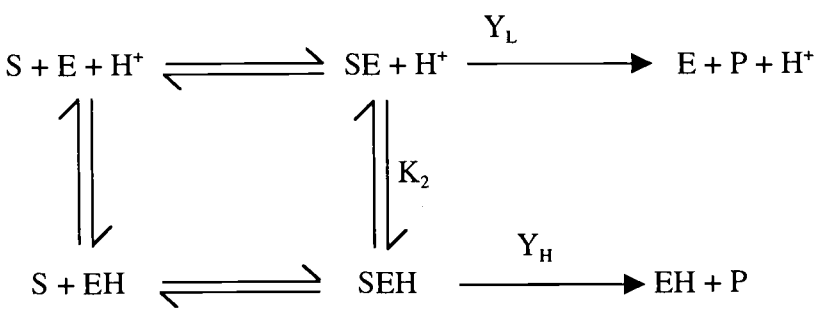

(Scheme 3.1)

While (V/K) profiles generally show a loss of activity when groups are incorrectly protonated, V profiles may show changes to a new plateau level when ionization of a group increases the rate of the step that is normally rate-limiting (233). Thus according to eq 3.7, the ionization of a group that leads to an increase in a rate-limiting step may affect hydride transfer, k_3, the steady-state isomerization of E_3 to E_3', k_7 and/or the rate of electron transfer to DCIP, k_{11}.

To discern which of these rate constants may be affected by pH, the log $(V/K)_{NADPH}$ and the log $(V/K)_{DCIP}$ profiles were investigated. $(V/K)_{NADPH}$ and $(V/K)_{DCIP}$ are defined by the following rate and equilibrium constants.

$$\left(\frac{V/E_t}{K_A}\right)_{NADPH} = \frac{k_3}{K_{iA}(1+1/K)} \tag{3.10}$$

$$\left(\frac{V/E_t}{K_B}\right)_{DCIP} = \frac{k_7 k_{11}}{K_{iB}(k_7+k_8)} \tag{3.11}$$

The log $(V/K)_{NADPH}$ pH profiles with and without Ca^{2+}-CaM were a similar in shape (Figure 3.3). On the acidic limb, $(V/K)_{NADPH}$ increased due to the protonation of a group with a pK_a of 6.47. As the pH increased, $(V/K)_{NADPH}$ increased as two groups both with a pK_a of 7.5-7.6 ionized. The ionization of one of these groups is responsible for an increase rate of catalysis, since the same pK_a value also appears in the log V profile. As shown in eq. 3.10 the only catalytic rate constant which appears in $(V/K)_{NADPH}$ is k_3, the rate of hydride transfer. Thus the ionization of this group, with a pK_a of 7.5-7.6 increases the rate of k_3. If k_3 is slow, or rate limiting compared to k_7 and k_{11}, then V is largely dependent on k_3. Thus the pK_a of 7.5-7.6 which appears in the log V pH profile may represent a group whose ionization status affects the rate of hydride transfer to from the nictotinamde ring to FAD.

The second group with a pK_a of 7.5-7.6 and the group with a pK_{a1} of 6.47, effect the binding of the nucleotide since they only appear in the log $(V/K)_{NADPH}$ profile and not the log V profile. The value of 6.47 for pK_{a1} was observed in the titration of NADPH 2'-phosphate (Figure 3.1A) suggesting that this pK_a originates from the nucleotide. If this were the case, then the monoanionic form of 2'-phospahate of NADPH preferentially

binds nNOS. This is in contrast to a number of other nicotinamide-binding enzymes including CPR (258), iso-citrate dehydrogenase (257), dihydrofolate reductase (260), and glyceraldehyde-3-phosphate dehydrogenase (261) in which the dianionic form of NADPH preferentially binds. Interestingly, NADPH complexed with these enzymes typically exhibits a lower the pK_a value (5-5.5) for the 2'-phosphate, suggesting that it interacts one or more positively charged groups in the active site or there is distortion of the O-P-O angles (261). The dianionic form of NADPH may also binds to nNOS, provided that the pK_a of the 2'-phosphate is shifted to a lower pH value, as with the above nucleotide-binding enzymes, to prevent it from being observed in the $(V/K)_{NADPH}$ pH profiles. This situation would place the group with a pK_{a1} of 6.47 on nNOS. The second acidic group with a pK_{a2} equal to 7.5 likely originates on nNOS since NADPH does not have an ionizable group with this pK_a value.

Amino acid sequence of the NOS NADPH/FAD binding motif in the reductase domain is homologous to a class of flavoproteins, the transhydrogenases, which include ferridoxin-NADP$^+$ reductase (FNR), CPR, NADH-nitrate reductase, NADH-cytochrome b5 reductase and phthalate dioxygenase reductase (66). The three-dimensional structure of FNR•2'phosphate-AMP complex shows interaction between the 2'-phosphate and residues Ser234, Arg235, Tyr236 and possibly Lys224 (250). These conserved residues have been also been implicated in the binding 2'-phosphate of NADPH with other members of the transhydrogenase family. The corresponding residues in nNOS, Ser1327, Arg1328, Lys1334 and Tyr1336 may also play a role in stabilizing the 2'-phosphate. Site directed mutagenesis combined with pH studies identified Arg597 on CPR with a pK_a of 9.5 as a residue involved in ionic interactions with the 2'-phosphate

of NADPH (262). The log $(V/K)_{NADPH}$ profile for nNOS could not be extended beyond 9.0 due to enzyme instability, preventing a similar pK_a value on the basic limb of the profile from being observed. Assignment of these residues in stabilizing NADPH in nNOS awaits the three-dimensional crystal structure of the enzyme and/or site directed mutagenesis of these residues.

The pH profiles for $(V/K)_{DCIP}$ and $(V/K)_{NADPH}$ are similar in that $(V/K)_{DCIP}$ increases at the low pH limit. A fit of the data to eq 3.4 or eq 3.5 does not generate a defined value for this pK_a, because of an inability to obtain data at the lower pH value. If we assume that this pK_a originates from the ionization of the DCIP hydroxyl, and fix this parameter at 5.87 (Figure 3.1B), then the remaining parameters can be defined through a nonlinear least squares fit of eq 3.5 to the data.

pH-dependence studies on CPR-catalyzed reduction of DCIP revealed that $(V/K)_{DCIP}$ decreases at low pH as a group with a pK_a of 5.9 is protonated (258), which was suggested to originate from the ionization of the DCIP hydroxyl. In contrast, an increase in $(V/K)_{DCIP}$ in both the basal and CaM-stimulated activities indicates that protonated form of DCIP has a higher affinity for nNOS. If this pK_a corresponds to the DCIP hydroxyl group, the change in the direction of the nNOS and CPR $(V/K)_{DCIP}$ pH profiles at acidic pH may be attributed to the two enzymes having different binding sites for DCIP. Alternate binding sites may explain why nNOS depleted of the FMN can reduce DCIP (81), while CPR cannot (226). Alternatively, the lower pK_a may originate from a group on nNOS that facilitates DCIP binding.

A fit of equation 3.5 to the data in Figure 3.4 generated pK_{a2} values for the ionization of two groups ranging between 6.9-7.1 and a pK_a of 8.8-9.2 for the ionization

Site-1:

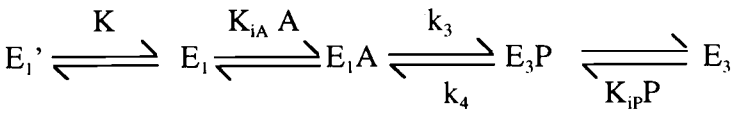

Site-2:

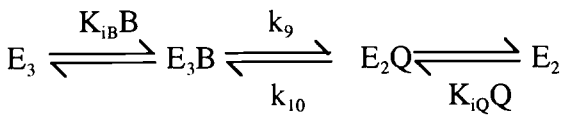

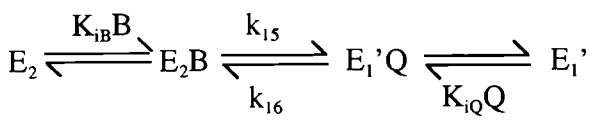

Figure 3.8 The kinetic scheme illustrating the iso (two-site) ping-pong mechanism for the nNOS-catalyzed reduction of cytochrome c^{3+}. *A*, *B*, *P*, *Q*, and *I* represent NADPH, cytochrome c^{3+}, $NADP^+$, and cytochrome c^{2+}, and 2'-AMP, respectively. E_1 and E_1' are the one-electron (FAD/FMNH•) forms of nNOS that exclusively bind NADPH and 2'-AMP, respectively. E_2 and E_3 represent two (FAD/$FMNH_2$) and three-electron (FADH•/$FMNH_2$) reduced form of nNOS. *K* is the equilibrium constant for the conversion of the two enzyme forms, E_1 and E_1'.

of a third group. The presence of Ca^{2+}-CaM did not significantly influence the values of these groups. According to eq 3.12, these pK_a values may be a function of rate constants defining the following (1) steady-state isomerization of E_3 to E_3', k_7 and k_8, (2) dissociation of DCIP, K_{iB} or (3) the rate of electron transfer from the flavins to nNOS, k_{11}.

3.5.2 Interpretation of pH profiles for cytochrome c^{3+} reductase activity

Initial velocity, product, and dead-end inhibition studies for basal and CaM-stimulated reduction of cytochrome c^{3+} are consistent with an iso two-site ping-pong mechanism shown in Figure 3.8 (254). Although the reaction consists of two-half reactions, the two active sites operate independently; therefore, unlike the classical one-site ping-pong mechanism, formation of a ternary complex is possible. NADPH binds in a uni-uni fashion at site 1 and converts the enzyme from E_1 to E_3. Cytochrome c^{3+}, binds in a tert-uni ping-pong fashion at site 2. Similar to the mechanism described for DCIP, after the release second molecule of cytochrome c^{2+}, there is a rapidly equilibrating isomerization of the free enzyme form prior to the binding of NADPH, (i.e E_1' to E_1). E_1', is able to bind the NADPH analog, 2'-AMP, but not the substrate NADPH. According to the derivation of the rate equation for the iso two-site ping-pong mechanism shown in Figure 3.8, the maximum rate of catalysis, V and the Michaelis constants for substrates NADPH and cytochrome c^{3+} are defined in terms of the following rate constants.

$$\frac{V}{E_t} = \frac{k_3 k_9 k_{15}}{(k_3 k_9 + k_3 k_{15} + k_9 k_{15})} \tag{3.12}$$

$$K_A = \frac{(K_{iA})(k_9 k_{15})(1 + 1/K)}{(k_3 k_9 + k_3 k_{15} + k_9 k_{15})} \tag{3.13}$$

$$K_B = \frac{(K_{iB})(k_3 k_{15} + k_3 k_9)}{(k_3 k_9 + k_3 k_{15} + k_9 k_{15})} \tag{3.14}$$

where K_A and K_B are the Michaelis constants for NADPH and cytochrome c^{3+} and K_{iA} and K_{iB} are their corresponding dissociation constants. The rate constants are the same as those in Figure 3.8, and K (equal to E_1/ E_1') is the equilibrium constant for the conversion of the two free enzyme forms.

The log V versus pH profile for the basal cytochrome c^{3+} reductase activity forms a wave where the ionization of a group with a pK_a of 8.6 optimizes catalysis (Figure 3.5A). The V profile may exhibit high and low plateaus at varying pH if ionization of this group increases the rate of the step that is normally rate-limiting (233). According to eq 3.12, the rate-limiting catalytic step is either hydride transfer, k_3 or electron transfer from FMN to cytochrome c^{3+}, k_9, k_{15}.

The pH-dependence on cytochrome c^{3+} reduction is dramatically altered in the presence of Ca^{2+}-CaM as the log V profile is bell-shaped with catalysis dependent on the deprotonation of an acidic group with a pK_a of 6.4 and protonation of basic group with a pK_a of 9.2. The binding of Ca^{2+}-CaM may change the rate-limiting step(s). For example, if the rate of hydride transfer is slower than electron transfer from the flavins to

cytochrome c^{3+} ($k_3 < k_9$, k_{15}), then the pK_a observed in the log V profile for the basal cytochrome c^{3+} reductase activity will reflect the pH-dependence of the former step. The increased rate of k_3 with respect to k_9 and k_{15}, induced by the binding of Ca^{2+}-CaM could potentially shift the pK_a from 8.6 to 6.4. Alternatively, the conformational changes associated with the binding of Ca^{2+}-CaM may change which ionizable groups on nNOS participate in hydride transfer or electron transfer from FMN to cytochrome c^{3+}.

Several candidates for ionizable residues on nNOS that could participate in hydride transfer include Cys1348, Ser1177, and Asp1407. The three dimensional crystal structures of FNR and CPR reveal that these conserved residues are close to the FAD isoalloxazine ring. Substitution of the corresponding cysteine in CPR (Cys630) to an alanine shifted the pK_a of a ionizable group necessary for catalysis from 6.9 to 7.8, indicating that it may be a proton donor/acceptor to FAD the prosthetic group. The corresponding residue in nNOS (Cys1348) is in the putative NADPH-adenine binding motif, adjacent in primary sequence to the C-terminal, which has been shown to inhibit electron transfer to FAD in the absence of CaM (78). The C-terminal tail may affect the location of the Cys1348, Ser1177 and/or Asp1407 by distancing these residues from the FAD causing them to be ineffective in hydride transfer. This may explain the different pK_a values observed in the log V versus pH profile for cytochrome c^{3+} in the presence and absence of Ca^{2+}-CaM. Alternatively the pK_a exhibited in these profiles may also originate from the flavins themselves which exhibit pK_a values in the range studied, and are known to be perturbed dramatically with changes in flavin redox state or when the flavins are protein bound (263, 264).

The pH-dependence of $(V/K)_{cytc}$ was also investigated for basal and CaM-stimulated reduction of cytochrome c^{3+}. Both profiles showed that $(V/K)_{cytc}$ increased with the ionization of an acidic group with a pK_a of 7.1(basal) and 7.6 (Ca^{2+}-CaM) and decreased when a group with a pK_a of 9.4 – 9.6 ionized. According to equation 3.15, which is the expression for $(V/K)_{cytc}$ the pK_a values observed in these pH profiles may reflect groups on nNOS , whose ionization status effect the rates of electron transfer from FMN to cytochrome c^{3+}, k_9 and k_{15} or the binding of cytochrome c^{3+}.

$$\left(\frac{V/E_t}{K_B}\right) = \frac{k_9 k_{15}}{(K_{iB})(k_{15} + k_9)} \tag{3.15}$$

The two groups in the $(V/K)_{cytc}$ also appear in the log V versus pH profile for the CaM-stimulated reduction of cytochrome c^{3+}, indicating that they do not originate from residues on nNOS or cytochrome c^{3+} that effect binding of the substrate. Thus they represent groups involved in electron transfer from the flavins to cytochrome c^{3+}, k_9 and k_{15}. The outward displacement of the acidic pKa by 1.2 pH units from the log $(V/K)_{cytc}$ profile (pK_a = 7.6) to the log V profile (pK_a = 6.4) for CaM-stimulated cytochrome c^{3+} may indicate that k_3 is partially rate limiting such that it effects the observed pK_a value in the log V profile. Alternatively, the shift in pK_a may be attributed to differences in the microenvironment of cytochrome c^{3+}-free nNOS compared to the cytochrome c^{3+}-nNOS complex (i.e. solvent exclusion; 233). Sem and Kasper also noted a 1 pH unit perturbation (7.23 to 6.21) in the log $(V/K)_{cytc}$ to log V pH profiles for CPR reduction of cytochrome c^{3+} (258). Interestingly, the two enzymes exhibit the same pH profiles when they elicit similar kinetic mechanisms (two-site ping-pong) and turnover rates. The former occurs when the steady-state kinetic analysis of CPR-cytochrome c^{3+} reductase is

performed in high ionic strength (850 mM) and the latter occurs when nNOS cytochrome c^{3+} reductase activity is stimulated by Ca^{2+}-CaM.

The pK_a of 9.38, appearing in the $(V/K)_{cytc}$ versus pH profile, is not present in the pH profile for V for basal cytochrome c^{3+} reduction, indicating that this residue is involved in the binding of cytochrome c^{3+}. The ionizable group may originate from cytochrome c^{3+}, which is known to have several lysine residues involved in binding interaction with other electron transfer pairs including CPR (258). The corresponding pK_a may not occur in the $(V/K)_{cytc}$ for CaM-stimulated cytochrome c^{3+} reduction because the group ionizes at high pH, and it is difficult to resolve two versus one pK_a in this region. Alternatively, Ca^{2+}-CaM may induce a conformational change such that this ionizable group no longer participates in the binding interaction between cytochrome c^{3+} and nNOS.

3.6 Acknowledgements

We are grateful to Drs. Sonia Anderson and Dean Malencik for supplying CaM and the CaM-sepharose column and to Dr. Ted Dawson for giving us the cDNA plasmid construct for rat neuronal NOS. We thank Dr. Victor Hsu and Joshua Hicks for performing the NMR studies. We would also like to acknowledge the Nucleic Acids and Proteins Core Facilities of Oregon State University Environmental Health Sciences Center in conducting these studies.

Chapter 4

Neuronal Nitric-oxide Synthase: Substrate and Solvent Kinetic Isotope Effects on the Steady State Kinetic Parameters for the Reduction of 2,6-Dichloroindolphenol and Cytochrome c^{3+}

Kirsten R. Wolthers and Michael I. Schimerlik

4.1 Summary

The neuronal nitric-oxide synthase basal and calmodulin-stimulated reduction of 2,6-dichloroindophenol and cytochrome c^{3+} follow ping-pong mechanisms [Wolthers and Schimerlik (2001) *Biochemistry* 40; 4721-4737]. Primary deuterium (NADPH(D)) and solvent deuterium isotope effects on the kinetic parameters were studied to determine rate-limiting step(s) in the kinetic mechanisms for the two substrates. nNOS was found to abstract the pro-*R* (A-side) hydrogen from NADPH. Values for ^{D}V and $^{D}(V/K)_{NADPH}$ were similar for the basal (1.3-1.6) and CaM-stimulated (1.5-2.1) reduction of DCIP, while ^{D}V (2.1-2.8) was higher than $^{D}(V/K)_{NADPH}$ (1.1-1.5) for cytochrome c^{3+} reduction with and without CaM. The data suggests the overall reaction rate may be limited by the rate of the reductive half-reaction (NADPH oxidation) versus the oxidative half reaction (reduction of the DCIP or cytochrome c^{3+}). A value for $^{D}(V/K)_{NADPH}$ close to 1 indicates the intrinsic isotope effect on hydride transfer is suppressed by a slower step in the reductive half reaction. The oxidative half reaction is insensitive to the NADPD isotopic effects as both $^{D}(V/K)_{DCIP}$ and $^{D}(V/K)_{cytc}$ equal one within experimental error. Large solvent kinetic isotope effects (SKIE) observed for $(V/K)_{cytc}$ for basal (~8) and CaM-stimulated (~31) reduction of cytochrome c^{3+} suggests that proton uptake from the solvent limits the rate of the oxidative half reaction. This step does not severely limit the overall reaction rate as ^{D2O}V equaled 2 and $^{D2O}(V/K)_{NADPH}$ was between 0.87 and 1.3 for basal and CaM-stimulated cytochrome c^{3+} reduction. Proton inventory analysis indicates that multiple transition-state protons contribute to the observed SKIE.

4.2 Introduction

Mammalian nitric-oxide synthase (NOS)[1] produces the physiologically ubiquitous molecule nitric oxide (NO; 265-267). One reaction cycle consumes 1.5 NADPH and two O_2 in the two-step conversion of L-arginine to NO and L-citrulline (3, 268). In the first step, NADPH-derived electrons and O_2 are used to hydroxylate L-arginine to form the intermediate N^{ω}-hydroxy-L-arginine and H_2O (114). The second step utilizes 0.5 mol of NADPH and one O_2 to oxidize N^{ω}-hydroxy-L-arginine to produce L-citrulline, NO, and H_2O (6, 130). All three known isoforms of NOS, neuronal (nNOS), endothelial (eNOS) and inducible (iNOS) function as homodimers (4, 114, 268). Each polypeptide subunit is divided into an oxygenase domain, which contains a P450-type heme and the binding sites for (6*R*)-5,6,7,8-tetrahydrobiopterin (H_4B) and L-arginine (11, 12, 14) and a reductase domain, which contains FAD, FMN, and the binding site for NADPH (15, 62, 149). During catalysis the flavins transfer NADPH-derived electrons to the oxygenase domain to enable heme-based oxygen-activation and subsequent oxidation of L-arginine (114). The binding of Ca^{2+}-activated calmodulin (Ca^{2+}-CaM) to the calmodulin-binding motif located between the two domains facilitates electron transfer between the flavins and heme (18). A rise in intracellular Ca^{2+} concentration triggers the binding of CaM to eNOS and nNOS (24); however, CaM remains tightly bound to iNOS at basal levels of Ca^{2+} (220).

The NOS reductase domain is structurally and functionally homologous to cytochrome P450 reductase (CPR). Amino acid alignment of the last 641 residues on

nNOS revealed 36% sequence identity and 58% sequence similarity with CPR (15). nNOS and CPR are both composed of an NADPH-FAD module, homologous to ferridoxin-$NADP^+$ reductase (FNR) and an FMN module that is homologous to bacterial flavodoxin (15, 66, 250). The mode of electron transfer in NOS and CPR is proposed to proceed from NADPH to FAD to FMN and then finally to a P-450 heme (73, 81, 222, 226). The flavins on NOS and CPR are thought to cycle between the one and three-electron reduced states during catalysis (74, 224, 225). Finally, both NOS and CPR are able reduce non-physiological electron acceptors such as DCIP, ferricyanide (FeCN), and cytochrome c^{3+} (31, 75). The binding of Ca^{2+}-CaM to nNOS and eNOS alleviates partial inhibition of electron transfer to these substrates (30, 74, 76, 269), as DCIP and FeCN reduction increases 2- to 3- fold and cytochrome c^{3+} reduction increases 10 to 20-fold (30, 76). The CaM-stimulated reduction of these non-physiological acceptors is not linked to electron transfer to the heme, production of superoxide (74, 76, 269), or a change in the redox potentials of the flavins (73). Ca^{2+}-CaM does increase pre-steady-state flavin reduction (76, 78) and induces conformational changes in the diflavin domain (30, 74, 270). The structural rearrangement may remove the autoinhibitory effects of a 40-50 amino acid insert located in middle of the FMN-binding domain of eNOS and nNOS (82). This insert, which is not found in other structurally related flavoproteins or iNOS, was shown to promote the dissociation of CaM at low intracellular Ca^{2+} concentrations and inhibit electron transfer in the absence of Ca^{2+} (79, 80). Additionally, Ca^{2+}-CaM may realign a 20-amino acid C-terminal tail to promote interflavin electron transfer. The C-terminal tail, unique to the NOS isoforms, was also

shown to block electron transfer to non-physiological electron acceptors in the absence of Ca^{2+}-CaM (78, 83).

In lieu of a three-dimensional crystal structure of NOS depicting the specific structural role of CaM, an understanding of how the activated cofactor imparts control of electron transfer relies on the above mentioned and future biochemical and mutagenic studies as well as comparative analysis with structurally related enzymes. Recently, steady–state kinetic data for the basal and CaM-stimulated reduction of cytochrome c^{3+} catalyzed by nNOS was shown to be consistent with a nonclassical iso two-site ping-pong mechanism, which is similar to the mechanism previously described for the CPR cytochrome c^{3+}-reductase activity (254). Ternary complexes are permissible for this kinetic mechanism as the substrate active sites and the catalytic activities do not overlap. In contrast, the kinetic mechanism for basal and CaM-stimulated reduction of DCIP is limited to the formation of binary complexes as initial velocity and inhibition data with this substrate is consistent with a di-iso ping-pong bi bi mechanism. In this manuscript, primary deuterium isotope effects using NADPD and solvent isotope effects were employed to identify possible rate limiting step(s) in these kinetic mechanisms. nNOS was found to be an A-side dehydrogenase as the enzyme abstracts the pro-*R* hydrogen from NADPH. Primary deuterium (NADPH(D)) isotope effects on *V* and (*V/K*) for basal and CaM-stimulated DCIP and cytochrome c^{3+} reduction revealed that of the two half reactions, the reductive half-reaction involving NADPH oxidation limits the overall reaction rate but hydride transfer to FAD is not the slow step. Large solvent kinetic isotope effects (SKIE) observed for $(V/K)_{cytc}$ suggests that proton uptake is the rate-limiting step in the oxidative half reaction. However, proton uptake does not limit the

overall reaction rate as small SKIE on V and $(V/K)_{NADPH}$ were observed. The proton inventory technique was used to assess the number of transition state protons that contribute to the observed SKIE.

4.3 Experimental Procedures

4.3.1 Materials

The cDNA for rat neuronal NOS was kindly provided by T.M. Dawson (Johns Hopkins University, Baltimore, MD; 271), and the pCWori(+) expression vector was a gift form F.W. Dalhquist (University of Oregon, Eugene, OR; 228). Tetrahydrobiopterin (H_4B) was purchased from Cayman Chemical (Ann Arbor, MI), 2', 5 'ADP-Sepharose was from Amersham Pharmacia Biotech (Piscataway, NJ), and the TSK-GEL TOYOPEARL™ DEAE-650M (65 micron resin) was bought from Supelco (Bellefont, PA). Hepes was purchased from Research Organics (Cleveland, OH). Ammonium acetate, from EM Scientific, (Gibbstown, NJ) was prepared from reagent grade crystals and the pH was adjusted to 7.5 with NH_4OH. NADPH, $NADP^+$, DCIP, cytochrome c^{3+}, dihydrofolate, yeast glucose 6-phosphate dehydrogenase (G6PDH) (260 UI/mg), *Aspergillus niger* glycerol dehydrogenase (0.227 U/mg), and yeast hexokinase (270 UI/mg) were also purchased from Sigma (St. Louis, MO). The D-[1-^{3}H(N)]-glucose (specific activity of 11.3 Ci/mmol) was obtained from New England Nuclear (Boston, MA). D_2O (D, 99.9%) and deuterated glycerol (1, 1, 2, 3, 3-D_5, 99 %) were from Cambridge Isotope Laboratories (Andover, MA). T4 bacteriophage dihydrofolate reductase (DHFR) was a gift from Dr. Christopher Mathew's laboratory (Oregon State

University), and calmodulin and calmodulin-Sepharose were donated by Drs. Sonia Anderson and Dean Malencik (Oregon State University).

4.3.2 Preparation of [4(S)-^{3}H]NADPH

The procedure for the synthesis of [4(*R*)-^{3}H]NADPH and [4(*S*)-^{3}H]NADPH was adapted from Moran *et al* (272). A 0.1 mL sample containing 1 μCi (8.7 nmol) of [^{3}H]-glucose dissolved in 95 % ethanol was dried with a gentle stream of argon. The [1-^{3}H]-glucose was then dissolved in 100 μL of 50 mM Tris-HCl (pH 7.8) containing 1 μmol of $MgCl_2$, 0.1 μmol of ATP and phosphorylated to give [1-^{3}H]-glucose-6-phosphate with the addition of 0.5 U of hexokinase (273). After incubation at room temperature for 10 minutes, the reaction volume was brought to 0.2 mL with H_2O. Ten nmol of $NADP^+$ and 0.5 U of G6PDH were added to generate [4(*S*)-^{3}H]NADPH. The reaction was incubated at room temperature for 30 minutes then brought to a volume of 1 mL with H_2O and applied to an 8 mL (1.2 cm^2 × 7 cm) TSK-GEL TOYOPEARL™ DEAE-650M (65 micron resin) column equilibrated with 10 mM ammonium acetate (NH_4OAc) at 4 °C. An 80 mL linear gradient from 10 mM to 0.75 M NH_4OAc was applied to the column at a flow rate of 0.5 mL/min and 0.8 mL fractions were collected. The amount of radioactivity in a 10 μL sample was determined by liquid scintillation counting. Fractions with an absorbance ratio $A_{260}/A_{340} \leq 2.4$ and a high specific activity (~8.5 Ci/mmol) were pooled.

4.3.3 Preparation of [4(R)-^{3}H]NADPH

To synthesize [4(*R*)-^{3}H]NADPH, the purified [4(*S*)-^{3}H]NADPH was converted to [4-^{3}H]NADP$^+$ by dihydrofolate reductase which stereospecifically removes the unlabeled 4 pro-*R* hydrogen (274). The reaction mixture containing the pooled fraction of [4(*S*)-^{3}H]NADPH, 42 mM β-mercaptoethanol, 0.133 mM dihydrofolate, and 0.5 U of T4 bacteriophage DHFR was incubated at room temperature for 10 minutes and then diluted to 60 mL with H_2O and applied to an 8 mL (1.2 cm^2 × 7 cm) TSK-GEL TOYOPEARL™ DEAE-650M (65 micron resin) column equilibrated with 10 mM NH_4OAc at 4 °C. An 80 mL linear gradient from 10 mM to 750 mM NH_4OAc was applied to the column at a flow rate of 1 mL/min. Fractions were collected (1 mL) and fractions with a specific activity of ~3 Ci/mmol and an A_{260} absorbance without an A_{340} absorbance were pooled. B-face reduction of the nicotinamide ring was accomplished using G6PDH by adding the following to approximately 6 mL ~0.5 μM of [4-^{3}H]NADP$^+$: 19.8 mM glucose-6-phosphate, 60 mM $MgCl_2$ and 0.5 U of G6PDH. The reaction was incubated at room temperature for 10 minutes before dilution with 50 mL of H_2O and purification on TSK-GEL TOYOPEARL™ DEAE-650 as described above. Fractions with an absorbance ratio $A_{260}/A_{340} \leq 2.4$ and a high specific activity (~2.5 Ci/mmol) were combined.

4.3.4 Preparation of [4(R)-^{2}H]NADPH

[4(*R*)-^{2}H]NADPH was synthesized with the addition of 0.1 U of glycerol dehyrdrogenase from *Aspergillus niger* to a 1 mL mixture containing 2 mM $NADP^+$ and 10 mM deuterated (1, 1, 2, 3, 3-D_5)-glycerol in 50 mM glycine/NaOH (pH 9.0). The reaction was incubated at room temperature for 45 minutes, and the production of NADPH was followed by an increase in absorbance at 340 nm. The enzyme was then heat inactivated by immersing the reaction for 2 minutes in a water bath at 41 °C. The reaction was applied to a 20 mL (1.2 cm^2 × 14 cm) TSK-GEL TOYOPEARL™ DEAE-650M column pre-equilibrated with 10 mM NH_4OAc pH 7.5. A 100 mL linear gradient from 0.01 M to 1 M NH_4OAc was applied to the column at a flow rate of 0.75 mL/min and 1 mL fractions were collected. Fraction with an A_{260}/A_{340} absorbance ratio ≤ 2.4 were pooled and used in the substrate kinetic isotope studies. The concentration of NADP(H/D) was determined spectrophotometrically using ε_{340}= 6.22 mM^{-1} cm^{-1} (275).

4.3.5 Enzyme expression and purification

Recombinant rat nNOS was purified from *E. coli* strain BL21(DE3) after over expression of the cDNAwith the pCWori (+) vector. The enzyme was purified according to the protocol published by Gerber and Ortiz de Montellano, with slight modification (229). nNOS was more than 85% pure as judged by SDS-polyacrylamide gel electrophoresis with a specific activity of 150 nmol NO min^{-1} mg^{-1} at 25 °C. The rate of NO production was measured by the hemoglobin-NO capture assay following the

procedures of Stuehr *et al.* (22). Protein concentration was determined with the Lowry Assay using bovine serum albumin as a standard (230).

4.3.6 Determining the stereospecificty of nNOS-catalyzed NADPH hydride transfer

The procedure for determining the stereospecificity of hydride transfer was adapted from Vanoni and Matthews (276). The oxyhemoglobin assay was used to determine which hydrogen was transferred under conditions of NO synthesis. A 1 mL reaction mixture containing ~ 0.3-0.7 μM [4(*R*)-^{3}H]NADPH or [4(*S*)-^{3}H]NADPH and 4 μM of oxygenated hemoglobin, 5 μM FAD, 100 μM L-arginine, 10 μM $CaCl_2$, 100 nM CaM, and 8 μM H_4B was incubated with 1 μg of nNOS at 25 C° for 30 mins. Duplicate reaction mixtures, lacking nNOS, were also incubated under the oxyhemoglobin assay conditions to determine the extent of nonenzymatic tritium release into the solvent. The stereospecificity of hydride transfer under uncoupled NADPH oxidation conditions was determined by adding 10 μM $CaCl_2$, 100 nM CaM to the reaction containing 0.3-0.7 μM [4(*R*)-^{3}H]NADPH or [4(*S*)-^{3}H]NADPH. Finally, to examine if Ca^{2+}-CaM influences the stereospecificity of hydride transfer, 0.3-0.7 μM [4(*R*)-^{3}H]NADPH] or [4(*S*)-^{3}H]NADPH was incubated along with 50 μM DCIP and 1 μg of nNOS at 25 C° for 30 mins. At the completion of the reaction, 1 mL aliquots were withdrawn and the ^{3}H-radioactivity released from the solvent was separated from radioactive NADPH and/or $NADP^+$ by condensation of the solvent on a cold finger. Solvent fractions from reactions with and without nNOS were collected from the cold finger (~ 1 mL) and solute fractions from

the enzymatic and the nonenzymatic reactions were collected and redissolved in 1 mL of H_2O. The amount of ^{3}H-radioactivity in each sample was then analyzed by liquid scintillation fluorometry.

4.3.7 Determination of $^D(V/K)$ and $^D(V)$ associated with the oxidation of [4(R)-^{2}H]NADPH

The [4(*R*)-^{2}H]NADPH eluted from the column at 0.5 M NH_4OAc. Fractions containing [4(*R*)-^{2}H]NADPH were pooled and the concentration was determined at 340 nm using ε_{340} = 6.22 $mM^{-1}\,cm^{-1}$. A stock of the same concentration was then made of [4(*R*)-^{1}H]NADPH from Sigma in 0.5 M NH_4OAc. Primary kinetic substrate isotope effects were measured by direct comparison of the initial rates measured by reduction of cytochrome c^{3+} ($\Delta\,\varepsilon$ = 21.1 $mM^{-1}\,cm^{-1}$) at 550 nm or DCIP ($\Delta\,\varepsilon$ = 21 $mM^{-1}\,cm^{1}$) at 600 nm (231) with [4(*R*)-^{2}H]NADPH or [4(*R*)-^{1}H]NADPH. Reactions were performed in 3.5 mL at 25 °C using a 5 cm path length cuvette. Reaction mixtures contained 50 mM Hepes-NaOH (pH 7.5), variable concentrations of substrates [4(*R*)-^{2}H]NADPH or [4(*R*)-^{1}H]NADPH, cytochrome c^{3+} or DCIP, and where appropriate, 10 μM $CaCl_2$ and 100 nM CaM. Reactions were initiated with the addition of 0.5-2 μg of nNOS. nNOS catalyzed reductions of DCIP and cytochrome c^{3+} follow ping-pong mechanisms; thus, ^DV and $^D(V/K)_{NADPH}$ were obtain by directly fitting initial velocities at varying [4(*R*)-^{2}H]NADPH or [4(*R*)-^{1}H]NADPH concentrations with varying DCIP or cytochrome c^{3+} concentrations to the following equation with Origin v 4.0 software (MicroCal Software Inc., North Hampton, MA).

$$v_i = \frac{VAB}{(K_A B + K_B A + AB)} \qquad (4.1)$$

where v_i is the initial velocity, A is the concentration of [4(R)-^{2}H]NADPH or [4(R)-^{1}H]NADPH and B is the concentration of DCIP or cytochrome c^{3+}, and K_A and K_B are their corresponding Michaelis constants. Reciprocal initial velocities were plotted against the reciprocal substrate concentrations and, in all cases, the plots were linear. A control experiment showed that [4(R)-^{1}H]NADPH prepared in the same manner as [4(R)-^{2}H]NADPH exhibited the same kinetic parameters as [4(R)-^{1}H]NADPH purchased from Sigma.

4.3.8 Solvent kinetic isotope effects

A 50 mM Hepes-NaOH solution in D_2O was prepared by two lyophilizations of a 50 mM Hepes-NaOH solution in H_2O, each time re-dissolving the dry residue in D_2O. pD values were determined by adding 0.4 to the pH meter reading (pD = pH + 0.4; 277). For the reactions performed in D_2O, nNOS and CaM were diluted in D_2O and stock solutions of NADPH, cytochrome c^{3+}, DCIP, and $CaCl_2$ were prepared by dissolving their lyophilzed powders into D_2O. The SKIE on $(V/K)_{DCIP}$ was determined by measuring the initial rate of DCIP reduction at varying DCIP concentrations with a fixed sub-saturating concentration of NADPH (0.25 μM). Since both the basal and CaM-stimulated reductions of DCIP follow a ping-pong mechanism, the concentration of NADPH will not influence the value of $(V/K)_{DCIP}$ (254). The data was fit to the Michaelis-Menton equation (eq. 4.2) by non-linear least squares analysis with Origin v 4.0 software.

$$v_i = \frac{VA}{K_m + A} \qquad (4.2)$$

where v_i is the initial velocity, V is the maximal velocity, A is the variable substrate concentration, and K_m is the Michaelis constant for A. The SKIE on V and $(V/K)_{cytc}$ was determined by comparing the initial rate of cytochrome c^{3+} reduction at increasing concentrations of cytochrome c^{3+} and saturating concentrations of NADPH (10 μM) in 50 mM Hepes (pH/D 7.5) prepared in H_2O and D_2O. A non-linear least squares fit of the data to eq 2 gave values for V and $(V/K)_{cytc}$. Since concentrations of cytochrome $c^{3+} > 5K_m$ inhibit the reduction of the electron acceptor, the SKIE effects on $(V/K)_{NADPH}$ was determined by measuring cytochrome c^{3+} reduction with varying NADPH concentrations at a fixed sub-saturating concentration of cytochrome c^{3+} (0.4 μM). The data was fit to the Michaelis-Menton equation (eq. 2.2) by non-linear least squares analysis.

4.3.9 Proton inventories

The proton inventory method was used to obtain the number of proton(s) being transferred in the transition-state. The initial rate of DCIP or cytochrome c^{3+} reduction was measured at a fixed concentration of NADPH (10 μM) and fixed concentrations of DCIP (100 μM) or cytochrome c^{3+} (10 μM) at different fractional concentrations of D_2O in the reaction mixture. Data where fit to various forms of the Gross-Butler equation (eq. 4.3; 278, 279) by non-linear least squares analysis.

$$k_n = k_0 \frac{\prod^{v}\left(1-n+n\phi_i^{T}\right)}{\prod^{v}\left(1-n+n\phi_i^{G}\right)} \tag{4.3}$$

In equation 4.3, ϕ_i^G and ϕ_i^T are the ground and transition state fractionation factor at the *i*th exchangeable site, v is the number of protons involved in the reaction, k_n is the observed rate measured at n, where n is the fractional concentration of D_2O, and k_0 is the observed rate measured at 0% D_2O. Although proteins consist of numerous exchangeable hydrogenic sites, the magnitude of the SKIE is often limited to difference between ϕ_i^G and ϕ_i^T at a few sites. Thus, proton inventory analysis begins with simplified forms of equation 4.3, which assumes one (eq. 4.4) or two protons (eq. 4.5) in the transition state contribute to the observed SKIE and $\phi_i^G = 1$ (true for most protein hydrogenic sites, with the exception of sulfhydryl groups where $\phi^G = 0.65$; 280).

$$k_n = k_0(1-n+n\phi^{T}_1) \tag{4.4}$$

$$k_n = k_0(1-n+n\phi^{T}_1)(1-n+n\phi^{T}_2) \tag{4.5}$$

To determine if equation 4.4 or 4.5 provides a better fit to the proton inventory data, equation 4.5 was expanded to the following, where ϕ_1^T equals ϕ_2^T:

$$k_n = k_0 + 2k_0\left(\phi_1^{T}-1\right)n + Ck_0\left(\phi_1^{T}-1\right)^2 n^2 \tag{4.6}$$

For assessing the lack of fit a third parameter, C, was added to the expanded equation which is now an unconstrained quadratic in n. If a nonlinear least squares fit of the data

to this equation gives a value of C=0, the data is consistent with one proton in the transition state contributing to the observed SKIE, as eq 4.6 reduces to eq 4.5. If $C \geq 1$, then the data describes a model in which two or more protons in the transition-state contribute to the observed SKIE. The data were also fit to equation 4.7, which assumes two protons, which have equal values for their fractionation factors (i.e. $\phi_1^T = \phi_2^T$), are transferred in the transition-state.

$$k_n = k_0(1 - n + n\phi^T{}_1)^2 \qquad (4.7)$$

4.4 Results

4.4.1 Stereospecificity nNOS-catalyzed NADPH oxidation

The stereospecificity of NADPH oxidation was determined under conditions for NO-synthesis, uncoupled NADPH oxidation, and NADPH oxidation with DCIP as an electron acceptor. Table 4.1 shows that under each of these conditions, the pro-*R* hydrogen is abstracted. Approximately 85% of the tritium was released into the solvent in the presence of nNOS with [4(*R*)-^{3}H]NADPH as the substrate; whereas, the majority of the tritium remained with the particulate fraction in the absence of nNOS. The percentage of tritium released into the solvent was approximately the same in the absence and presence of the enzyme with [4(*S*)-^{3}H]NADPH as the substrate. On the basis of these results, nNOS catalyzes the stereospecific removal of the pro-*R* hydrogen at the 4-position of NADPH and the subsequent exchange of this hydrogen with the solvent occurs, possibly on the enzyme bound flavin.

Table 4.1: Stereospecificity of the oxidation of NADP(H/T) catalyzed by nNOS

	dpm released into solvent		dpm retained in residue	
Substrate	+enzyme	-enzyme	+enzyme	-enzyme
[4(R)-^{3}H]NADPH				
HbO_2[a]	217,223 (74%)	22,218 (10%)	57,336 (26%)	211,839 (90%)
	664,264 (84%)	74,046 (13%)	109,134 (16%)	570,954 (87%)
	753,876 (89%)	92,192 (14%)	88,408 (11%)	640,829 (86%)
uncoupled[b]	641,646 (81%)		123,281 (19%)	
DCIP[c]	814,592 (87%)		110,381 (13%)	
[4(S)-^{3}H]NADPH				
HbO_2	99,201 (3 %)	154, 542 (5 %)	2,933,589 (97 %)	3,345,873 (96%)
	78,604 (3 %)	140,567 (4 %)	2,993,746 (97 %)	3,133,32 (97%)
	228,073 (9 %)	55,513 (2 %)	2,465,362 (91 %)	3,138,312 (98%)
uncoupled	100,706 (3 %)		3,213,992 (97 %)	
DCIP	487,964 (17 %)		2,869,820 (83 %)	

[a] NADPH oxidation was performed under conditions of the HbO_2 assay described in the *Experimental Procedures*

[b] NADPH oxidation was performed in the absence of L-arginine

[c] DCIP was used as the terminal electron acceptor for NADPH oxidation.

4.4.2 Substrate isotope effects with [4(R)-^{3}H]NADPH.

[4(*R*)-^{1}H]NADPH was prepared in the same manner as [4(*R*)-^{2}H]NADPH to ensure that the synthesized NADPH had the same properties as NADPH purchased from Sigma. The synthesized [4(*R*)-^{1}H]NADPH exhibited the same V and K_m for NADPH compared to [4(*R*)-^{1}H]NADPH purchased from Sigma (data not shown). The primary deuterium isotope effects on the basal and CaM-stimulated reduction of NADPH are summarized in Table 4.2.. The values for $^D(V)$ in the presence and absence of Ca^{2+}-CaM with DCIP as the terminal electron acceptor were 1.56 ± 0.10 and 1.91 ± 0.33, respectively. $^D(V/K)_{NADPH}$ for basal activity was 1.42 ± 0.13 while CaM-stimulated activity produced a value of 1.60 ± 0.17. The primary isotope effect of $^D(V/K)_{DCIP}$ with and without Ca^{2+}-CaM was 1.01 ± 0.10 and 1.02 ± 0.10, respectively, indicating that the oxidative half reaction in isotopically insensitive to hydride transfer.

$^D(V)$ for basal reduction of cytochrome c^{3+} was 2..72 ± 0.07. In the presence of Ca^{2+}-CaM, $^D(V)$ equaled 2.24 ± 0.16 The value for $^D(V/K)_{NADPH}$ was 1.31 ± 0.16 and 1.19 ± 0.10 in the presence and absence of Ca^{2+}-CaM, respectively. $(V/K)_{cytc}$ did not exhibit an NADPH(D) primary isotope effect in either the presence (0.97 ± 0.04) or absence (0.98 ± 0.07) of Ca^{2+}-CaM, since the values were one, within experimental error. The lack of an observed NADPD isotope effect on the oxidative half reaction with DCIP and cytochrome c^{3+} is consistent with the reactions following ping-pong mechanisms and

Table 4.2 Measurement of ^{D}V and $^{D}(V/K)$ for nNOS-catalyzed NADPH oxidation[a]

Substrate	Ca^{2+}-CaM	^{D}V	$^{D}(V/K)_{NADPH}$	$^{D}(V/K)_{acc}$
DCIP	-	1.56 ± 0.10	1.42 ± 0.13	1.01 ± 0.10
DCIP	+	1.91 ± 0.33	1.60 ± 0.17	1.02 ± 0.10
cytochrome c^{3+}	-	2.72 ± 0.07	1.19 ± 0.10	0.98 ± 0.07
cytochrome c^{3+}	+	2.24 ± 0.16	1.31 ± 0.16	0.97 ± 0.04

[a] Reaction conditions are described under *Experimental Procedures*. Values are from a global fit of 3 experiments to eq. 4.1 to the data ± standard errors.

further suggests that the label exchanges with the solvent prior to reduction of these two substrates.

4.4.3 Solvent kinetic isotope effects on kinetic parameters

Kinetic solvent isotope studies involve comparing the values of V and (V/K) for various substrates (NADPH, DCIP and cytochrome c^{3+}) in buffer prepared in H_2O versus D_2O. The deuterium in D_2O exchanges with all the hydrogenic sites on nNOS and the substrates, therefore D_2O has the potential to affect V and (V/K) by altering substrate binding, and/or altered stability or conformation of the enzyme (281).

To determine if the latter contributed to the observed SKIE, nNOS and the substrates (NADPH, DCIP, and cytochrome c^{3+}) were equilibrated in D_2O and the catalytic rates of DCIP and cytochrome c^{3+} reduction were compared to nNOS and the three substrates diluted in H_2O under identical conditions. No differences in catalytic rates were observed; therefore, the observed solvent isotope effects is not attributed an irreversible change in the structure of the enzyme itself. The solvent isotope effects on the kinetic parameters for the reduction of DCIP and cytochrome c^{3+} are summarized in Table 4.3. An inverse solvent isotope effect, 0.72 ± 0.07, was observed for $(V/K)_{DCIP}$ for the basal reduction of this electron acceptor. However, in the presence of Ca^{2+}-CaM the value for $^{D2O}(V/K)_{DCIP}$ was equal to 3.97 ± 0.32. A large SKIE was observed for the basal reduction of cytochrome c^{3+} with $^{D2O}(V/K)_{cytc}$, 8.38 ± 0.69. This value increased approximately 4-fold in the presence of Ca^{2+}-CaM to 31.00 ± 2.99. The values for ^{D2O}V

Table 4.3 Kinetic solvent isotope effect on kinetic parameters for NADPH oxidation[a]

Substrate	Ca^{2+}-CaM	^{D}V	$^{D}(V/K)$
NADPH	-		0.87 ± 0.08[b]
NADPH	+		1.17 ± 0.07[b]
DCIP	-	nd[c]	0.72 ± 0.07
DCIP	+	nd	3.97 ± 0.32
cytochrome c^{3+}	-	1.99 ± 0.06	8.38 ± 0.69
cytochrome c^{3+}	+	2.07 ± 0.09	31.00 ± 2.99

[a] Reaction conditions are described under *Experimental Procedures*. Values are generated from a fit of equation 4.2 ± standard errors.

[b] Determined with cytochrome c^{3+} as the second substrate.

[c] Not determined

for the basal and CaM-stimulated reduction of cytochrome were equal within error, 1.99 ± 0.06 (basal) and 2.07 ± 0.09 (Ca^{2+}-CaM). The large SKIE associated with $(V/K)_{cytc}$ indicates that proton uptake from the solvent is the rate-determining step in the half reaction involving the reduction of this substrate. However, since the value for $^{D2O}(V)$ is ~2 for the basal and CaM-stimulated reduction of cytochrome c^{3+}, proton uptake does not completely limit the rate of the overall reaction. A value for $^{D2O}(V/K)_{NADPH}$ of 0.87 ± 0.08 and 1.17 ± 0.07 for the basal and CaM-stimulated reduction of cytochrome c^{3+}, respectively, indicates proton transfer is not a rate limiting-step in the reductive half-reaction.

4.4.4 Proton inventory studies

The proton inventory method was used to determine the number of protons which contribute to the SKIE (282). The technique involves measuring the reaction rate in various binary mixtures of H_2O and D_2O and plotting the observed rate, ^{n}k, versus the fraction of deuterium in the solvent, n. As shown in Figure 4.1, plots of basal DCIP (A) and cytochrome c^{3+} (B) reduction rates, ^{n}k against the atom fraction of D_2O in the solvent, n, bulge downwards. The characteristic bowl-shaped curvatures of the experimental data points suggest that multiple protons are transferred or "in flight" in the conversion from the initial (reactant) state to the transition-state. A nonlinear least-squares fit eq 4.6 to the data in Figure 4.1A and 4.1B gave values of C equal to 1.13 ±

Figure 4.1: Proton inventory for the basal nNOS-catalyzed reduction of (A) DCIP and (B) cytochrome c^{3+}. The fraction of deuterium (n) is plotted against the rate of steady-state activity measured in the H_2O/ D_2O mixture (k_n). A non-linear least squares fit of the experimental data in A to eq 4.6, represented by solid lines, gave values for $C = 1.13 \pm 0.06$, $\phi^T_1 = 0.19 \pm 0.06$, and k_o (rate of DCIP reduction in 0% D_2O) = 329.2 ± 10.9 min^{-1}. A fit of eq 4.7 to the data yielded a value of $k_o = 321.65$ min^{-1} and $\phi^T_1 = 0.28 \pm 0.05$. A non-linear least squares fit of the experimental data in B to eq 4.6 gave values for $C = 1.22 \pm 0.10$, $\phi^T_1 = 0.33 \pm 0.06$, and k_o (rate of cytochrome c^{3+} reduction in 0% D_2O) = 118.7 ± 10.9 min^{-1}. A fit of eq 4.7 to the data yielded a value of $k_o = 107.6 \pm 3.0$ min^{-1} and $\phi^T_1 = 0.30 \pm 0.03$.

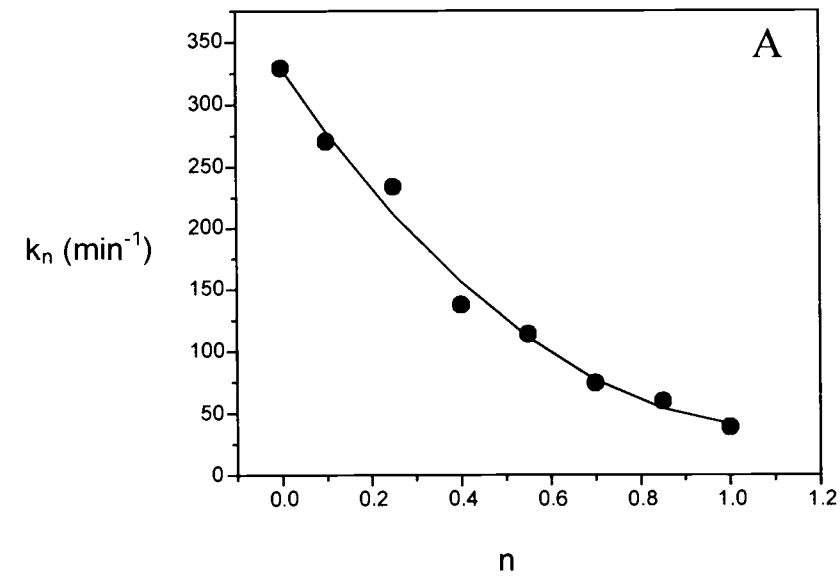
A
350
300
250
200
150
100
50
0
0.0
0.2
0.4
0.6
0.8
1.0
1.2
k_n (min^{-1})
n

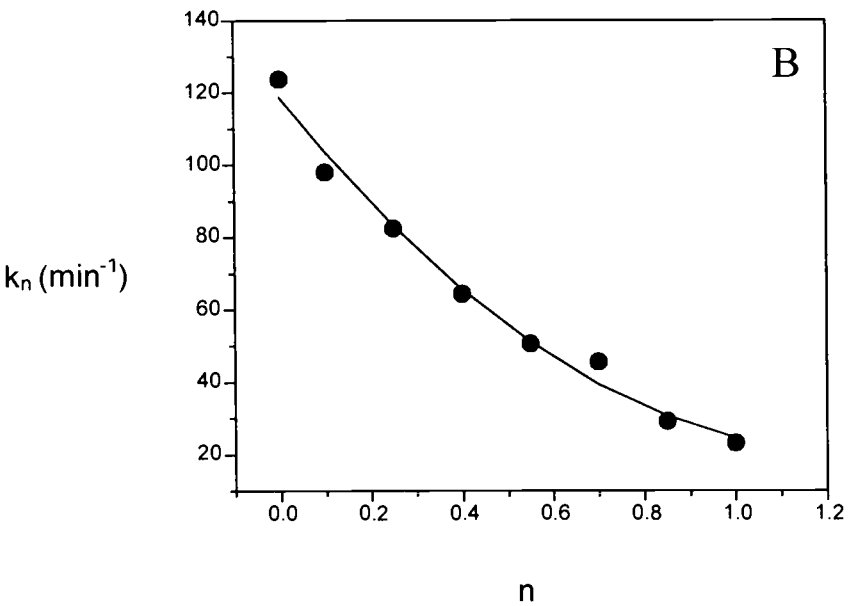
B
140
120
100
80
60
40
20
0.0
0.2
0.4
0.6
0.8
1.0
1.2
k_n (min^{-1})
n

Figure 4.1

0.06 and 1.22 ± 0.10, respectively, indicating that the isotope effect originates from two or more protons in flight. A fit of eq 4.5, which describes two protons in flight, to the data gave undefined values for ϕ_1^T and ϕ_2^T. A fit of eq 4.7, which is a function of two protons in flight with equal fractionation factors generated defined values for the fractionation factor (Panel A ϕ^T= 0.29 ± 0.05 and Panel B ϕ^T= 0.30 ± 0.03).

4.5 Discussion

4.51 .Stereospecificity of oxidation of NADPH catalyzed by nNOS

The separate NADPH/FAD and FMN binding modules of nNOS and other related dual flavoproteins such as CPR (66), sulfite reductase (67), and methionine synthase reductase (68) are homologous to FNR and flavodoxin, respectively. FNR is the prototypic member of the transhydrogenases family of proteins which also includes NADH-nitrate reductase and NADH-cytochrome b5 reductase (65, 250). Enzymes in this family catalyze the transfer of electrons between nicotinamide nucleotides (obligate two-electron or hydride donors/acceptors) and obligate one-electron donors (65). The stereospecifity of hydride transfer appears to be a conserved feature for this enzyme family as members including FNR (283), CPR (284), NADPH-cytochrome b5 reductase (285) and NADH-nitrate reductase (286) were shown to abstract the pro-*R* hydrogen. A second class of flavin containing enzymes, the carbon-sulfur transhydrogenase family, are stereospecific for the pro-*S* hydrogen (65). Enzymes of this family, including glutathione reductase (273), thioredoxin reductase (287), and lipoamide dehydrogenase

(288) catalyze two-electron transfers between nicotinamide nucleotides and disulfide-dithiol pairs.

As shown in Table 4.1, the pro-*R* hydrogen is abstracted during nNOS-catalyzed NADPH oxidation. Therefore, nNOS maintains the relationship between the class of transhydrogenases and stereospecifity of hydride transfer.

4.5.2 Substrate isotope effects.

Establishing that the A-side hydrogen is stereospecifically removed permitted further investigation of the primary isotope effects on DCIP and cytochrome c^{3+} reduction. The basal and CaM-stimulated reduction of these two substrates is proposed to occur in two-half reactions, whereby the reduction of enzyme bound flavin by NADPH and release of the oxidized nucleotide is followed by binding of the oxidant, DCIP or cytochrome c^{3+}, and reoxidation of the reduced flavin. The steady-state initial velocity and inhibition studies were consistent with DCIP following a di-iso ping-pong mechanism (Figure 4.2; 254). There are two isomerization steps. After the release of $NADP^+$, the three electron reduced state of nNOS, E_3 is proposed to isomerize at steady-state to E_3' prior to the binding of DCIP. A rapidly equilibrating isomerzation of the one-electron reduced state is also proposed to occur between the free enzyme form, which appears after the release of reduced DCIP, E_1', and the enzyme form which binds NADPH, E_1.

Like the reduction of DCIP, the basal and CaM-stimulated reduction of cytochrome c^{3+} also occurs in two-half reactions. However the initial velocity and inhibition patterns are consistent with the iso (two-site) ping-pong mechanism illustrated in Figure 4.3 (254). The salient feature of this mechanism is the ability of NADPH and

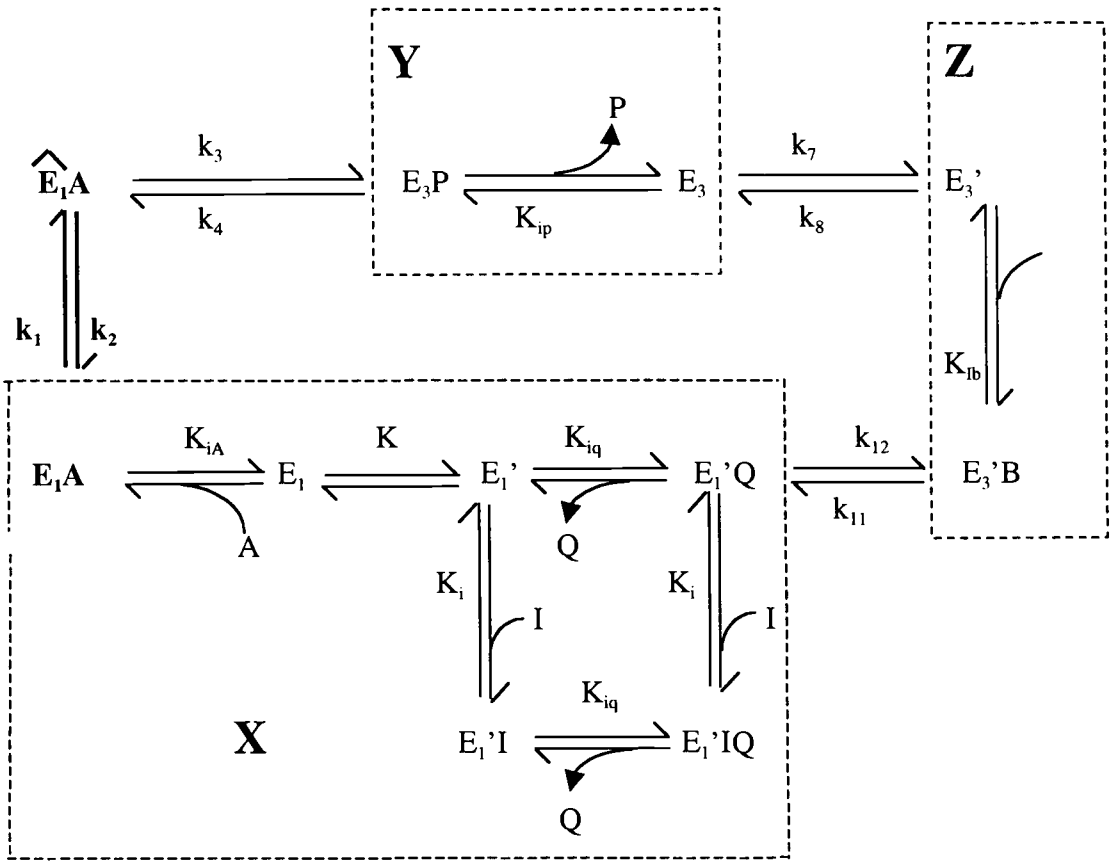

Figure 4.2 Kinetic scheme for a di-iso ping-pong bi-bi mechanism for the nNOS-catalyzed reduction of DCIP with a step representing the formation of the charge transfer complex (E_1A to $\hat{E}_1$A). *A, B, P, Q* and *I* represent NADPH, $DCIP_{ox}$, $NADP^+$, $DCIP_{red}$, 2'-AMP and the K_i values refer to their respective dissociation constants. E_1 and E_1' are the one-electron (FAD/FMNH•) forms of nNOS that exclusively bind NADPH and 2'-AMP, respectively. E_3 and E_3' are the three-electron (FADH•/$FMNH_2$) or ($FADH_2$/FMNH•) forms of nNOS that exclusively bind $NADP^+$ and $DCIP_{ox}$, respectively. *K* is the equilibrium constant for the conversion of the two enzyme forms, E_1 and E_1'. The dotted boxes labeled *X, Y,* and *Z* indicate the proposed rapid equilibrium segments for the reaction mechanism, where $X = E_1 + E_1' + E_1'I + E_1'IQ + E_1'Q + E_1A$, $\hat{E}_1$A; $Y = E_3P + E_3$; $Z = E_3' + E_3'B$.

Site-1:

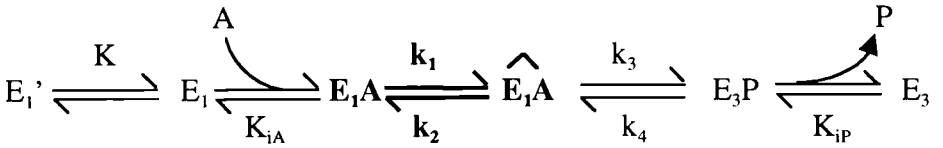

Site-2:

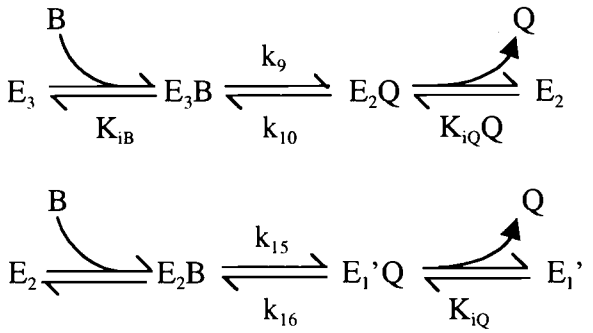

Figure 4.3 The kinetic scheme illustrating the iso (two-site) ping-pong mechanism for the nNOS-catalyzed reduction of cytochrome $c^{3+}$with a step representing the formation of the charge transfer complex (E_1A to $\hat{E}_1A$). *A*, *B*, *P*, *Q* and *I* represent NADPH, cytochrome c^{3+}, $NADP^+$, and cytochrome c^{2+}, and 2'AMP, respectively. E_1 and E_1' are the one-electron (FAD/FMNH•) forms of nNOS that exclusively bind NADPH and 2'-AMP, respectively. E_2 and E_3 represent two (FAD/$FMNH_2$) and three-electron (FADH•/$FMNH_2$) reduced form of nNOS. *K* is the equilibrium constant for the conversion of the two enzyme forms, E_1 and E_1'.

cytochrome c^{3+} to act at catalytically independent sites on nNOS. Figure 4.3 depicts NADPH binding to site 1 in a uni-uni fashion and two molecules of cytochrome c^{3+} binding to site 2 in a tetra-uni fashion. Unlike the single site ping-pong mechanism, ternary complex formation is not precluded by the two-site kinetic mechanism. The name of the kinetic mechanism is prefixed with iso to acknowledge the rapidly equilibrating isomerization of E_1 to E_1'.

With the assumption that the substrates bind in rapid equilibrium, the derivation of the kinetic mechanisms for DCIP and cytochrome c^{3+} produced identical expressions for $(V/K)_{NADPH}$ (eq. 4.8; (254).

$$\left(\frac{V/E_t}{K_A}\right)=\frac{k_3}{K_{iA}\left(1+1/K\right)} \tag{4.8}$$

where V is the maximal velocity, E_t is the concentration of nNOS, K_A is the Michaelis constant for NADPH, K_{iA} is the NADPH dissociation constant, K is the equilibrium constant for the conversion of E_1 to E_1' and k_3 is the rate of hydride transfer.

In the kinetic mechanisms illustrated in Figures 4.2 and 4.3, only the rate constant representing hydride transfer, k_3, is sensitive to isotopic substitution; thus, the expression for substrate isotope effect on $(V/K)_{NADPH}$ is as follows:

$$^{D}\left(\frac{V}{K}\right)_{NADPH}={}^{D}k_3 \tag{4.9}$$

where ${}^{D}k_3$, or the intrinsic isotope effect, equals k_{3H}/k_{3D} with k_{3H} defining the rate of NADPH hydride transfer, and k_{3D} the rate of NADPD deuteride transfer. Equation 4.9

shows that $^{D}(V/K)_{NADPH}$ is a function only of the intrinsic isotope effect. Typically, $^{D}k_3$ ranges between 5-8, which corresponds to the differences between the zero-point energy vibrational energies of C-H and C-D bonds in the ground and transition-state; however, values are observed outside this range due to the nature of the transition-state or tunneling (289).

The intrinsic isotope effect was not estimated by method of Northrop (290) where the tritium isotope effects on $(V/K)_{NADPH}$ are compared with $^{D}(V/K)_{NADPH}$ with the assumption that the tritium intrinsic isotope effect, $^{T}k_3$ is 1.44 the power of the deuterium isotope effects, $^{D}k_3$ (291), because the over all tritium isotope effect is measured by the release of tritium from the reduced flavin into the water, which constitutes the first irreversible step. In contrast, the first irreversible step for NADPD oxidation is transfer of the deuteride to FAD. Hence, $^{D}(V/K)$ and $^{T}(V/K)$ are comprise different rate constants; therefore, there values can not be used to determine the intrinsic isotope effect (see ref (292) for further details).

As shown in Table 4.2, the value for $^{D}(V/K)_{NADPH}$ was much lower than the intrinsic isotope effect for either the basal or CaM-stimulated reduction of DCIP or cytochrome c^{3+} indicating that the full value of $^{D}k_3$ in the expression for $^{D}(V/K)_{NADPH}$ is suppressed by a more rate-limiting isotopically insensitive step(s) (293). Thus, $(V/K)_{NADPH}$ is probably defined by other microscopic rate constants, such as NADPH binding, NADPH dissociation, or conformational changes associated with the formation of a charge-transfer complex (E_1-NADPH).

To simplify the original derivation of the kinetic mechanism for DCIP and cytochrome c^{3+} reduction it was assumed that substrate binding occurs in rapid

equilibrium, (i.e. the rate of NADPH dissociation is greater than the rate of nNOS and NADPH complex formation). This assumption was validated by the competitive inhibition exhibited by the NADPH-analog, 2'AMP against varying concentrations of NADPH observed for both electron acceptors. If NADPH binding and release were at steady-state, then the 2'AMP would be a non-competitive inhibitor of NADPH since they bind to different forms of the one-electron reduced state of nNOS (254). Thus, the binding and release of NADPH are not the rate-limiting steps in the reductive-half reaction.

However, comparative analysis with the structurally and functionally related enzymes, FNR and CPR suggest that putative structural rearrangements in nNOS prior to hydride transfer may be rate-limiting steps in the reductive-half reaction. Biochemical and structural studies of FNR and CPR indicate that both enzymes undergo a structural rearrangement to form a charge-transfer complex between the binding of the nucleotide and hydride transfer. The crystal structures of rat CPR (70) and pea FNR (250, 251) revealed that the aromatic ring of a tryptophan residue in the former and a tyrosine residue in the latter shield the isoalloxazine ring of the FAD from the nicotinamide cofactor. It is clear that both aromatic side chains need to reposition themselves for the nicotinamide ring to be at an appropriate distance from the N5 of FAD for hydride transfer. Stopped-flow fluorescence studies have demonstrated that the conserved tryptophan residue in human CPR is mobile (i.e. "flips away" from the isoalloxazine ring) during the formation of the charge-transfer complex (294). Movement of the homologous residue in nNOS, Phe1395, in the formation and/or decay

of the charge-transfer complex, may be the origin of the isotopically insensitive rate-limiting step.

The kinetic mechanisms for the reduction of DCIP and cytochrome c^{3+} were modified to incorporate the formation of the charge-transfer complex (bold portions of Figures 4.2 and 4.3, respectively). In both kinetic mechanisms, k_1 and k_2 represent the formation and decay rate of charge-transfer complex, respectively. The derivations of the kinetic mechanisms with this additional step are consistent with the steady-state initial velocity and inhibition data obtained previously (254), and $(V/K)_{NADPH}$ is now described by the following equation:

$$\left(\frac{V/E_t}{K_A}\right) = \frac{k_1 k_3}{K_{ia}(1+1/K)(k_2+k_3)} \tag{4.10}$$

The expression for $^{D}(V/K)_{NADPH}$, assuming that k_3 is the only isotopically sensitive step would then be defined in the following equation.

$$^{D}(V/K)_{NADPH} = \frac{^{D}k_3 + k_{3H}/k_2}{1 + k_{3H}/k_2} \tag{4.11}$$

Equation 4.11 illustrates that $^{D}(V/K)_{NADPH}$ would also be a function of k_2, or the dissociation of the change transfer-complex, assuming that this step also occurs in nNOS. If $k_2 < k_{3H}$ then full expression of $^{D}k_3$ would be reduced in $^{D}(V/K)_{NADPH}$. For example, if $^{D}k_3$ obeys the classical limit for the intrinsic isotope effect and has a value ~ 7, then for $^{D}(V/K)_{NADPH}$ to range between 1.2 and 1.6, then k_{3H} must be 10- to 30-fold greater than k_2. Alternatively, if $^{D}k_3$ approaches only 3, observed if there is a small change in the C-H and C-D vibrational energy difference between the ground state and

the transition state, then k_{3H} need only be 2.5- to 10-fold greater than k_2. There is precedent for considering $k_2 < k_{3H}$ since several research groups have characterized NADPH as a "sticky" substrate (255, 276, 295). A substrate is considered "sticky" if partitioning of the enzyme-substrate complex towards catalysis is favored compared to release from the enzyme (i.e $k_2 < k_3$; (255). Vanoni and Mathews proposed that dehydrogenases which exhibit suppression of the isotope effect of hydride transfer in $^{D}(V/K)_{NADPH}$ are optimized for catalytic efficiency of their reductive half-reaction (276, 296). Thus, nNOS would be exhibiting high forward commitment to catalysis since the E_1-NADPH charge-transfer complex, once formed, preferably would undergo oxidoreduction to form the E_3-$NADP^+$ complex rather than dissociate to form E_1 and NADPH.

Although the expressions for $^{D}(V/K)_{NADPH}$ for DCIP and cytochrome c^{3+} reduction are defined by the same rate constants and hence exhibit similar values for $^{D}(V/K)$, the expressions for ^{D}V are not a function of the same rate constants; therefore, the two substrates will not necessarily exhibit similar ^{D}V values. As shown in Table 2, the experimentally observed values for ^{D}V for the basal and CaM-stimulated for DCIP (1.5-2) reduction were significantly smaller compared to cytochrome c^{3+} (2.4-2.7). According to the mechanism illustrated in Figure 4.2, V for DCIP reduction is defined in the following equation

$$\frac{V}{E_t} = \frac{k_1 k_3 k_7 k_{11}}{k_1 k_3 k_7 + k_1 k_{11}(k_3 + k_7) + k_7 k_{11}(k_2 + k_3)} \qquad (4.12)$$

where the rate constants are the same as those in Figure 2. Following the mechanism illustrated in Figure 4.3, V for the basal and CaM-stimulated reduction of cytochrome c^{3+} is a function of the following rate constants.

$$\frac{V}{E_t} = \frac{k_1 k_3 k_9 k_{15}}{k_9 k_{15}(k_1 + k_2 + k_3) + k_1 k_3 (k_9 + k_{15})} \tag{4.13}$$

where k_1, k_2, k_3, k_9, and k_{15} are the same as those in Figure 4.3. With k_3 defined as the isotopically sensitive step, ${}^{D}V$ equals eq. 4.14 and eq. 4.15 for DCIP and cytochrome c^{3+} reduction, respectively.

$${}^{D}V = \frac{{}^{D}k_3\left(1 + \frac{k_1}{k_2}\right) + \frac{k_{3H}}{k_2}\left(1 + \frac{k_1}{k_7} + \frac{k_1}{k_{11}}\right)}{1 + \frac{k_1}{k_2} + \frac{k_{3H}}{k_2}\left(1 + \frac{k_1}{k_7} + \frac{k_1}{k_{11}}\right)} \tag{4.14}$$

$${}^{D}V = \frac{{}^{D}k_3\left(1 + \frac{k_1}{k_2}\right) + \frac{k_{3H}}{k_2}\left(1 + \frac{k_1}{k_9} + \frac{k_1}{k_{15}}\right)}{1 + \frac{k_1}{k_2} + \frac{k_{3H}}{k_2}\left(1 + \frac{k_1}{k_9} + \frac{k_1}{k_{15}}\right)} \tag{4.15}$$

The ratio of k_1, rate of formation of the charge-transfer complex, over the rate constants defining the forward rate constants in the oxidative half-reaction differentiate eqs 4.14 and 4.15. If the ratio of k_1 over k_7 (steady-state isomerization of E_3 to E_3') and/or k_{11}, (electron transfer from the flavins to DCIP) is less then k_1 over k_9 and/or k_{15} (electron transfer from the flavins to cytochrome c^{3+}) then the ${}^{D}V$ value for DCIP reduction would

be less compared to cytochrome c^{3+} reduction, because there would be more attenuation of the ratio k_{3H}/k_2, which was assumed to be ≥10 based on a value of $^{D}(V/K)_{NADPH}$ near unity and the intrinsic isotope effect equals the classical limit.

Comparison of ^{D}V and $^{D}(V/K)$ values provides information concerning the relative rates of the two half reactions in ping-pong mechanism (297). For example, a value for ^{D}V similar to $^{D}(V/K)$, as observed for the reduction of DCIP, or slightly larger then $^{D}(V/K)$, as seen for cytochrome c^{3+} reduction with and without Ca^{2+}-CaM, suggests that the reductive-half reaction limits the overall reaction rate (297). If the oxidative half reaction is more rate-limiting k_1, and/or $k_3 < k_7$ or k_{11}, for DCIP reduction and k_1, and/or k_3 is $< k_9$ or k_{15} for cytochrome c^{3+} reduction. Due to the complexity of the ping-pong mechanisms, i.e the addition of isomerization steps and rate constants in the expressions for ^{D}V, it can not be determined if k_1 and or k_3 is less then or greater then k_7 or k_{11} (DCIP reduction) or k_9 or k_{15} (cytochrome c^{3+} reduction).

Stopped-flow experiments with CPR revealed that there was rapid formation of the charge transfer complex as the apparent rate constant was >500 s^{-1} followed an isomerization of a second transfer complex (~200 s^{-1}), while the rate of hydride transfer much slower was ~3 s^{-1} (69). If nNOS were to exhibit the same relative rates in the k_1 and k_3, then it follows that the ratio of $k_{3H}/k_2 < k_1/k_2$ since $k_{3H} > k_2$ and $k_1 > k_3$. When equations 4.14 and 4.15 are rewritten to equations 4.16 and 4.17, respectively, one can see the relative importance of k_{3H}/k_2 and k_1/k_2 in the value of ^{D}V for reduction of the two electron acceptors.

$$^{D}V = \frac{^{D}k_3\left(1 + k_1/k_2\right) + k_{3H}/k_2\left(1 + k_1/k_7 + k_1/k_{11}\right)}{1 + k_1/k_2 + k_{3H}/k_2\left(1 + k_1/k_7 + k_1/k_{11}\right)} \quad (4.16)$$

$$^{D}V = \frac{^{D}k_3\left(1 + k_1/k_2\right) + k_{3H}/k_2\left(1 + k_1/k_9 + k_1/k_{15}\right)}{1 + k_1/k_2 + k_{3H}/k_2\left(1 + k_1/k_9 + k_1/k_{15}\right)} \quad (4.17)$$

If $k_1/k_2 >> k_{3H}/k_2$ and $k_1 > k_7$ and k_{11}, (eq 4.16) or k_9, and k_{15} (eq 4.17) then ^{D}V would be equal for reduction of the oxidants and the value of the intrinsic isotope effect $^{D}k_3$. However, this is clearly not the case, thus the value of ^{D}V must be suppressed by different amounts in equation 4.16 and 4.17 by the second term in the numerator, i.e. the value of k_{3H}/k_2 multiplied the combination of rate constants enclosed in parenthesis. If the opposite is true, such that $k_1/k_2 << k_{3H}/k_2$ and $k_1 < k_7$ and k_{11}, (eq 4.16) or k_9, and k_{15} (eq 4.17) then ^{D}V equals $^{D}(V/K)_{NADPH}$ for the reduction of either DCIP or cytochrome c^{3+}. Since this is clearly not the case for cytochrome c^{3+} reduction, where $^{D}V > {}^{D}(V/K)_{NADPH}$, the value k_1/k_2 must contribute substantially to the value of ^{D}V causing it to be greater than $^{D}(V/K)_{NADPH}$.

The values for $^{D}(V/K)_{DCIP}$ and $^{D}(V/K)_{cytc}$ were equal to one within experimental error. This is consistent with the proposed ping-pong mechanism for these substrates (254) since $^{D}(V/K)_{DCIP}$ and $^{D}(V/K)_{cytc}$ and functions of k_3. The data is also suggests that the label exchanges with the solvent prior to reduction of the DCIP or cytochrome c^{3+}. This conclusion is supported by the NADPH stereospecifity study described above as the pro-R ^{3}H appeared in the solvent fraction, presumably through solvent exchange while bound to the flavin.

4.5.3 Solvent kinetic isotope effects

Unlike substrate isotope effects, which investigate changes in the catalytic rate associated with one isotopic substitution, solvent isotope effects relate the changes associated with the complete replacement of exchangeable solvent protons with deuterons on the enzyme and substrate. Due to the global nature of solvent isotope studies, one must exercise caution in the interpretation of results since deuterium oxide could change the reaction rate by effecting several steps in a multi-step mechanism, substrate binding, and/or the stability or conformation of the enzyme (281).

The magnitude of the observed SKIE provides information regarding its origin. Large SKIE are thought to arise in a partially rate determining step(s) in which there is direct proton or hydride transfer in the transition-state (281). The isotope effect would likely be primary, where water is the reactant or functional group(s) on the enzyme or substrate become labeled by exchange with the solvent. In contrast, secondary isotope effects, defined by those involving conformational changes in the enzyme caused by the properties of hydrogen bonds, hydrophobic bonds and other factors typically yield small (~2) SKIE.

A large SKIE value of 8 for $^{D20}(V/K)_{cytc}$ was observed for the basal reduction of cytochrome c^{3+}, suggesting that proton uptake directly from the solvent or from an exchangeable site(s) on nNOS or cytochrome c^{3+} is the rate-limiting step in the oxidative half-reaction. The substrate cytochrome c^{3+} has numerous exchangeable hydrogenic sites; therefore, one can not exclude that the magnitude of SKIE in part arises from the effects D_2O on protein conformation and thus on substrate binding. The 4-fold increase in the SKIE on the observed $(V/K)_{cytc}$ may be attributed to a combination of events

including further rate limitation of proton transfer, an increase in the number of protons transferred, or the solvent effects on cytochrome c^{3+} binding becoming more pronounced. The level of Ca^{2+}-CaM stimulated cytochrome c^{3+} reductase activity was approximately 20% greater in D_2O compared to H_2O, indicating that deuterium oxide does not impair the affinity or behavior of the activated cofactor.

The solvent isotope effect on V was approximately 2 for the basal and CaM-stimulated reduction of cytochrome c^{3+}. A significantly smaller value for ^{D2O}V compared to $^{D2O}(V/K)_{cytc}$ suggests that while proton transfer is rate-limiting step in the oxidative half reaction, it does not completely limit the over all reaction rate. These results agree with the primary NADPH(D) substrate isotope effects showing that the reductive half reaction is more rate-limiting. Alternatively, structural differences in cytochrome c^{3+} induced by D_2O affecting its affinity for nNOS and the value for $^{D}(V/K)_{cytc}$, would not be observed in ^{D}V as it is not a function of substrate binding.

Small SKIE were observed for $^{D}(V/K)_{NADPH}$ for the basal and CaM-stimulated reduction of cytochrome c^{3+} indicating that proton transfer is not a rate-limiting step. The expression for $(V/K)_{NADPH}$ encompasses all the rate constants from the binding of NADPH up to the first irreversible step. If hydride transfer from C-4 of the nicotinamide ring to the N-5 of the flavin constitutes the first irreversible step, then one would not observe SKIE on subsequent proton transfer steps, such as protonation of the N-1 of the FAD isoalloxazine ring. Alternatively, hydride transfer could be a reversible step and SKIE on $(V/K)_{NADPH}$ could be suppressed by slower steps in the reaction.

4.5.4 Proton inventory analysis

The existence of an isotope effect does imply that some protonic restructuring does occur in the reaction. To obtain information concerning the number of protons and their individual contributions to the SKIE, a proton inventory experiment performed in which rate measurements were made in binary mixtures of H_2O and D_2O. The shape of a plot which compares the catalytic rate, ${}^{n}k$, against the fraction of deuterium in the solvent, n, shows if the SKIE arises from the transfer of one of more protons in the transition state. If a single transition state-proton contributes to SKIE the plot will generate a straight line since ${}^{n}k$ will be a linear function of n (eq. 4.4). However, if two or more protons contribute to SKIE, the plots will be bowl-shaped since ${}^{n}k$ becomes a polynomial function of n (eq. 4.5). The characteristic bowl-shaped curvature of the experimental data points in Figure 4.1 suggests the involvement of multiple protons in the conversion from the reactant-state to the transition-state in the basal reduction of DCIP and cytochrome c^{3+}. To verify whether the one- or multi-proton model better represents the proton inventory data in Figure 4.1, the data was fit to equation 4.6. For both data sets, a fit generated a value for C (1.13 and 1.22 for Figure 4.1, Panels A and B, respectively) that did not equal zero, indicating that the data does not accommodate a linear (one-proton) model. A fit of the data to eq 4.5, which assumes 2 protons are in flight, gave equal values for ϕ_1^T and ϕ_2^T; however, values ϕ_1^T and ϕ_2^T were undefined do to large standard errors. A fit of equation 4.7, where the number of parameters are reduced by assuming $\phi_1^T = \phi_2^T$; to the data in Figure 4.1 did generate defined values for the fractionation factor (Panel A, $\phi^T = 0.29 \pm 0.05$ and Panel B, $\phi^T = 0.30 \pm 0.03$). Although,

it was possible to statistically demonstrate that more then one proton is in flight, it was not possible to specify the exact number of protons in flight or the magnitude of their fractionation factors.

In summary, both primary substrate isotope effects and solvent isotope effects suggest that the reductive half-reaction is more rate determining then the subsequent oxidative half reaction in the ping-pong mechanisms for DCIP and cytochrome c^{3+} reduction and the presence of Ca^{2+}-CaM does not alter this behavior. The slow step in the reductive half reaction is not hydride transfer, but may be formation of the energetically unfavorable charge-transfer complex (E_1-NADPH), known to form in CPR and FNR. The slow step in the cytochrome c^{3+} oxidative half reaction appears to be multiple proton transfer from the solvent or an exchangeable site on nNOS or the substrate.

4.6 Acknowledgements

We are grateful to Drs. Sonia Anderson and Dean Malencik for supplying CaM and the CaM-Sepharose column, to Dr. Ted Dawson for giving us the cDNA plasmid construct for rat neuronal NOS and to Dr. Chris Mathews for T4 bacteriophage dihydrofolate reductase. We would also like to acknowledge the Nucleic Acids and Proteins Core Facilities of Oregon State University Environmental Health Sciences Center in conducting these studies.

Chapter 5

Conclusion

The flavoprotein domain nNOS shares considerable structural and functional similarity with CPR. During catalysis both enzymes shuttle NADPH-derived reducing equivalents from FAD to FMN and then finally to a P450-heme to enable heme-based oxygen activation. However, nNOS is unique in that the binding of Ca^{2+}-CaM enables electron transfer from FMN to the heme and alleviates inhibition of electron transfer within the flavoprotein domain. The latter of these roles for Ca^{2+}-CaM is correlated with the cofactor's ability to stimulate the reduction of flavin electron acceptors, DCIP and cytochrome c^{3+}. The uniqueness of nNOS in terms of Ca^{2+}-CaM stimulating electron transfer have encouraged evaluation of the steady-state kinetic mechanism for electron transfer to DCIP and cytochrome c^{3+} in the presence and absence of the cofactor. In addition the effect of Ca^{2+}-CaM on the rate limiting steps in the reaction cycle and the ionizable groups involved in catalysis or the binding of substrates was also investigated. Kinetic mechanisms in the presence and absence of Ca^{2+}-CaM for the reduction of DCIP and cytochrome c^{3+} were proposed based on steady-state initial velocity and inhibition studies. The pH-dependence on basal and CaM-stimulated reduction of DCIP and cytochrome c^{3+} was investigated to determined if the activated cofactor influences ionizable groups involved in the binding of substrates or catalysis. Finally, primary deuterium isotope effects (NADP(D)) and solvent isotope kinetic effects (SKIE) were to employed to probe for Ca^{2+}-CaM affects on rate-limiting steps in either mechanism.

A family of parallel lines on double reciprocal plots of initial velocity studies indicates that both DCIP and cytochrome c^{3+} are reduced *via* two-half reactions in a ping-pong mechanism. In the reductive half reaction NADPH reduces the nNOS flavins from the one-electron (E_1) to the three-electron reduced state (E_3). DCIP is reduced via two-electron donation; however, one electron is required to reduce cytochrome c^{3+}; therefore, the oxidative half reaction is different for the two substrates. Abstraction of two-electrons by DCIP returns nNOS to E_1, where reduction of two molecules of cytochrome c^{3+} is required to return the enzyme back to E_1. Product and dead-end inhibition data with DCIP were consistent with a ping-pong bi-bi mechanism; however, a steady-state isomerization step of E_3 was proposed based on the noncompetitive inhibition of $NADP^+$ at varying concentrations of DCIP. Hence the name of the mechanism was prefixed with iso (i.e. iso ping-pong bi bi). In contrast, product and dead-end inhibition studies with cytochrome c^{3+} were consistent with the nonclassical (two-site) ping-pong mechanism previously described for the NADPH-cytochrome P450 reductase-catalyzed reduction of cytochrome c^{3+}. In the former mechanism only binary complexes form; however, for the latter, ternary complexes are permissible. The differences in the kinetics mechanism may be related to the ability of DCIP to be reduced by nNOS with the FMN cofactor removed, where as the FMN cofactor is essential for cytochrome c^{3+} reduction. In other words, cytochrome c^{3+} requirement of the low potential flavin may effectively separate the catalytic sites for NADPH and cytochrome c^{3+} allowing a ternary complex to form and the reaction sequence to follow a two-site ping pong mechanism.

To accommodate competitive dead-end inhibition by 2'-AMP versus NADPH for both electron acceptors, the NADPH-analog was proposed to bind to E_1 in both kinetic mechanisms. However, 2'-AMP exhibited different binding affinities in the presence of cytochrome c^{3+} versus DCIP. Both kinetic mechanisms incorporated a rapid equilibrating isomerization step after the release of the electron acceptor and prior to the binding of NADPH to account for the difference in the apparent affinity of 2'-AMP. Thus, the kinetic mechanisms for reduction of DCIP and cytochrome c^{3+} were renamed di-iso ping-pong bi-bi and iso (two-site) ping-pong mechanism, respectively.

The presence Ca^{2+}-CaM did not alter the proposed kinetic mechanisms; however, it did effect to varying degrees, the $(k_{cat}/K_m)_{NADPH}$, for the various substrates and inhibition constants. The presence of Ca^{2+}-CaM caused a ~2-fold increase in the inhibition constant for 2'-AMP and $NADP^+$ versus NADPH suggesting that the activated cofactor may slightly reduce the affinity of the enzyme for these two inhibitors. Ca^{2+}-CaM caused a 1.5- to 2-fold increase in $(k_{cat}/K_m)_{NADPH}$, a 4.5-fold increase $(k_{cat}/K_m)_{DCIP}$, and a 23-fold increase in $(k_{cat}/K_m)_{cytc.}$. Based on the ratio of rate constants defining (k_{cat}/K_m) for the various substrates, Ca^{2+}-CaM may stimulate the rate of electron transfer to the electron acceptors by increasing the forward rate constants for the catalysis of these substrate and/or decreasing the dissociation constant for the electron acceptor.

The pH-dependence the kinetic parameters associated with the basal and CaM-stimulated rate of electron transfer to DCIP and cytochrome c^{3+} were investigated to determine the effects of the cofactor on ionizable groups involved in catalysis or the binding of substrates. The interpretation of the pH-dependence of V and (V/K) for the various substrates was done in the context of the proposed kinetic mechanisms. The

log V pH profile for the basal and CaM-stimulated reduction of DCIP forms a wave where the ionization of a group with a pK_a of 7.5 to 7.6 lead to an increase of a step that is normally rate-limiting. This step may be hydride transfer, the steady-state isomerization of the three-electron reduced state of nNOS, and/or the rate of electron transfer from the flavins to DCIP. The pH-dependencies of $(V/K)_{NADPH}$ and $(V/K)_{DCIP}$, indicate that of these rate constants, hydride transfer is more-rate limiting compared to the other two. The pH profiles $(V/K)_{NADPH}$ exhibited additional pK_a values associated with ionizable groups involved in the binding of the nucleotide. One of these groups may represent the 2'-phoshate of NADPH, as suggest by the titration profile of this substrate. If this were the case, then NADPH preferentially binds to nNOS in its monoanionic form. The $(V/K)_{DCIP}$ pH profile also exhibits additional pK_a groups that affect the binding of this substrate. The above mentioned pH profiles for the reduction are the same in the presence and absence of Ca^{2+}-CaM indicating that the cofactor does not influence ionizable groups associated with catalytic steps in DCIP reduction or the binding of NADPH or DCIP.

This is in contrast to the pH-dependencies observed for the basal and CaM-stimulated reduction of cytochrome c^{3+}. The log V versus pH profile for the basal cytochrome c^{3+} reductase activity is wave-shaped where the ionization of a group with a pK_a of 8.6 optimizes of catalysis. The rate-limiting catalytic step that is affected by pH is either hydride transfer or electron transfer from FMN to cytochrome c^{3+}. The pH-dependence on cytochrome c^{3+} reduction is dramatically altered in the presence of Ca^{2+}-CaM as the log V profile is bell-shaped with catalysis dependent on the deprotonation of an acidic group with a pK_a of 6.4 and protonation of group with a pK_a of 9.2. If the

binding of Ca^{2+}-CaM affects the relative rates of k_9 and k_{15} with respect to k_3, such that k_3 is no as longer rate limiting, then this could potentially shift the acidic pK_a from 8.6 to 6.4 and incorporate an additional pK_a at a higher pH. Alternatively, Ca^{2+}-CaM may affect which ionizable groups (through conformational change) on nNOS that participate in hydride transfer or electron transfer from FMN to cytochrome c^{3+}. The pH-profiles for $(V/K)_{cytc}$ for basal and CaM-stimulated reduction of cytochrome c^{3+} were bell-shaped as $(V/K)_{cytc}$ increased with the ionization of an acidic group with a pK_a of 7.1(basal) and 7.6 (Ca^{2+}-CaM) and decreased when a group with a pK_a of 9.4 – 9.6 ionized.

nNOS was found to abstract the pro-*R* (A-side) hydrogen from NADPH, consistent with it belonging to the electron/transferase family of dehydrogenases. Determination of the stereospecificity of hydride transfer permitted investigation of the primary deuterium isotope effects with (NADPH(D)) on V and (V/K) for the various substrates in the basal and CaM-stimulated reduction of DCIP and cytochrome c^{3+}. Interpretation of the primary isotope effects was done in the context of the ping-pong mechanism described for DCIP and cytochrome c^{3+}. The value for $^{D}(V/K)_{NADPH}$ was 1.2-1.7 in the presence of either electron acceptor; however, $^{D}(V/K)_{NADPH}$ for the reduction the substrates is defined by the same rate constant, $^{D}k_3$ which is the intrinsic isotope effect on hydride transfer, and this value typically ranges between 5-8. Thus, it was concluded that $^{D}(V/K)_{NADPH}$ incorporates an additional rate-limiting step that suppresses the full expression of the intrinsic isotope effect in $^{D}(V/K)_{NADPH}$. It was assumed that $(V/K)_{NADPH}$ is probably a function of other microscopic rate constants that define a conformational change associated with the formation of a charge-transfer complex (E_1-NADPH), which is

known to form in the related enzymes, CPR and FNR. The derivations of the kinetic mechanisms with this additional step are consistent with the steady-state initial velocity and inhibition data obtained previously, and the expression for $^{D}(V/K)_{NADPH}$ becomes a function of k_2, or the dissociation of the change transfer-complex. If $k_2 < k_{3H}$ then the full value of $^{D}k_3$ would be suppressed in $^{D}(V/K)_{NADPH}$. NADPH would be considered a "sticky" substrate where partitioning of the enzyme-substrate complex towards catalysis is favored compared to release from the enzyme.

The value of ^{D}V was slightly lower for DCIP reduction compared to cytochrome c^{3+} reduction. The expressions ^{D}V for the two substrates are distinguished by the ratio of the formation rate for the charge-transfer complex over the forward rate constants for the oxidative half reaction. If the ratio were smaller for DCIP reduction compared to cytochrome c^{3+} reduction then the ^{D}V value would be smaller for the former oxidant. Values for $^{D}(V/K)_{DCIP}$ and $^{D}(V/K)_{cytc}$ close to unity were consistent with the oxidative half reaction being isotopically insensitive in their respective ping-pong mechanisms.

Similar ^{D}V and $^{D}(V/K)_{NADPH}$ values were obtained for the basal and CaM-stimulated reduction of DCIP, while the value for ^{D}V was slightly greater than value for $^{D}(V/K)_{NADPH}$ for the basal and CaM-stimulated reduction of cytochrome c^{3+}, indicating that of the two half reactions, the reductive half reaction is more rate-limiting. This conclusion is supported by the SKIE, where a value $^{D20}(V/K)_{cytc}$ of 8 for the basal and 31 for CaM-stimulated reduction of cytochrome c^{3+} was reported, while small SKIE where associated both with V and $(V/K)_{NADPH}$. The large SKIE value for $^{D20}(V/K)_{cytc}$ indicates that proton uptake directly from the solvent or from an exchangeable site on nNOS or cytochrome c^{3+} is the rate-limiting step in the oxidative half-reaction. The 4-

fold increase in the SKIE on the observed $(V/K)_{cytc}$ may be attributed to further rate limitation of proton transfer, an increase in the number of protons transferred, or the solvent effects on cytochrome c^{3+} binding becoming more pronounced. Proton inventory analysis suggests that multiple protons are involved the conversion from the initial (reactant) state to the transition-state for both the basal reduction of DCIP and cytochrome c^{3+}.

Bibliography

1. Choi, D. (1993) Nitric Oxide: Foe or friend in the injured brain? *Proc. Natl. Acad. Sci.* **90**, 9741-9743.

2. Marletta, M.A., Tayeh, M.A., and Hevel, J.M. (1990) Unraveling the biological significance of nitric oxide. *Biofactors* **2**, 219-225.

3. Knowles, R.G. and Moncada, S. (1994) Nitric oxide synthases in mammals. *Biochem. J.* **298**, 249-258.

4. Marletta, M.A. (1994) Nitric oxide synthase: aspects concerning structure and catalysis. *Cell* **78**, 927-930.

5. Kwon, N.S., Nathan, C.F., Gilker, C., Griffith, O.W., Matthews, D.E., and Stuehr, D.J. (1990) L-citrulline production from L-arginine by macrophage nitric oxide synthase. The ureido oxygen derives from dioxygen. *J. Biol. Chem.* **265**, 13442-13445.

6. Stuehr, D.J., Kwon, N.S., Nathan, C.F., Griffith, O.W., Feldman, P.L., and Wiseman, J. (1991) N omega-hydroxy-L-arginine is an intermediate in the biosynthesis of nitric oxide from L-arginine. *J. Biol. Chem.* **266**, 6259-6263.

7. Klatt, P., Schmidt, K., Uray, G., and Mayer, B. (1993) Multiple catalytic functions of brain nitric oxide synthase. Biochemical characterization, cofactor-requirement, and the role of N omega-hydroxy-L-arginine as an intermediate. *J. Biol. Chem.* **268**, 14781-17487.

8. Pufahl, R.A., Nanjappan, P.G., Woodard, R.W., and Marletta, M.A. (1992) Mechanistic probes of N-hydroxylation of L-arginine by the inducible nitric oxide synthase from murine macrophages. *Biochemistry* **31**, 6822-6828.

9. Korth, H.G., Sustmann, R., Thater, C., Butler, A.R., and Ingold, K.U. (1994) On the mechanism of the nitric oxide synthase-catalyzed conversion of N omega-hydroxyl-L-arginine to citrulline and nitric oxide. *J. Biol. Chem.* **269**, 17776-17779.

10. Marletta, M.A. (1993) Nitric oxide synthase: function and mechanism. *Adv. Exp. Med. Biol*. **338**, 281-284.

11. McMillan, K., Bredt, D.S., Hirsch, D.J., Snyder, S.H., Clark, J.E., and Masters, B.S. (1992) Cloned, expressed rat cerebellar nitric oxide synthase contains stoichiometric amounts of heme, which binds carbon monoxide. *Proc. Natl. Acad. Sci. U. S. A.* **89**, 11141-11145.

12. Stuehr, D.J. and Ikeda-Saito, M. (1992) Spectral characterization of brain and macrophage nitric oxide synthases. Cytochrome P-450-like hemeproteins that contain a flavin semiquinone radical. *J. Biol. Chem.* **267**, 20547-20550.

13. Mayer, B., John, M., and Bohme, E. (1990) Purification of a Ca^{2+}/calmodulin-dependent nitric oxide synthase from porcine cerebellum. Cofactor-role of tetrahydrobiopterin. *FEBS Lett* **277**, 215-219.

14. White, K.A. and Marletta, M.A. (1992) Nitric oxide synthase is a cytochrome P-450 type hemoprotein. *Biochemistry* **31**, 6627-6631.

15. Bredt, D.S., Hwang, P.M., Glatt, C.E., Lowenstein, C., Reed, R.R., and Snyder, S.H. (1991) Cloned and expressed nitric oxide synthase structurally resembles cytochrome P-450 reductase. *Nature* **351**, 714-718.

16. Siddhanta, U., Wu, C., Abu-Soud, H.M., Zhang, J., Ghosh, D.K., and Stuehr, D.J. (1996) Heme iron reduction and catalysis by a nitric oxide synthase heterodimer containing one reductase and two oxygenase domains. *J. Biol. Chem.* **271**, 7309-7312.

17. Siddhanta, U., Presta, A., Fan, B., Wolan, D., Rousseau, D.L., and Stuehr, D.J. (1998) Domain swapping in inducible nitric-oxide synthase. Electron transfer occurs between flavin and heme groups located on adjacent subunits of the dimer. *J. Biol. Chem.* **273**, 18950-18958.

18. Abu-Soud, H.M. and Stuehr, D.J. (1993) Nitric oxide synthases reveal a role for calmodulin in controlling electron transfer. *Proc. Natl. Acad. Sci. U. S. A.* **90**, 10769-10772.

19. Bredt, D.S. and Snyder, S.H. (1990) Isolation of nitric oxide synthetase, a calmodulin-requiring enzyme. *Proc. Natl. Acad. Sci. U.S.A.* **87**, 682-685.

20. Presta, A., Liu, J., Sessa, W.C., and Stuehr, D.J. (1997) Substrate binding and calmodulin binding to endothelial nitric oxide synthase coregulate its enzymatic activity. *Nitric Oxide* **1**, 74-87.

21. Stevens-Truss, R. and Marletta, M.A. (1995) Interaction of calmodulin with the inducible murine macrophage nitric oxide synthase. *Biochemistry* **34**, 15638-15645.

22. Stuehr, D.J., Cho, H.J., Kwon, N.S., Weise, M.F., and Nathan, C.F. (1991) Purification and characterization of the cytokine-induced macrophage nitric oxide synthase: an FAD- and FMN-containing flavoprotein. *Proc. Natl. Acad. Sci. U. S. A.* **88**, 7773-7777.

23. Haufschild, T., Nava, E., Meyer, P., Flammer, J., Luscher, T.F., and Haefliger, I.O. (1996) Spontaneous calcium-independent nitric oxide synthase activity in porcine ciliary processes. *Biochem. Biophys. Res. Commun.* **222**, 786-789.

24. Schimdt, H.H.H.W., Pollock, J.S., Nakane, M., Gorsky, L.D., Forestermann, U., and Murad, F. (1991) Purification of a soluble isoform of guanylyl cyclase-activating cofactor synthase. *Proc. Natl. Acad. Sci. U.S.A.* **88**, 365-369.

25. Pollock, J.S., Forstermann, U., Mitchell, J.A., Warner, T.D., Schmidt, H.H., Nakane, M., and Murad, F. (1991) Purification and characterization of particulate endothelium-derived relaxing factor synthase from cultured and native bovine aortic endothelial cells *Proc. Natl. Acad. Sci. U.S.A.* **88**, 10480-10484.

26. Stuehr, D.J., Cho, H.J., Kwon, N.S., Weise, M.F., and Nathan, C.F. (1991) Purification and characterization of the cytokine-induced macrophage nitric oxide synthase: and FAD and FMN-containing flavoprotein. *Proc. Natl. Acad. Sci. USA* **88**, 7773-7777.

27. Cho, K.-O., Hunt, C.A., and Kennedy, M.B. (1992) The rat brain post-synaptic density fraction contains a homolog of the Drosophila large-disc tumor suppressor protein. *Neuron* **9**, 929-924.

28. Rodriguez-Crespo, I., Moenne-Loccoz, P., Loehr, T.M., and Ortiz de Montellano, P.R. (1997) Endothelial nitric oxide synthase: modulations of the distal heme site produced by progressive N-terminal deletions. *Biochemistry* **36**, 8530-8538.

29. Klatt, P., Schmidt, K., Lehner, D., Glatter, O., Bachinger, H.P., and Mayer, B. (1995) Structural analysis of porcine brain nitric oxide synthase reveals a role for tetrahydrobiopterin and L-arginine in the formation of an SDS- resistant dimer. *Embo J* **14**, 3687-3695.

30. Sheta, E.A., McMillan, K., and Masters, B.S. (1994) Evidence for a bidomain structure of constitutive cerebellar nitric oxide synthase. *J. Biol. Chem.* **269**, 15147-15153.

31. Klatt, P., Heinzel, B., John, M., Kastner, M., Bohme, E., and Mayer, B. (1992) Ca2+/calmodulin-dependent cytochrome c reductase activity of brain nitric oxide synthase. *J. Biol. Chem.* **267**, 11374-11378.

32. Venema, R.C., Ju, H., Zou, R., Ryan, J.W., and Venema, V.J. (1997) Subunit interactions of endothelial nitric-oxide synthase. Comparisons to the neuronal and inducible nitric-oxide synthase isoforms. *J Biol Chem* **272**, 1276-1282.

33. Ghosh, D.K. and Stuehr, D.J. (1995) Macrophage NO synthase: characterization of isolated oxygenase and reductase domains reveals a head-to-head subunit interaction. *Biochemistry* **34**, 801-807.

34. Abu-Soud, H.M., Loftus, M., and Stuehr, D.J. (1995) Subunit dissociation and unfolding of macrophage NO synthase: relationship between enzyme structure, prosthetic group binding, and catalytic function. *Biochemistry* **34**, 11167-11175.

35. Reif, A., Lothar, G., Kotsonis, P., Frey, A., Bommel, H.M., Wink, D.A., Pfleiderer, W., and Schmidt, H.H.H.W. (1999) Tetrahydrobiopeterin inhibits monomerization and is consumed during catalysis of neuronal NO synthesis. *J. Biol. Chem.* **274**, 24921-24929.

36. Klatt, P., Pfeiffer, S., List, B.M., Lehner, D., Glatter, O., Bachinger, H.P., Werner, E.R., Schmidt, K., and Mayer, B. (1996) Characterization of heme-deficient neuronal nitric-oxide synthase reveals a role for heme in subunit dimerization and binding of the amino acid substrate and tetrahydrobiopterin. *J Biol Chem* **271**, 7336-7342.

37. List, B.M., Klosch, B., Volker, C., Gorren, A.C., Sessa, W.C., Werner, E.R., Kukovetz, W.R., Schmidt, K., and Mayer, B. (1997) Characterization of bovine endothelial nitric oxide synthase as a homodimer with down-regulated uncoupled NADPH oxidase activity: tetrahydrobiopterin binding kinetics and role of haem in dimerization. *Biochem J* **323**, 159-165.

38. Nishida, C.R. and Ortiz de Montellano, P.R. (1998) Electron transfer and catalytic activity of nitric oxide synthases. *J. Biol. Chem.* **273**, 5566-5571.

39. Renodon, A., Boucher, J., Wu, C., Gachhui, R., Sari, M., Mansuy, D., and Stuehr, D. (1998) Formation of nitric oxide synthase-iron(II) nitrosoalkane complexes: severe restriction of access to the iron(II) site in the presence if tetrahydrobiopeterin. *Biochemistry* **37**, 6367-6374.

40. Ghosh, D.K., Abu-Soud, H.M., and Stuehr, D.J. (1996) Domains of macrophage N(O) synthase have divergent roles in forming and stabilizing the active dimeric enzyme. *Biochemistry* **35**, 1444-1449.

41. Crane, B.R., Arvai, A.S., Ghosh, D.K., Wu, C., Getzoff, E.D., Stuehr, D., and Tainer, J.A. (1998) Structure of nitric oxide synthase oxygenase dimer with pterin and substrate. *Science* **279**, 2121-2126.

42. Raman, C.S., Huiying, L., Martasek, P., Kral, V., Siler Masters, B.S., and Poulos, T.L. (1998) Crystal structure of constitutive endothelial nitric oxide synthase: a paradigm for pterin function involving a novel metal center. *Cell* **95**, 939-950.

43. Chen, P.F., Tsai, A.L., and Wu, K.K. (1994) Cysteine 184 of endothelial nitric oxide synthase is involved in heme coordination and catalytic activity. *J. Biol. Chem.* **269**, 25062-25066.

44. Richards, M.K. and Marletta, M.A. (1994) Characterization of neuronal nitric oxide synthase and a C415H mutant, purified from a baculovirus overexpression system. *Biochemistry* **33**, 14723-14732.

45. McMillan, K. and Masters, B.S. (1995) Prokaryotic expression of the heme- and flavin-binding domains of rat neuronal nitric oxide synthase as distinct polypeptides: identification of the heme-binding proximal thiolate ligand as cysteine-415. *Biochemistry* **34**, 3686-3693.

46. Cubberley, R.R., Alderton, W.K., Boyhan, A., Charles, I.G., Lowe, P.N., and Old, R.W. (1997) Cysteine-200 of human inducible nitric oxide synthase is essential for dimerization of haem domains and for binding of haem, nitroarginine and tetrahydrobiopterin. *Biochem J* **323**, 141-146.

47. Crane, B.R., Arvai, A.S., Gachhui, R., Wu, C., Ghosh, D.K., Getzoff, E.D., Stuehr, D.J., and Tainer, J.A. (1997) The structure of nitric oxide synthase oxygenase domain and inhibitor complexes .*Science* **278**, 425-431.

48. White, R.E. and Coon, M.J. (1982) Heme-ligand replacement reactions of cytochrome P450. *J. Biol. Chem.* **257**, 3077-3083.

49. Dawson, J.H., Andersson, L.A., and Sono, M. (1983) The diverse spectroscopic properties of ferrous cytochrome P-450-CAM. *J. Biol. Chem.* **258**, 13637-13645.

50. Poulos, T.L., Finzel, B.C., Gunsalus, I.C., Wagner, G.C., and Kraut, J. (1985) The 2.6 A crystal struture of Pseudomonas putida cytochrome P-450. *J. Biol. Chem.* **260**, 16122-16130.

51. Wang, J., Stuehr, D.J., Ikeda-Saito, M., and Rousseau, D.L. (1993) Heme coordination and structure of the catalytic site in nitric oxide synthase. *J. Biol. Chem.* **268**, 22255-22258.

52. McMillan, K. and Masters, B.S. (1993) Optical difference spectrophotometry as a probe of rat brain nitric oxide synthase heme-substrate interaction. *Biochemistry* **32**, 9875-9880.

53. Salerno, J.C., Frey, C., McMillan, K., Williams, R.F., Masters, B.S., and Griffith, O.W. (1995) Characterization by electron paramagnetic resonance of the interactions of L-arginine and L-thiocitrulline with the heme cofactor region of nitric oxide synthase *J. Biol. Chem.* **270**, 27423-27428.

54. Wolff, D.J., Datto, G.A., Samatovicz, R.A., and Tempsick, R.A. (1993) Calmodulin-dependent nitric-oxide synthase. Mechanism of inhibition by imidazole and phenylimidazoles *J. Biol. Chem.* **268**, 9425-9429.

55. Matsuoka, A., Stuehr, D.J., Olson, J.S., Clark, P., and Ikeda-Saito, M. (1994) L-arginine and calmodulin regulation of the heme iron reactivity in neuronal nitric oxide synthase. *J. Biol. Chem.* **269**, 20335-20339.

56. Sono, M., Ledbetter, A.P., McMillian, K., Roman, L.J., Shea, T.M., Siler Masters, B.S., and Dawson, J.H. (1999) Essential thiol requirement to restore pterin- or substrate-binding capability and to regenerate native enzyme-type high-spin heme spectra in the *Escherchia coli*-expressed tertrahydrobiopterin-free oxygenase domain of neuronal nitric oxide synthase. *Biochemistry* **38**, 15853-15862.

57. Gorren, A.C., Schrammel, A., Schmidt, K., and Mayer, B. (1997) Thiols and neuronal nitric oxide synthase: complex formation, competitive inhibition, and enzyme stabilization. *Biochemistry* **36**, 4360-4366.

58. Li, H., Raman, C.S., Glaser, C.B., Blasko, E., Young, T.A., Parinson, J.F., Whitlow, M., and Poulos, T.L. (1999) Crystal structures of zinc-free and -bound heme domain of human inducible nitric oxide synthase. *J. Biol. Chem.* **274**, 21276-21284.

59. Crane, B.R., Rosenfeld, R.J., Arval, A.S., Ghosh, D.K., Ghosh, S., Tainer, J.A., Stuehr, D.J., and Getzoff, E.D. (1999) N-terminal domain swapping and metal ion binding in nitric oxide synthase dimerization. *EMBO Journal* **18**, 6271-6281.

60. Fischmann, T.O., hruza, A., Nui, X.D., Fossetta, J.D., Lunn, C.A., Dolphin, E., Prongay, A.J., Reichert, P., Lundell, D.J., Narula, S.K., and Weber, P.C. (1999) Structural characterization of nitric oxide synthase isoform reveal stiking active site conservation. *Nat. Struct. Biol.* **6**, 233-241.

61. Gorren, A.C., List, B.M., Schrammel, A., Pitters, E., Hemmens, B., Werner, E.R., Schmidt, K., and Mayer, B. (1996) Tetrahydrobiopterin-free neuronal nitric oxide synthase: evidence for two identical highly anticooperative pteridine binding sites. *Biochemistry* **35**, 16735-16745.

62. Mayer, B., John, M., Heinzel, B., Werner, E.R., Wachter, H., Schultz, G., and Bohme, E. (1991) Brain nitric oxide synthase is a biopterin- and flavin-containing multi- functional oxido-reductase. *FEBS Lett* **288**, 187-191.

63. Richards, M.K., Clague, M.J., and Marletta, M.A. (1996) Characterization of C415 mutants of neuronal nitric oxide synthase. *Biochemistry* **35**, 7772-7780.

64. Hevel, J.M. and Marletta, M.A. (1992) Macrophage nitric oxide synthase: relationship between enzyme-bound tetrahydrobiopterin and synthase activity. *Biochemistry* **31**, 7160-7165.

65. Massey, V. and Hemmerich, P. (1980) Active site probes for flavoproteins. *Biochem. Soc. Trans.* **8**, 246-258.

66. Porter, T.D. and Kasper, C.D. (1986) NADPH-cytochrome P-450 oxidoreductase flavin mononucleotide and flavin adenine dinucleotide domains evolved from different flavoproteins. *Biochemistry* **25**, 1682-1687.

67. Gruez, A., Pignol, D., Zeghouf, M., Coves, J., Fontecave, M., Ferrer, J.L., and Fontecilla-Camps, J.C. (2000) Four crystal structures of the 60 KDa flavoprotein monomer of the sulfite reductase indicate a disordered flavodoxin-linke module. *J. Mol. Biol.* **26**, 199-212.

68. Leclerc, D., Wilson, A., Dumas, R., Gafuik, C., Song, D., Watins, D., Heng, H.H.Q., Rommens, J.M., Scherer, S.W., Roseblatt, D.S., and Gravel, R.A. (1998) Cloning and mapping of a cDNA for methionine synthethase reductase, a flavoprotein defective in patients with homocytinuria. *Proc. Natl. Acad. Sci. U.S.A.* **95**, 3059-3064.

69. Gutierrez, A., Lian, L.-Y., Wolf, C.R., Scrutton, N.S., and Roberts, G.C.K. (2001) Stopped-flow kinetic studies of flavin reduction in human cytochrome P450 reductase and its component domains. *Biochemistry* **40**, 1964-1975.

70. Wang, M., Roberts, D.L., Paschke, R., Shea, T.M., Masters, B.S., and Kim, J.J. (1997) Three-dimensional structure of NADPH-cytochrome P450 reductase: prototype for FMN- and FAD-containing enzymes. *Proc Natl Acad Sci U S A* **94**, 8411-8416.

71. Galli, C., MacArthur, R., Abu-Soud, H.M., Clark, P., Steuhr, D.J., and Brudvig, G.W. (1996) EPR spectroscopic characterization of neuronal NO synthase [published erratum appears in Biochemistry 1996 Jun 4;35(22):7298]. *Biochemistry* **35**, 2804-2810.

72. Witteveen, C.F.B., Giovanelli, J., Yim, M.B., Gachhui, R., Stuehr, D.J., and Kaufman, S. (1998) Reactivity of the flavin semiquinone of nitric oxide synthase in the oxygenation of arginine to NG-hydroxyarginine, the first step of nitric oxide synthesis [In Process Citation]. *Biochem. Biophys. Res. Commun.* **250**, 36-42.

73. Noble, M.A., Munro, A.W., Rivers, S.L., Robledo, L., Daff, S., Yellowlees, L.J., Shimizu, T., Sagami, I., Gullemette, G., and Chapman, S.K. (1999) Potentiometric analysis of the flavin cofactors of nitric oxide synthase. *J. Biol. Chem.* **38**, 16413-16418.

74. Gachhui, R., Presta, A., Bentley, D.F., Abu-Soud, H.M., McArthur, R., Brudvig, G., Ghosh, D.K., and Stuehr, D.J. (1996) Characterization of the reductase domain of rat neuronal nitric oxide synthase generated in the methylotrophic yeast Pichia pastoris. Calmodulin response is complete within the reductase domain itself. *J. Biol. Chem.* **271**, 20594-20602.

75. Williams, C.H.J. and Kamin, H. (1962) Microsomal triphosphopyridine nucleotide-cytochrome c reductase of liver. *J. Biol. Chem.* **237**, 587-595.

76. Abu-Soud, H.M., Yoho, L.L., and Stuehr, D.J. (1994) Calmodulin controls neuronal nitric-oxide synthase by a dual mechanism. Activation of intra- and interdomain electron transfer. *J. Biol. Chem.* **269**, 32047-32050.

77. Wolff, D.J., Datto, G.A., Samatovicz, R.A., and Tempsick, R.A. (1993) Calmodulin-dependent nitric-oxide synthase. Mechanism of inhibition by imidazole and phenylimidazoles. *J. Biol. Chem.* **268**, 9425-9429.

78. Roman, L.J., Martasek, P., Miller, T., Harris, D.E., de la Garza, M.A., Shea, T.M., Kim, J., and Siler Masters, B.S. (2000) The C termini of constiutive nitric-oxide synthases control electron flow through the flavin and heme domains and affects modulation by calmodulin. *J. Biol. Chem.* **275**, 29225-29232.

79. Daff, S., Sagami, I., and Shimizu, T. (1999) The 42-amino acid insert in the FMN domain of neuronal nitric oxide synthase exerts control over Ca2+/Calmodulin-dependent electron transfer. *J Biol. Chem.* **274**, 30589-30595.

80. Chen, P. and Wu, K.K. (2000) Characterization of the roles of the 594-645 region of human endothelial nitric-oxide synthase in regulating calmodulin binding and electron transfer. *J. Biol. Chem.* **275**, 13155-13163.

81. Adak, S., Ghosh, S., Abu-Soud, H.M., and Stuehr, D.J. (1999) Role of reductase domain cluster 1 acidic residues in neuronl nitric-oxide synthase. *J. Biol. Chem.* **274**, 22313-22320.

82. Salerno, J.C., Harris, D.E., Irizarry, K., Patel, B., Morales, A.J., Smith, S.M., Martasek, P., Roman, L.J., Masters, B.S., Jones, C.L., Weissman, B.A., Lane, P., Liu, Q., and Gross, S.S. (1997) An autoinhibitory control element defines calcium-regulated isoforms of nitric oxide synthase. *J. Biol. Chem.* **272**, 29769-29777.

83. Roman, L., Miller, T., de la Garaza, M., and J., K. (2000) The C terminus of mouse macrophage inducible nitric-oxide synthase attenutates electron flow through the flavin domain. *J. Biol. Chem.* **275**, 21914-21919.

84. Vorherr, T., Knopfel, L., Hofmann, F., Mollner, S., Pfeuffer, T., and Carafoli, E. (1993) The calmodulin binding domain of nitric-oxide synthase and adenylyl cyclase. *Biochemistry* **32**, 6081-6088.

85. Matsubara, M., Hayashi, N., Titani, K., and Taniguchi, H. (1997) Circular dichroism and 1H NMR studies on the structures of peptides derived from the calmodulin-binding domains of inducible and endothelial nitric-oxide synthase in solution and in complex with calmodulin. Nascent alpha-helical structures are stabilized by calmodulin both in the presence and absence of Ca2+. *J. Biol. Chem.* **272**, 23050-23056.

86. Zhang, M. and Vogel, H.J. (1994) Characterization of the calmodulin-binding domain of rat cerebellar nitric oxide synthase. *J. Biol. Chem.* **269**, 981-985.

87. Ruan, J., Xie, Q., Hutchinson, N., Cho, H., Wolfe, G.C., and Nathan, C. (1996) Inducible nitric oxide synthase requires both the canonical calmodulin- binding domain and additional sequences in order to bind calmodulin and produce nitric oxide in the absence of free Ca2+. *J. Biol. Chem.* **271**, 22679-22686.

88. Lee, S.-J. and Stull, J.T. (1998) Calmodulin-dependent regulation of inducible and neuronal nitric-oxide synthase. *J. Biol. Chem.* **273**, 27430-27437.

89. Persechini, A., White, H.D., and Gansz, K.J. (1996) Different mechanisms for Ca2+ dissociation from complexes of calmodulin with nitric oxide synthase or myosin light chain kinase. *J. Biol. Chem.* **271**, 62-67.

90. Stevens-Truss, R., Beckingham, K., and Marletta, M.A. (1997) Calcium binding sites of calmodulin and electron transfer by neuronal nitric oxide synthase. *Biochemistry* **36**, 12337-12345.

91. Su, Z., Blazing, M.A., Fan, D., and George, S.E. (1995) The calmodulin-nitric oxide synthase interaction. Critical role of the calmodulin latch domain in enzyme activation. *J. Biol. Chem.* **270**, 29117-29122.

92. Miller, T.R., Martasek, P., Omura, T., and Siler Masters, B.S. (1999) Rapid kinetic studies of electron transfer in the three isoforms of nitric-oxide synthases. *Biochem. Biophys. Res. Comm.* **265**, 184-188.

93. Mayer, B., Pfeiffer, S., Leopold, E., Muller, J., Weser, U., and Schmidt, K. (1996) Structural and functional analogs of CuZn superoxide dismutase inhibit rat brain nitric oxide synthase by interference with the reductase (diaphorase) domain. *Neurosci Lett* **209**, 169-172.

94. Heinzel, B., John, M., Klatt, P., Bohme, E., and Mayer, B. (1992) Ca2+/calmodulin-dependent formation of hydrogen peroxide by brain nitric oxide synthase. *Biochem. J.* **281**, 627-630.

95. Pou, S., Keaton, L., Surichamorn, W., and G.M., R. (1999) Mechanism of superoxide generation by neuronal nitric-oxide synthase. *J. Biol. Chem.* **274**, 9573-9580.

96. Xia, Y. and Zweier, J.L. (1997) Superoxide and peroxynitrite generation from inducible nitric oxide synthase in macrophages. *Proc. Natl. Acad. Sci. U. S. A.* **94**, 6954-6958.

97. Xia, Y., Tsai, A.L., Berka, V., and Zweier, J.L. (1998) Superoxide Generation from Endothelial Nitric-oxide Synthase. A Ca2+/calmodulin-dependent and tetrahydrobiopterin regulatory process. *J. Biol. Chem.* **273**, 25804-25808.

98. Vasquez-Vivar, J., Martasek, P., Hogg, N., Masters, B.S., Pritchard, K.A., Jr., and Kalyanaraman, B. (1997) Endothelial nitric oxide synthase-dependent superoxide generation from adriamycin. *Biochemistry* **36**, 11293-11297.

99. Xia, Y., Roman, L.J., Masters, B.S., and Zweier, J.L. (1998) Inducible nitric-oxide synthase generates superoxide from the reductase domain. *J. Biol. Chem.* **273**, 22635-22639.

100. Wever, R.M.F., van Dam, T., van Rijn, H.J., de Groot, F., and Rabelink, T.J. (1997) Tetrahydrobiopterin regulates superoxide and nitric oxide generation by recombinant endothelial nitric oxide synthase. *Biochem. Biophys. Res. Commun.* **237**, 340-344.

101. Presta, A., Weber-Main, A.M., Stankovich, M.T., and Stuehr, D.J. (1998) Comparative effects of substrates and pterin cofactors on the heme midpoint potential of inducible and neuronal nitric oxide synthases. *J. Am. Chem. Soc.* **120**, 9460-9465.

102. Abu-Soud, H.M., Wang, J., Rousseau, D.L., Fukuto, J.M., Ignarro, L.J., and Stuehr, D.J. (1995) Neuronal nitric oxide synthase self-inactivates by forming a ferrous- nitrosyl complex during aerobic catalysis. *J. Biol. Chem.* **270**, 22997-23006.

103. Boggs, S., Huang, L., and Stuehr, D.J. (2000) Formation and reactions of the heme-dioxygen intermediate in the first and second steps of nitric oxide

synthesis as studied by stopped-flow spectroscopy under single-turnover conditions. *Biochemistry* **39**, 2332-2339.

104. Adak, S., Wang, Q., and Stuehr, D.J. (2000) Arginine conversion to nitricoxide by tetrahydrobiopterin-free neuronal nitric-oxide synthase. *J. Biol. Chem.* **275**, 33554-33561.

105. Tsubaki, M., Hiwatashi, A., Ichikawa, Y., Fujimoto, Y., Ikekawa, N., and Hori, H. (1988) Electron paramagentic resonance study of the ferrous cytochrome P45O-scc nitric oxide complexes: effects of 20(R), 22(R) dihydroxycholesterol and reduced adrenodoxin. *Biochemisrty* **27**, 4856-4862.

106. Abu-Soud, H.M., Gachhui, R., Raushel, F.M., and Stuehr, D.J. (1997) The ferrous-dioxy complex of neuronal nitric oxide synthase. Divergent effects of L-arginine and tetrahydrobiopterin on its stability. *J. Biol. Chem.* **272**, 17349-17353.

107. Migita, C.T., Salerno, J.C., Masters, B.S., Martasek, P., McMillan, K., and Ikeda-Saito, M. (1997) Substrate binding-induced changes in the EPR spectra of the ferrous nitric oxide complexes of neuronal nitric oxide synthase. *Biochemistry* **36**, 10987-10992.

108. Adak, S., Croos, C., Wang, Q., Crane, B.R., Tainer, J.A., Getzoff, E.D., and Steuhr, D.J. (1999) Tryptophan 409 controls the activity of neuronal nitric-oxide synthase by regulating nitric oxide feedback inhibition. *J. Biol. Chem.* **274**, 26907-26911.

109. Negrerie, M., Berka, V., Vos, M.H., Liebl, U., Lambry, J., Tsai, A., and Martin, J. (1999) Geminate recombination of nitric oxide to endothelial nitric-oxide synthase and mechanistic implications. *J. Biol. Chem.* **274**, 24694-24702.

110. Abu-Soud, H.M., Ichimori, K., Presta, A., and Stuehr, D.J. (2000) Electron transfer, oxygen binding, and nitric oxide feedback inhibition in endothelial nitric oxide synthase. *J. Biol. Chem.* **275**, 17349-17357.

111. Ortiz de Montellano, P.R., *Cytochrome P-450 structure, mechanism and biochemistry*. 2nd ed, ed. P.R. Ortiz de Montellano. 1995, New York: Plenum Press. 245-303.

112. Sono, M., Roach, M.P., Coulter, E.D., and Dawson, J.H. (1996) Heme containing oxygenases *Chem. Rev.* **96**, 2841-2887.

113. Crane, B.R., Arvil, A.S., Ghosh, S., Getzoff, E.D., Stuehr, D.J., and Tainer, J.A. (2000) Stucture of the N-omega-hydroxy-L-arginine complex of inducible nitric oxide synthase oxygenase dimer with active and inactive pterins. *Biochemisty* **39**, 4608-4621.

114. Griffith, O.W. and Stuehr, D.J. (1995) Nitric oxide synthases: properties and catalytic mechanism. *Annu. Rev. Physiol.* **57**, 707-736.

115. Iwanaga, T., Yamazai, T., and Komoinami, S. (1999) Kinetic studies on the successive reaction of neuronal nitric oxide synthase from L-arginine to nitric oxide and citrulline. *Biochemistry* **38**, 16629-16635.

116. Clague, M.J., Wishnok, J.S., and Marletta, M.A. (1997) Formation of N-hydroxy-L-arginine and hydrogen peroxide by neuronal nitric oxide synthase: implications for mechanism. *Biochemistry* **36**, 14465-14473.

117. Mayer, B. and Hemmens, B. (1997) Biosynthesis and action of nitric oxide in mammalian cells. *Trends in Biochemical Sciences* **22**, 477-481.

118. Ghosh, D.K., Wu, C., Pitters, E., Moloney, M., Werner, E.R., Mayer, B., and Stuehr, D.J. (1997) Characterization of the inducible nitric oxide synthase oxygenase domain identifies a 49 amino acid segment required for subunit dimerization and tetrahydrobiopterin interaction. *Biochemistry* **36**, 10609-10619.

119. Gerber, N.C., Nishida, C.R., and Ortiz de Montellano, P.R. (1997) Characterization of human liver inducible nitric oxide synthase expressed in *Escherichia coli*. *Arch. Biochem. Biophys.* **343**, 249-253.

120. Mayer, B., Wu, C., Gorren, A.C., Pfeiffer, S., Schmidt, K., Clark, P., Stuehr, D.J., and Werner, E.R. (1997) Tetrahydrobiopterin binding to macrophage inducible nitric oxide synthase: heme spin shift and dimer stabilization by the potent pterin antagonist 4-amino-tetrahydrobiopterin. *Biochemistry* **36**, 8422-8427.

121. Rusche, K.M., Spierling, M.M., and Marletta, M.A. (1998) Reactions catalyzed by tetrahydrobiopterin-free nitric oxide synthase. *Biochemistry* **37**, 15503-15512.

122. Abu-Soud, H.M., Wu, C., Ghosh, D.K., and Stuehr, D.J. (1998) Stopped-flow analysis of CO and NO binding to nitric oxide synthase. *Biochemistry* **37**, 3777-3786.

123. Ghosh, S., Wolan, D., Adak, S., Crane, B.R., Kwon, N.S., Tainer, J.A., Getzoff, E.D., and Stuehr, D.J. (1999) Mutational Analysis of the tetrahydrobiobpterin-binding site in Inducible Nitric-oxide Synthase. *J. Biol. Chem.* **274**, 24100-24112.

124. Reid, J.J. (1993) Endothelin-1 may be a physiologic modulator of vasoconstriction in rat kidney. *J. Cardiovasc Pharmacol.* **22**, 267-270.

125. Reithmuller, C., Gorren, A.C.F., Pitters, E., Hemmens, B., Habisch, H., Heales, S.J.R., Schmidt, K., Werner, E.R., and Mayer, B. (1999) Activation of neuronal nitric oxide synthase by the 5-methyl analog of tetrahydrobiopterin. *J. Biol. Chem.* **274**, 16047-16051.

126. Witteveen, C.F.B., Giovanelli, J., and Kaufman, S. (1999) Reactivity of tetrahydrobiopterin bound to ntric oxide synthase. *J. Biol. Chem.* **274**, 29755-29762.

127. Witteveen, C.F., Giovanelli, J., and Kaufman, S. (1996) Reduction of quinonoid dihydrobiopterin to tetrahydrobiopterin by nitric oxide synthase. *J. Biol. Chem.* **271**, 4143-4147.

128. Vasquez-Vivar, J., Hogg, N., Martasek, P., Karoui, H., Pritchard, K.A., and Kalyanaraman, B. (1999) Tetrahydrobiopterin-dependent inhibition of superoxide generation from neuronal nitric oxide synthase. *J. Biol. Chem.* **274**, 41436-41442.

129. Hurshman, A.R., Krebs, C., Edmondson, D.E., Huynh, B.H., and Marletta, M.A. (1999) Formation of a Pterin radical in the reaction of the heme domain of inducible nitric-oxide synthase with oxygen. *Biochemistry* **38**, 15689-15696.

130. Abu-Soud, H.M., Presta, A., Mayer, B., and Stuehr, D.J. (1997) Analysis of neuronal NO synthase under single-turnover conditions: conversion of Nomega-hydroxyarginine to nitric oxide and citrulline. *Biochemistry* **36**, 10811-10816.

131. Presta, A., Siddhanta, U., Wu, C., Sennequier, N., Huang, L., Abu Soud, H.M., Erzurum, S., and Stuehr, D. (1998) Comparitive functioning of the dihyro- and tetrahydropterins in supporting electron transfer, catalysis and subunit dimerization in inducible nitric oxide synthase. *Biochemistry* **37**, 298-310.

132. Bec, N., Gorren, A.C.F., Voelker, C., Mayer, B., and Lang, R. (1998) Reaction of neuronal nitric-oxide synthase with oxygen at low temperature. *Journal of Biological Chemistry* **273**, 13502-13508.

133. Schmidt, H.H., Pollock, J.S., Nakane, M., Gorsky, L.D., Forstermann, U., and Murad, F. (1991) Purification of a soluble isoform of guanylyl cyclase-activating-factor synthase. *Proc. Natl. Acad. Sci. U. S. A.* **88**, 365-369.

134. Bredt, D.S., Hwang, P.M., and Snyder, S.H. (1990) Localization of nitric oxide synthase indicating a neural role for nitric oxide. *Nature* **347**, 768-770.

135. Schmidt, H.H., Gagne, G.D., Nakane, M., Pollock, J.S., Miller, M.F., and Murad, F. (1992) Mapping of neural nitric oxide synthase in the rat suggests frequent co- localization with NADPH diaphorase but not with soluble guanylyl cyclase, and novel paraneural functions for nitrinergic signal transduction. *J. Histochem. Cytochem.* **40**, 1439-1356.

136. Asano, K., Chee, C., Gaston, B., Lilly, C.M., Gerard, C., Drazen, J.M., and Stamler, J.S. (1994) Constitutive and inducible nitric oxide synthase gene expression, regulation, and activity in human lung epithelial cells. *Proc. Natl. Acad. Sci. U.S.A.* **91**, 10,089-10,093.

137. Schmidt, H.H., Warner, T.D., Ishii, K., Sheng, H., and Murad, F. (1992) Insulin secretion from pancreatic B cells caused by L-arginine-derived nitrogen oxides [see comments]. *Science* **255**, 721-723.

138. Nakane, M., Schmidt, H.H., Pollock, J.S., Forstermann, U., and Murad, F. (1993) Cloned human brain nitric oxide synthase is highly expressed in skeletal muscle. *FEBS Lett* **316**, 175-180.

139. Kobzik, L., Reid, M.B., Bredt, D.S., and Stamler, J.S. (1994) Nitric oxide in skeletal muscle [see comments]. *Nature* **372**, 546-548.

140. Marsden, P.A., Heng, H.H., Scherer, S.W., Stewart, R.J., Hall, A.V., Shi, X.M., Tsui, L.C., and Schappert, K.T. (1993) Structure and chromosomal localization of the human constitutive endothelial nitric oxide synthase gene. *J. Biol. Chem.* **268**, 17478-17488.

141. Larrson, B. and Phillips, S.C. (1998) Isolation and characterization of novel, human neuronal nitric oxide synthase cDNA. *Biochem. Biophys. Res. Comm.* **251**, 898-902.

142. Silvagno, F., Xia, H., and Bredt, D.S. (1996) Neuronal nitric-oxide synthase-mu, an alternatively spliced isoform expressed in differentiated skeletal muscle. *J Biol Chem* **271**, 11204-11208.

143. Schepens, J., Cuppen, E., Wieringa, B., and Hendriks, W. (1997) The neuronal nitric oxide synthase PDZ motif binds to -G(D,E)XV* carboxyterminal sequences. *FEBS Lett* **409**, 53-56.

144. Brenman, J.E., Chao, D.S., Xai, H., Aldape, K., and Bredt, D.S. (1995) Nitric oxide synthase complexed with dystrophin and absent from skeletal muscle sarcolemma in duchenne muscular dystrophy. *Cell* **82**, 743-752.

145. Brenman, J.E., Chao, D.S., Gee, S.H., McGee, A.W., Craven, S.E., Santillano, D.R., Wu, Z., Huang, F., Xia, H., Peters, M.F., Froehner, S.C., and Bredt, D.S.

(1996) Interaction of nitric oxide synthase with the postsynaptic density protein PSD-95 and alpha1-syntrophin mediated by PDZ domains. *Cell* **84**, 757-767.

146. Jaffrey, S.R. and Snyder, S.H. (1996) PIN: an associated protein inhibitor of neuronal nitric oxide synthase. *Science* **274**, 774-777.

147. Fan, J., Zhang, Q., Li, M., Tochio, H., Yamazaki, T., Shimizu, M., and Zhang, M. (1998) Protein inhibitor of neuronal nitric-oxide synthase, PIN, binds to a 17-amino acid fragment of the enzyme. *J. Biol. Chem.* **273**, 33472-33481.

148. Hemmens, B., Woschitz, S., Pitters, E., Kllsch, B., Volker, C., Schmidt, K., and Mayer, B. (1998) The protein inhibitor on neuronal nitric oxide synthase (PIN): characterization of its action of pure nitric oxide synthases. *Febs Lett.* **430**, 397-400.

149. Hevel, J.M., White, K.A., and Marletta, M.A. (1991) Purification of the inducible murine macrophage nitric oxide synthase. Identification as a flavoprotein. *J. Biol. Chem.* **266**, 22789-22791.

150. Bandaletova, T., Brouet, I., Barsch, H., Sugimura, T., Esumi, H., and Ohshima, H. (1993) Immunohistochemical localization of inducible form of nitric oxide synthase in various organs of rats treated with propionibacterium-acnes and lippopolysaccahride. *APMIS* **101**, 330-336.

151. Xie, Q.W., Whisnant, R., and Nathan, C. (1993) Promoter of the mouse gene encoding calcium-independent nitric oxide synthase confers inducibility by interferon gamma and bacterial lipopolysaccharide. *J. Exp. Med.* **177**, 1779-1784.

152. Xie, Q.-W., Kashiwabara, Y., and Nathan, C. (1994) Role of transcription factor NF-KB/rel in induction of nitric oxide synthase. *J. Biol. Chem.* **269**, 4705-4708.

153. Forrester, K., Ambs, S., Lupold, S.E., Kapust, R.B., Spillare, E.A., Weinberg, W.C., Felley-Bosco, E., Wang, X.W., Geller, D.A., Tzeng, E., Billiar, T.R., and Harris, C.C. (1996) Nitric oxide-induced p53 accumulation and regulation of inducible nitric oxide synthase expression by wild-type p53. *Proc. Natl. Acad. Sci. U. S. A.* **93**, 2442-2447.

154. Ratovitski, E.A., Bao, C., Quic, R.A., McMillan, A., Kozlovsky, C., and Lowenstein, C.J. (1999) An inducible nitric-oxide synthase (NOS)-associated protein inhibits NOS dimerization and activity. *J. Biol. Chem.* 30250-30257.

155. Pollock, J.S., Nakane, M., Buttery, L.K., Martinez, A., Springall, D., Polak, J.M., Forstermann, U., and Murad, F. (1983) Characterization and localization of endothelial nitric oxide synthase using specific monoclonial antibodies. *Am. J. Physiol.* **265**, 1379-1387.

156. Myatt, L., Brockman, D.E., Eis, A.L., and Pollock, J.S. (1993) Immunohistochemical localization of nitric oxide synthase in the human placenta. *Placenta* **14**, 487-495.

157. Tracey, W.R., Pollock, J.S., Murad, F., Nakane, M., and Forstermann, U. (1994) Identification of a type III (endothelial-like) articulate nitric oxide synthase in LLC-PK1 kidney tubular cells. *Am. J. Physiol.* 22-26.

158. Xue, C. and Johns, R.A. (1995) Endothelial nitric oxide synthase in the lungs of patients with pulmonary hypertension [letter]. *N. Engl. J. Med.* **333**, 1642-1644.

159. Dinerman, J.L., Dawson, T.M., Schell, M.J., Snowman, A., and Snyder, S.H. (1994) Endothelial nitric oxide synthase localized to hippocampal pyramidal cells: implications for synaptic plasticity. *Proc. Natl. Acad. Sci. U. S. A.* **91**, 4214-4218.

160. Shesely, E.G., Maeda, N., Kim, H.S., Desai, K.M., Krege, J.H., Laubach, V.E., Sherman, P.A., Sessa, W.C., and Smithies, O. (1996) Elevated blood pressures in mice lacking endothelial nitric oxide synthase. *Proc. Natl. Acad. Sci. U. S. A.* **93**, 13176-13181.

161. Shaul, P.W., Smart, E.J., Robinson, L.J., German, Z., Yuhanna, I.S., Ying, Y., Anderson, R.G., and Michel, T. (1996) Acylation targets emdothelial nitric-oxide synthase to plasmalemmal caveolae. *J. Biol. Chem.* **271**, 6518-6522.

162. Anderson, R.G.W. (1993) Caveolae: where incoming ans outcoming messangers meet. *Proc. Natl. Acad. Sci. U.S.A.* **90**, 10909-10913.

163. Lisanti, M.P., Tang, Z., Scherer, P.E., and Sargiacomo, M. (1995) caveolae purification and glycosylphophatidylinositol-linked protein sorting in polarized epithelial *Methods Enzymol.* **250**, 665-668.

164. Feron, O., Belhassen, L., Kobzik, L., Smith, T.W., Kelly, R.A., and Michel, T. (1996) Endothelial nitric oxide synthase targeting to caveolae. Specific interactions with caveolin isoforms in cardiac myocytes and endothelial cells. *J. Biol. Chem.* **271**, 22810-22814.

165. Venema, V.J., Zou, R., Ju, H., Marrero, M.B., and Venema, R.C. (1997) Caveolin-1 detergent solubility and association with endothelial nitric oxide synthase is modulated by tyrosine phosphorylation. *Biochem. Biophys. Res. Commun.* **236**, 155-161.

166. Michel, J.B., Feron, O., Sacks, D., and Michel, T. (1997) Reciprocal regulation of endothelial nitric-oxide synthase by Ca2+- calmodulin and caveolin. *J. Biol. Chem.* **272**, 15583-15586.

167. Feron, O., Smith, T.W., Michel, T., and Kelly, R.A. (1997) Dynamic targeting of the agonist-stimulated m2 muscarinic acetylcholine receptor to caveolae in cardiac myocytes. *J. Biol. Chem.* **272**, 17744-17748.

168. Ju, H., Zou, R., Venema, V.J., and Venema, R.C. (1997) Direct interaction of endothelial nitric-oxide synthase and caveolin-1 inhibits synthase activity. *J. Biol. Chem.* **272**, 18522-18525.

169. Ghosh, S., Gachhui, R., Crooks, C., Wu, C., Lisanti, M.P., and Stuehr, D.J. (1998) Interaction between caveolin-1 and the reductase domain of endothelial nitric-oxide synthase. Consequences for catalysis. *J. Biol. Chem* . **273**, 22267-22271.

170. Hensely, K., Tababaie, T., Stewart, C.A., Pye, Q., and Floyd, R.A. (1996) Nitric oxide and derived species as toxic agents in stroke, aids dimentia and chronic neurodegenerative diseases. *Chem. Res.Toxicol.* **10**, 527-532.

171. Wood, J. and Garthwaite, J. (1994) Models of the diffusional spread of nitric oxide: implications for neural nitric oxide signalling and its pharmalogical properties. *Neuropharmacology* **33**, 1235-1244.

172. Pryor, W.A. and Squadrito, G.L. (1995) The chemistry of peroxinitrite: a product from the reaction of nitric oxide with superoxide. *Am J. Physiol* **268**, 669-722.

173. Gow, A.J. and Stamler, J.S. (1998) Reactions between nitric oxide and hemoglobin under physiological conditions. *Nature* **391**, 169-173.

174. Lipton, S.A., Singel, D.J., and Stamler, J.S. (1994) Neuroprotective and neurodesructive effects of nitric oxide and redox congeners. *Ann. N.Y. Acad. Sci.* **738**, 382-387.

175. Huie, R.E. and Padmaja, S. (1993) The reaction of NO wih superoxide. *Free Radical Research Commun.* **188**, 195-199.

176. Radi, R., Beckman, J.S., Bush, K.M., and Freeman, B.A. (1991) Peroxynitrite-induced lipid peroxidation: The cytotoxic potential of superoxide and nitric oxide. *Arch. Biochem. Biophs.* **288**, 481-489.

177. Halfpenny, E. and Robinson, P.L. (1952) The nitration and hydroxylation of aromatic compounds by pernitrous acid. *J. Chem. Soc.* **A**, 928-946.

178. Wiseman and Halliwel, B. (1996) Damage to DNA by reactive oxygen and nitrogen species: Role in inflammatory disease and progression to cancer. *Biochem. J.* **313**, 17-29.

179. Lymar, S.V., Jiang, Q., and Hurst, J. (1995) Mechanisms of carbon dioxide-catalyzed oxidation of tyrosine by peroxynitrite *Biochemistry* **35**, 7855-7861.

180. Caulfield, J.L., Wishnok, J.S., and Tannenbaum, S.R. (1998) Nitric oxide-induced deamination of cytosine and guanine in deoxynucleotides and oligonucleotides. *J. Biol. Chem.* **273**, 12689-12695.

181. Zhang, J., Dawson, V.L., Dawson, T.M., and Snyder, S.H. (1994) Nitric oxide activation of poly(ADP-ribose) synthetase in neurotoxcity. *Science* **263**, 687-689.

182. Moncada, S. and Higgs, A. (1993) The L-arginine-nitric oxide pathway. *N. Engl. J. Med.* **329**, 2002-2012.

183. Moncada, S. and Higgs, E.A. (1995) Molecular mechanisms and therapeutic strategies related to nitric oxide. *Faseb J.* **9**, 1319-1330.

184. McAndrew, J., Patel, R.P., Jo, H., Cornwell, T., Lincoln, T., Moellering, D., White, C.R., Matalon, S., and Darley-Usmar, V. (1997) The interplay of nitric oxide and peroxynitrite with signal transduction pathways: implications for disease. *Semin. Perinatol.* **21**, 351-366.

185. Huang, Z., Huang, P.L., Panahian, N., Dalkara, T., Fishman, M.C., and Moskowitz, M.A. (1994) Effects of cerebral ischemia in mice deficient in neuronal nitric oxide synthase. *Science* **265**, 1883-1885.

186. Nathan, C. (1995) Inducible nitric oxide synthase: regulation subserves function. *Cur.r Top. Microbiol. Immunol.* **196**, 1-4.

187. Roman, L.J., Sheta, E.A., Martasek, P., Gross, S.S., Liu, Q., and Masters, B.S. (1995) High-level expression of functional rat neuronal nitric oxide synthase in Escherichia coli. *Proc. Natl. Acad. Sci. U. S. A.* **92**, 8428-8432.

188. Furfine, E.S., Harmon, M.F., Paith, J.E., and Garvey, E.P. (1993) Selective inhibition of constitutive nitric oxide synthase by L-NG-nitroarginine. *Biochemistry* **32**, 8512-8517.

189. Furfine, E.S., Harmon, M.F., Paith, J.E., Knowles, R.G., Salter, M., Kiff, R.J., Duffy, C., Hazelwood, R., Oplinger, J.A., and Garvey, E.P. (1994) Potent and selective inhibition of human nitric oxide synthases. Selective inhibition of neuronal nitric oxide synthase by S-methyl-L- thiocitrulline and S-ethyl-L-thiocitrulline. *J. Biol. Chem.* **269**, 26677-26683.

190. Furchgott, R.F., *Studies on the relaxation of rabbit arota by sodium nitrite: The basis for the proposal that the acid-activatable inflammatory inhibitory factor from bovine retactor penis is inorganic nitrite and the endothelium-derived relaxing factor is nitric oxide.* Vasodilation; Vascular Smooth Muscle, Peptides, Autonomic nerves, and Endothelium, ed. P.M. Vanhoutte. 1988, New York: Raven Press.

191. Ignarro, L.J., BUga, G.M., Wood, K.S., and Byrns, R.E. (1987) Endothelium-derived relaxing factor produced and released from artery and vein is nitric oxide. *Proc. Natl. Acad. Sci. U.S.A.* **84**, 9265-9269.

192. Ignarro, L.J. (1993) Nitric oxide-mediated vasorelaxation. *Thromb. Haemost.* **70**, 148-151.

193. Radomski, M.W. and Moncada, S. (1993) Regulation of vascular homeostasis by nitric oxide. *Thromb. Haemost.* **70**, 36-41.

194. Moro, M.A., Russel, R.J., Cellek, S., Lizasoain, I., Su, Y., Darley-Usmar, V.M., Radomski, M.W., and Moncada, S. (1996) cGMP mediates the vascular and platelet actions of nitric oxide: confirmation using an inhibitor of the soluble guanylyl cyclase. *Proc. Natl. Acad. Sci. U. S. A.* **93**, 1480-1485.

195. Brandish, P.E., Buechler, W., and Marletta, M.A. (1998) Regeneration of the ferrous heme of soluble guanylate cyclase fron nitric oxide complex: acceleration by thiols and oxyhemoglobin. *Biochemistry* **37**, 16898-16907.

196. Hibbs, J.B., Taintor, R.R., Chapman, H.A.J., and Weinberg, J.B. (1977) Macrophage tumor killing: influence of the local environement. *Science* **197**, 279-287.

197. Lancaster, J.R., Jr. and Hibbs, J.B., Jr. (1990) EPR demonstration of iron-nitrosyl complex formation by cytotoxic activated macrophages. *Proc. Natl. Acad. Sci. U. S. A.* **87**, 1223-1227.

198. Henry, Y., LePoivre, M., and Drapier, J.C. (1993) EPR characterization of molecular targets for NO in mammalian cells and organelles. *FASEB J.* **7**, 2224-2234.

199. Lepoivre, M., Flaman, J.M., Bobe, P., Lemaire, G., and Henry, Y. (1994) Quenching of the tyrosyl free radical of ribonucleotide reductase by nitric oxide. Relationship to cytostasis induced in tumor cells by cytotoxic macrophages. *J. Biol. Chem.* **269**, 21891-21897.

200. Garthwaite, J., Charles, S.L., and Chess-Williams, R. (1988) Endothelium-derived relaxing factor release on activation of NMDA receptors suggests a role as an intracellular messenger. *Nature* **336**, 385-388.

201. Garthwaite, J. and Boulton, C.L. (1995) Nitric oxide signaling in the central nervous system. *Annu. Rev. Physiol.* **57**, 683-706.

202. Bredt, D.S. and Snyder, S.H. (1989) Nitric oxide mediates glutamate-mediated enhancement of cGMP levels in the cerebellum. *Proc. Natl. Acad. Sci. U.S.A.* **86**, 9030-9033.

203. Knowles, R.G., Palacios, M., Palmer, R.M.J., and Moncada, S. (1989) Formation of nitric oxide from L-arginine in the central nervous system: a transduction mechanism for the stimulation of the soluble guanyate cyclase. *Proc. Natl. Acad. Sci. U.S.A.* **86**, 5159-5162.

204. O'Dell, T.J., Hawkins, R.D., Kandel, E.R., and Arancio, O. (1991) Tests of the role of of two diffusible substances in long term potentiation: Evidence for nitric oxide as a possible retrograde messenger. *Proc. Natl. Acad. Sci. U.S.A.* **88**, 11285-11289.

205. Schuman, E.M. and Madison, D.V. (1991) A requirement for the intercellular messenger nitric oxide in long-term potentiation. *Science* **254**, 1503-1506.

206. Shibuki, K. and Okada, D. (1991) Endogenous nitric oxide release required for long-term synaptic depression in the cerebellum. *Nature* **349**, 326-328.

207. Arancio, O., Kiebler, M., Lee, C.J., Lev-Ram, V., Tsien, R.Y., Kandel, E.R., and Hawkins, R.D. (1996) Nitric oxide acts directly in the presynaptic neuron to produce long term potentiation in cultured hippocampal neurons. *Cell* **87**, 1025-1035.

208. Holscher, C. (1997) Nitric oxide, the enigmatic neuronal messenger: its role in synaptic plasticity [see comments]. *Trends Neurosc.i* **20**, 298-303.

209. Son, H., Hawkins, R.D., Martin, K., Kiebler, M., Huang, P.L., Fishman, M.C., and Kandel, E.R. (1996) Long-term potentiation is reduced in mice that are doubly mutant in endothelial and neuronal nitric oxide synthase. *Cell* **87**, 1015-1023.

210. Dawson, T.M., Zhang, J., Dawson, V.L., and Snyder, S.H. (1994) Nitric oxide: cellular regulation and neuronal injury. *Prog. Brain Res.* **103**, 365-369.

211. Sattler, R., Xiong, Z., Lu, W., Hafner, M., MacDonald, J.F., and Tymianski, M. (1999) Specific coupling of NMDA recepetor activation to nitric oxide neurotoxicity by PSD-95 protein. *Science* **284**, 1845-1848.

212. Lei, S.Z., Pan, Z.-H., Aggarwal, S.K., chen, H.-S.V., Hartman J., Sucher, N.J., and Lipton, S.A. (1992) Effect of nitric oxide production on the redox modulatory site of the NMDA receptor-channel complex. *Neuron* **8**, 1087-1099.

213. Rand, M.J. and Li, C.G. (1995) Nitric oxide as a neurotransmitter in peripheral nerves: nature of transmitter and mechanism of transmission. *Annu. Rev. Physiol.* **57**, 659-682.

214. Burleigh, D.E. (1992) N-nitro-L-arginine reduces nonadrenergic noncholinergic relaxtions of human gut. *Gastroenterology* **102**, 679-683.

215. Burnett, A.L., Lowenstein, C.J., Bredt, D.S., Chang, T.S., and Snyder, S.H. (1992) Nitric oxide: a physiologic mediator of penile erection. *Science* **257**, 401-403.

216. Belvisi, M.G., Stretton, C.D., Miura, M., Verleden, G.M., Tadjkarimi, S., Yacoub, M.H., and Barnes, P.J. (1992) Inhibitory NANC nerves in human tracheal smooth muscle: a quest for the neurotransmitter. *J. Appl. Physiol.* **73**, 2505-2510.

217. Moncada, S. and Higgs, E.A. (1991) Endogenous nitric oxide: physiology, pathology and clinical relevance. *Eur. J. Clin. Invest.* **21**, 361-374.

218. Nathan, C.F. (1991) Role of nitric oxide synthesis in macrophage antimicrobial activity. *Curr. Opin. Immunol.* **3**, 65-70.

219. Stuehr, D.J. and Griffith, O.W. (1992) Mammalian nitric oxide synthases. *Adv. Enzymol. Relat. Areas Mol. Biol.* **65**, 287-346.

220. Cho, H.J., Xie, Q.W., Calaycay, J., Mumford, R.A., Swiderek, K.M., Lee, T.D., and Nathan, C. (1992) Calmodulin is a subunit of nitric oxide synthase from macrophages. *J. Exp. Med.* **176**, 599-604.

221. Nishimura, J.S., Martasek, P., McMillan, K., Salerno, J., Liu, Q., Gross, S.S., and Masters, B.S. (1995) Modular structure of neuronal nitric oxide synthase: localization of the arginine binding site and modulation by pterin. *Biochem. Biophys. Res. Commun.* **210**, 288-294.

222. Vermilion, J.L. and Coon, M.L. (1978) Identification of the high and low potential flavins of liver microsomal NADPH-cytochrome P-450 reductase. *J Biol. Chem.* **253**, 8812-8819.

223. Oprian, D.D., Vatsis, K.P., and Coon, M.J. (1979) Kinetics of reduction of cytochrome P-450LM4 in a reconstituted liver microsomal enzyme system. *J. Biol. Chem.* **254**, 8895-8902.

224. Iyanagi, T. and Mason, F. (1973) Some properties of hepatic reduced nicotinamide adenine phosphate cytochrome c reductase. *Biochemistry* **12**, 2297-2308.

225. Vermillion, J.L., Balloou, D.P., Massey, V., and Coon, M.J. (1981) Separate Role for FMN and FAD in Catalysis by Liver Microsomal NADPH-cytochrome P450 reductase. *J. Biol. Chem.* **256**, 266-277.

226. Iyanagi, T., Makino, N., and Mason, H.S. (1974) Redox properties of the reduced nicotinamide andenine dinucleotide phosphate cytochrome P-450 and reduced nictotinamide adenine dinucleotide-cytochrome b5 reductase. *Biochemistry* **13**, 1701-1710.

227. Dawson, V.L. and Dawson, T.M. (1996) Nitric oxide actions in neurochemistry. *Neurochem. Int.* **29**, 97-110.

228. Muchmore, D.C., McIntosh, L.P., Russell, C.B., Anderson, D.E., and Dahlquist, F.W. (1989) Expression and nitrogen-15 labeling of proteins for proton and nitrogen-15 nuclear magnetic resonance. *Methods Enzymol.* **177**, 44-73.

229. Gerber, N.C. and Ortiz de Montellano, P.R. (1995) Neuronal nitric oxide synthase. Expression in *Escherichia coli*, irreversible inhibition by phenyldiazene, and active site topology. *J. Biol. Chem.* **270**, 17791-17796.

230. Peterson, G. (1977) A simplification of the protein assay method of Lowry *et al.* which is generally more applicable. *Anal. Biochem.* **83**, 346-356.

231. Gelder, B.F.V. and Slater, E.C. (1962) The extinction coefficient for cytochrome c^{3+}. *Biochim. Biophys. Acta* **58**, 593-595.

232. Renosto, F., Ornitz, D.M., Peterson, D., and Segal, I.H. (1981) Nitrate reductase from *Penicillium chryogenum*. Purification and kinetic mechanism. *J. Biol. Chem.* **25**, 8616-8625.

233. Cleland, W.W. (1977) Determining the chemical mechanisms of enzyme catalyzed reactions by kinetic studies. *Adv. Enzymol. Relat. Area Mol. Biol.* **45**, 273-387.

234. Cleland, W.W. (1963) The kinetics of enzyme-catalyzed reactions with two or more substrates or products: nomenclature and rate equations. *Biochim. Biophys. Acta* **67**, 104-137.

235. Wolff, D.J. and Datto, G.A. (1992) Identification and characterization of a calmodulin-dependent nitric oxide synthase from GH3 pituitary cells. *Biochem. J.* **285**, 201-206.

236. Sem, D. and Kasper, C. (1994) Kinetic mechanism for the model reaction of NADPH-cytochrome P450 oxidoreductase with cytochrome c. *Biochemistry* **33**, 12012-12021.

237. Northrop, D.B. (1969) Transcarboxylase-kinetic analysis of the reaction mechanism. *J. Biol. Chem.* **244**, 5808-8519.

238. Cleland, W.W. (1963) The kinetics of enzyme-catalyzed reactions with two or more substrates or products: prediction of initial velocity and inhibition patterns by inspection. *Biochim. Biophys. Acta* **67**, 188-202.

239. Abu-Soud, H.M., Feldman, P.L., Clark, P., and Stuehr, D.J. (1994) Electron transfer in the nitric-oxide synthases. Characterization of L-arginine analogs that block heme iron reduction. *J. Biol. Chem.* **269**, 32318-32326.

240. Barden, R.E., Fung, C.-H., Utter, M.F., and Scrutton, M.C. (1981) Pyruvate carboxylase from chicken liver. Steady state kinetic studies indicates a "two-site" ping pong mechanism. *J. Biol. Chem.* **247**, 1323-1333.

241. Tsai, C.S., Burgett, M.W., and Reed, L.J. (1973) Alha-keto acid dehydrogenase complexes: A kinetic study of the pyruvate dehydrogenase complex from bovine kidney. *J. Biol. Chem.* **248**, 8348-8352.

242. Coughlan, M.P. and Rajagopalan, K.V. (1980) The kinetic mechanism of xanthine dehydrogenase and related enzymes. *Eur. J. Biochem.* **105**, 81-84.

243. Rendina, A.R. and Orme-Johnson, W.H. (1978) Glutamate synthetase: on the kinetic mechanism of the enzyme from *Escherchia coli* W. *Biochemistry* **12**, 5388-5393.

244. Livingston, D.J., Fox, J.A., Orme-Johnson, W.H., and Walsh, C.T. (1987) 8-Hydroxy-5-deazaflavin-reducing hydrgenase from *Methanobacterium thermoautophicum*: 2. Kinetic and hydrogen-transfer studies. *Biochemistry* **14**, 4228-4237.

245. Arp, D.J. and Burris, R.H. (1981) Kinetic mechanism of the hydrogen-oxidizing hydrogenase from soybean nodule bacteriods. *Biochemistry* **20**, 2234-2240.

246. Hines, V. and Johnston, M. (1989) Analysis of the kinetic mechanism of the bovine liver mitochondrial dihydroorotate dehydrogenase. *Biochemistry* **28**, 1222-1226.

247. Sem, D. and Kasper, C. (1995) Effect of ionic strength on the kinetic mechanism and relative rate limitation of steps in the model NAPH-cytochrome P450 oxidoreducatase reaction with cytochrome c. *Biochemistry* **34**, 12768-12774.

248. Murataliev, M.B., Klein, M., Fulco, A.J., and Feyereisen, R. (1997) Functional interactions in Cytochrome P450BM3: Flavin semiquinone interemediates, role of NADP(H), and mechansim of electron transfer by the flavoprotein domian. *Biochemistry* **36**, 8401-8412.

249. Labeth, J.D. and Klamin, H. (1976) Adrenodoxin reductase-properties of reduced enzyme with $NADP^+$ and NADPH. *J. Biol. Chem.* **251**, 4299-4306.

250. Karplus, P.A., Daniels, M.J., and Herriott, J.R. (1991) Atomic structure of ferredoxin-NADP+ reductase: prototype for a structurally novel flavoenzyme family. *Science* **251**, 60-66.

251. Deng, Z., Alivert, A., Zanetti, G., Arakak, A.K., Ottado, J., Orellano, E.G., Clacaterra, N.B., Ceccarelli, E.A., Carrillo, N., and Karplus, P.A. (1999) A productive NADP+ binding mode of ferredoxin-NADP+ reductase revealed by protein engineering and crystallographic studies. *Nat. Struct. Biol.* **6**, 847-853.

252. Nathan, C. and Xie, Q.W. (1994) Nitric oxide synthases: roles, tolls, and controls. *Cell* **78**, 915-918.

253. Gachhui, R., Ghosh, D.K., Wu, C., Parkinson, J., Crane, B.R., and Stuehr, D.J. (1997) Mutagenesis of acidic residues in the oxygenase domain of inducible nitric-oxide synthase identifies a glutamate involved in arginine binding. *Biochemistry* **36**, 5097-5103.

254. Wolthers, K.R. and Schimerlik, M.I. (2001) The reaction of neuronal nitric oxide 2, 6-Dicholorindophenol and Cytochrome c^{3+}: Influence of electron acceptor and the binding of Ca^{2+}-activated Calmodulin on the Kinetic Mechanism. *Biochemistry* **40**, 4722-4737.

255. Cleland, W.W. (1982) The use of pH studies to determine chemical mechanisms of enzyme-catalyzed reactions. *Methods Enzymol.* **87**, 390-405.

256. Feeney, J., Birdsall, B., Roberts, G.C.K., and Burgen, A.S.V. (1975) 31P NMR studies of NADPH and NADP+ binding to *L. casi* dihydrofolate reductase. *Nature* **257**, 564-568.

257. Mas, M.T. and Colman, R.F. (1984) Phosphorous-31 nuclear magnetic resonance studies of the binding of nucleotides to NADP+-specific isocitrate dehydrogenase. *Biochemistry* **23**, 1675-1683.

258. Sem, D.S. and Kasper, C.B. (1993) Enzyme-substrate binding interactions of NADPH-Cytochrome P-450 oxidoreductase characterized with pH and alternate substrate/inhibitor studies. *Biochemistry* **32**, 11539-11547.

259. Steyn-Parve, E.P. and Beinert, H. (1958) On the mechanism of dehydrogenation of fatty acyl derivatives of coenzyme A *J. Biol. Chem.* **233**, 843-852.

260. Hyde, E.I., Birdsall, B., Roberts, G.C.K., Feeney, J., and Burgen, A.S.V. (1980) Phosphorous-31 nuclear magnetic resonance studies of the binding of oxidized coenzyme to *Lactobacillus casei* dihyrofolate reductase. *Biochemistry* **19**, 3746-3754.

261. Eyschen, J., Vitoux, B., Rahuel-Clermont, S., Marraud, M., Branlant, G., and Cung, M.T. (1996) Phosphorous-31 nuclear magnetic resonance studies on coenzyme binding and specificity in glyceraldehyde-3-phosphate dehydrogenase. *Biochemistry* **35**, 6064-6072.

262. Sem, D.S. and Kasper, C.B. (1993) Interaction of L-arginine 597 of NADPH-cytochrome P450 oxidoreductase as a primary source of uniform binding energy used to discriminate between NADH and NADPH. *Biochemistry* **32**, 11548-11558.

263. Draper, R.D. and Ingraham, L.L. (1968) A potentiometric study of the flavin semiquinone equilibrium. *Arch. Biochem. Biophys.* **125**, 802-808.

264. Theorell, H. and Nygaard, A.P. (1954) Kinetics and equilibria in flavoprotein systems: the effects of pH, anions and temperature on the dissociation and reassociation of the old yellow enzyme. *Acta Chem. Scand.* **8**, 1649.

265. Masters, B.S. (1994) Nitric oxide synthases: why so complex? *Annu. Rev. Nut.* **14**, 131-145.

266. Bredt, D.S. and Snyder, S.H. (1994) Nitric oxide: a physiologic messenger molecule. *Annu. Rev. Biochem.* **63**, 175-195.

267. MacMicking, J., Xie, Q.W., and Nathan, C. (1997) Nitric oxide and macrophage function. *Annu. Rev. Immunol.* **15**, 323-350.

268. Marletta, M.A., Hurshman, A.R., and Rusche, K.M. (1998) Catalysis by nitric oxide synthase. *Curr. Opin. Chem. Biol.* **2**, 656-663.

269. Wolff, D.J., Datto, G.A., and Samatovicz, R.A. (1993) The dual mode of inhibition of calmodulin-dependent nitric-oxide synthase by antifungal imidazole agents. *J. Biol. Chem.* **268**, 9430-9436.

270. Brunner, K., Tortschanoff, A., Hemmens, B., Andrew, P.J., Mayer, B., and Kungl, A.J. (1998) Sensitivity of flavin fluorescence dynamics in neuronal nitric oxide synthase to cofactor-induced conformational changes and dimerization. *Biochemistry* **37**, 17545-17553.

271. Dawson, T.M. and Dawson, V.L. (1996) Nitric oxide synthase: role as a transmitter/mediator in the brain and endocrine system. *Annu. Rev. Med.* **47**, 219-27.

272. Moran, R., Sartori, P., and Reich, V. (1984) A rapid and convient preparation of [4-3H]NADP and stereospecifically tritiated NADP^{3}H. *Anal. Biochemistry* **138**, 196-204.

273. Stern, B.K. and Vennesland, B. (1960) The enzymatic transfer of hydrogen: the reactions catalyzed by glucose-6-phosphate dehydrogenase and phosphogluconic acid. *J. Biol. Chem.* **235**, 205-210.

274. Pastore, E.J. and Freidkin, M. (1962) The enzymatic synthesis of thymidylate: transfer of tritium from tetrahydrofolate to methly groups of thymidylate *J. Biol. Chem.* **237**, 3802-3810..

275. Kornberg, A. and Hornberg, B.L., Biochem. Preparations. Vol. 3. 1953, New York, NY: E.E. Snell, J. Wiley and Son. 27.

276. Vanoni, M. and Matthews, R.G. (1984) Kinetic isotope effects on the oxidation of reduced nicotinamide adenine dinucleotide phosphate by the flavoprotein methylenetetrahydrofolate reductase. *Biochemistry* **23**, 5272-5279.

277. Schowen, K.B. and Schowen, R.L. (1982) Solvent isotope effects on enzyme systems. *Methods Enzymol.* **87**, 551-568.

278. Kresage, A.J. (1964) Solvent isotope effects in H_2O-D_2O mixtures. *Pure Appl. Chem.* **8**, 243-258.

279. Gold, V. (1972) Protolytic process in H_2O and D_2O mixtures. *Adv. Phys. Org. Chem.* **7**, 259-331.

280. Quinn, D.M. and Sutton, L.D., *Theoretical basis and mechanistic utility of solvent isotope effects*. Enzyme Mechanism from Isotope Effects, ed. P.F. Cook. 1991, Boca Raton, FL: CRC Press Inc. 73-126.

281. Schowen, R.L., *Solvent isotope effects on enzymatic reactions*. Isotope Effects on enzyme catalyzed reactions, ed. W.W. Cleland, M.H. O'Leary, and D.B. Northrop. 1977, Baltimore: University Park Press. 64-99.

282. Quinn, D.M. and Sutton, L.D., *Enzyme Mechanisms from Isotope Effects*, ed. P.F. Cook. 1991, Boca Raton, FL: CRC Press. 73-126.

283. Krakow, G., Ameraal, N., and Vennesland, B. (1965) The stereospecificity of the Hill Reaction with triphosphopyridine nucleotide. *J. Biol. Chem.* 1820-1827.

284. Sem, D.S. and Kasper, C.B. (1992) Geometric relationship between the nicotinamide and isoalloxazine rings in NADPH-cytochrome P-450 oxidoreductase: implications for the classification of the evolutionary and functionally related flavoproteins. *Biochemistry* **31**, 3391-3398.

285. Drysdale, G.R., Spiegle, M.J., and Sprittmatter, P. (1961) Flavoprotein-catalyzed direct hydrogen transfer between pyridine nucleotides. *J. Biol. Chem.* **236**, 2323-2328.

286. Guerreo, M.G. and Vennesland, B. (1975) The stereospecifity of hydrogen removal from pyridine nucleotide: the reactions catalyzed by nitrate reductase and by xanthine oxidase *FEBBS Lett.* **51**, 284-289.

287. Larsson, A. and Thelander, L. (1965) The stereospecificty of thioredoxin reductase triphospyridine nucleotide. *J. Biol. Chem.* 2691-2697.

288. Ammeraal, R.N., Krakow, G., and Vennesland, B. (1965) The stereospecificity of the hill reaction with diphosphopyridine nucleotide. *J. Biol. Chem.* **240**, 1824-1830.

289. Kresage, A.J., *Magnitude of primary hydrogen isotope effects*. Isotope effects on enzyme catalyzed reactions, ed. W.W. Cleland, O.L. M.H., and D.B. Northrop. 1977, Baltimore: University Park Press. 37-63.

290. Northrop, D.B. (1975) Steady-state kinetic analysis of kinetic isotope effects on enzyme catalyzed reactions. *Biochemistry* **14**, 2644-2651.

291. Swain, C.G., Stiver, E.C., Reuwer, J.F., and Schaad, L. (1958) the use of hydrogen isotope effects to identify the attacking nucleoophile in the enolization of etones catalyzed by acetic acids. *J. Am. Chem. Soc.* **80**, 5885-5890.

292. Cummings Ryerson, C., Ballou, D.P., and Walsh, C. (1982) Kinetic isotope effects in the oxidation of isotopically labeled NAD(P)H by bacerial flavoprotein monooxygenases. *Biochemistry* **21**, 1144-1151.

293. Northrop, D.B., *Determining the absolute magnitude of hydrogen isotope effects*. Isotope Effects on Enzyme Catalyzed Reactions, ed. W.W. Cleland, M.H. O'Leary, and D.B. Northrop. Vol. 122. 1977, Baltimore: University Park Press. 112-152.

294. Gutierrez, A., Doehr, O., Paine, M., Wolf, C.R., Scrutton, N.S., and Roberts, G.C.K. (2001) Trp-676 facilitates nicotinamide exchange in the reductive half-reaction of cytochrome P450 reductase: properties of soluble W676H ans W676A mutant reductases. *Biochemistry* **39**, 15990-15999.

295. Podschun, B., Jahnke, K., Schnackerz, K.D., and Cook, P.F. (1993) Acid base catalytic mechanism of the dihydropyrimidine dehydrogenase from pH studies. *J Biol Chem* **268**, 3407-3413.

296. Albery, W.J. and Knowles, J.R. (1976) Evolution of enzyme function and the development of catalytic efficiency *Biochemistry* **15**, 5631-5640.

297. Cook, P.F., *Enzyme Mechanism from Isotope Effects*. CRC, ed. P.F. Cook. 1991, Boca Raton, FL: CRC Press, Inc. 203-230.

298. Vogelstein, B., Gillespie, D. (1979) Preparation and analytical purification of DNA from agarose *Proc. Natl. Acad. Sci. U.S.A.* **76**, 615-9.

299. Chung, C.T., Miller, R.H.(1993) Preparation and storage of competent *Escherichia coli* cells *Methods. Enzymol.* **218**, 621-7.

300. Tartof, K. D, Hobbs, C. A. (1987) Improved media for growing plasmid and cosmid clones *Bethesda Res. Lab.* 1**19**, 205.

301. Benesch, R.E., Benesch,R., Yung,S. (1973) Equations for the spectrophotometric analysis of hemoglobin mixtures. *Anal. Biochemistry* **55** 205-210.

302. Cha, S. (1968) A simple method for derivation of rate equations for enzyme-catalyzed reactions under the rapid equilibrium assumption or combined assumptions of equilibrium and steady-state. *J. Biol. Chem.* **243**, 820-825

303. Maniatis, T., Fritsch, E.F., Sambrook, J. *Molecular cloning a laboratory manual* (1982) Cold Springs Harbor Laboratory, NY.

Appendices

Appendix 1

Neuronal Nitric-oxide Synthase: Cloning, Expression, Purification, and Activity

A1.1 Cloning of Rat Neuronal NOS cDNA into the pCWori (+) vector.

The cDNA for rat neuronal nitric oxide synthase nNOS was cloned into a pCWori(+) expression vector for expression in *E coli.* pCWori(+), a derivative of the plasmid pHSe5, contains a pBR322 origin of replication, the lac I^q gene, the β-lactamase gene conferring ampicillan resistance, and a bacteriophage origin of replication. The transcription/translation region contains the following: a lacUV5 promoter and two copies of a tac promoter cassette followed by a translation initiation region derived from the phage T4 lysozyme gene. This DNA sequence contains a seven-base pair Shine-Delgarno element located three nucleotides 5' of the initiation codon, which is contained in an Nde I restriction site. pCWori(+) has proven to be a successful expression vector for yielding soluble and sufficient quantities of cytochrome P450 and NOS (229); therefore, this plasmid was used to generate a expression construct for nNOS. The key element for successful expression of these enzymes is a weak tac-tac promoter; efforts to use strong promoters (including T7) led either to no expression or, in few cases, to the appearance of inclusion bodies.

The pCWori(+) was cut with Nde I and Hind III and the complete digest was separated by electrophoreses on a 1.5% agarose gel using Tris acetate buffer. The gel slice containing large 5 kb fragment was removed and the DNA was isolated using the

glass milk procedure (298). A pET3a vector containing the nNOS cDNA (pET3anNOS) was digested with Nde I and the digest was electrophoresed on a 1.5 % agarose gel and the linear DNA was isolated using the glass milk procedure (298). A Hind III restriction site was inserted in the 3' untranslated region of nNOS by PCR amplifying the last 350 bp of nNOS with the 3' primer containing and Hind III restriction site in the linker region. The PCR reactions contained the following: 0.1 μg of pET3anNOS, 100 pmol of the NOS20 oligonucleotide (5' GGA ATT CCA GGA ATT GGA ATT CCC GGG AAC CGG ACA GGC C' containing the Nde I and Sma I restriction sites), 100 pmol of oligonucleotide NOS 21 (5' CCC AAG CTT GGG ATT AGG AGC TGA AAA CCT CAT CTG CG 3' containing the Hind III restriction sites), 50 μM dNTPs, 1.5 mM $MgCl_2$, Promega reaction buffer, and 5 U Taq DNA Polymerase from Promega). The total volume of the reaction was 100 μL. The melting temperature was set at 94°C for 30 sec; the primers were annealed at 55°C for 30 sec and the extension time was set at 72°C for 30 sec. The cycle was repeated 30 times. The reaction mixture was electrophoresed on a 1.5 % agarose gel and the 300 base pair amplified PCR fragment was gel purified using the glass milk/NaI procedure (298). The PCR fragment was digested with Hind III and Nde I in NEB 2 buffer (New England Biolabs) at 37°C. The reaction mixture was electrophoresed on a 1.5 % agarose gel and the 300 bp fragment was gel isolated again using the glass milk/NaI procedure. The isolated 300 bp DNA fragment was ligated with the Hind III and Nde I digested pCWori(+) vector with T4 DNA ligase buffer from New England Biolabs and 20 U of T4 DNA ligase plus 1 mM ATP. The ligation reaction mixtures where incubated overnight at 16°C. The ligation mixture was transformed into

E. coli strain C38 using the method of Chung (299) and cells were plated on ampicillin (Amp; 100 μg/mL) LB plates. Several colonies were grown up in LB broth and the plasmid DNA was isolated using alkaline lysis protocol (303). Mini preps were screened using restriction digests for the newly ligated plasmid, referred to as pCWORI 3'NOS. One pCWORI 3'NOS clone was grown in *E. coli* in a large volume (1L) and the plasmid was isolated by CsCl gradient method (303). The 300 base pair segment of the clone that was amplified by PCR was sequenced by the Center for Gene Research and Biotechnology central services laboratory at Oregon State University to determine that the sequence was free of mutations. The pCWORI 3'NOS and pET3aNOS were then cut with Nde I and Sma I and the reaction mixture was loaded on a 1.5 % agarose gel. The 5.4 kb fragment from the pCWORI3'NOS digest and the 4 kb fragment from the pET3anNOS digest were excised from the gel and the DNA was isolated using the glass milk/NaI procedure. The two fragments were then ligated together overnight at 16 °C using T4 DNA ligase. The ligation mixture was transformed into *E coli* strain C38 using the method of Chung (299) and the cells were plated selecting for Amp resistance. Colonies were chosen to grow in LB broth overnight and plasmid DNA was isolated using alkaline lysis protocol. Mini preps were screened using restriction digests with Nde I and Sma I and Nde I and Hind III.

A digest with correct restriction pattern was transformed into the *E. coli* BL21 (DE3) strain (Novagen). Twenty-five mLs of L-broth containing 0.35 μg/ml of Cm was inoculated with 0.1 to 0.2 mL of fresh overnight culture of *E. coli* BL21 (DE3). The cells were grown to an OD_{600nm} of 0.4 to 0.6 and then centrifuged for 5 min at 8,000 rpm with the SS-34 Sorvall Rotor at 4°C. The pellet was resuspend in 5 mL of sterile RbCl buffer

(100 mM RbCl, 45 mM $MnCl_2$, 10 mM $CaCl_2$ and 35 mM KCH_3CO_2, 15 % sucrose pH 6.0). The cells were divided into 5 sterile 1.5 mL microfuge tubes and stored on ice for 5 mins. The cells were centrifuged for 1 min at 14,000 rpm and the pellet was resuspended in 0.2 mL of ice cold RbCl buffer. Ten ng of plasmid DNA was incubated with the cells and held on ice for 1 hour. The cells were then incubated in a 42 °C water bath for 2 min. One mL of L-broth was added to the cells and they were grown at 37 °C Transformed cells were grown on plates containing 100 μg/mL of Amp and 35 μg/mL of chloremphenicol (Cm).

A1.2 Expression and Purification of nNOS from *E. coli* BL21(DE3) Cells

The media formation that has been found to be most useful for nNOS expression is Terrific Broth (300). This phosphate buffered media maintains the culture pH near neutrality, even at high cell densities, and contains a readily utilizable carbon source, glycerol. nNOS expression began with the inoculation of 4 mL of LB containing 100 μg/mL of Amp and 35 μg/mL of Cm with BL21(DE3) pCWNOS from a fresh plate containing the same concentrations of Amp and Cm. The cells were grown at 37°C overnight and 4-1 L Fernbach flasks containing 35 μg/mL of Cm and 100 μg/mL of Amp were then each inoculated with 1 mL of overnight culture. The cells were grown in Terrific Broth media at 37°C to an OD_{600} = 1.2 at which time the flasks were cooled to room temperature by running under cold water, swirling the flask constantly. Then 0.1 mM of IPTG and 4 μg/mL of hemin chloride were added. The hemin chloride stock was

prepared by dissolving 16 mg of hemin chloride, which is stored at 4 °C, in 1 mL of 0.1 N NaOH. The cells were then grown for an additional 16-20 hr at 23°C at 250 rpm before harvesting. The cells were pelleted at 5,000 for 10 min in a J-6 Beckman centrifuge. Cells were then washed in a solution of 50 mM Tris-HCl (pH 7.8), 10 % (w/v) sucrose, and 150 mM NaCl then pelleted by centrification and frozen at –70° C. The enzyme was purified according to the protocol published by Gerber *et al.* with slight modification (229). Cells were thawed and re-suspended in Buffer A which contained the following: 50 mM Hepes-NaOH (pH 7.5), 10% glycerol (w/v), 100 mM DTT, 10 μM H_4B, and the protease inhibitors (1 mM EDTA, 1 μg/mL of trypsin inhibitor, 1 μg/mL pepstatin A, 17 μg/mL of PMSF, 1 μg/mL benzamidine, 10 μg/mL bacitracin, 2.5 μg/mL leupeptin, 2.5 μg /mL aprotinin and 1.0 μg /mL E-64). The cells (~150 mL) were transferred to a glass beaker and stored on ice. Lysozyme (20 mg) was added to the cells and incubated on ice for 15 min before sonicated (4 × 30 sec pulses at 80% power with a one min rest in between pulses). The lysate was transferred to 35 mL round bottom centrifuge tubes and the cell debris was then pelleted at 18,000 rpm for 45 min at 4°C with the J21 Beckman rotor. The lysate was applied to a 10 mL ADP-Sepharose (Amersham Pharmacia) column equilibrated with Buffer A. The column was washed with 100 mL of Buffer A at ~1 mL/min followed by 50 mL of Buffer A containing 0.5 M NaCl. The protein was eluted with 50 mL of Buffer A plus 0.5 M NaCl and a 20 mM mixture of 2'-and 3'- AMP. 2'AMP will not elute nNOS from the resin alone, but the

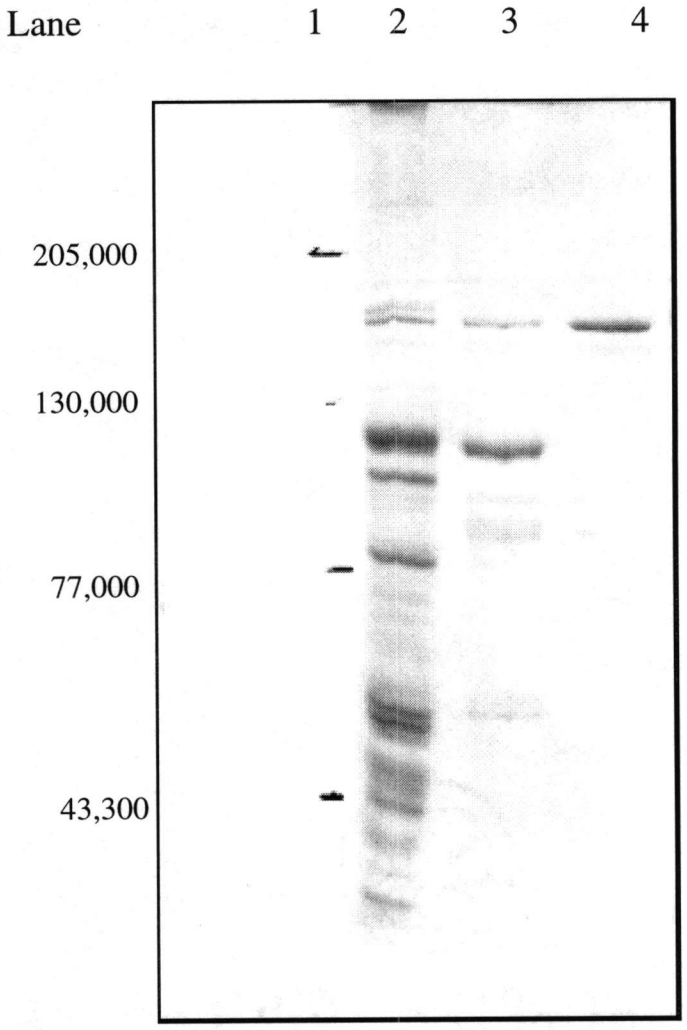

FIGURE A1.1 Analysis of purification of nNOS determined by 8% SDS-polyacrylamide gel electrophoresis. The gel was stained with Coomaisse Blue. Lane 1 represents the molecular weight markers from BioRad (205,000, Myosin; 130,000, β-galactosidase, 77,000 bovine serum albumin, 43,300 carbonic anhydrase). Lane 2 is the IPTG induced *E. coli* strain BL21(DE3) with the pCWori vector containing the nNOS cDNA lysate, Lane 3 is the ADP-Sepharose eluate, and Lane 4 is the CaM affinity column eluate.

presence of 0.5 M NaCl along with 20mM 2'-AMP elicits the sharp elution of nNOS. Two millimolar of $MgCl_2$ and 1 mM $CaCl_2$ were added to the ADP-eluate, which was then applied an 8 mL (1.2 $cm^2 \times 6$ cm) CaM-Sepharose column equilibrated with Buffer A plus 2 mM $MgCl_2$ and 1 mM $CaCl_2$. The column was washed with 50 mL of Buffer A plus 2 mM $MgCl_2$, 1 mM $CaCl_2$ and 0.3 M NaCl. Finally the protein was eluted with Buffer A plus 0.3 M NaCl and 3 mM EDTA. Protein concentration was determined with the Lowery Assay using BSA as a standard (230). The recombinant purified protein was more than 85% pure as judged a densometric scan of the by SDS-polyacrylamide gel and determining the dots per inch (dpi) for each band (Figure A1.1) with a specific activity of 150 nmol NO min^{-1} mg^{-1} at 25°C.

In the absence of added pterin, purified NOS that is frozen or left at 4°C loses activity rapidly. Thus during the purification procedure 8 μM of H_4B must be freshly added to all the purification buffers and purified nNOS must be stored with this concentration of H_4B. H_4B is readily oxidized in air; therefore, it is prepared as an anaerobic solution under argon or nitrogen or prepared in buffer containing DTT. An 8 mM H_4B solution is prepared in 100 mM Hepes (pH 7.5) and 100 mM DTT and can be frozen at –80C for over three months without any observable oxidation. The concentration of H_4B can be determined spectrally using $\varepsilon_{297} = 8710$ mM^{-1} cm^{-1} at pH 8.0.

A1.3. Determining nNOS Activity by the Oxyhemoglobin (HbO_2) Assay.

The hemoglobin assay is a simple, continuous assay based on the reaction of NO and HbO_2. The reaction between HbO_2 and NO is stoichiometric and occurs at a rate that is faster than molecular O_2 and NO; therefore, the formation of NO can be measured under initial rate conditions. Although the affinity of hemoglobin for NO is 3×10^5 higher than that for O_2, NO does not react with HbO_2 by displacing bound dioxygen, but rather by attacking the oxygen molecule directly, forming metHb. The soret peak for HbO_2 at 415 nm shifts towards 406 nm for metHb. The wavelength where there is a maximal change in absorbance is at 401 nm (increasing) in the conversion of HbO_2 to metHb, and catalytic activity is measured by following the absorbance change at this wavelength.

The HbO_2 stock was prepared by dissolving 5 mg of pig lyophilized hemoglobin in 5 mL of 100 mM potassium phosphate buffer pH 7.4. The solution was divided between 4 Eppendorf microfuge tubes. The large particulates were pelleted for 1 min at 14,000 rpm in a microfuge and the supernatent was put in a 25 mL Erlenmeyer Flask. Dithionite (2-3 fold molar excess) was added and the color of the solution changed immediately from brownish red to a dark red (deoxyhemoglobin). The flask was swirled to oxygenate (5-7 min) the hemoglobin; the solution turned bright red. The oxyHb solution was purified and desalted by passing 1 mL of the solution over a 2 mL (3.2 cm $\times$ 0.785 cm^2) Sephadex G-25 column. The concentration of the desalted HbO_2 stock was determined spectrophotometrically. The absorbance maximum should be at 415 nm. If the maximum occurs at lower wavelengths, then metHb is a contaminant in the HbO_2. MetHb does not interfere with the use of the HbO_2 in the NO assay as long as enough

HbO_2 is present such that it is not depleted at the end of the experiment. The HbO_2 was prepared fresh each day since it is subject to autooxidation and microbial contamination when stored. The following formula was used to determined the concentration of HbO_2: [oxy Hb]mM = $(1.013A_{576} - 0.3269A_{630} - 0.7353A_{560}) \times 10^{-4}$ (301).

A significant problem with the assay is an irreproducible extinction coefficient for the absorbance change at 401 nm. If quantitative measurements of NOS activity are to be done with the assay, the extinction coefficient should be made for a particular solution of HbO_2 prior to such experiments. The extinction coefficient was determined by measuring the 401 nm absorbance of HbO_2 solutions at varying concentrations (1-5 μM) in 100 mM phosphate buffer pH 7.4. The NO releaser, sodium nitroprusside was added to each solution to oxidize the HbO_2 to metHb. At the completion of the reaction, the absorbance change for each concentration at 401 nm was recorded. The molar extinction coefficient was determined from the slope of the calibration curve (plot of absorbance change versus the HbO_2 concentration). An extinction coefficient of ~ 60 $mM^{-1} cm^{-1}$ at 401 nm was calculated using this protocol; therefore, this value was used to determine the activity of nNOS. The reaction mixtures (1mL) contained 20 μM L-arginine, 10 μM $CaCl_2$, 100 nM CaM, 10 μM NADPH, 8 μM H_4B and the reaction was initiated with the addition of nNOS.

A1.4 Analysis of Heme Incorporation

The amount of heme incorporation into nNOS was determined by measuring the difference CO-heme spectra. Carbon monoxide was gently bubbled through 2 mL of the enzyme solution (~ 0.1 to 0.5 μM) on ice for 2 min to allow the CO to bind to the ferric iron of the heme. The spectrum is recorded, and then the iron was reduced to its ferrous state with the addition of sodium dithoinate. The difference spectrum was then recorded, and the ferrous-CO complex gave a difference spectrum with a peak at 444 nm. The heme content was calculated with $\Delta \varepsilon = 75\ mM^{-1}\ cm^{-1}$ at 444 nm.

A1.5 Determining of nNOS Activity with the L-Citrulline Assay

The citrulline assay is a sensitive, discontinuous assay, which employs the use of small Dowex 50 cation-exchange column to separate radiolabeled L-citrulline from L-arginine. L-[2, 3, 4, 5-^{3}H] arginine was purchased from New England Nuclear with a specific activity 40 mCi/mmol. A working solution ~3 μCi/umol was prepared by diluting the stock with unlabeled L-arginine. Dowex resin (50 × 8-499) in the sodium form is a strong acidic cation exchanger and was used for the separation of L-citrulline, which at pH 5.5 is of neutral charge, from L-arginine which is cationic. nNOS was incubated with 10 μM of L-arginine, 10 μM NADPH, 100 nM CaM, 10 μM $CaCl_2$ and 8 μM H_4B and 4 mL of stop buffer (50 mM Hepes-NOH, (pH 5.5), 5 mM EDTA) was added to the

reaction test tube after an incubation period. This mixture was applied to a 0.5 mL (0.64 cm × 0.785 cm^2) column of Dowex resin (50X8-499) equilibrated with stop buffer. The column was washed with 2 mL of H_20 and the flow trough was collected in 20 mL scintillation vials. The amount of citrulline that eluted was quantitated using liquid scintillation counting based on the specific activity of the L-arginine used. The activity of nNOS measured with this assay was plotted at varying concentrations of L-arginine and the data was fit to the Michaelis-Menton equation to determine the Km for the substrate. The specific assay of nNOS was determined to be 227 nmol/min/mg at 37 °C and the Km was 0.8 ± 0. 3 μM.

Appendix 2

Derivation of Kinetic Mechanisms

A2.1 Derivation of the Rate Equation for a Di-Iso Ping-Pong Bi-Bi Mechanism for nNOS Catalyzed Reduction of DCIP

Figure 2.3. shows the kinetic scheme for the di-iso ping-pong bi-bi mechanism proposed for the nNOS catalyzed reduction of DCIP. The basic features of the proposed mechanism are as follows: (a) The reaction consists of two-half reactions with NADPH oxidation reducing the enzyme to three-electron reduced state, E_3, followed by reduction of DCIP which converts the enzyme back to the one-electron reduced state, E_1. (b) A steady-state isomerization step occurs between two forms of the three-electron reduced state of the enzyme, E_3 and E_3', one that binds $NADP^+$ and one that binds DCIP. (c) An alternate form of the free enzyme, E_1', exists in the reaction sequence, which is in rapid equilibrium with E_1 and is able to bind the NADPH analog, 2'-AMP, but not the substrate NADPH. The binding of substrates/inhibitors and the release of products is assumed to occur in rapid equilibrium; thus, the kinetic mechanism is divided into three rapid equilibrium segments, labeled X, Y, and Z. The derivation of steady-state equation is according to the method of Cha (302). For the purposes of illustrating how dead-end inhibition studies with 2'-AMP lead to the proposal of the rapid isomerization of E_1 to E_1' in the overall reaction scheme, the enzyme-inhibitor complexes that would form with the substrate analog, 2'-AMP (I), are also included in Figure 2.3. The fractionation factors for the mechanism drawn in Figure 2.3 are as follows:

$$f_3 = \frac{E_1 A}{X} = \frac{A/K_{iA}}{1 + A/K_{iA} + 1/K(1 + I/K_{iI} + Q/K_{iQ} + QI/K_{iQ}K_{iI})} \quad \text{(A2.1)}$$

$$f_4 = \frac{E_3 P}{Y} = \frac{P/K_{iP}}{1 + P/K_{iP}} \quad \text{(A2.2)}$$

$$f_7 = \frac{E_3}{Y} = \frac{1}{1 + P/K_{iP}} \quad \text{(A2.3)}$$

$$f_8 = \frac{E_3'}{Z} = \frac{1}{1 + B/K_{iB}} \quad \text{(A2.4)}$$

$$f_{11} = \frac{E_3' B}{Z} = \frac{B/K_{iB}}{1 + B/K_{iB}} \quad \text{(A2.5)}$$

$$f_{12} = \frac{E_1' Q}{X} = \frac{Q/K_{iQ}}{1 + A/K_{iA} + 1/K(1 + I/K_{iI} + Q/K_{iQ} + QI/K_{iQ}K_{iI})} \quad \text{(A2.6)}$$

A, *B*, *P*, *Q* and *I* represent NADPH, $DCIP_{ox}$, $NADP^+$, $DCIP_{red}$, and 2'-AMP respectively, and the K_i values refer to their respective dissociation constants. E_1 and E_1' are the one-electron (FAD/FMNH•) forms of nNOS that exclusively bind NADPH and 2'-AMP, respectively. E_3 and E_3' are the three-electron ($FADH•/FMNH_2$) or ($FADH_2/FMNH•$) forms of nNOS that exclusively bind $NADP^+$ and $DCIP_{ox}$, respectively. K (equal to E_1/E_1') is the equilibrium constant for the conversion of the two free enzyme forms, E_1 and E_1'. $X = E_1 + E_1' + E_1'I + E_1'IQ + E_1'Q + E_1A$; $Y = E_3P + E_3$; $Z = E_3' + E_3'B$, and $E_t = X + Y + Z$. Using the scheme shown in Figure A2.1 as the basic King-Altman figure, the following velocity equation is obtained:

$$\frac{v_i}{E_t} = \frac{k_3k_7k_{11}f_3f_7f_{11} - k_4k_8k_{12}f_4f_8f_{12}}{k_4k_8f_4f_8 + k_4k_{11}f_4f_{11} + k_7k_{11}f_7f_{11} + k_3k_8f_3f_8 + k_3k_{11}f_3f_{11} + k_8k_{12}f_8f_{12} + k_3k_7f_3f_7 + k_4k_{12}f_4f_{12} + k_7k_{12}f_7f_{12}} \quad \text{(A2.7)}$$

Under initial velocity conditions (P=Q=I=O) substitution of the fractionation factors (eqs A2.1-A2.6) into equation A2.7 yields the following equation:

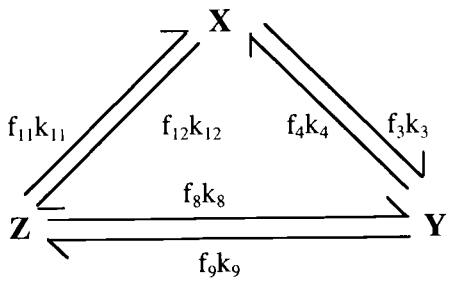

Figure A2.1 The steady-state steps for the nNOS-catalyzed reduction of DCIP. *X*, *Y* and *Z* refer the rapid equilibrium segments drawn in Figure 2.3. *X* represents all the enzyme species that bind NADPH, 2'-AMP and $DCIP_{red}$; *Y* represents all the enzyme species that bind $NADP^+$, and *Z* represents all the enzyme species that bind $DCIP_{ox}$ (i.e. $X = E_1 + E_1' + E_1'I + E_1'IQ + E_1'Q + E_1A$; $Y = E_3P + E_3$; $Z = E_3' + E_3'B$. The f_i represents the fractional concentration of rapid equilibrium segment involved in the reaction given by the rate constants k_i (eqs A2.1-A2.6).

$$\frac{v_i}{E_t} = \frac{[A][B]\dfrac{k_3k_7k_{11}}{(k_3k_7 + k_3k_{11} + k_7k_{11})}}{[A][B] + [B]\dfrac{(K_{iA})(1+1/K)(k_7k_{11})}{(k_3k_7 + k_3k_{11} + k_7k_{11})} + [A]\dfrac{(K_{iB})(k_3k_7 + k_3k_8)}{(k_3k_7 + k_3k_{11} + k_7k_{11})}} \qquad \text{(A2.8)}$$

The kinetic constants are defined as follows:

$$k_{cat} = \frac{k_3k_7k_{11}}{(k_3k_7 + k_3k_{11} + k_7k_{11})} \qquad \text{(A2.9)}$$

$$K_A = \frac{K_{iA}(k_7k_{11})(1+1/K)}{(k_3k_7 + k_3k_{11} + k_7k_{11})} \qquad \text{(A2.10)}$$

$$K_B = \frac{K_{iB}(k_3k_7 + k_3k_8)}{(k_3k_7 + k_3k_{11} + k_7k_{11})} \qquad \text{(A2.11)}$$

Equation A2.8 simplifies to equation A2.12.

$$\frac{v_i}{E_t} = \frac{V[A][B]}{[A][B] + K_B[A] + K_A[B]} \qquad \text{(A2.12)}$$

which has the same form as the rate equation for a ping-pong mechanism, eq. 2.1. Thus, the proposed mechanism for nNOS reduction of DCIP is consistent with the observed initial velocity patterns and yields the same patterns expected for a standard ping-pong mechanism.

The equation describing product inhibition by $NADP^+$, P, is derived letting $Q = I = 0$ and substituting the fractionation factors A2.1 to A2.6 into equation A2.7:

$$\frac{v_i}{E_t} = \frac{V[A][B]}{[A][B] + K_B[A] + K_A[B] + [P]\frac{D_1}{K_{iP}} + [A][P]\frac{D_2}{K_{iP}} + [B][P]\frac{D_3}{K_{iP}} + [A][B][P]\frac{D_4}{K_{iP}}} \quad \text{(A2.13)}$$

where

$$D_1 = \frac{K_{iB}K_{iA}k_4k_8(1+1/K)}{(k_7k_{11} + k_3k_{11} + k_3k_7)} \quad \text{(A2.14)}$$

$$D_2 = \frac{K_{iB}(k_3k_8 + k_4k_8)}{(k_7k_{11} + k_3k_{11} + k_3k_7)} \quad \text{(A2.15)}$$

$$D_3 = \frac{K_{iA}k_4k_{11}(1+1/K)}{(k_7k_{11} + k_3k_{11} + k_3k_7)} \quad \text{(A2.16)}$$

$$D_4 = \frac{(k_3k_{11} + k_4k_{11})}{(k_7k_{11} + k_3k_{11} + k_3k_7)} \quad \text{(A2.17)}$$

The double reciprocal form of equation A2.13 predicts noncompetitive inhibition patterns for *P* with either *A* or *B* as the variable substrate. Thus, the mechanism correctly predicts the product inhibition patterns which where obtained experimentally.

For dead-end inhibition by the substrate analog, 2'-AMP (*I*), *P*=*Q*=O, substitution of equations A2.1 to A2.6 into equation A2.7 yields the following velocity equation:

$$\frac{v_i}{E_t} = \frac{V[A][B]}{[A][B] + K_B[A] + K_A[B]\left(1 + \frac{[I]}{K_{il}(1+K)}\right)} \quad \text{(A2.18)}$$

With *A* as the varied substrate, the double reciprocal form of the equation A2.18 is

$$\frac{E_t}{v_i} = \frac{1}{V}\left(1 + \frac{K_B}{B}\right) + \frac{K_A}{V}\left(1 + \frac{[I]}{K_{il}(1+K)}\right)\frac{1}{[A]} \qquad \text{(A2.19)}$$

The equation predicts a competitive pattern for I when A is the variable substrate, consistent with the experimental results. Arranging A2.19 with B as the variable substrate, the equation becomes

$$\frac{E_t}{v_i} = \frac{1}{V}\left(1 + \frac{K_A}{[A]}\left(1 + \frac{[I]}{K_{il}(1+K)}\right)\right) + \frac{K_B}{V}\frac{1}{[B]} \qquad \text{(A2.20)}$$

Uncompetitive inhibition is predicted for I when B is the variable substrate, consistent with the experimental results. Comparison of equation 2.3 with A2.19 and equation 2.4 with A2.20, show that the K_{is} and K_{ii} values are both a function of the dissociation constant, K_{iI} and the equilibrium constant, K, between E_1 and E_1'.

A2.2 Derivation of Rate Equations of an Iso Two-Site Ping-Pong Mechanism for nNOS-Catalyzed Reduction of Cytochrome c^{3+}

Figure 2.4 shows the kinetic scheme for the iso two-site ping-pong mechanism with NADPH binding in a uni-uni fashion at site 1 and cytochrome c^{3+} binding in a tert-uni ping-pong fashion at site 2. Although the reaction consists of two-half reactions, the two active sites operate independently and formation of a ternary complex is possible. Since the difference in the apparent affinity for 2'AMP obtained with DCIP compared to cytochrome c^{3+} as an electron acceptor led to the proposal that the reaction proceeds *via* an iso mechanism, Figure 2.4 also shows 2'AMP forming a dead-end complex with E_1'. To simplify the derivation of the rate equation the following assumptions were made: (1) all ligand binding steps occur in rapid equilibrium; (2) the binding of a ligand at site one

does not effect of binding of the ligands at second site; and (3) the values of all ligand dissociation constants are unaffected by the oxidation state of the enzyme. Figure A2A illustrates the number of different binary and ternary complexes that can form with nNOS and the various ligands, and Figure A2B shows the additional dead-end complexes that form with E_1' in the presence of 2'-AMP. Equations were derived using the method of Cha (302) with the fractionation factors defined as follows:

$$f_A = \frac{E_1A + E_1AB + E_1AQ}{E_{tX}} = \frac{A/K_{iA}}{1 + A/K_{iA} + P/K_{iP} + 1/K(1 + I/K_{il})} \quad \text{(A2.21)}$$

$$f_B = \frac{E_2B + E_2AB + E_2PB}{E_{t2}} = \frac{E_3B + E_3AB + E_3PB}{E_{t3}} = \frac{B/K_{iB}}{1 + B/K_{iB} + Q/K_{iQ}} \quad \text{(A2.22)}$$

$$f_P = \frac{E_3P + E_3PB + E_3PQ}{E_{t3}} = \frac{P/K_{iP}}{1 + A/K_{iA} + P/K_{iP}} \quad \text{(A2.23)}$$

$$f_Q = \frac{E_2Q + E_2AQ + E_2PQ}{E_{t2}} = \frac{Q/K_{iQ}}{1 + B/K_{iB} + Q/K_{iQ}} \quad \text{(A2.24)}$$

$$f_Q' = \frac{E_1'Q}{E_{tX}} = \frac{Q/KK_{iQ}}{\left[1 + B/K_{iB} + Q/K_{iQ}\right]\left[1 + A/K_{iA} + P/K_{iP} + 1/K(1 + I/K_{il})\right]} \quad \text{(A2.25)}$$

Figure A2.2 Kinetic scheme showing the various rapid equilibrium enzyme-ligand complexes that form in the iso (two-site) ping-pong mechanism for the nNOS catalyzed reduction of cytochrome c^{3+}. *A, B, P, Q*, and I represent the same molecules as in Figure 2.4, and the rate and equilibrium constants are the same as those in Figure 2.4. In Figure A2.2A, *E* represents E_1, E_2, or E_3. Figure A2.2B illustrates the equilibrium between E_1, the free enzyme form that binds NADPH, but not 2'-AMP and E_1', the free enzyme form that binds 2'-AMP and not NADPH.

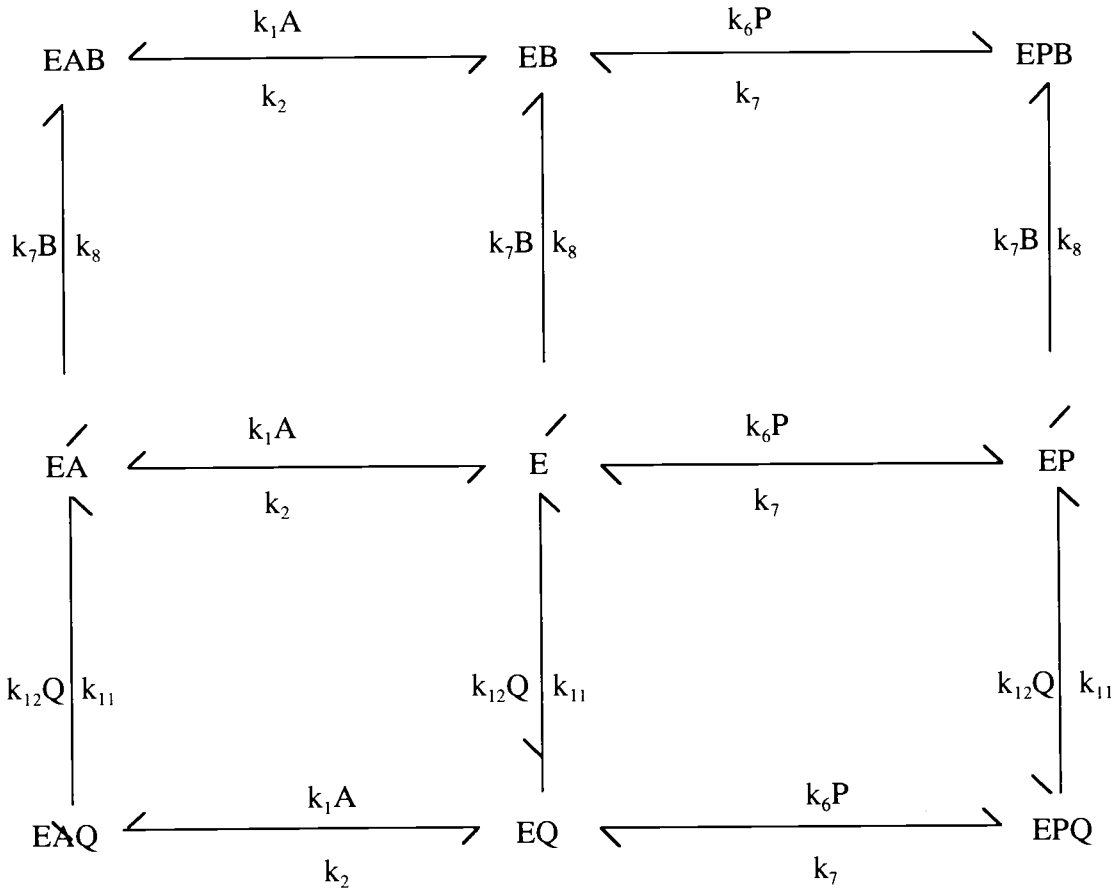

Figure A2.2A

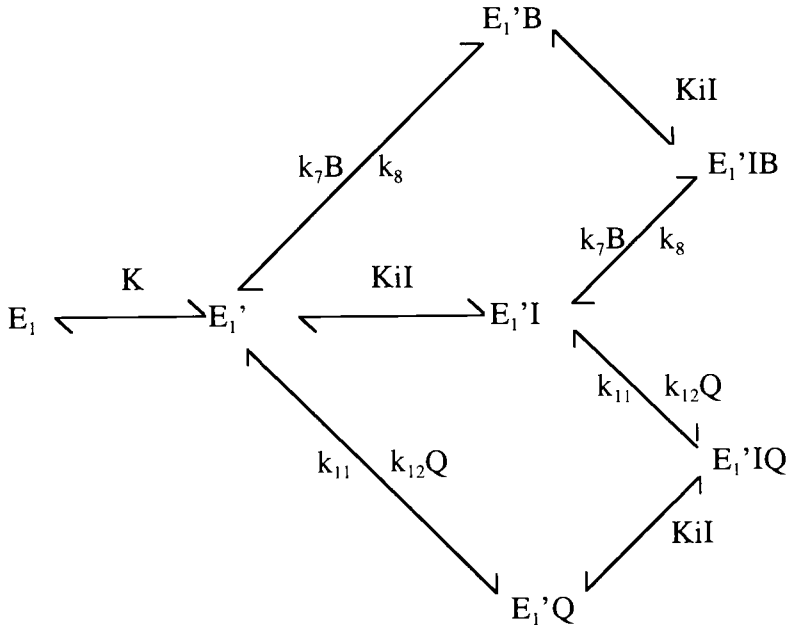

Figure A2.2B

A, *B*, *P*, *Q* and *I* represent NADPH, cytochrome c^{3+}, $NADP^+$, cytochrome c^{2+}, and 2'-AMP respectively, and the K_i values refer to their respective dissociation constants. E_1 and E_1' are the one-electron (FAD/FMNH•) forms of nNOS that exclusively bind NADPH and 2'-AMP, respectively. E_2 is the two-electron ($FAD/FMNH_2$) enzyme form and E_3 is the three-electron ($FADH•/FMNH_2$) form of the enzyme. K (equal to E_1/E_1') is the equilibrium constant for the conversion of the two free enzyme forms. $E_{t2}= E_2+ E_2A + E_2B + E_2P + E_2Q + E_2AB + E_2BP + E_2AQ + E_2PQ$. $E_{t3}= E_3+ E_3A + E_3B + E_3P + E_3Q + E_3AB + E_3BP + E_3AQ + E_3PQ$. $E_{tX}= E_1 + E_1A + E_1B, + E_1P + E_1Q+ E_1AB + E_1BP + E_1AQ + E_1PQ + E_1' + E_1'I + E_1'B + E_1'Q + E_1'IB + E_1'IQ$. Using the fractionation factors and the scheme in Figure A2.3 as the basic King-Altman pattern, one can derive the following velocity equation:

$$\frac{v_i}{E_t} = \frac{k_3k_9k_{15}f_Af_Bf_B - k_4k_{10}k_{16}f_Pf_Qf_Q'}{k_4k_{10}f_Pf_Q + k_4k_{15}f_Pf_B + k_9k_{15}f_Bf_B + k_3k_9f_Af_B + k_4k_6f_Pf_Q' + k_9k_{16}f_Bf_Q' + k_3k_{10}f_Af_Q + k_3k_{15}f_Af_B + k_{10}k_{16}f_Qf_Q'} \qquad \text{(A2.26)}$$

Under initial velocity conditions (P=Q=I=0), substitution of the fractionation factors A2.21 to A2.25 simplifies the overall rate equation to the following equation.

$$\frac{v_i}{E_t} = \frac{\dfrac{k_3k_9k_{15}[A][B]}{(k_3k_9 + k_3k_{15} + k_9k_{15})}}{[A][B] + [A]\dfrac{(K_{iB})(k_3k_{15} + k_3k_9)}{(k_3k_9 + k_3k_{15} + k_9k_{15})} + [B]\dfrac{(K_{iA})(k_9k_{15})(1+1/K)}{(k_3k_9 + k_3k_{15} + k_9k_{15})}} \qquad \text{(A2.27)}$$

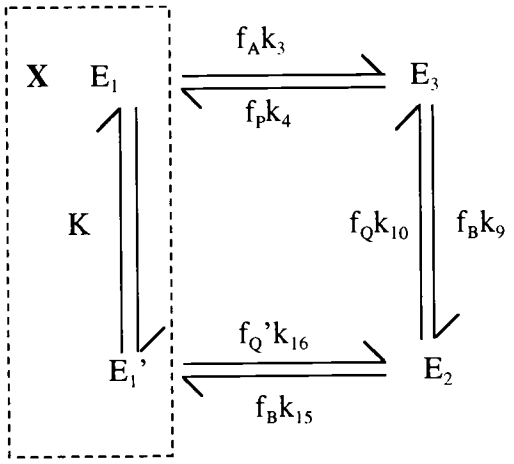

Figure A2.3 The steady-state steps for the nNOS catalyzed reduction of cytochrome c^{3+}. E_1, E_1', E_2, and E_3, the rate constants, and K are the same as in Figure 2.4. The dotted box labeled X represents the rapid equilibrium segments between E_1 and E_1' and the values for the fractionation factors, f_i, are given in equations A2.21 to A2.25.

Kinetic constants are defined in equation A2.28 to A2.30.

$$k_{cat} = \frac{k_3 k_9 k_{15}}{(k_3 k_9 + k_3 k_{15} + k_9 k_{15})} \quad \text{(A2.28)}$$

$$K_A = \frac{(K_{iA})(k_9 k_{15})(1 + 1/K)}{(k_3 k_9 + k_3 k_{15} + k_9 k_{15})} \quad \text{(A2.29)}$$

$$K_B = \frac{(K_{iB})(k_3 k_{15} + k_3 k_9)}{(k_3 k_9 + k_3 k_{15} + k_9 k_{15})} \quad \text{(A2.30)}$$

Thus the rate equation reduces to the following:

$$\frac{v_i}{E_t} = \frac{V[A][B]}{[A][B] + K_B[A] + K_A[B]} \quad \text{(A2.31)}$$

The K_A and K_B refer to the Michaelis constants of NADPH and cytochrome c^{3+}, respectively, and V is the maximal velocity. Equation A2.31 has the same form as equation 2.1 to which the parallel initial velocity patterns were fit. Thus, the proposed two-site ping-pong mechanism for nNOS reduction of cytochrome c^{3+} is consistent with the observed initial velocity patterns. However, a hexa-uni one-site ping-pong mechanism would also generate a rate equation having the same form as the equation for the two-site ping-pong mechanism under initial velocity conditions. Therefore, product and dead-end inhibition studies were required to distinguish which mechanism is valid for nNOS.

In the CPR-catalyzed reduction of cytochrome c^{3+}, $NADP^+$ is uncompetitive *versus* cytochrome c^{3+}. Sem and Kasper accounted for this inhibition pattern by assuming that electron transfer from E_3 to cytochrome c^{3+} is much faster than electron transfer from E_3 to $NADP^+$ (i.e. $k_9 >> k_4$; 236). This assumption was supported by the

absence of pronounced curvature in the double reciprocal plots with cytochrome c^{2+} as an inhibitor. Since $NADP^+$ is uncompetitive *versus* cytochrome c^{3+} and the double-reciprocal plots with cytochrome c^{2+} as an inhibitor are linear, the same assumptions were made for the nNOS mechanism. In the presence of P ($Q = I = 0$), substitution of the fractionation factors A2.21-A2.25 into equation A2.26 and omission of terms in equation A2.26 containing k_4 gave the following equation:

$$\frac{v_i}{E_t} = \frac{V[A][B]}{[A][B] + [B]K_A + [A]K_B + [B][P]\left(\frac{K_A}{K_{iP}(1+1/K)}\right)} \qquad \text{(A2.32)}$$

Equation A2.32 predicts competitive inhibition by P when A is the variable substrate. The corresponding equation describing product inhibition by P with B as the variable substrate predicts uncompetitive inhibition. Thus, the mechanism correctly predicts the product inhibition patterns obtained experimentally.

With product inhibition by Q ($P=I=0$), substitution of the fractionation factors A2.21 to A2.25 into equation A2.26 produces the following rate equation:

$$\frac{v_i}{E_t} = \frac{V[A][B]^2}{[A][B]^2 + [B]^2K_A + [A][B]K_B + [A][B][Q]\left(\frac{C_1}{K_{iQ}}\right) + [B][Q]\left(\frac{C_2}{KK_{iQ}}\right) + [A][Q]\frac{C_3}{K_{iQ}} + [A][Q]^2\left(\frac{C_3}{K_{iQ}^2}\right) + [Q]^2\left(\frac{C_4}{KK_{iQ}^2}\right)} \qquad \text{(A2.33)}$$

where

$$C_1 = K_{iB}\left(\frac{k_3k_9 + k_3k_{10} + k_3k_{15}}{k_3k_9 + k_9k_{15} + k_3k_{15}}\right) \tag{A2.34}$$

$$C_2 = K_{iA}K_{iB}\left(\frac{k_9k_{16}}{k_3k_9 + k_9k_{15} + k_3k_{15}}\right) \tag{A2.35}$$

$$C_3 = K_{iB}^{\,2}\left(\frac{k_3k_{10}}{k_3k_9 + k_9k_{15} + k_3k_{15}}\right) \tag{A2.36}$$

$$C_4 = K_{iA}K_{iB}^{\,2}\left(\frac{k_{10}k_{16}}{k_3k_9 + k_9k_{15} + k_3k_{15}}\right) \tag{A2.37}$$

The terms C_1 and C_2 predominate over C_3 and C_4 in equation A2.33 since k_{10} and k_{16}, which represent the rate of cytochrome c^{2+} reduction of E_2 and E_1, respectively, are assumed to be much slower then electron transfer to cytochrome c^{3+}, k_9 and k_{15}. This assumption is based on the absence of curvature in the initial velocity patterns. Furthermore, if hydride transfer, k_3, is much slower than electron transfer to cytochrome c^{3+} then $C_2 >> C_3$. Both of these assumptions were also made in the derivation of the rate equation for cytochrome c^{2+} inhibition studies with CPR (236). Thus, equation A2.33 reduces to the following equation:

$$\frac{v_i}{E_t} = \frac{V[A][B]}{[A][B] + [B]K_A + [A]K_B + [A][Q]\left(\frac{C_1}{K_{iQ}}\right) + [Q]\left(\frac{C_2}{KK_{iQ}}\right)} \tag{A2.38}$$

Equation A2.38 predicts product inhibition by Q with B as the variable substrate to be competitive. The corresponding equation describing product inhibition by Q with A as the variable substrate predicts noncompetitive inhibition. Therefore, the proposed iso

two-site ping-pong mechanism is consistent with the cytochrome c^{2+} product inhibition patterns obtained experimentally.

In the presence of 2'-AMP, *I*, (*P*=*Q*=O), substitution of the fractionation factors A2.21 to A2.25 into equation A2.26 leads to the following equation:

$$\frac{v_i}{E_t} = \frac{V[A][B]}{[A][B] + K_B[A] + K_A[B]\left(1 + \frac{[I]}{K_{il}(1+K)}\right)} \qquad \text{(A2.39)}$$

Equation A2.39 predicts that *I* will be competitive *versus A* and uncompetitive *versus B*. As with the di-iso ping-pong mechanism described for DCIP as an electron acceptor, the overall apparent affinity for 2'-AMP is a function of its dissociation constant and the equilibrium constant, *K* (equal toE_1/E_1'), i.e. $K_{is}=K_{il}(1+K)$ and $K_{ii}=K_{il}(1+K)$.

A2.3 Derivation of Rate Equation Describing a Hexa-Uni Ping-Pong Mechanism for nNOS-Catalyzed Reduction of Cytochrome c^{3+}

Scheme A2.1 shows the kinetic scheme for the hexa-uni ping-pong mechanism with NADPH binding in a uni-uni fashion followed by the binding of cytochrome c^{3+} in a tert-uni ping-pong fashion. The reaction consists of two-half reactions with only the formation of binary complexes possible. Using Scheme A2.1 as the basic King-Altman figure, the following rate equation is obtained.

$$\frac{v}{E_t}=\frac{k_1k_3k_5k_7k_9k_{11}[A][B]^2-k_2k_4k_6k_8k_{10}k_{12}[P][Q]^2}{[A][B]^2(k_1k_5k_7k_9k_{11}+k_1k_3k_5k_9k_{11}+k_1k_3k_5k_7k_9)+} \quad \text{(A2.40)}$$

$$[B]^2(k_3k_5k_7k_9k_{11}+k_2k_5k_7k_9k_{11})+$$

$$[A][B](k_1k_3k_7k_9k_{11}+k_1k_3k_6k_9k_{11}+k_1k_3k_5k_7k_{11}+k_1k_3k_5k_7k_{10})+$$

$$[B][P](k_2k_4k_6k_9k_{11}+k_2k_4k_7k_9k_{11})+[A][B][P](k_1k_4k_6k_9k_{11}+k_1k_4k_7k_9k_{11})+$$

$$[Q]^2(k_3k_6k_8k_{10}k_{12}+k_2k_6k_8k_{10}k_{12})+[A][Q](k_1k_3k_6k_8k_{11}+k_1k_3k_6k_8k_{10})+$$

$$[B][Q]^2(k_3k_5k_8k_{10}k_{12}+k_2k_5k_8k_{10}k_{12})+[A][B][Q](k_1k_3k_5k_8k_{11}+k_1k_3k_5k_8k_{10})+$$

$$[B][Q](k_3k_5k_7k_{10}k_{12}+k_2k_5k_7k_{10}k_{12})+[B]^2[Q](k_3k_5k_7k_9k_{12}+k_2k_5k_7k_9k_{12})+$$

$$[P][Q](k_2k_4k_7k_{10}k_{12}+k_2k_4k_6k_{10}k_{12}+k_2k_4k_6k_8k_{11}+k_2k_4k_6k_8k_{10})+$$

$$[P][Q]^2(k_2k_4k_8k_{10}k_{12}+k_2k_4k_6k_8k_{12}+k_2k_4k_8k_{10}k_{12})+$$

$$[A][P][Q](k_1k_4k_6k_8k_{11}+k_1k_4k_6k_8k_{10})+[B][P][Q](k_2k_4k_7k_9k_{12}+k_2k_4k_6k_9k_{12})$$

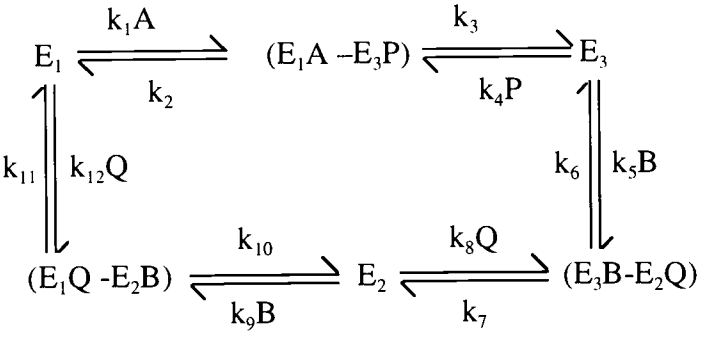

(Scheme A2.1)

Equation A2.40 simplifies to the following equation under initial velocity conditions (P=Q=0).

$$\frac{v_i}{E_t}=\frac{k_1k_3k_5k_7k_9k_{11}[A][B]}{[A][B](k_1k_5k_7k_9k_{11}+k_1k_3k_5k_9k_{11}+k_1k_3k_5k_7k_9)+[B](k_3k_5k_7k_9k_{11}+k_2k_5k_7k_9k_{11})} \quad \text{(A2.41)}$$

$$[A](k_1k_3k_7k_9k_{11}+k_1k_3k_6k_9k_{11}+k_1k_3k_5k_7k_{11}+k_1k_3k_5k_7k_{10})$$

The kinetic constants are defined in equations A2.42 to A2.44.

$$k_{cat} = \frac{k_3 k_7 k_{11}}{\left(k_7 k_{11} + k_3 k_{11} + k_3 k_7\right)} \tag{A2.42}$$

$$K_A = \frac{k_7 k_{11}\left(k_2 + k_3\right)}{k_1\left(k_7 k_{11} + k_3 k_{11} + k_3 k_7\right)} \tag{A2.43}$$

$$K_B = \frac{k_3\left(k_7 k_9 k_{11} + k_6 k_9 k_{11} + k_5 k_7 k_{11} + k_5 k_7 k_{10}\right)}{k_5 k_9\left(k_7 k_{11} + k_3 k_{11} + k_3 k_7\right)} \tag{A2.44}$$

where K_A and K_B refer to the Michaelis constant of NADPH and cytochrome c^{3+}, respectively. Equation A2.41 reduces to the following equation:

$$\frac{v_i}{E_t} = \frac{V[A][B]}{[A][B] + K_B[A] + K_A[B]} \tag{A2.45}$$

which has the same form as equation 2.1 to which the parallel initial velocity patterns were fit. Thus, the proposed hexa-uni ping-pong mechanism for nNOS reduction of cytochrome c^{3+} is consistent with the observed initial velocity patterns.

With product inhibition by P (Q=0) the equation A2.40 reduces to the following equation:

$$\frac{v_i}{E_t} = \frac{k_1 k_3 k_5 k_7 k_9 k_{11}[A][B]}{\begin{aligned}&[A][B]\left(k_1 k_5 k_7 k_9 k_{11} + k_1 k_3 k_5 k_9 k_{11} + k_1 k_3 k_5 k_7 k_9\right) + \\ &[B]\left(k_3 k_5 k_7 k_9 k_{11} + k_2 k_5 k_7 k_9 k_{11}\right) \\ &[A]\left(k_1 k_3 k_7 k_9 k_{11} + k_1 k_3 k_6 k_9 k_{11} + k_1 k_3 k_5 k_7 k_{11} + k_1 k_3 k_5 k_7 k_{10}\right) + \\ &[P]\left(k_2 k_4 k_6 k_9 k_{11} + k_2 k_4 k_7 k_9 k_{11}\right) + [A][P]\left(k_1 k_4 k_6 k_9 k_{11} + k_1 k_4 k_7 k_9 k_{11}\right)\end{aligned}} \tag{A2.46}$$

Equation A2.46 can be rewritten as

$$\frac{v_i}{E_t} = \frac{V[A][B]}{[A][B]+[A]K_B+[B]K_A+[P]/G_1+[A][P]/G_2} \qquad \text{(A2.47)}$$

where K_A, K_B and k_{cat} are defined as above and

$$G_1 = \frac{k_1k_5k_9(k_7k_{11}+k_3k_{11}+k_3k_7)}{k_2k_4k_6k_{11}(k_6+k_7)} \qquad \text{(A2.48)}$$

$$G_2 = \frac{k_5(k_7k_{11}+k_3k_{11}+k_3k_7)}{k_4k_{11}(k_6+k_7)} \qquad \text{(A2.49)}$$

In double reciprocal form equation A2.47 becomes

$$\frac{E_t}{v_i} = \frac{K_A}{V}\left(1+\frac{[P]}{[B]K_AG_1}\right)\frac{1}{[A]}+\frac{1}{V}\left[1+\frac{K_B}{[B]}\left(1+\frac{[P]}{K_BG_2}\right)\right] \qquad \text{(A2.50)}$$

which shows that *P* will be noncompetitive with *A*. as the variable substrate. This inhibition pattern is inconsistent with the competitive inhibition pattern observed for $NADP^+$ (*P*) *versus* NADPH (*A*) with cytochrome c^{3+} as the electron acceptor. Arranging equation A2.50 with *B* as the variable substrate gives

$$\frac{E_t}{v_i} = \frac{K_B}{V}\left(1+\frac{[P]}{[A]K_BG_1}+\frac{[P]}{K_BG_2}\right)\frac{1}{[B]}+\frac{1}{V}\left[1+\frac{K_A}{[A]}\right] \qquad \text{(A2.51)}$$

Equation A2.51 predicts that *P* will be competitive versus *B*. This inhibition pattern is also inconsistent with the uncompetitive inhibition pattern observed for $NADP^+$ (*P*) *versus* cytochrome c^{3+} (*B*) in Table 2.3. Therefore, the hexa-uni ping-pong mechanism is not consistent with the basal and CaM-stimulated reduction of cytochrome c^{3+}.

With Q as a product inhibitor (P=0) equation A2.40 becomes

$$\frac{v_i}{E_t} = \frac{k_1k_3k_5k_7k_9k_{11}[A][B]^2}{\begin{aligned}&[A][B]^2(k_1k_5k_7k_9k_{11} + k_1k_3k_5k_9k_{11} + k_1k_3k_5k_7k_9) + \\ &[B]^2(k_3k_5k_7k_9k_{11} + k_2k_5k_7k_9k_{11}) + [A][Q](k_1k_3k_6k_8k_{11} + k_1k_3k_6k_8k_{10}) + \\ &[A][B](k_1k_3k_7k_9k_{11} + k_1k_3k_6k_9k_{11} + k_1k_3k_5k_7k_{11} + k_1k_3k_5k_7k_{10}) + \\ &[Q]^2(k_3k_6k_8k_{10}k_{12} + k_2k_6k_8k_{10}k_{12}) + +[B][Q]^2(k_3k_5k_8k_{10}k_{12} + k_2k_5k_8k_{10}k_{12}) \\ &+[A][B][Q](k_1k_3k_5k_8k_{11} + k_1k_3k_5k_8k_{10}) + \\ &[B][Q](k_3k_5k_7k_{10}k_{12} + k_2k_5k_7k_{10}k_{12}) + [B]^2[Q](k_3k_5k_7k_9k_{12} + k_2k_5k_7k_9k_{12})\end{aligned}} \quad \text{(A2.52)}$$

Equation A2.52 reduces to the following equation

$$\frac{v_i}{E_t} = \frac{V[A][B]^2}{\begin{aligned}&[A][B]^2 + K_B[A][B] + K_A[B]^2 + \\ &[Q]^2/J_1 + [A][Q]/J_2 + [B][Q]^2/J_3 + [A][B][Q]/J_4 + [B][Q]/J_5 + [B]^2[Q]/J_6\end{aligned}} \quad \text{(A2.53)}$$

where K_A, K_B and k_{cat} are defined in A2.42 to A2.44.

$$J_1 = \frac{k_1 k_5 k_9 \left(k_7 k_{11} + k_3 k_{11} + k_3 k_7\right)}{k_6 k_8 k_{10} k_{12} \left(k_2 + k_3\right)} \tag{A2.54}$$

$$J_2 = \frac{k_5 k_9 \left(k_7 k_{11} + k_3 k_{11} + k_3 k_7\right)}{k_3 k_6 k_8 \left(k_{10} + k_{11}\right)} \tag{A2.55}$$

$$J_3 = \frac{k_1 k_9 \left(k_7 k_{11} + k_3 k_{11} + k_3 k_7\right)}{k_8 k_{10} k_{12} \left(k_2 + k_3\right)} \tag{A2.56}$$

$$J_4 = \frac{k_9 \left(k_7 k_{11} + k_3 k_{11} + k_3 k_7\right)}{k_3 k_8 \left(k_{10} + k_{11}\right)} \tag{A2.57}$$

$$J_5 = \frac{k_1 k_9 \left(k_7 k_{11} + k_3 k_{11} + k_3 k_7\right)}{k_7 k_{10} k_{12} \left(k_2 + k_3\right)} \tag{A2.58}$$

$$J_6 = \frac{k_1 k_9 \left(k_7 k_{11} + k_3 k_{11} + k_3 k_7\right)}{k_7 k_{12} \left(k_2 + k_3\right)} \tag{A2.59}$$

In double reciprocal form with A as the variable substrate equation A2.53 becomes.

$$\frac{E_t}{v_i} = \frac{1}{V}\left(K_A + \frac{[Q]^2}{J_1[B]^2} + \frac{[Q]^2}{J_5[B]^2} + \frac{[Q]}{J_6} + \frac{[Q]^2}{J_3[B]}\right)\frac{1}{[A]} + \frac{1}{V}\left(1 + \frac{K_B}{[B]} + \frac{[Q]}{J_2[B]^2} + \frac{[Q]}{J_4[B]}\right) \tag{A2.60}$$

Inhibition by Q would generate a double reciprocal plot in which both the intercept and slope are affected and are non-linear functions of Q and/or B. Although Table 2.3 shows that cytochrome c^{2+}, Q, is noncompetitive *versus* NADPH, A, the inhibition patterns did not exhibit any curvature; therefore, they are not consistent the hexa-uni ping-pong mechanism. Rearranging equation A2.60 to show B as the variable substrate gives

$$\frac{E_t}{v_i} = \frac{1}{V}\left\{\left(K_B + \frac{[Q]^2}{J_3[A]} + \frac{[Q]}{J_4} + \frac{[Q]}{J_5[A]}\right)\frac{1}{[B]} + \left(\frac{[Q]^2}{J_1[A]}\right)\frac{1}{[B]^2}\right\} + \frac{1}{V}\left(1 + \frac{K_A}{[A]} + \frac{[Q]}{J_6[A]}\right) \tag{A2.61}$$

When B is the variable substrate, inhibition by Q is expected to have an affect on the intercept and the slope, with the slope a nonlinear function of Q. As shown in Table 2.3, cytochrome c^{2+}, Q, is competitive *versus* cytochrome c^{3+}, B; therefore, the product inhibition pattern is not consistent with the hexa-uni ping-pong mechanism.

Appendix 3

Derivation of Kinetic Mechanisms with the Charge-transfer Complex

A3.1 Derivation of the Rate Equation for a Di Iso Ping-Pong Bi-Bi Mechanism for nNOS Catalyzed Reduction of DCIP Incorporating the Steady-state Isomerization of the Charge-transfer Complex

Figure 3.2 shows the kinetic scheme for the di-iso ping-pong mechanism with the steady-state isomerization of the charge-transfer complex with NADPH-FAD proposed for the nNOS catalyzed reduction of DCIP. The basic features of the proposed mechanism are the same as outlined in the Appendix of Wolthers and Schimerlik (255). As before, the binding of substrates/inhibitors and the release of products is assumed to occur in rapid equilibrium; thus, the kinetic mechanism is divided into four rapid equilibrium segments, labeled E_1A, X, Y, and Z.. The derivation of steady-state equation is according to the method of Cha (302).

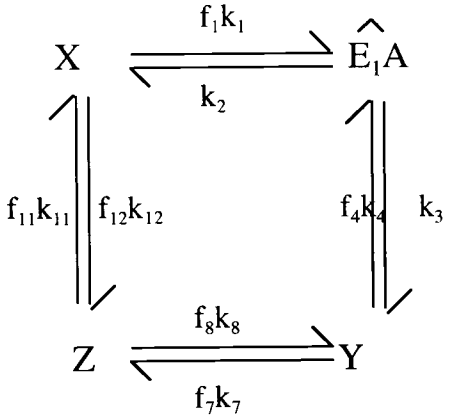

Scheme 3.1

The fractionation factors for the mechanism drawn in Figure 3.2 are as follows:

$$f_1 = \frac{E_1 A}{X} = \frac{A/K_{iA}}{1 + A/K_{iA} + 1/K(1 + I/K_{iI} + Q/K_{iQ} + QI/K_{iQ}K_{iI})} \quad \text{(A3.1)}$$

$$f_4 = \frac{E_3 P}{Y} = \frac{P/K_{iP}}{1 + P/K_{iP}} \quad \text{(A3.2)}$$

$$f_7 = \frac{E_3}{Y} = \frac{1}{1 + P/K_{iP}} \quad \text{(A3.3)}$$

$$f_8 = \frac{E_3'}{Z} = \frac{1}{1 + B/K_{iB}} \quad \text{(A3.4)}$$

$$f_{11} = \frac{E_3' B}{Z} = \frac{B/K_{iB}}{1 + B/K_{iB}} \quad \text{(A3.5)}$$

$$f_{12} = \frac{E_1' Q}{X} = \frac{Q/K_{iQ}}{1 + A/K_{iA} + 1/K(1 + I/K_{iI} + Q/K_{iQ} + QI/K_{iQ}K_{iI})} \quad \text{(A3.6)}$$

A, *B*, *P*, *Q* and *I* represent NADPH, $DCIP_{ox}$, $NADP^+$, $DCIP_{red}$, and 2'-AMP respectively, and the K_i values refer to their respective dissociation constants. E_1 and E_1' are the one-electron (FAD/FMNH•) forms of nNOS that exclusively bind NADPH and 2'-AMP, respectively. E_3 and E_3' are the three-electron (FADH•/$FMNH_2$) or ($FADH_2$/FMNH•) forms of nNOS that exclusively bind $NADP^+$ and $DCIP_{ox}$, respectively. *K* (equal to E_1/E_1') is the equilibrium constant for the conversion of the two free enzyme forms, E_1 and E_1'. $X = E_1 + E_1' + E_1'I + E_1'IQ + E_1'Q + E_1A$; $Y = E_3P + E_3$; $Z = E_3' + E_3'B$, and $E_t = X + Y + Z$. Using Scheme A3. 1 as the basic King-Altman pattern, the following velocity equation is obtained:

$$\frac{v_i}{E_t} = \frac{k_1k_3k_7k_{11}f_1f_7f_{11} - k_2k_4k_8k_{12}f_4f_8f_{12}}{k_7k_{11}f_7f_{11}(k_1 + k_2 + k_3) + k_2k_4f_4(k_8f_8 + k_{11}f_{11}) + k_4k_8f_4f_8(k_1f_1 + k_{12}f_{12}) + k_2k_8k_{12}f_8f_{12}(k_2 + k_3) + k_1k_{11}f_1f_{11}(k_3 + k_4f_4) + k_1k_3f_1(k_7f_7 + k_8f_8) + k_2k_7k_{12}f_7f_{12}(k_2 + k_3) + k_2k_4k_{12}f_4f_{12}} \quad \text{(A3.7)}$$

Under initial velocity conditions (P=Q=I=O) substitution of the fractionation factors (eqs A3.1-A3.6) into equation A3.7 yields the following equation:

$$\frac{v_i}{E_t} = \frac{[A][B]\dfrac{k_1k_3k_7k_{11}}{(k_1k_3k_7 + k_1k_{11}(k_3 + k_7) + k_7k_{11}(k_2 + k_3))}}{[A][B] + [B]\dfrac{(K_{iA})(1 + 1/K)(k_7k_{11}(k_2 + k_3))}{(k_1k_3k_7 + k_1k_{11}(k_3 + k_7) + k_7k_{11}(k_2 + k_3))} + [A]\dfrac{(K_{iB})(k_1k_3(k_7 + k_8))}{(k_1k_3k_7 + k_1k_{11}(k_3 + k_7) + k_7k_{11}(k_2 + k_3))}} \quad \text{(A3.8)}$$

The kinetic constants are defined as follows:

$$k_{cat} = \frac{k_1k_3k_7k_{11}}{(k_1k_3k_7 + k_1k_{11}(k_3 + k_7) + k_7k_{11}(k_2 + k_3))} \quad \text{(A3.9)}$$

$$K_A = \frac{(K_{iA})(1 + 1/K)(k_7k_{11}(k_2 + k_3))}{(k_1k_3k_7 + k_1k_{11}(k_3 + k_7) + k_7k_{11}(k_2 + k_3))} \quad \text{(A3.10)}$$

$$K_B = \frac{(K_{iB})(k_1k_3(k_7 + k_8))}{(k_1k_3k_7 + k_1k_{11}(k_3 + k_7) + k_7k_{11}(k_2 + k_3))} \quad \text{(A3.11)}$$

Equation A3.8 simplifies to equation A3.12.

$$\frac{v_i}{E_t} = \frac{V[A][B]}{[A][B] + K_B[A] + K_A[B]} \quad \text{(A3.12)}$$

which has the same form as the rate equation for a ping-pong mechanism, eq. 2.1. Thus, the proposed mechanism for nNOS reduction of DCIP is consistent with the observed initial velocity patterns and yields the same patterns expected for a standard ping-pong mechanism.

The equation describing product inhibition by $NADP^+$, P, is derived letting $Q = I = 0$ and substituting the fractionation factors A3.1-A3.6 into equation A3.7:

$$\frac{v_i}{E_t} = \frac{V[A][B]}{[A][B]\left(1+\frac{D_4P}{K_{iP}}\right)+[A]\left(K_B+\frac{D_2P}{K_{ip}}\right)+[B]\left(K_A+\frac{D_3P}{K_{iP}}\right)+[P]\frac{D_1}{K_{iP}}} \qquad \text{(A3.13)}$$

where

$$D_1 = \frac{K_{iB}k_4k_8\left(k_1+k_2K_{iA}\left(1+1/K\right)\right)}{k_7k_{11}\left(k_2+k_3\right)+k_1k_{11}\left(k_3+k_7\right)+k_1k_3k_7} \qquad \text{(A3.14)}$$

$$D_2 = \frac{K_{iB}k_8\left(k_2k_4+k_1k_3\right)}{k_7k_{11}\left(k_2+k_3\right)+k_1k_{11}\left(k_3+k_7\right)+k_1k_3k_7} \qquad \text{(A3.15)}$$

$$D_3 = \frac{K_{iA}k_2k_4k_{11}\left(1+1/K\right)}{k_7k_{11}\left(k_2+k_3\right)+k_1k_{11}\left(k_3+k_7\right)+k_1k_3k_7} \qquad \text{(A3.16)}$$

$$D_4 = \frac{k_{11}\left(k_2k_4+k_1k_4+k_1k_3\right)}{k_7k_{11}\left(k_2+k_3\right)+k_1k_{11}\left(k_3+k_7\right)+k_1k_3k_7} \qquad \text{(A3.17)}$$

With A as the variable substrate, the double reciprocal form of equation A3.13 becomes

$$\frac{E_t}{v} = \frac{K_a}{V}\left(1+\frac{P}{K_{iP}}\left(D_3+\frac{D_1}{B}\right)\frac{1}{K_a}\right)\frac{1}{A}+\frac{1}{V}\left(1+\frac{K_b}{B}+\frac{P}{K_{iP}}\left(D_4+\frac{D_2}{B}\right)\right) \qquad \text{(A18)}$$

which predicts that inhibition by *P* will produce a noncompetitive inhibition pattern. The double reciprocal form of equation A3.13 with *B* as the variable substrate is the following

$$\frac{E_t}{v} = \frac{K_b}{V}\left(1 + \frac{P}{K_{iP}}\left(D_2 + \frac{D_1}{A}\right)\frac{1}{K_b}\right)\frac{1}{B} + \frac{1}{V}\left(1 + \frac{K_a}{A} + \frac{P}{K_{iP}}\left(D_4 + \frac{D_3}{A}\right)\right) \qquad \text{(A19)}$$

which also predicts that inhibition by *P* will produce a noncompetitive inhibition pattern. Thus, the mechanism correctly predicts the product inhibition patterns which where obtained experimentally.

For dead-end inhibition by the substrate analog, 2'-AMP (*I*), *P*=*Q*=O, substitution of equations A3.1-A3.6 into equation A3.7 yields the following velocity equation:

$$\frac{v_i}{E_t} = \frac{V[A][B]}{[A][B] + K_B[A] + K_A[B]\left(1 + \dfrac{[I]}{K_{il}(1+K)}\right)} \qquad \text{(A3.20)}$$

With *A* as the varied substrate, the double reciprocal form of the equation A3.20 is

$$\frac{E_t}{v_i} = \frac{1}{V}\left(1 + \frac{K_B}{B}\right) + \frac{K_A}{V}\left(1 + \frac{[I]}{K_{il}(1+K)}\right)\frac{1}{[A]} \qquad \text{(A3.21)}$$

The equation predicts a competitive pattern for *I* when *A* is the variable substrate, consistent with the experimental results. Arranging A3.20 with *B* as the variable substrate, the equation becomes

$$\frac{E_t}{v_i} = \frac{1}{V}\left(1 + \frac{K_A}{A}\left(1 + \frac{[I]}{K_{il}(1+K)}\right)\right) + \frac{K_B}{V}\frac{1}{[B]} \qquad \text{(A3.22)}$$

Uncompetitive inhibition is predicted for I when B is the variable substrate, consistent with the experimental results. Ifk_3 is the isotopically sensitive step, then the observed isotope effect on V and $(V/K)_{NADPH}$

A3.1 Derivation of Rate Equations of an Iso Two-Site Ping-Pong Mechanism for nNOS-Catalyzed Reduction of Cytochrome c^{3+} Incorporating the Charge-Transfer Complex

Figure 2.4 shows the kinetic scheme for the iso two-site ping-pong mechanism with NADPH and the formation of a conformationally distinct charge transfer complex. The following assumptions were made in the derivation of the rate equation: (1) all ligand binding steps occur in rapid equilibrium; (2) the binding of a ligand at site one does not effect of binding of the ligands at second site; and (3) the values of all ligand dissociation constants are unaffected by the oxidation state of the enzyme. Scheme A3.2 illustrates the King-Altman pattern used for the following derivation. Equations were derived using the method of Cha (62) with the fractionation factors defined as follows:

$$f_A = \frac{E_1A + E_1AB + E_1AQ}{E_{tX}} = \frac{A/K_{iA}}{1 + A/K_{iA} + P/K_{iP} + 1/K(1 + I/K_{il})} \quad \text{(A3.25)}$$

$$f_B = \frac{E_2B + E_2AB + E_2PB}{E_{t2}} = \frac{E_3B + E_3AB + E_3PB}{E_{t3}} = \frac{B/K_{iB}}{1 + B/K_{iB} + Q/K_{iQ}} \quad \text{(A3.26)}$$

$$f_P = \frac{E_3P + E_3PB + E_3PQ}{E_{t3}} = \frac{P/K_{iP}}{1 + A/K_{iA} + P/K_{iP}} \quad \text{(A3.27)}$$

$$f_Q = \frac{E_2Q + E_2AQ + E_2PQ}{E_{t2}} = \frac{Q/K_{iQ}}{1 + B/K_{iB} + Q/K_{iQ}} \quad \text{(A3.28)}$$

$$f_Q' = \frac{E_1'Q}{E_{tX}} = \frac{Q/KK_{iQ}}{\left[1 + B/K_{iB} + Q/K_{iQ}\right]\left[1 + A/K_{iA} + P/K_{iP} + 1/K(1 + I/K_{il})\right]} \quad \text{(A3.29)}$$

A, B, P, Q and *I* represent NADPH, cytochrome c^{3+}, $NADP^+$, cytochrome c^{2+}, and 2'AMP respectively, and the K_i values refer to their respective dissociation constants. E_1 and E_1' are the one-electron (FAD/FMNH•) forms of nNOS that exclusively bind NADPH and 2'AMP, respectively. E_2 is the two-electron ($FAD/FMNH_2$) enzyme form and E_3 is the three-electron ($FADH•/FMNH_2$) form of the enzyme. K (equal to E_1/E_1') is the equilibrium constant for the conversion of the two free enzyme forms. $E_{t2} = E_2 + E_2A + E_2B + E_2P + E_2Q + E_2AB + E_2BP + E_2AQ + E_2PQ$. $E_{t3} = E_3 + E_3A + E_3B + E_3P + E_3Q + E_3AB + E_3BP + E_3AQ + E_3PQ$. $E_{tX} = E_1 + E_1A + E_1B, + E_1P + E_1Q + E_1AB + E_1BP + E_1AQ + E_1PQ + E_1' + E_1'I + E_1'B + E_1'Q + E_1'IB + E_1'IQ$. Using the fractionation factors and the scheme in Figure 2.7 as the basic King-Altman pattern, one can derive the following velocity equation:

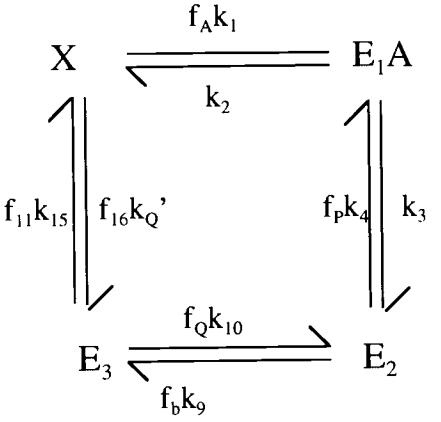

Scheme A3.2

$$\frac{v_i}{E_t} = \frac{k_1k_3k_9k_{15}f_Af_Bf_B - k_2k_4k_{10}k_{16}f_Pf_Qf_Q'}{k_2k_4k_{10}f_Pf_Q + k_9k_{15}f_B^2(k_2+k_3) + k_2k_4k_{15}f_Bf_P + k_1k_4k_{10}f_Af_Pf_Q + k_4k_{10}k_{16}f_Pf_Qf_Q' + k_1k_9k_{15}f_Af_B^2 + k_1k_4k_{15}f_Af_Bf_P + k_1k_3k_9f_Af_Q + k_{10}k_{16}f_Qf_Q'(k_2+k_3) + k_1k_3f_Af_B(k_9+k_{15}) + k_9k_{16}f_Bf_Q'(k_2+k_3) + k_2k_4k_{16}f_Pf_Q'} \tag{A3.30}$$

Under initial velocity conditions (P=Q=I=0), substitution of the fractionation factors A3.25 to A3.29 simplifies the overall rate equation to the following equation.

$$\frac{v_i}{E_t} = \frac{\dfrac{k_1k_3k_9k_{15}[A][B]}{k_9k_{15}(k_1+k_2+k_3)+k_1k_3(k_9+k_{15})}}{[A][B]+[A]\dfrac{k_1k_3(K_{iB})(k_9+k_{15})}{k_9k_{15}(k_1+k_2+k_3)+k_1k_3(k_9+k_{15})}+ [B]\dfrac{k_9k_{15}(K_{iA})(k_2+k_3)(1+1/K)}{k_9k_{15}(k_1+k_2+k_3)+k_1k_3(k_9+k_{15})}} \tag{A3.31}$$

Kinetic constants are defined in equation A3.32 to A3.34.

$$\frac{V}{E_t} = \frac{k_1 k_3 k_9 k_{15}}{k_9 k_{15}(k_1 + k_2 + k_3) + k_1 k_3 (k_9 + k_{15})} \tag{A3.32}$$

$$K_A = \frac{k_1 k_3 k_9 k_{15}}{k_9 k_{15}(k_1 + k_2 + k_3) + k_1 k_3 (k_9 + k_{15})} \tag{A3.33}$$

$$K_B = \frac{k_1 k_3 (K_{iB})(k_9 + k_{15})}{k_9 k_{15}(k_1 + k_2 + k_3) + k_1 k_3 (k_9 + k_{15})} \tag{A3.34}$$

Thus the rate equation reduces to the following:

$$\frac{v_i}{E_t} = \frac{V[A][B]}{[A][B] + K_B[A] + K_A[B]} \tag{A3.35}$$

The K_A and K_B refer to the Michaelis constants of NADPH and cytochrome c^{3+}, respectively, and V is the maximal velocity. Equation A3.35 has the same form as equation expected for a ping-pong mechanism. Thus, the proposed two-site ping-pong mechanism for nNOS reduction of cytochrome c^{3+} is consistent with the observed initial velocity patterns.

Since $NADP^+$ is uncompetitive *versus* cytochrome c^{3+} and the double-reciprocal plots with cytochrome c^{2+} as an inhibitor are linear the assumptions were made (i.e. $k_9 >> k_4$) for the nNOS mechanism. In the presence of P ($Q = I = 0$), substitution of the fractionation factors A3.25-A3.29 into equation A3.30 and omission of terms in equation A30 containing k_4 gave the following equation:

$$\frac{v_i}{E_t} = \frac{V[A][B]}{[A][B] + [B]K_A + [A]K_B + [B][P]\left(\frac{K_A}{K_{iP}(1 + 1/K)}\right)} \tag{A3.36}$$

Equation A3.36 predicts competitive inhibition by P when A is the variable substrate. The corresponding equation describing product inhibition by P with B as the variable substrate predicts uncompetitive inhibition. Thus, the mechanism correctly predicts the product inhibition patterns obtained experimentally.

With product inhibition by Q (P=I=0), substitution of the fractionation factors A3.25 to A3.29 into equation A3.30 produces the following rate equation:

$$\frac{v_i}{E_t} = \frac{V[A][B]^2}{[A][B]^2 + [B]^2 K_A + [A][B]K_B + [A][B][Q]\left(\frac{C_1}{K_{iQ}}\right) + [B][Q]\left(\frac{C_2}{KK_{iQ}}\right) + [A][Q]\frac{C_3}{K_{iQ}} + [A][Q]^2\left(\frac{C_3}{K_{iQ}^{\ 2}}\right) + [Q]^2\left(\frac{C_4}{KK_{iQ}^{\ 2}}\right)} \qquad \text{(A3.37)}$$

where

$$C_1 = K_{iB}\left(\frac{k_1k_3(k_9 + k_{10} + k_{15})}{k_3k_9 + k_9k_{15} + k_3k_{15}}\right) \qquad \text{(A3.38)}$$

$$C_2 = K_{iA}K_{iB}\left(\frac{k_9k_{16}(k_2 + k_3)}{k_3k_9 + k_9k_{15} + k_3k_{15}}\right) \qquad \text{(A3.39)}$$

$$C_3 = K_{iB}^{\ 2}\left(\frac{k_1k_3k_{10}}{k_3k_9 + k_9k_{15} + k_3k_{15}}\right) \qquad \text{(A3.40)}$$

$$C_4 = K_{iA}K_{iB}\left(\frac{k_{10}k_{16}(k_2 + k_3)}{k_3k_9 + k_9k_{15} + k_3k_{15}}\right) \qquad \text{(A3.41)}$$

The terms C_1 and C_2 predominate over C_3 and C_4 in equation A3.37 since k_{10} and k_{16}, which represent the rate of cytochrome c^{2+} reduction of E_2 and E_1, respectively, are

assumed to be much slower then electron transfer to cytochrome c^{3+}, k_9 and k_{15}. Thus, equation A3.37 reduces to the following equation:

$$\frac{v_i}{E_t} = \frac{V[A][B]}{[A][B] + [B]K_A + [A]K_B + [A][Q]\left(\frac{C_1}{K_{iQ}}\right) + [Q]\left(\frac{C_2}{KK_{iQ}}\right)} \qquad \text{(A3.42)}$$

Equation A3.42 predicts product inhibition by Q with B as the variable substrate to be competitive. The corresponding equation describing product inhibition by Q with A as the variable substrate predicts noncompetitive inhibition. Therefore, the proposed iso two-site ping-pong mechanism is consistent with the cytochrome c^{2+} product inhibition patterns obtained experimentally.

In the presence of 2'-AMP, I, (P=Q=O), substitution of the fractionation factors A3.25 to A3.29 into equation A3.30 leads to the following equation:

$$\frac{v_i}{E_t} = \frac{V[A][B]}{[A][B] + K_B[A] + K_A[B]\left(1 + \frac{[I]}{K_{il}(1+K)}\right)} \qquad \text{(A3.43)}$$

Equation A3.43 predicts that I will be competitive *versus* A and uncompetitive *versus* B. As with the di-iso ping-pong mechanism described for DCIP as an electron acceptor, the overall apparent affinity for 2'-AMP is a function of its dissociation constant and the equilibrium constant, K (equal toE_1/E_1'), i.e. K_{is}=K_{il}(1+K) and K_{ii}=K_{il}(1+K).